

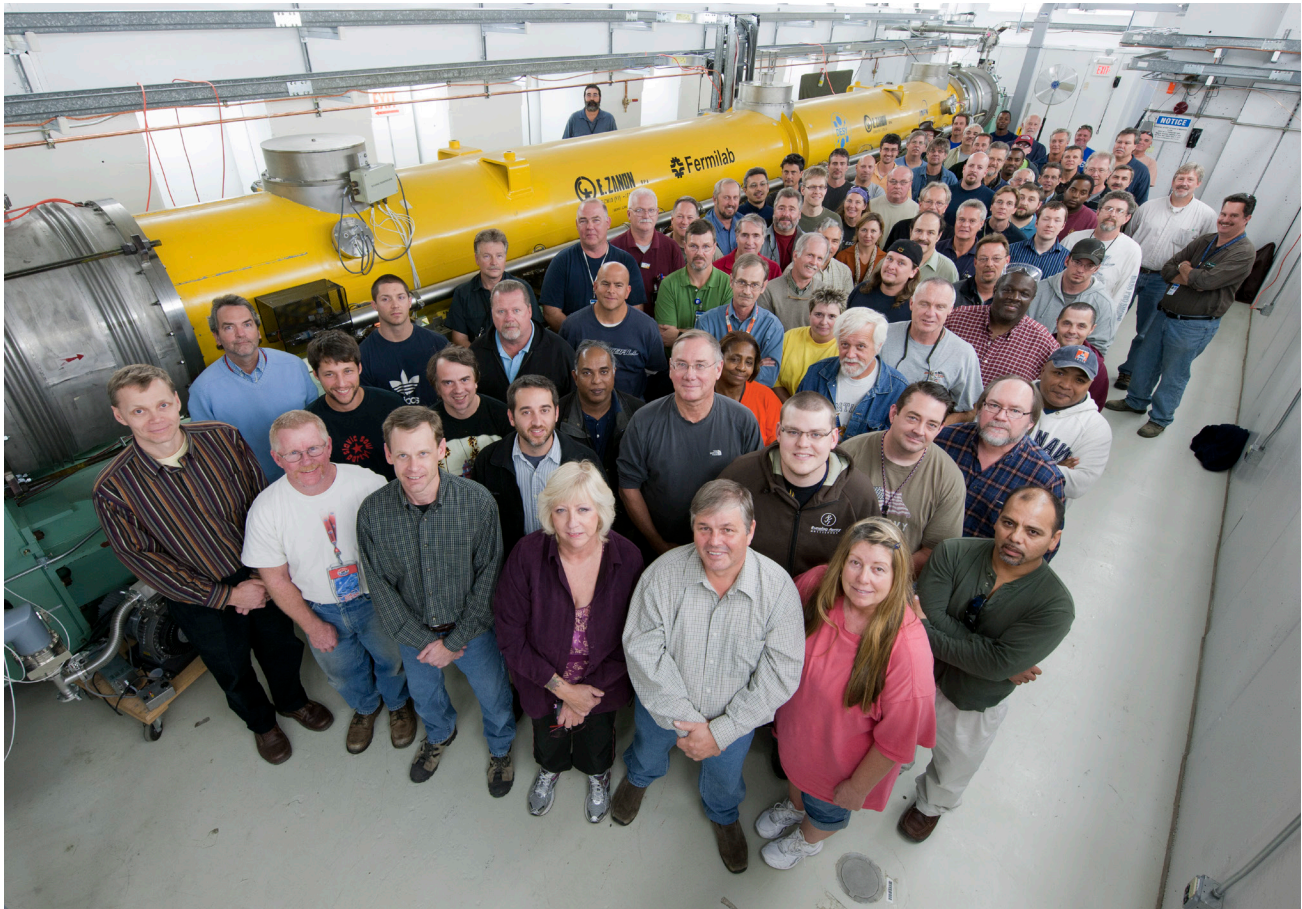
Proposal for an  
Accelerator R&D User Facility  
at Fermilab's

Advanced Superconducting  
Test Accelerator (ASTA)

Proposal for an

# Accelerator R&D User Facility at Fermilab's Advanced Superconducting Test Accelerator (ASTA)

December 2012



Managed by Fermi Research Alliance, LLC for the Department of Energy

## List of Authors and Contributors

### ASTA Facility

M. Church<sup>1</sup>, H. Edwards<sup>1</sup>, E. Harms<sup>1</sup>, S. Henderson<sup>1</sup>, S. Holmes<sup>1</sup>, A. Lumpkin<sup>1</sup>, R. Kephart<sup>1</sup>, V. Lebedev<sup>1</sup>, J. Leibfritz<sup>1</sup>, S. Nagaitsev<sup>1</sup>, P. Piot<sup>1,2</sup>, C. Prokop<sup>2</sup>, V. Shiltsev<sup>1</sup>, Y.E. Sun<sup>1</sup>, A. Valishev<sup>1</sup>

### Scientific Case

C. Ankenbrandt<sup>3</sup>, B. Carlsten<sup>4</sup>, C. Brau<sup>5</sup>, J. Byrd<sup>6</sup>, B. Chase<sup>1</sup>, D. Christian<sup>1</sup>, M. Chung<sup>1</sup>, M. Church<sup>1</sup>, J. Corlett<sup>6</sup>, V. Danilov<sup>7</sup>, Ya. Derbenev<sup>8</sup>, N. Eddy<sup>1</sup>, H. Edwards<sup>1</sup>, P. Emma<sup>6</sup>, R. Holt<sup>11</sup>, R. Johnson<sup>3</sup>, G. Krafft<sup>8</sup>, F. Lemery<sup>2</sup>, A. Lumpkin<sup>1</sup>, V. Lebedev<sup>1</sup>, D. Mihalcea<sup>2</sup>, A. Murokh<sup>9</sup>, S. Nagaitsev<sup>1</sup>, E. Nissen<sup>8</sup>, M. Palmer<sup>1</sup>, P. Piot<sup>1,2</sup>, M. Reinsch<sup>6</sup>, T. Roberts<sup>3</sup>, J. Ruan<sup>1</sup>, V. Scarpine<sup>1</sup>, V. Shiltsev<sup>1</sup>, Y.M. Shin<sup>1,2</sup>, N. Solyak<sup>1</sup>, A. Sonnenschein<sup>1</sup>, Y.E. Sun<sup>1</sup>, R. Thurman-Keup<sup>1</sup>, R. Tschirhart<sup>1</sup>, A. Valishev<sup>1</sup>, N. Vinokurov<sup>10</sup>, R. Wilcox<sup>6</sup>, V. Yakovlev<sup>1</sup>, Y. Zhang<sup>8</sup>, M. Zolotorev<sup>6</sup>, R. Zwaska<sup>1</sup>

### Editorial Support

P. Garbincius<sup>1</sup>

<sup>1</sup>Fermi National Accelerator Laboratory

<sup>2</sup>Northern Illinois University

<sup>3</sup>Muons, Inc.

<sup>4</sup>Los Alamos National Laboratory

<sup>5</sup>Vanderbilt University

<sup>6</sup>Lawrence Berkeley National Laboratory

<sup>7</sup>Oak Ridge National Laboratory

<sup>8</sup>Thomas Jefferson National Laboratory

<sup>9</sup>RadiaBeam Technologies

<sup>10</sup>Budker Institute of Nuclear Physics

<sup>11</sup>Argonne National Laboratory

[http://apc.fnal.gov/programs2/ASTA\\_TEMP/index.shtml](http://apc.fnal.gov/programs2/ASTA_TEMP/index.shtml)

## Table of Contents

|   |    |
|---|----|
| List of Authors and Contributors .....  | 2  |
| Table of Contents.....  | 3  |
| 1.0 Executive Summary .....   | 6  |
| 2.0 Introduction.....   | 9  |
| 2.1 The Role of Particle Physics in Accelerator Development.....                      | 9  |
| 2.2 ASTA’s Role in Furthering the HEP Mission .....                                   | 10 |
| 2.3 Overview of Scientific Opportunities at ASTA .....                                | 13 |
| 2.4 Organization of This Proposal.....  | 15 |
| 3.0 The Fermilab Context .....  | 16 |
| 3.1 Connection to Fermilab’s Mission .....  | 16 |
| 3.2 Fermilab’s Historical Contributions in Advanced Accelerator R&D.....              | 18 |
| 3.2.1 Fermilab’s AARD Contributions .....   | 18 |
| 3.2.2 Selected AARD Publications from Fermilab.....                                   | 19 |
| 3.2.3 PhD Theses in Advanced Accelerator R&D from Fermilab-based Research .....       | 20 |
| 4.0 Scientific Drivers in Advanced Accelerator R&D .....                              | 21 |
| 4.1 References .....  | 24 |
| 5.0 Comparison with other AARD Facilities .....                                       | 25 |
| 5.1 References .....  | 30 |
| 6.0 ASTA Facility Overview and Capabilities .....                                     | 31 |
| 6.1 RF Photoinjector .....  | 33 |
| 6.2 1.3 GHz SRF Cryomodules.....  | 35 |
| 6.3 IOTA Ring.....  | 36 |
| 6.4 3.9 GHz SRF Cavity .....  | 36 |
| 6.5 Other Equipment and Experimental Areas.....                                       | 37 |
| 6.6 ASTA Timeline .....   | 38 |
| 6.7 References .....  | 40 |
| 7.0 Scientific Opportunities at ASTA .....  | 41 |
| 7.1 Overview of Research Thrusts .....  | 41 |
| 7.1.1 Accelerator R&D for Particle Physics at the Intensity and Energy Frontiers..... | 41 |
| 7.1.2 Accelerator R&D for Stewardship and Applications.....                           | 41 |

|        |   |     |
|--------|---|-----|
| 7.2    | Accelerator R&D Opportunities at ASTA: Toward HEP Discovery Science at the Intensity and Energy Frontiers.....                    | 42  |
| 7.2.1  | Demonstration of High Power High Gradient SRF Cryomodules with Intense Beams .....  | 42  |
| 7.2.2  | Integrable-optics test accelerator (IOTA) ring construction and operation.....  | 50  |
| 7.2.3  | Space Charge Compensation in High Intensity Circular Accelerators .....   | 62  |
| 7.2.4  | Optical Stochastic Cooling Experiment at ASTA .....   | 64  |
| 7.2.5  | Investigation of Acceleration and Cooling of Carbon-Based Crystal Structures for Muon Accelerators .....                          | 71  |
| 7.2.6  | Electron Wave Function Size Measurements in IOTA Ring .....   | 81  |
| 7.2.7  | LBNE Targetry Experiments at ASTA.....  | 83  |
| 7.2.8  | A Tagged Photon Beam at ASTA for Detector R&D .....   | 87  |
| 7.2.9  | Applications of Inverse Compton Scattered Photons.....  | 89  |
| 7.3    | Accelerator R&D Opportunities at ASTA: Stewardship and Applications.....  | 91  |
| 7.3.1  | High-brightness X-ray channeling radiation source.....  | 91  |
| 7.3.2  | Advanced phase space manipulations.....   | 98  |
| 7.3.3  | Demonstration of techniques to generate and manipulate ultra-low emittance beams for future hard X-ray free-electron lasers ..... | 108 |
| 7.3.4  | Beam-beam kicker for electron-ion collider .....  | 116 |
| 7.3.5  | Feasibility of an XUV FEL Oscillator at ASTA .....  | 120 |
| 7.3.6  | Production of Narrow Band Gamma-Rays.....   | 134 |
| 7.3.7  | Inverse Compton Scattering Gamma-Ray Source at ASTA.....  | 136 |
| 7.3.8  | Attosecond vacuum-ultraviolet pulses via space-charge-driven amplification of shot-noise density fluctuations .....               | 139 |
| 7.3.9  | Potential for Critical Laser-Induced Microbunching Studies with the High-Micropulse-Repetition-Rate Electron beams at ASTA .....  | 141 |
| 7.3.10 | Proposed Coherent Diffraction Radiation Measurements of Bunch Length at ASTA .....  | 154 |
| 7.3.11 | Non-intercepting Optical Diffraction Radiation Diagnostics at ASTA.....   | 160 |
| 7.3.12 | Towards Ultra-Stable Operation of ASTA with Beam Based Feedback .....   | 173 |
| 7.3.13 | Proposed Wakefield Measurements at ASTA.....  | 181 |
| 7.3.14 | Flat-Beam-Driven Dielectric-Wakefield Acceleration in Slab Structures.....  | 185 |
| 8.0    | Technical Description of ASTA.....  | 193 |
| 8.1    | Facility Overview .....   | 193 |
| 8.2    | Injector .....  | 195 |
| 8.2.1  | Electron gun .....  | 195 |

|        |   |     |
|--------|---|-----|
| 8.2.2  | Photocathode laser .....                          | 196 |
| 8.2.3  | Beamline elements .....                           | 197 |
| 8.2.4  | Diagnostics .....                                 | 197 |
| 8.3    | Cryomodules .....                                 | 198 |
| 8.3.1  | Description .....                                 | 198 |
| 8.3.2  | Initial operation.....                            | 199 |
| 8.4    | High energy beamlines .....                       | 201 |
| 8.4.1  | Beamline elements .....                           | 201 |
| 8.4.2  | Diagnostics .....                                 | 201 |
| 8.4.3  | Beam dump.....                                    | 201 |
| 8.5    | Beam dynamics calculations and simulations .....  | 202 |
| 8.6    | References .....                                  | 203 |
| 9.0    | Accelerator Science Education at ASTA .....       | 205 |
| 10.0   | Scope, Cost and Schedule.....                     | 208 |
| 10.1   | Scope.....  | 208 |
| 10.2   | Cost .....  | 210 |
| 10.2.1 | Stage I Cost.....                                 | 210 |
| 10.2.2 | IOTA Cost.....                                    | 212 |
| 10.2.3 | Stage II Cost.....                                | 212 |
| 10.2.4 | Stage III Cost.....                               | 213 |
| 10.2.5 | Stage IV Cost .....                               | 214 |
| 10.2.6 | Operating Cost .....                              | 215 |
| 10.2.7 | Cost Breakdown .....                              | 216 |
| 10.3   | Schedule.....                                     | 217 |
| 11.0   | Management of the Scientific User Program.....    | 219 |
| 12.0   | List of Acronyms .....                            | 221 |
| 13.0   | Appendix - Letters of Institutional Interest..... | 227 |

## 1.0 Executive Summary

Fermilab is the nation's particle physics laboratory, supported by the DOE Office of High Energy Physics (OHEP). Fermilab is a world leader in accelerators, with a demonstrated track-record – spanning four decades – of excellence in accelerator science and technology. While the US accelerator-based HEP program is oriented toward the Intensity Frontier, which requires modern superconducting linear accelerators and advanced high-intensity storage rings, there are no accelerator test facilities that support the accelerator science of the Intensity Frontier. Further, nearly all proposed future accelerators for Discovery Science will rely on superconducting radiofrequency (SRF) acceleration, yet there are no dedicated test facilities to study SRF capabilities for beam acceleration and manipulation in prototypic conditions. Finally, there are a wide range of experiments and research programs beyond particle physics that require the unique beam parameters that will only be available at Fermilab's Advanced Superconducting Test Accelerator (ASTA). To address these needs we submit this proposal for an Accelerator R&D User Facility at ASTA.

The ASTA program is based on the capability provided by an SRF linac (which provides electron beams from 50 MeV to nearly 1 GeV) and a small storage ring (with the ability to store either electrons or protons) to enable a broad range of beam-based experiments to study fundamental limitations to beam intensity and to develop transformative approaches to particle-beam generation, acceleration and manipulation which cannot be done elsewhere. It will also establish a unique resource for R&D towards Energy Frontier facilities and a test-bed for SRF accelerators and high brightness beam applications in support of the OHEP mission of Accelerator Stewardship.

ASTA is unique among accelerator user facilities in six principal ways:

- High repetition-rate: ASTA accelerates 1 msec long bunch trains, with 3 MHz micro-pulse repetition rate, with up to 3000 bunches per train
- High average power: ASTA accelerates 1 msec long bunch trains at up to five pulses per second, providing the highest beam power and highest average brightness of any accelerator test facility in the U.S.
- High energy: ASTA accelerates beam to ~1 GeV, which is important for a number of photon-science and FEL-related experiments
- Extremely stable beams: ASTA, based on ILC technology, is capable of providing exceptional beam stability, which has been demonstrated at the FLASH facility at DESY
- Superconducting technology: ASTA necessarily brings SRF and beams together. As nearly all future large scale accelerator facilities will rely on SRF technology, ASTA will be the only GeV-scale test facility which is capable of supporting R&D in prototypical conditions.
- Storage ring: ASTA includes a small, very flexible storage ring, based on innovative optics, capable of supporting a broad range of ring-based advanced beam dynamics experiments.

These unique features enable a broad program in advanced accelerator R&D which cannot be carried out elsewhere. A national User Facility for Accelerator R&D based at Fermilab's ASTA will further the mission of OHEP by addressing several needs:

- Furthering the strategic priorities for particle physics
- Strengthening the nation's Accelerator Test Facility infrastructure
- Establishing a test-bed for Superconducting RF Accelerators
- Fulfilling the Accelerator Stewardship Mission
- Educating and training the next generation of accelerator scientists

Construction of the ASTA Facility at NML began in 2006 as part of the International Linear Collider/SRF R&D Program and later the American Recovery and Reinvestment Act (ARRA) within the DOE OHEP. Construction of the facility was motivated by the goal of building, testing and operating a complete ILC RF unit to demonstrate industrial and laboratory capability for producing state-of-the-art superconducting linear accelerator components, and assembling them into a fully functioning system. ASTA, configured as a single ILC RF unit, would consist of an electron photo-injector, accelerating cavities, a bunch compressor, and three 1.3 GHz ILC cryomodules powered together from a single high-power klystron. Each cryomodule provides 250 MeV of energy gain for total output energy of approximately 800 MeV.

It was recognized early in the planning process that an electron beam meeting the demanding ILC performance parameters was itself a powerful resource of interest to the wider Advanced Accelerator R&D (AARD) community as expressed at the Workshop "Future Directions for Accelerator R&D at Fermilab" (May 2009 - Lake Geneva, WI). For those reasons the ARRA-funded facility construction incorporated space for the installation of additional SRF cryomodules to increase the beam energy to a maximum of 1.5 GeV, space for multiple high-energy beamlines, as well as provisions for a small circular ring for the exploration of advanced accelerator concepts, for transporting laser light into and out of the accelerator enclosure, and an adequately-sized control room.

With the completion of the ILC R&D Program in FY2012, DOE/OHEP has directed Fermilab to submit a proposal for funding the completion of the ASTA facility and establishing an accelerator R&D user program there. This Proposal is submitted in recognition of the tremendous opportunity that the ASTA facility, based on a state-of-the-art superconducting linear accelerator, represents to the national and international Advanced Accelerator R&D user community.

The ASTA facility at NML presently consists of the following:

- A 47 meter long, 4,500 ft<sup>2</sup> shielded accelerator enclosure housed inside the 12,000 ft<sup>2</sup> NML building.
- A 70 meter long, 8,000 ft<sup>2</sup> newly constructed tunnel enclosure to the North of the NML building.

- An 2,800 ft<sup>2</sup> support building
- A control room
- An radio-frequency photo-injector system, including the drive laser system, which is scheduled to be commissioned in FY 2013
- Operating high-power and low-level RF systems, RF distribution system and controls
- Refrigeration system capable of 120 W @ 2K.

Two SRF cryomodules have been assembled and a third is presently under construction. All parts, including cavities, couplers, vacuum vessels, etc., for a total of 6 cryomodules have been purchased. ASTA experimental beamline equipment, including 154 magnets, all vacuum chambers, 22 beam position monitors, etc. have also been purchased. To date, a total of \$ 74 M has been spent to construct and operate the facility. The ARRA-funded construction of the facility has been completed at a total investment of approximately \$ 18 M.

To enable a broad range of scientific opportunities, the completion of the ASTA facility requires establishing beams to low-energy (50 MeV) and high-energy (300-800 MeV) experimental areas and to complete construction of the Integrable Optics Test Accelerator (IOTA), a 38-m circumference ring designed for the study of novel, non-linear accelerator lattices and high-brightness beam dynamics. With this proposal, we request funds totaling \$ 19.4 M for the completion of the ASTA facility, and provide an estimate of the annual operating cost to support a user program at ASTA of \$ 3.9 M/yr. This estimate assumes nine months of beam operation per year.

The completion of ASTA and operation of a user program builds upon Fermilab's strong history and experience in the operation of the A0 Photoinjector and its associated R&D program. That program has produced 9 PhDs in AARD since its inception in the mid-1990's. The scientific strength of that program and the assembled staff which operates it and directs the R&D program has resulted, just in the last two years, in 21 high-quality publications in accelerator science.

With the substantial investment already made in the ASTA facility, and the additional funds requested to complete the facility, OHEP has the opportunity to support a unique, state-of-the-art, modern AARD user facility which is expected to have a broad impact, influencing fields from particle physics to basic-energy sciences to national security. As the nation's particle physics laboratory, Fermilab intends to play a leading role in the development of tomorrow's accelerators. A key element of that vision is a world-leading user facility for accelerator science.

## 2.0 Introduction

### 2.1 The Role of Particle Physics in Accelerator Development

Since the invention of the cyclotron eighty years ago, the multitude of historic breakthroughs in our understanding of the subatomic world has been inextricably linked to advances in accelerator technologies. These advances have enabled the construction of a remarkably compact and, thus far, complete picture of the subatomic world. Beginning approximately three decades ago, accelerator technologies developed for particle and nuclear physics began to be deployed to further the understanding of materials, leading to a revolution in our understanding of the atomic and molecular worlds as well. Today, large user facilities support the research of thousands of biologists, chemists and materials scientists by exploiting the accelerator technologies developed for particle and nuclear physics.

Industry has come to rely on technologies such as the cyclotron and the electrostatic accelerator for myriad industrial processes ranging from curing plastics to sterilizing medical equipment. The health sciences field recognized the critical capabilities that accelerator technology could play in treating cancer, in producing valuable radioisotopes and in expanding medical imaging. The security field has recently deployed accelerators to serve a security function that would be impossible to achieve otherwise. Today, the total value of all goods and products touched by accelerators exceeds \$ 500 B per year.

Nearly all the fundamental accelerator technology that has enabled these remarkable achievements of the last eight decades can be traced to the need to develop accelerators for particle physics with ever increasing energy, intensity and particle densities. In the U.S., DOE's Office of High Energy Physics (OHEP) (and its progenitor agencies) has supported the bulk of this development. Indeed, the importance of research in accelerator science and technology is made explicit in the Mission of the Department of Energy's Office of High Energy Physics:

*"The mission of the High Energy Physics program is to understand how our universe works at its most fundamental level. We do this by discovering the most elementary constituents of matter and energy, exploring the basic nature of space and time itself, and probing the interactions between them. These fundamental ideas are at the heart of physics and hence all of the physical sciences. To enable these discoveries, HEP supports theoretical and experimental research in both elementary particle physics and fundamental accelerator science and technology. HEP underpins and advances the DOE missions and objectives through this research, and by the development of key technologies and trained manpower needed to work at the cutting edge of science."*

The importance of basic research in accelerator science and technology in support of High Energy Physics and the larger national needs is widely recognized and acknowledged. The P5 Panel (2008) recognized this need and recommended a broad strategic program in accelerator R&D:

*“The US must continue to make advances in accelerator and detector R&D to maintain leadership at the Intensity and Cosmic Frontiers of particle physics; to allow for a return to the Energy Frontier in the US; and to develop applications for the benefit of society.*

***The panel recommends a broad strategic program in accelerator R&D, including work on ILC technologies, superconducting rf, high-gradient normal-conducting accelerators, neutrino factories and muon colliders, plasma and laser acceleration, and other enabling technologies, along with support of basic accelerator science.”***

Recently, the special role that HEP has traditionally played in expanding the frontiers of accelerator science and technology has been codified through OHEP's Accelerator Stewardship Mission, which charges OHEP with managing an accelerator R&D program in accordance with the broader scientific and societal needs for accelerator technology. This Accelerator Stewardship Mission recognizes the pivotal role that accelerators have played and will continue to play in furthering Discovery Science, Medicine, Industry, National Security, and challenges confronting the nation in Energy and the Environment.

## **2.2 ASTA's Role in Furthering the HEP Mission**

It is in this context that we propose completing the construction of the Advanced Superconducting Test Accelerator (ASTA) at Fermilab, and establishing a User Facility for Accelerator R&D based upon it.

Construction of the Advanced Superconducting Test Accelerator (ASTA) Facility at NML began in 2006 as part of the International Linear Collider/SRF R&D Program and later the American Recovery and Reinvestment Act (ARRA) within the Department of Energy, Office of High Energy Physics. Construction of the facility was motivated by the goal of building, testing and operating a complete ILC RF unit to demonstrate industrial and laboratory capability for producing state-of-the-art superconducting linear accelerator components, and assembling them into a fully functioning system. ASTA, configured as a single ILC RF unit, would consist of an electron photo-injector, accelerating cavities, a bunch compressor, and three 1.3 GHz ILC cryomodules powered together from a single high-power klystron. Each cryomodule provides 250 MeV of energy gain for total output energy of approximately 800 MeV.

It was recognized early in the planning process that an electron beam meeting the demanding ILC performance parameters was itself a powerful resource of interest to the wider Advanced Accelerator R&D (AARD) community. For those reasons the ARRA-funded facility construction incorporated space for the installation of additional cryomodules to increase the beam energy to a maximum of 1.5 GeV, space for multiple high-energy beamlines, as well as provision for a small circular ring for the exploration of ring-based advanced accelerator concepts. The facility design incorporated features necessary for the operation of an AARD user program, including adequate experimental beamline and insertion space, an appropriately sized support building, provision for transporting laser light into and out of the accelerator enclosure, and an adequately-sized control room.

ASTA is unique among accelerator user facilities in six principal ways:

- High repetition-rate: ASTA accelerates 1 msec long bunch trains, with 3 MHz micro-pulse repetition rate, with up to 3000 bunches per train.
- High average power: ASTA accelerates 1 msec long bunch trains at up to five pulses per second, providing the highest beam power and highest average brightness of any accelerator test facility in the U.S.
- High energy: ASTA accelerates beam to  $\sim 1$  GeV, which is important for a number of photon-science and FEL-related experiments.
- Extremely stable beams: ASTA, based on ILC technology, is capable of providing exceptional beam stability, which has been demonstrated at the FLASH facility at DESY
- Superconducting technology: ASTA necessarily brings SRF and beams together. As nearly all future large scale accelerator facilities will rely on SRF technology, ASTA will be the only GeV-scale test facility which is capable of supporting R&D in prototypical conditions.
- Storage ring: ASTA includes a small, very flexible storage ring, based on innovative optics, capable of supporting a broad range of ring-based advanced beam dynamics experiments.

A national User Facility for Accelerator R&D based at Fermilab's ASTA will further the mission of OHEP by addressing several needs:

### **Furthering the Strategic Priorities for Particle Physics:**

While the domestic accelerator-based HEP program is oriented toward the Intensity Frontier, there are no accelerator test facilities that support Intensity Frontier accelerator science. ASTA, with both a modern superconducting linear accelerator and a small storage ring (with the capability of storing either electrons or protons) enables of class of beam-based experiments which seek to study fundamental limitations to beam intensity which cannot be carried out elsewhere.

### **Strengthening the Nation's Accelerator Test Facility Infrastructure:**

Historically, much of the accelerator R&D needed to build the next generation accelerators and accelerator-based facilities was carried out at operating facilities. The last decade and a half has witnessed the shutdown of a substantial accelerator infrastructure for particle physics in the US (SLC, PEP-II, CESR, Fermilab's Tevatron and Antiproton Complex) and abroad (LEP, HERA, DAFNE). The P5 Panel recognized this need in their report:

*"Finally, the field must address the critical lack of accelerator test facilities that R&D requires. Historically, much accelerator R&D took place using operating high-energy physics facilities. However, as the operating facilities have turned off in the US, the opportunities for experimental demonstrations have correspondingly decreased. Some dedicated facilities have been proposed; and, while such facilities tend to be expensive to operate, they are essential for progress."*

### **Establishing a Test-Bed for Superconducting RF Accelerators:**

Nearly all large-scale accelerator user facilities envisioned for the future are based on superconducting RF technology. This includes Project-X, a MW-class accelerator facility for Intensity Frontier Physics based on a high-power superconducting linac; the International Linear Collider; LBNL's Next Generation Light Source (NGLS), a high repetition rate soft x-ray FEL based on ILC/TESLA technology; the Facility for Rare Isotope Beams (FRIB) at MSU, a superconducting linac for heavy-ions; Cornell's Energy Recovery Linac, a superconducting linac-based photon science facility. Despite the ambitions of the accelerator field to deploy SRF technology in myriad future projects, there does not exist on U.S. soil an SRF test accelerator to meet the R&D needs of these future projects. ASTA will fill a need for a superconducting test accelerator based on state-of-the-art SRF technology. ASTA will deliver prototypic beam conditions that cannot be reproduced elsewhere.

### **Fulfilling the Accelerator Stewardship Mission:**

While ASTA is intended to support the particle physics mission, it will strengthen OHEP's stewardship portfolio at the same time by supporting a broad range of accelerator R&D which will have a broad impact, ranging from particle physics, to photon sciences, to security.

### **Educating and Training the Next Generation of Accelerator Scientists:**

With the closure of many of the accelerators that accommodated substantial machine studies programs, there is a critical lack of experimental beam facilities to allow training the next generation of accelerator scientists. As an accelerator R&D User Facility, ASTA could be expected to support the educational needs of dozens of Ph.D. students over a decade of operation.

### **2.3 Overview of Scientific Opportunities at ASTA**

The unique features and capabilities of ASTA, as outline above, will allow the exploration of a wide range of advanced accelerator R&D topics, which are summarized in Table 1 and explained in detail in Section 7 below. ASTA will enable a world-leading program in AARD for HEP Discovery Science at both the Intensity and Energy Frontiers, making use of the capabilities of ASTA's stat-of-the-art superconducting linac, and flexible storage ring. With its high energy, high brightness, high repetition-rate beams, and the capability for emittance manipulation built into the design, ASTA is an ideal platform for exploring novel approaches for producing bright photon beams, which aligns with OHEP's Stewardship and Applications mission.

The experiments and research topics described in this proposal are mapped according to their applicability to the Intensity Frontier, the Energy Frontier, and Stewardship and Application thrusts, in Table 1.

Table 1: Proposed ASTA Experiments and Accelerator R&D thrusts.

| Experiment   | HEP Discovery Science |                 | Stewardship & Applications |
|--|-----------------------|-----------------|----------------------------|
|  | Intensity Frontier    | Energy Frontier |                            |
| IOTA Test of non-linear, but integrable, accelerator lattices                                      | ✓                     |                 | ✓                          |
| Demonstration of technology and beam parameters for the Project X pulsed linac                     | ✓                     | ✓               | ✓                          |
| Beam dynamics studies and halo diagnostics in space-charge dominated proton rings                  | ✓                     |                 |                            |
| Test of space charge compensation using an electron lens or electron columns                       | ✓                     | ✓               |                            |
| Development and test of a beam-beam kicker   |                       | ✓               | ✓                          |
| Test of Optical Stochastic Cooling   |                       | ✓               |                            |
| Flat-beam-driven dielectric-wakefield acceleration in slab structures                              |                       | ✓               | ✓                          |
| Plasma-wakes in long bunch-trains  |                       | ✓               | ✓                          |
| Demonstration of technology and beam parameters of a high gradient SRF-unit                        |                       | ✓               |                            |
| Measurement of the electron wave function  |                       | ✓               |                            |
| Investigation of acceleration and cooling of carbon-based crystal structures for muon accelerators |                       | ✓               |                            |
| High brightness X-ray channeling as a compact x-ray radiation source                               |                       | ✓               | ✓                          |
| Coherent diffraction radiation measurements of bunch length  |                       | ✓               | ✓                          |
| Non-intercepting optical diffraction radiation diagnostics   |                       |                 | ✓                          |
| Ultra-low emittance techniques for X-ray FELs  |                       |                 | ✓                          |
| Advanced phase-space manipulations   |                       |                 | ✓                          |
| Inverse Compton scattering gamma-ray source  |                       |                 | ✓                          |
| Attosecond VUV pulses via space-charge driven amplification of shot-noise density fluctuations     |                       |                 | ✓                          |
| Laser-induced microbunching studies with high micropulse-repetition rate electron beams            |                       |                 | ✓                          |
| Ultrastable operation of SRF Linacs  | ✓                     | ✓               | ✓                          |
| Feasibility of an XUV FEL oscillator   |                       |                 | ✓                          |
| Production of narrow-band gamma-rays   |                       |                 | ✓                          |
| Target Studies for LBNE  | ✓                     |                 |                            |
| Studies with Tagged Photons  | ✓                     |                 |                            |
| Studies with Inverse Compton Scattered Photons   | ✓                     | ✓               |                            |

## **2.4 Organization of This Proposal**

Section 3 describes the context of ASTA within Fermilab's broader mission, as well as Fermilab's historical contributions within the field of Advanced Accelerator R&D.

Section 4 describes the scientific drivers in the field of advanced accelerator R&D.

Section 5 presents a comparison of ASTA's parameters, capabilities, and costs with those of other advanced accelerator R&D user facilities.

Section 6 describes the ASTA Facility and its capabilities. A staged approach for build-out is described in which the linac beam energy is increased from an initial 300 MeV with a single ILC cryomodule to 800 MeV with the full build-out of three cryomodes. A small ring, the Integrable Optics Test Accelerator (IOTA), enables a broad range of AARD experiments already in the first stage.

Section 7 describes the scientific opportunities at ASTA. Those opportunities are aligned along research thrusts including Discovery Science at the Intensity and Energy Frontiers and Accelerator Stewardship and Applications. Taken together, ASTA provides a platform upon which a very broad range of accelerator science experiments can be carried out.

Section 8 provides a technical description of the ASTA linac and user facility.

Section 9 describes the role that ASTA will play in Accelerator Science education.

Section 10 presents the estimated costs to complete ASTA and establish the capability to support a user program, as well as the estimated costs to operate the facility in support of a user program.

Finally, Section 11 describes the management of the Scientific User Program.

### **3.0 The Fermilab Context**

#### **3.1 Connection to Fermilab's Mission**

Since the invention of the cyclotron eighty years ago the multitude of historic breakthroughs in particle physics has been inextricably linked to advances in accelerator technologies. Much of the accelerator development in the U.S. over this period has taken place within the Office of High Energy Physics in the Department of Energy (and its progenitor agencies). OHEP's unique role is now formally recognized through the assumption of stewardship responsibility for long-range accelerator development within the U.S., independent of the final application.

Fermilab is the sole remaining U.S. laboratory devoted to providing facilities for accelerator based high energy physics. Since it's founding in the late 1960s Fermilab's history has been closely linked to leadership in the advancement of accelerator technologies, most notably the development of superconducting magnets for accelerator applications, but also including the development of large scale cryogenics systems, electron and stochastic cooling systems, and novel beam manipulations utilizing radiofrequency systems. All these advances have been supported by comprehensive integrated theoretical concepts and simulations of complete future facilities on both the energy and intensity frontiers. More recently Fermilab has established cutting edge capabilities and infrastructure for the development of superconducting radio-frequency acceleration based on its promise as an enabling technology for high energy physics. At present Fermilab (i) supplies integrated design concepts and technology development for a multi-MW proton source (Project X) to support world-leading programs in long baseline neutrino and rare processes experiments; (ii) plays a leading role in the development of ionization cooling technologies required for muon storage ring facilities at the energy (multi-TeV Muon Collider) and intensity (Neutrino Factory) frontiers, and supplies integrated design concepts for these facilities; (iii) provides leadership on the development of next generation superconducting magnet technologies for application in upgrades to the Large Hadron Collider in Europe and a possible next generation hadron collider; and (iv) carries out a program of advanced accelerator R&D (AARD) in the field of high quality beam sources, and novel beam manipulation techniques.

The advanced accelerator R&D program described within this report builds upon accomplishments of the prior decade while leveraging multiple assets unique to Fermilab. Foremost among these assets is the Advanced Superconducting Test Accelerator, consisting of an ILC RF-unit, currently nearing completion in the New Muon Lab (NML) complex. The facility is configured to eventually produce electron beams with energies close to 1 GeV, and is unique in its ability to produce long pulse beams at GeV-scale energies. Fermilab envisions that this facility will eventually support a world-leading, vibrant user-driven research program in Accelerator Science and beyond.

Beyond the NML complex Fermilab brings a number of additional assets in support of the ASTA program:

Staff capabilities and core competencies: Fermilab staff possesses unique capabilities and skills in accelerator design, construction, and operations, in leading edge accelerator technologies, and in advanced accelerator R&D. In particular the staff is well experienced in superconducting rf and superconducting magnet development, in beam physics and simulations, in the management of significant accelerator projects, and in the construction and operations of accelerators. Personnel who work within the accelerator operations programs are available to support the ASTA program on either temporary or longer term bases via full or part time assignments.

Infrastructure: Beyond the very significant infrastructure in place in the NML complex Fermilab has available very substantial cryogenics, RF power, assembly, testing, and electrical infrastructure within the laboratory.

Accelerator computation/simulation tools: A variety of advanced computation and simulation tools are available in the Accelerator Physics Center and via the SciDAC sponsored national accelerator computational program, which is led by Fermilab.

Collaborative Connections: Fermilab has strong collaborative connections with a large number of national and international laboratories and universities within the ongoing accelerator development programs. In addition several local universities, plus Argonne National Laboratory, are active or potential participants in the Fermilab AARD program.

Educational Programs: Fermilab has a long established accelerator PhD program that typically support 5-10 students at any given time. Many leaders within the U.S. accelerator community have come through this program. In addition Fermilab hosts the U.S. Particle Accelerator School.

Post-doctoral Program: The Peoples and Bardeen Fellowship programs bring the most accomplished post-doctoral accelerator scientists and engineers in the world to Fermilab, where they become vital contributors to the development and operations programs.

ASTA contributes to Fermilab's Mission in at least two important ways. First, ASTA enables the exploration of several accelerator science topics of direct relevance to future Intensity Frontier facilities that cannot be carried out elsewhere. Secondly, as the national particle physics laboratory, Fermilab plays a unique role in ensuring that the accelerators of tomorrow can support the ambitions of the field. A vibrant Accelerator R&D program is a requirement for serving that unique mission.

## 3.2 Fermilab's Historical Contributions in Advanced Accelerator R&D

### 3.2.1 Fermilab's AARD Contributions

Fermilab – as the leading US HEP laboratory and one of the leading accelerator institutions in the world – was always in the forefront of accelerator research and development in general (broadly understood as efforts toward improvement of existing accelerators and near future facilities), and advanced accelerator R&D (AARD) in particular (which is focused on the next generation and beyond accelerators, fundamental beam physics issues, and novel accelerator technologies). The focus of the AARD efforts at Fermilab closely followed the priorities of HEP and sequentially was directed toward: in the mid-late 1990s – the Tevatron and Tevatron upgrades, LHC, VLHC and normal-conducting (NC) RF linear e+e-collider; in the 2000's – LHC, ILC and future multi-TeV lepton collider; in the early 2010's – on the next generation of intensity frontier accelerators, the LHC luminosity and energy upgrades, and multi-TeV Muon Colliders. It is to be noted, that many AARD activities at Fermilab developed in separate national programs – e.g., LHC Accelerator Research Program (US-LARP), and, recently, the Muon Accelerator Program (US-MAP). Over the decades, the AARD activities had been carried out at the operational facilities at Fermilab (Tevatron, Main Injector, Booster), other labs (LHC), dedicated R&D facilities elsewhere (CESR-TA, ATF, EMMA) and our own dedicated facilities – the A0 Photoinjector, which operated since the mid-1990's and was closed last year, and ASTA at NML which is being established at present. Results of the research are published in more than a hundred technical and peer-reviewed publications (the list of two dozen high-impact publications is given below). The research resulted in 11 PhDs over the past decade and a half, several of whom have gone on to become today's leaders in accelerator science and technology.

The highlights of the past Fermilab AARD program include many important contributions to the physics of beams, e.g.:

- Development of high-brightness particle sources, such as RF photo-injectors, combined with SRF
- Development of the relativistic electron cooling method
- Pioneering research on the method of electron lenses for beam-beam compensation and beam collimation
- Novel beam optics techniques, e.g., round colliding beams, non-scaling FFAGs and integrable optics accelerators
- First ever demonstration of high ratio round-to-flat beam transformation and transverse-to-longitudinal emittance exchange
- Advanced beam collimation by bent crystals, include first time demonstration of volume-reflection collimation in colliders
- Studies of ground motion and vibration effects for future colliders
- Development of advanced beam diagnostics

### 3.2.2 Selected AARD Publications from Fermilab

- [1] P. Piot, et al., Generation and Characterization of Electron Bunches with Ramped Current Profiles in a Dual-Frequency Superconducting Linear Accelerator , *Phys. Rev. Lett.* 108, 034801 (2012)
- [2] S. Machida et al., Acceleration in the linear non-scaling fixed-field alternating-gradient accelerator, *Nature Physics* (2012)
- [3] T. Maxwell, et al., Synchronization and characterization of an ultrashort pulse laser for photoemission and electron-beam diagnostics studies at a radio frequency photoinjector *JINST* 7 T11001 (2012)
- [4] J. Thangaraj, Experimental Studies on Coherent Synchrotron Radiation at an Emittance Exchange Line, *Phys. Rev. ST-AB*, 15, 110702 (2012).
- [5] A.H. Lumpkin, J. Ruan, and R.M. Thurman-Keup, Synchroscan streak camera imaging at a 15-MeV photoinjector with emittance exchange, *Nucl. Instr. and Methods Section A*, Vol. **687**, 92-100 (2012).
- [6] A. Shishlo, et al., First Observation of Intrabeam Stripping of Negative Hydrogen in a Superconducting Linear Accelerator, *Phys. Rev. Lett.* 108, 114801 (2012)
- [7] J. Thangaraj, et al., Demonstration of a real-time interferometer as a bunch-length monitor in a high-current electron beam accelerator, *Rev. Sci. Instrum.* 83, 043302 (2012)
- [8] G. Stancari, et al., Collimation with Hollow Electron Beams, *Phys. Rev. Lett.* 107 , 084802 (2011)
- [9] J. Ruan, et al., First observation of the exchange of transverse and longitudinal emittances, *Phys. Rev. Lett.* 106, 244801 (2011)
- [10] Y.-E Sun, et al., Tunable Subpicosecond Electron-Bunch-Train Generation Using a Transverse-To-Longitudinal Phase-Space Exchange Technique, *Phys. Rev. Lett.* 105, 23480 (2010)
- [11] V. Shiltsev, Observations of Random Walk of the Ground In Space and Time, *Phys. Rev. Lett.*, v.104, 238501 (2010)
- [12] V. Danilov, S. Nagaitsev, Nonlinear accelerator lattices with one and two analytic invariants, *Phys. Rev. ST Accel. Beams* 13, 084002 (2010)
- [13] A. Lumpkin, et al., Coherent optical transition radiation and self-amplified spontaneous emission generated by chicane-compressed electron beams, *Phys. Rev. ST Accel. Beams* 12, 040704 (2009)
- [14] V. Shiltsev, et al., Experimental Demonstration of Colliding-Beam-Lifetime Improvement by Electron Lenses, *Phys. Rev. Lett.* **99**, 244801 (2007)
- [15] S. Nagaitsev, et al., Experimental Demonstration of Relativistic Electron Cooling, *Phys. Rev. Lett.* **96**, 044801 (2006)
- [16] P. Piot, et al., Photoinjector generation of a flat electron beam with transverse emittance ratio of 100, *Phys. Rev. ST Accel. Beams* 9, 031001 (2006)
- [17] Y.-E Sun, et al., Generation of angular-momentum-dominated electron beams from a photoinjector, *Phys. Rev. ST Accel. Beams* 7, 123501 (2004)
- [18] M. Thompson, et al., Status of the UCLA/NICADD Plasma Density Transition Trapping Experiment , *AIP Conf. Proc.* 737, 440 (2004)

- [19] N. Barov, et al., Plasma Wakefield Experiments , *AIP Conf. Proc.* 647, 71 (2002)
- [20] B. Aune, et al., Superconducting TESLA cavities, *Phys. Rev. ST Accel. Beams* 3, 092001 (2000)
- [21] A. Burov, et al., Optical principles of beam transport for relativistic electron cooling, *Phys. Rev. ST Accel. Beams* 3, 094002 (2000)
- [22] B. Baklakov, et al., Ground vibration measurements for Fermilab future collider projects, *Phys. Rev. ST Accel. Beams* 1, 031001 (1998)
- [23] E. Colby, et al., Design of high brightness symmetric and asymmetric emittance RF photoinjectors for TESLA, *AIP Conf. Proc.* 335 (1995) 708-723

### 3.2.3 PhD Theses in Advanced Accelerator R&D from Fermilab-based Research

Alan Reilly Fry, 1996 University of Rochester, "Novel Pulse Train Glass Laser for RF Photoinjectors"

Eric Colby, 1997, UCLA, "Design, Construction, and Testing of a Radiofrequency Electron Photoinjector for the Next Generation Linear Collider"

Michael Fitch, 2000, University of Rochester, "Electro-optic Sampling of Transient Electric Fields from Charged Particle Beams"

Jean-Paul Carneiro, 2001, Paris XI, "Etude Experimentale du Photo-injecteur de Fermilab"

Matthew Thompson, 2004, UCLA, "Plasma Density Transition Trapping of Electrons in Plasma Wakefield Accelerators"

Kip Bishofberger, 2005, UCLA, "Tevatron Beam-Beam Compensation"

Sergei Seletskiy, 2005, University of Rochester, "Attainment of Electron Beam Suitable for Medium Energy Electron Cooling"

Yin-E Sun, 2005, University of Chicago, "Angular-momentum-dominated electron beams and flat beam generation"

Rodion Tikhoplav, 2006, University of Rochester, "Low Emittance Electron Beam Studies"

Pavel Snopok, 2007, Michigan State University, "Capture of a Large Phase Space Beam"

Timothy Koeth, 2009, Rutgers University, "The first observation of a Transverse to Longitudinal Emittance Exchange"

Tim Maxwell, 2012, Northern Illinois University, "Measurement of sub-picosecond electron bunches via electro-optic sampling of coherent transition radiation"

#### 4.0 Scientific Drivers in Advanced Accelerator R&D

The US domestic accelerator-based particle physics program is shifting focus from the Energy Frontier to the Intensity Frontier [1, 2]. The nation's and Fermilab's strategy is to develop the facilities to enable a world-leading program in Intensity Frontier Physics [3]. This will be accomplished by making use of the substantial existing infrastructure at Fermilab, and extending the capabilities of the accelerator complex by constructing a new high-power proton linear accelerator, called Project X. Figure 1 shows Fermilab's accelerator complex, as it will be configured in 2020, with the construction of Project X underway.

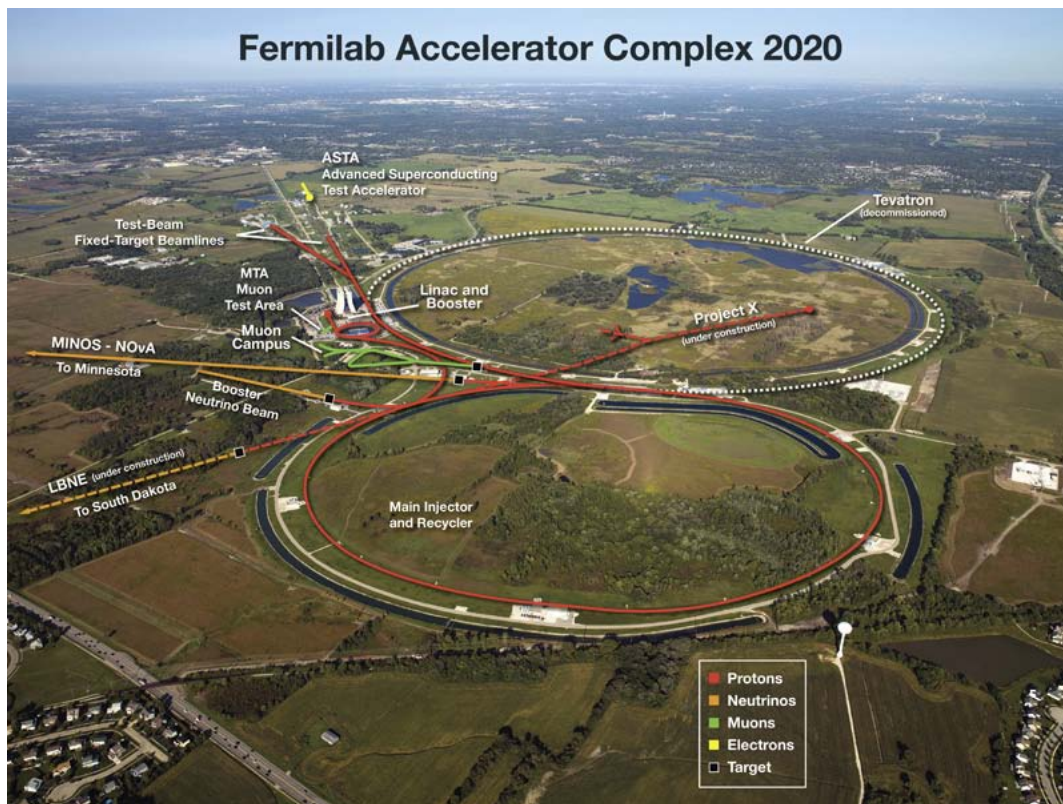


Fig.1: Fermilab's accelerator complex by the end of this decade [1].

The 2008 P5 report [2] specifically pointed out that "...advances in accelerator R&D are critical for the United States to maintain leadership not only at the energy frontier of particle physics, but also in the wider context of applications of particle accelerators and detectors reaching across science and society". Three major considerations shape the directions and scope of the accelerator research in the country [4]:

1. The recent Higgs discovery and the potential for discovering supersymmetry or other beyond standard-model physics (BSM) at the LHC will provide guidance for the next Energy Frontier accelerator:

- Perhaps a Higgs factory will be required to fully unravel its properties and couplings
  - Perhaps BSM results will motivate a multi-TeV lepton collider
  - Looking beyond, it is very difficult to probe well beyond LHC energies
2. There are two approaches to probing mass-scales well beyond the LHC:
    - Utilizing very intense beams to probe high mass-scales in rare decays and precision measurements [3].
    - Achieve very high energies, well beyond that which is routinely discussed today, enabled by advanced concepts, such as acceleration in crystal-channels, solid-state plasmas driven by high brightness x-rays, or similar approaches [5].
  3. Accelerator R&D beyond the field of particle physics is motivated by the growing recognition that:
    - Accelerators are essential tools for all fields of Discovery Science, including photon and neutron science, nuclear science and fusion energy science.
    - In addition to their role in Discovery Science, accelerators are vital to industry, medicine, national security, and have potential in energy and environment [6].
    - The path of accelerator development must be carried out in a socially and financially realistic way

As the nation's particle physics laboratory, Fermilab has a responsibility to ensure that the United States has a handle on technology needed to build the next generation facilities for particle physics, and that we're doing the necessary long-range R&D to support the ambitions of the field, and therefore the machines of the far future.

Regarding the Energy Frontier, there are several ideas to move into the few-TeV regime for lepton colliders which are presently being addressed by the AARD community (muon collider, two-beam and plasma-based e+e- colliders) [7], but beyond that, there is a great void in terms of direct searches beyond 10 times LHC energies. There is also a growing consensus that collisions of multi-TeV e+e- beams might not be feasible due to radiative energy losses and induced energy spreads which make such colliders ineffective – therefore, muons become the preferred particles for very high energy [5]. Correspondingly, there is a need to explore the issues associated with such a paradigm – muon sources, acceleration, manipulation, control, etc – which is being addressed by the US Muon Accelerator Program [8].

Similarly, the Intensity Frontier facilities of the near- and far- future have many challenges that require advancing the state-of-the-art through a dedicated R&D program. Key Challenges include:

- producing high-current, high-quality beams (high brightness);
- accelerating high beam currents to high energy;
- high-duty factor, high-power RF systems, structures and components;
- transporting high-power beams with extremely low beam loss, in order to allow routine hands-on maintenance (minimizing beam loss is the over-riding design constraint as a typical beam loss requirements for a MW proton beam are  $< 1$  Watt/m,  $< 1 \times 10^{-4}$  total beam loss in a ring);
- acceleration of beams from keVs to GeVs preserving emittance and minimizing growth in large-amplitude particles ("beam halo");
- target systems capable of handling extreme power densities and extreme radiation environments;
- producing intense, high-quality beams of secondary particles (muons, kaons, ...);
- achieving highly efficient H- stripping for high-intensity, high-power CW beams;
- overcoming beam dynamics issues of space-charge and instabilities , which ultimately limit all synchrotrons, accumulators, compressors and linacs;
- creating self-consistent beam distributions (i.e. linear space-charge force or space-charge compensated beams);
- generating large Landau-damping of coherent instabilities via non-linear (but stable) betatron motion
- novel ways to cleanly achieve slow spills of high intensity beams;
- more efficient non-standard methods of resonant extraction (e.g., can it be extended to higher orders? Can crystals be used for high-power proton extraction? Can electron beams be used to extract protons?)
- instrumentation for precise halo (and emittance) measurement and connection to simulations in a reliable way

One can see that the high intensity frontier accelerator research thrusts have direct connections to the high energy frontier development – for example, the Muon Collider concept has many similar challenging ingredients.

Other Discovery Science fields provide powerful motivation for advanced accelerator R&D. Accelerators have become essential tools in biology, health sciences, energy sciences, materials science, geophysics, in addition to those that have traditionally relied on them (nuclear and particle physics). Indeed, five of the last 15 Nobel Prizes in Chemistry have been awarded based on work carried out at synchrotron radiation facilities. The need for compact and affordable sources of particle probes for materials science drives much research throughout the world in new sources of photons and neutrons. The need for tunable photon sources with higher brightness and temporal and spatial coherence drives much of the Free Electron Laser (FEL) R&D that is carried out throughout the world.

Accelerator applications for industry, medicine, national security, energy and environment bring an increasing emphasis on applied accelerator technology, as they have real potential to make an impact, which in turn is becoming yet another powerful driver for advanced accelerator R&D [9].

Past developments have shown that the most effective way for AARD to address the scientific challenges faced by particle physics involves accelerator facilities. The 2008 P5 report recommendation summarized the situation: "... the field must address the critical lack of accelerator test facilities that R&D requires. Historically, much accelerator R&D took place using operating high-energy physics facilities. However, as the operating facilities have turned off in the US, the opportunities for experimental demonstrations have correspondingly decreased. Some dedicated facilities have been proposed; and, while such facilities tend to be expensive to operate, they are essential for progress." [2]

#### 4.1 References

- [1] *Fermilab: Plan for Discovery* (Fermilab, 2012), see at [https://www.fnal.gov/directorate/plan\\_for\\_discovery/](https://www.fnal.gov/directorate/plan_for_discovery/)
- [2] "US Particle Physics: Scientific Opportunities A Strategic Plan for the Next Ten Years" Report of the Particle Physics Project Prioritization Panel (2008), at [http://science.energy.gov/~media/hep/pdf/files/pdfs/p5\\_report\\_06022008.pdf](http://science.energy.gov/~media/hep/pdf/files/pdfs/p5_report_06022008.pdf)
- [3] Proc. "Fundamental Physics at the Intensity Frontier" Workshop, Nov.-Dec., 2011 (Rockville, MD, USA)
- [4] S. Henderson, "From Intensity Frontier to Energy Frontier", talk at the AAC-2012 Workshop, University of Texas, June 10-15, 2012 (Austin TX)
- [5] V. Shiltsev, "High energy particle colliders: past 20 years, next 20 years and beyond", *Phys. Uspekhy* 55 (10) 977 (2012), also at <http://arxiv.org/abs/1205.3087>
- [6] "Accelerators for America's Future", Report of "The Symposium on Accelerators for America's Future", Washington, DC (October 26, 2009).
- [7] V. Shiltsev, "Current Landscape of High Energy Particle Colliders", ICFA Beam Dynamics [Newsletter #58](#), pp.16-22 (August 2012).
- [8] Muon Accelerator Program <http://map.fnal.gov/>
- [9] DOE Accelerator R&D task Force report (2012) [http://www.acceleratorsamerica.org/report/accelerator\\_task\\_force\\_report.pdf](http://www.acceleratorsamerica.org/report/accelerator_task_force_report.pdf)

## 5.0 Comparison with other AARD Facilities

Particle physics research is strongly dependent on the use of high-energy beams provided by charged particle accelerators, storage rings and the associated detectors. Operating in the extreme domains that are essential for successful particle physics research demands very specialized technology that takes substantial time and expense to invent, design, build, maintain and upgrade. It has long been recognized that historically, much of accelerator R&D took place using operating high-energy physics facilities. However, only in the last decade, a great number of the operating frontier facilities have been turned off in the US and worldwide – SLC, LEP, HERA, PEP-II, CESR-c, Fermilab's Antiproton Accumulator, Debuncher and Tevatron, DAFNE, etc - and the opportunities for experimental AARD have correspondingly decreased. The critical lack of accelerator R&D test facilities has been appreciated and several dedicated facilities have been proposed and constructed, e.g., ATF at BNL [1], A0 Photoinjector at FNAL (recently closed and being moved to ASTA) [2], AWA at Argonne [3], BELLA at LBNL [4], FACET at SLAC [5], CESR-TA at Cornell University[6], UMER at UMD [7], TTF at DESY (recently converted into FLASH, a high-gain free-electron laser) [8]. Such facilities are essential for progress of the field, and in the US are supported primarily by the DOE Office of High Energy Physics (CESR-TA is an NSF-supported facility).

Among all the facilities, ASTA [9] has two unique features – i) it allows broad R&D in support of the program toward the intensity frontier accelerators and offers both linacs and ring, electrons and ions for accelerator research, ii) due to employment of the advanced SRF technology, record high average electron beam power and beam brightness are available to users. Figure 1 shows the energy and beam brightness available at the various AARD facilities.

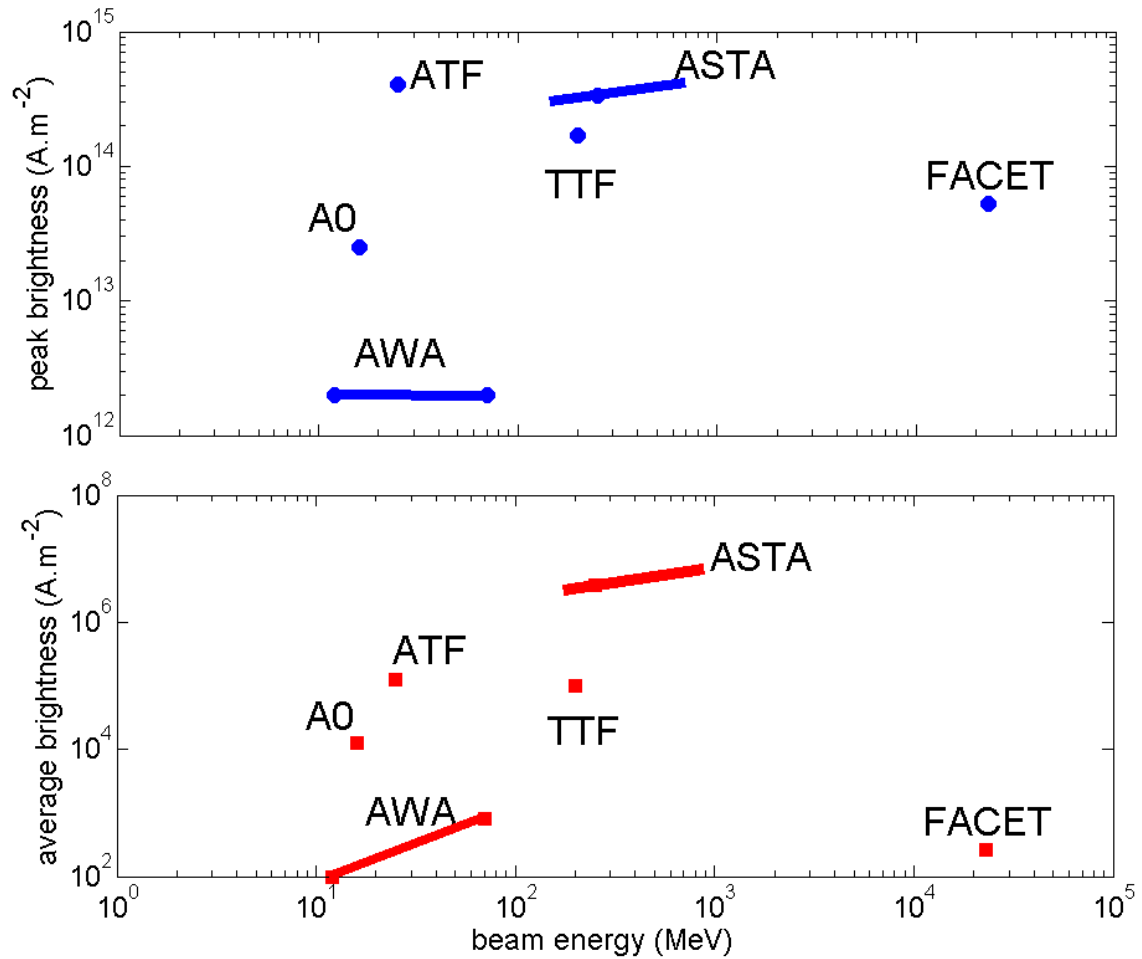


Fig.1: Comparison of beam parameters of AARD facilities. The peak brightness is computed as the ratio of peak current over the four-dimensional normalized transverse emittance, while the average uses the averaged beam current.

The ASTA facility will offer variable energy electron beams, from (~50 to ~800 MeV), high-repetition rate (1-ms trains), L-band SRF linac, small emittance photoinjector source, arbitrary emittance partition (with repartition of phase spaces to match final applications), and tailored current profiles. The Integrable Optics Test Accelerator (IOTA) ring will be capable of operating for a wide range of experiment with both 50-150 MeV electrons and 2.5 MeV ions/protons. Parameters of existing AARD facilities are shown in Table 1, together with those of ASTA.

Table 1: Beam parameters available to users at the accelerator R&D facilities.

| Facility              | Energy               | Particles/s                          | Macropulse duration | Rep rate/<br>max # of bunches |
|-----------------------|----------------------|--------------------------------------|---------------------|-------------------------------|
| ATF                   | 25-70 MeV e-         | $(3-10) \times 10^{11}$              | up to 3 $\mu$ s     | 1-3 Hz / 200                  |
| A0                    | 16 MeV e-            | $(0.5-2) \times 10^{11}$             | up to 100 $\mu$ s   | $\sim$ 1 Hz /<br>up to 100    |
| AWA                   | 70 MeV e-            | up to $2 \times 10^{13}$             | 2 $\mu$ s           | $\sim$ 1 Hz / 32              |
| BELLA                 | 1-5 GeV e-           | $\sim 0.1 \times 10^{11}$            | <0.3 ps             | <1 Hz / 1                     |
| FACET                 | 21 GeV e-, e+        | $0.6 \times 10^{11}$                 | 0.1 ps              | 30 Hz / 1                     |
| CESR-TA               | 1.8-5.3 GeV<br>e-,e+ | 1.6<br>$\times 10^{11}$ /bunch       | ring                | Ring / 45                     |
| UMER                  | 10 keV e-            | $(0.02-3) \times 10^{10}$            | 100's turns         | Ring/ 1                       |
| TTF                   | 1000 MeV, e-         | $5 \times 10^{13}$                   | 0.8 ms              | 5-10 Hz / 800                 |
| <b>ASTA Phase I.1</b> | <b>50 MeV e-</b>     | <b><math>3 \times 10^{14}</math></b> | <b>1 ms</b>         | <b>5 Hz / 3000</b>            |
| <b>Phase I.2</b>      | <b>300 MeV e-</b>    | <b><math>3 \times 10^{14}</math></b> | <b>1 ms</b>         | <b>5 Hz / 3000</b>            |
| <b>Phase II</b>       | <b>800 MeV e-</b>    | <b><math>3 \times 10^{14}</math></b> | <b>1 ms</b>         | <b>5 Hz / 3000</b>            |
| <b>Phase III</b>      | <b>2.5 MeV H-</b>    | <b><math>&gt; 10^{15}</math></b>     | <b>1 ms</b>         | <b>5 Hz / 1</b>               |

All of the current **Intensity Frontier** facilities and many of the future ones are based on circular accelerators with high intensity and high brightness beams. Accelerator R&D opportunities at the operational accelerators are practically non-existent; further, there is no circulating beam (ring) facility in the US dedicated for R&D. ASTA will address the need and will have a dual species (electrons and ions) IOTA storage ring. The experiments and tests planned there cover broad range of important subjects – from beam-loss control, beam dynamics, novel optics to space-charge compensation, collimation, and diagnostics. Together with studies enabled by SRF beam acceleration, ASTA promises to explore revolutionary techniques for intensity frontier facilities (Fermilab accelerator complex upgrades, Project-X, Neutrino Factory, etc).

The needs of all future **Energy Frontier** accelerators which are currently being considered in the US can and will be addressed – future e+e- collider (SRF beam studies and tests, high brightness electron sources, phase-space manipulations with them, positron production, etc), the LHC upgrades (space-charge studies and compensation, optical stochastic cooling test and new beam collimation techniques), Muon Collider and ultra-high energy colliders of the far future (high beam loading SRF acceleration, space-charge effects and compensation and OSC, use of crystals for beam shaping/acceleration).

Accelerator **Stewardship and Applications** research and development will employ the unique features of the ASTA facility - high power SRF, high brightness electron source, high energy – to test a variety of methods of relevance to future FEL accelerators, production of

very high energy  $\gamma$ 's via the Compton-scattering mechanism, SRF technology development and demonstration, materials, beam diagnostics and ultrafast choppers tests.

Table 2 summarizes relevance of the research proposed for ASTA and that of other facilities to the main thrusts of the DOE Office of HEP.

Table 2: Accelerator facilities and Accelerator R&D thrusts.

| Facility               | Main beams                | HEP Discovery Science  |  | Applications  |
|------------------------|---------------------------|--|--|---|
|                        |                           | Intensity Frontier   | Energy Frontier  |   |
| ATF (BNL)              | e-, CO <sub>2</sub> laser |  | PWFA, LPWA for e+e- LCs  | FEL, $\gamma$ 's, medical laser-gas   |
| A0 (FNAL)              | e-                        |  | e+e- LCs, PWFA   | FEL   |
| AWA (ANL)              | e-                        |  | e+e- LCs, DWFA   |   |
| BELLA (LBNL)           | laser                     |  | e+e- LCs, LWFA   | FEL, $\gamma$ 's, medical laser-gas   |
| FACET (SLAC)           | e-, e+                    |  | e+e- LCs, PWFA   |   |
| CESR-TA (Cornell)      | e-, e+                    | e-cloud (for e+)   | e+e- LCs   |   |
| UMER (UMD)             | e-                        | space charge   |  |   |
| TTF (DESY)             | e-                        |  | Initially – e+e- LC  | FEL, SRF technology   |
| <b>ASTA (Fermilab)</b> | <b>e-p/ions, laser</b>    | <b>Losses, beam dynamics, novel optics, collimation, space-charge &amp; compensation, diagnostics, SRF control</b> | <b>e+e- LCs, e+ sources, LHC &amp; upgrades, Muon Collider R&amp;D</b> | <b>FEL, <math>\gamma</math>'s, SRF technology, development &amp; testing, material test</b> |

On average, some 9-12 FTEs are needed to operate each of the US AARD facilities, similar to what is expected for ASTA. The facility will be embedded in, and leverage resources and infrastructure from, the much larger operations and general technology development programs at Fermilab which provided access to accelerator infrastructure (cryogenics,

electrical, LCW, etc), support functions (procurement, ESH, QA, accounting, etc.), skilled accelerator personnel (scientists, engineers, technicians), education programs closely connected with leading Universities and laboratories (IIT, NIU, UIUC, U of C, ANL, ICL, etc), accelerator theory, computation and simulations tools (SciDAC, CHEF, etc.), and will be synergistic with IARC (Illinois Accelerator Research Center). Table 3 summarizes the construction costs and operations costs of the various ASTA facilities.

Table 3: Cost of AARD Facilities.

| Facility                                 | Supporting Agencies | Cost                      |                   | Comments   |
|--|---------------------|---------------------------|-------------------|--|
|  |                     | Total Construction Cost   | Operating Cost    |  |
| ATF (BNL)                                | HEP, BES            | n/a                       | 2.7M\$/yr         | 2.2M\$/yr HEP + 0.5 M\$/yr BES; 120 days/yr          |
| A0 (FNAL)                                | HEP                 | n/a                       | 1.7M\$/yr         | Year-round, ca 2007-2008                             |
| AWA (ANL)                                | HEP, other          | n/a                       | ~2M\$/yr          | Year-round   |
| BELLA (LBNL)                             | HEP, other          | 33.5M\$                   | 2M\$/yr           | Not incl. support from DARPA, LDRD, SBIR; year-round |
| FACET (SLAC)                             | HEP, BES            | 14.5M\$                   | 14.2M\$/yr        | Incl.6.2M\$/yr from BES, few months/yr               |
| CESR-TA (Cornell)                        | NSF                 | 9 M\$                     | 4.25M\$/yr        | Beam ~80 days/ yr                                    |
| UMER (UMD)                               | HEP, ONR, DOD, JTO  | n/a                       | n/a               | Year-round   |
| TTF (DESY)                               | Germany             | >100MEuro                 | n/a               | Several months/yr                                    |
| <b>ASTA Stages I (FNAL) Stages II-IV</b> | <b>HEP</b>          | <b>8.1 M\$ + 11.2 M\$</b> | <b>3.9 M\$/yr</b> | <b>&gt;9 months/yr</b>                               |

## 5.1 References

- [1] BNL Accelerator Test Facility <http://www.bnl.gov/atf/>
- [2] FNAL A0/NICADD Photoinjector laboratory <http://nicadd.niu.edu/fnpl/>
- [3] ANL Argonne Wakefield Accelerator facility <http://www.hep.anl.gov/awa/>
- [4] LBNL BELLA (Berkeley Laboratory Laser Accelerator)  
<http://www.lbl.gov/Community/BELLA/index.html>
- [5] SLAC FACET (Facility for Advanced Accelerator Experimental Tests)  
<http://facet.slac.stanford.edu/>
- [6] CESR Damping Ring Test Accelerator  
<https://wiki.lepp.cornell.edu/ilc/bin/view/Public/CesrTA/>
- [7] University of Maryland Electron Ring/ UMER <http://www.umer.umd.edu/>
- [8] DESY Tesla Test Facility [http://tesla.desy.de/TTF\\_intro.html](http://tesla.desy.de/TTF_intro.html)
- [9] ASTA at Fermilab (Proc. Int'l PAC'2012, New Orleans)  
<http://accelconf.web.cern.ch/AccelConf/IPAC2012/papers/mooac02.pdf>

## 6.0 ASTA Facility Overview and Capabilities

The ASTA User Facility will evolve over time to address the demands of the accelerator R&D program. The main subsystems of ASTA include:

- Photoinjector source
- Linear accelerator based on superconducting RF cryomodules
- Electron storage ring (IOTA)
- Low- and high-power lasers
- Experimental areas for research with low-energy and high-energy beams.

Possibilities exist to further expand the capabilities of the R&D program, including

- An H<sup>-</sup> source and RFQ accelerator to expand the IOTA program to protons
- 3.9-GHz SRF accelerating cavity to enhance the peak current of compressed electron bunches and provide opportunities for bunch-current shaping
- Additional SRF cryomodules to increase the beam energy.

We envision a multi-staged approach to ASTA completion as shown in Figures 1 and 2. The first stage enables a low-energy AARD program based on the photoinjector and a 300 MeV program based on a single superconducting cryomodule, with associated beam transport lines and beam dumps. The first stage also enables one of the transformative beam dynamics experiments: exploration of novel, non-linear accelerator lattices in the Integrable Optics Test Accelerator (IOTA).

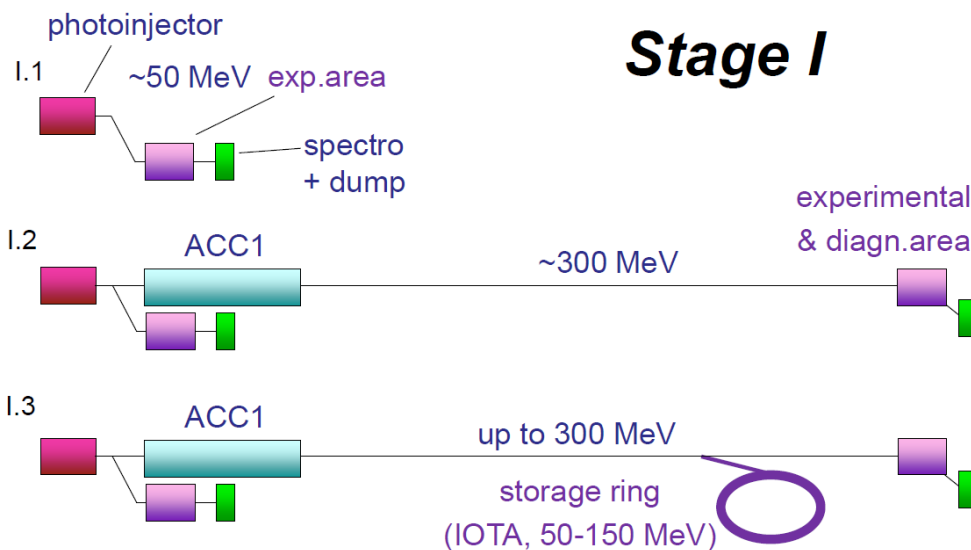


Fig.1: Stage I of the ASTA AARD User Facility construction and operation phases.

Stages II, III and IV allow a vast expansion of the ASTA capabilities for advanced accelerator research, as shown in Fig.2. In the second stage two additional cryomodules and associated

subsystems are added to provide high-energy beam up to 800 MeV. The AARD program will be expanded significantly with the higher beam energy capability, as outlined below. The IOTA program will also be expanded in Stage III to support beam-dynamics experiment on low-energy protons through the addition of proton beam injection capability for IOTA. Finally, Stage IV will allow a 3-fold increase of the electron peak current after installation of a linearizing 3.9-GHz cavity in the photoinjector area.

The beam energy can be further increased through the installation of up to 3 additional cryomodules.

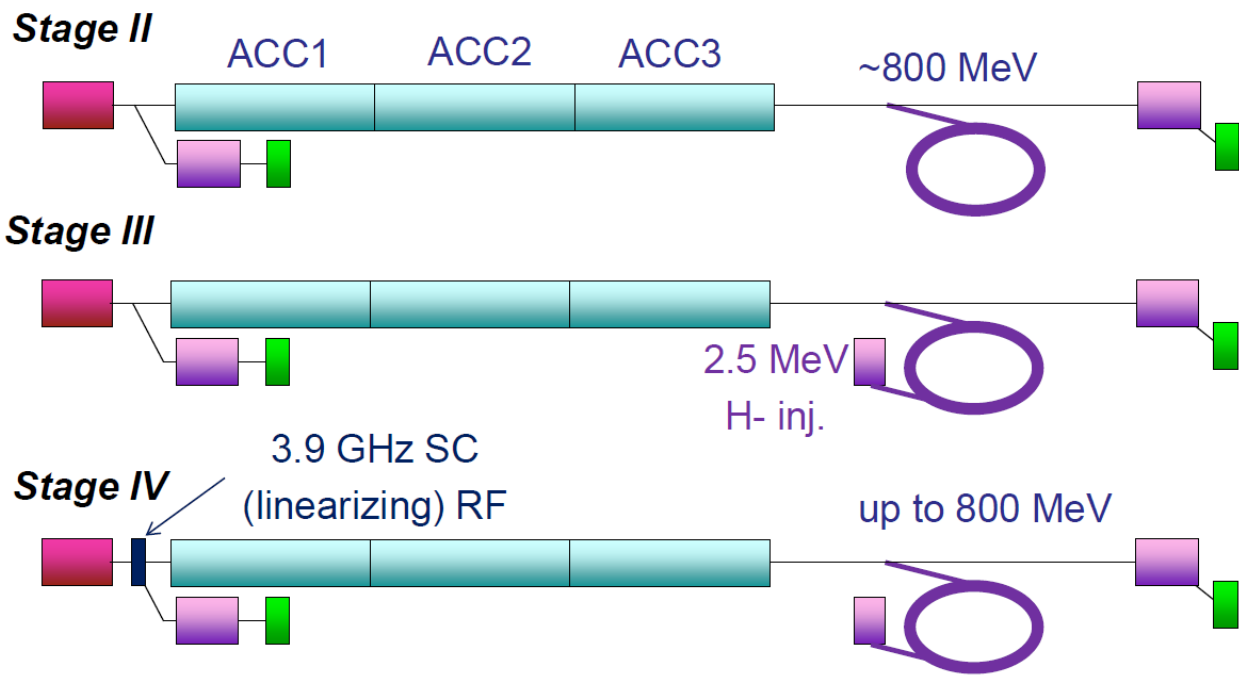


Fig.2: Stages II, III and IV of the ASTA AARD User Facility construction and operation.

The ASTA facility is located within the NML and is adjacent to the newly constructed Cryomodule Test Facility (CMTF), as shown in Figure. 3.

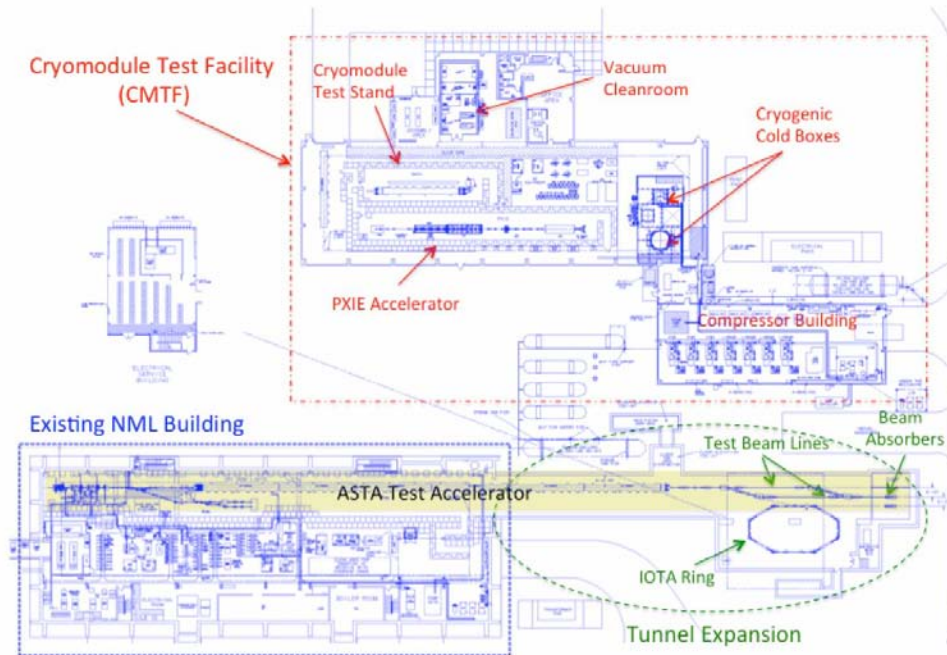


Figure 3: Layout of the ASTA Facility

## 6.1 RF Photoinjector

The backbone of the ASTA facility is a radio-frequency (RF) photoinjector, shown in Figure 4. The electron source is a 1-1/2 cell cylindrical-symmetric RF gun with a  $\text{Cs}_2\text{Te}$  photocathode. The cathode is illuminated by an ultraviolet (UV,  $\lambda=263$  nm) laser pulse produced via frequency quadrupling of an amplified infrared (IR,  $\lambda=1054$  nm) pulse [1]. The photocathode drive laser enables the generation of a train of bunches repeated at 3 MHz within a 1-ms-duration macropulse – see Figure 5. The parameters associated with the pulse format are summarized in Table I. The 5-MeV electron bunches exiting the RF gun are then accelerated with two superconducting radio-frequency (SRF) TESLA-type cavities (CAV1 and CAV2) to approximately 50 MeV. Downstream of this accelerating section the beamline includes quadrupole and steering dipole magnets, along with a four-bend magnetic compression chicane (BC1). The beamline also incorporates a round-to-flat-beam transformer (RFTB) capable of manipulating the beam to generate a high transverse-emittance ratio. In the early stages of operation, the bunches will be compressed in BC1 by operating CAV2 off crest. In this scenario the longitudinal phase space is strongly distorted and the achievable peak current limited to less than 3 kA. Eventually, a third-harmonic cavity (CAV39) operating at 3.9 GHz will be added. The prime purpose of this cavity is to linearize the longitudinal phase space and thereby enhance the compression scheme. In addition such a cavity could also be used to shape the current profile of the electron bunch [2]. The bunch generation and acceleration was extensively simulated and optimized using a multi-objective genetic optimizer [3].

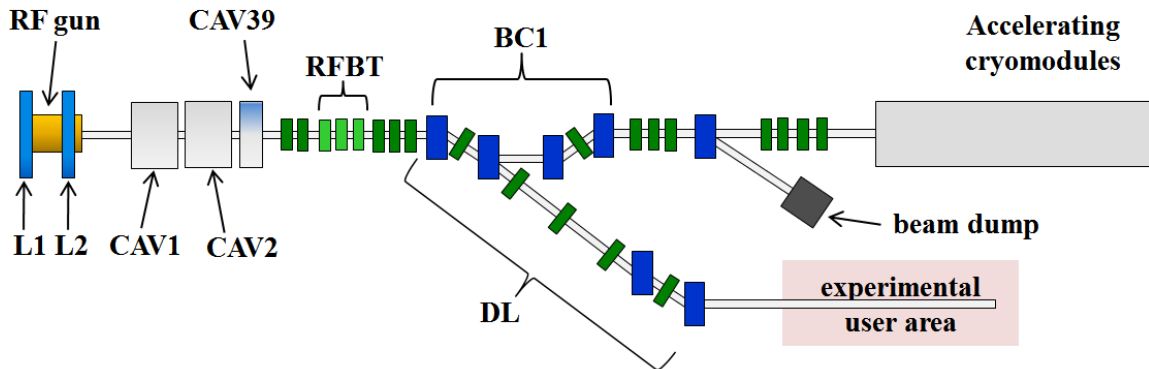


Figure 4: Overview of the ASTA photoinjector. The legend is L1, L2: solenoidal lenses, CAV1, CAV2 superconducting TESLA cavities, BC1: magnetic bunch compressor, DL: dogleg, green rectangles: quadrupole magnets, RFBT: round-to-flat-beam transformer.

Downstream of the accelerating section, the photoinjector includes an extensive diagnostics suite. In addition to conventional diagnostics (optical transition radiation screens, frequency-domain bunch-length measurement, etc), a deflecting cavity with a spectrometer will provide single-shot measurement of the longitudinal phase space (LPS diagnostics). Further developments of single-shot electro-optical imaging methods initiated at the A0 photoinjector are also planned downstream of BC1 [4].

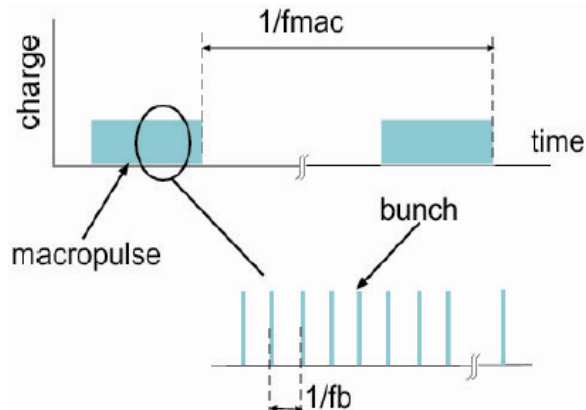


Figure 5: Time structure of the ASTA electron beam: macropulse rate  $f_{mac}=5$  Hz, macropulse length 1 ms, bunch frequency  $f_b \sim 3$  MHz (369 ns bunch spacing).

The photoinjector also includes an off-axis experimental beamline branching off at the second dipole of BC1 that will support beam physics experiments and diagnostics R&D.

Table I: ASTA electron beam pulse format

| Parameter                    | Value      | Unit |
|------------------------------|------------|------|
| Bunch charge                 | 0.02 – 3.2 | nC   |
| Bunch train duration         | 1          | ms   |
| Bunch frequency within train | 3          | MHz  |
| Number of bunches/train      | 1-3000     |      |
| Bunch train frequency        | 1 - 5      | Hz   |

## 6.2 1.3 GHz SRF Cryomodules

The 50-MeV beam is injected into the superconducting linear accelerator, which will eventually consist of three, 12-m long, 1.3 GHz superconducting accelerating modules. The linac consists of TESLA/ILC-type cryomodules, each of which includes eight 1.3 GHz nine-cell cavities. The first two cryomodules (CM1 and CM2) are a TESLA Type-III+ design, whereas the third (CM3), will be an ILC-Type IV design [5]. Together, these three cryomodules constitute a complete ILC RF Unit. It is expected that these three cryomodules will be capable of generating a beam energy gain of approximately 750 MeV. The installation of the cryomodules will be staged pending the completion of their construction as depicted in Figures 1 and 2. The first CM has already been tested in the ASTA Facility, as shown in Figure 6.



Figure 6: The first 1.3 GHz SRF cryomodule installed in the ASTA facility.

Downstream of the linac is the test beam line section, which consists of an array of multiple high-energy beam lines that transport the electron beam from the accelerating cryomodules to one of two beam absorbers. Each absorber is capable of dissipating up to 75 kW of power and is surrounded by a large steel and concrete shielding dump [6]. In addition to testing the accelerator components, the intent of this facility is to also test the support systems required for a future SRF linac.

During the first high energy beam operation and commissioning (referred to as Phase I.2 in Fig.1), only one cryomodule will be installed allowing for the production of bunches with energies up to ~300 MeV. Eventually, the second and third cryomodules will be installed in Phase II. Together, the three cryomodules plus the RF power systems will make up one complete ILC RF unit. During Phase II operation the beam energy will reach approximately 800 MeV. Beyond that stage several options are under consideration, including the installation of a 4<sup>th</sup> cryomodule downstream of a phase-space-manipulation beamline (either a simple magnetic bunch compressor or a phase space exchanger similar to the ones discussed below).

### **6.3 IOTA Ring**

The ASTA Facility was designed with the provision for incorporating a small storage ring to enable a ring-based AARD program in advanced beam dynamics of relevance to both Intensity and Energy Frontier accelerators. The Integrable Optics Test Accelerator (IOTA) ring is 39 meters in circumference and will be capable of storing electrons from 50 to 150 MeV in energy. Figure 3 shows the placement of the ring in the ASTA facility layout. IOTA will be described in detail in Section 7 below.

It is planned to expand capabilities for AARD in ASTA by the installation of the 2.5 MeV proton/H<sup>-</sup> RFQ accelerator which was previously used for High Intensity Neutrino Source research at Fermilab's Meson Detector Building (MDB) facility [7]. That accelerator starts with a 50 kV, 40 mA proton (or H<sup>-</sup> ion) source followed by a 2-solenoid Low Energy Beam Transport (LEBT) line. The protons/ions are then accelerated by the pulsed 325 MHz RFQ to 2.5 MeV (with ~1 ms pulse duration) before injection into IOTA, as discussed below.

### **6.4 3.9 GHz SRF Cavity**

In the early phases of ASTA, the electron bunch will be compressed using one magnetic bunch compressor located in the photoinjector. Because of the relatively long electron bunch (several mm depending on the charge) formed before acceleration in CAV1 and CAV2, significant longitudinal phase space distortion occurs during acceleration in these two cavities; see illustration in Figure 7. The resulting compressed bunch consists of a peaked distribution with a long trailing electron population. The addition of a 3.9-GHz harmonic cavity similar to the ones already developed at Fermilab and installed and operated at

FLASH [8] would allow to correct for the longitudinal phase space nonlinearities and significantly enhance the final peak current, as shown in Figure 7.

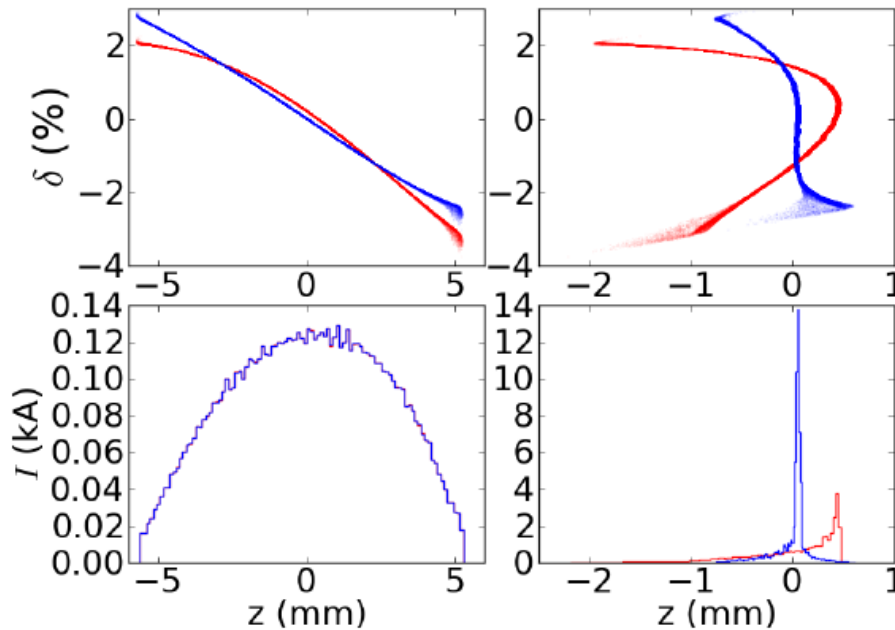


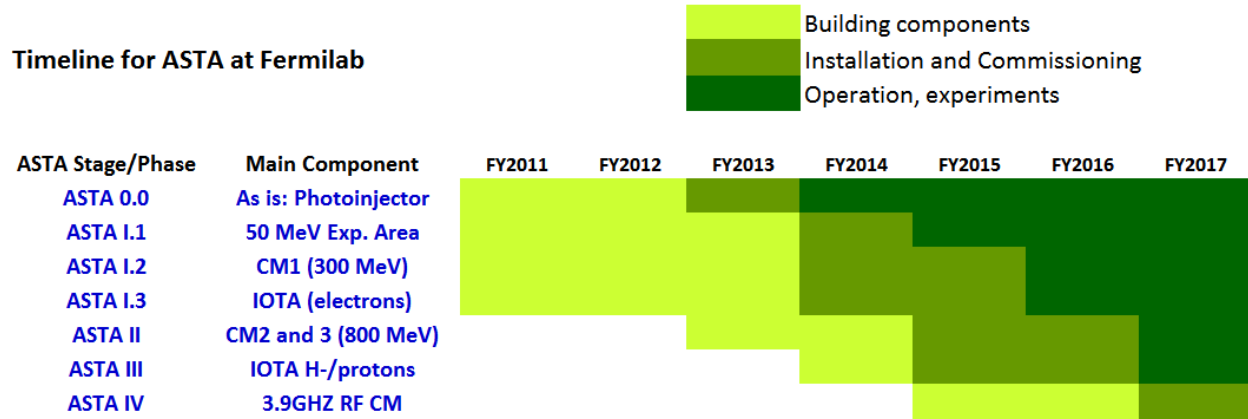
Fig. 7: Longitudinal phase space distribution (top row) and associated current profiles (bottom row) before (left column) and after (right column) the BC1 bunch compressor. The red and blue traces correspond respectively to the cases of a non-linearized and linearized longitudinal phase space upstream of BC1. The linearization is accomplished with a 3.9-GHz accelerating mode cavity and leads to a three-fold peak current increase (from Ref. [9]). Collective effects are not included in this plot.

## 6.5 Other Equipment and Experimental Areas

Operation and research at ASTA will require other equipment which will be provided by users (e.g., devices under test, specific beamline components, high power lasers, etc). There is significant space at ASTA reserved for as many as 10 experimental areas. Compared to the original NML building, there is 70 m-long tunnel expansion to the North that essentially doubled the length of the test facility from 75 m to 140 m. The expansion also includes a large 15 m-wide area for the high-energy test beam lines at the downstream end of the accelerator, as shown in Figure 3. This provides ample space for the experimental areas, which is a critical requirement for an AARD User Facility. An enclosure to house the high-energy beam absorbers and dump is situated at the end of the test beam lines and contains a pass-thru beam line that preserves the capability for further expansion of the accelerator in the future.

## 6.6 ASTA Timeline

The main purpose of ASTA is to serve a broader accelerator community and provide infrastructure for advanced research in accelerator science and technology. ASTA will offer a variety of beams and capabilities according to the timeline shown in Table I below.



The program of accelerator beam experiments will be determined by the ASTA Program Advisory Committee and its timeline will depend on the requirements and support of the studies. The ASTA beams required for the experiments and research programs presented in Section 7 are summarized in Table 2.

Table 2: Proposed ASTA experiments – beam/facility needs.

| Experiment   | 50 MeV area | High Energy |               | IOTA      |            |
|--|-------------|-------------|---------------|-----------|------------|
|  |             | CM1 300 MeV | CM1-3 800 MeV | electrons | protons/H- |
| Test of non-linear, but integrable, accelerator lattices (the Integrable Optics Test Accelerator)  | ✓           | ✓           |               | ✓         |            |
| Demonstration of technology and beam parameters for the Project X pulsed linac                     | ✓           | ✓           | ✓             |           |            |
| Beam dynamics studies and halo diagnostics in space-charge dominated proton rings                  |             |             |               |           | ✓          |
| Test of space charge compensation using an electron lens or electron columns                       |             |             |               |           | ✓          |
| Development and test of a beam-beam kicker   | ✓           |             |               |           |            |
| Test of Optical Stochastic Cooling   | ✓           | ✓           |               | ✓         |            |
| Flat-beam-driven dielectric-wakefield acceleration in slab structures                              | ✓           | ?           | ?             |           |            |
| Plasma-wakes in long bunch-trains  | ✓           | ✓           | ?             |           |            |
| Demonstration of technology and beam parameters of an ILC RF-unit                                  | ✓           | ✓           | ✓             |           |            |
| Measurement of the electron wavefunction   | ✓           | ✓           |               | ✓         |            |
| Investigation of acceleration and cooling of carbon-based crystal structures for muon accelerators | ✓           | ✓           |               |           |            |
| High brightness X-ray channeling as a compact x-ray radiation source                               | ✓           |             |               |           |            |
| Coherent diffraction radiation measurements of bunch length  | ✓           | ✓           | ?             |           |            |
| Non-intercepting optical diffraction radiation diagnostics   |             | ✓           | ✓             |           |            |
| Ultra-low emittance techniques for X-ray Free Electron Lasers                                      | ✓           | ✓           | ✓             |           |            |
| Advanced phase-space manipulations   | ✓           | ✓           |               | ✓         |            |
| Inverse Compton scattering gamma-ray source  | ✓           | ✓           | ✓             |           |            |
| Attosecond VUV pulses via space-charge driven amplification of shot-noise density fluctuations     |             | ✓           | ?             |           |            |
| Laser-induced microbunching studies with high micropulse-repetition rate electron beams            | ✓           | ✓           | ✓             |           |            |
| Ultrastable operation of SRF Linacs  | ✓           | ✓           | ✓             |           |            |
| Feasibility of an XUV FEL oscillator   |             | ✓           | ✓             |           |            |
| Production of narrow-band gamma-rays   | ✓           | ✓           |               |           |            |
| Target Studies for LBNE  |             | ✓           |               |           | ✓          |
| Studies with Tagged Photons  | ✓           | ✓           |               |           |            |
| Studies with Inverse Compton Scattered Photons   |             |             | ✓             |           |            |

## 6.7 References

- [1] J. Ruan, H. Edwards, R. P. Fliller III, J. K. Santucci, Proceedings of PAC07, Albuquerque, New Mexico, USA, 470 (2007)
- [2] P. Piot, Phys. Rev. Lett. **108**, 034801 (2012)
- [3] P. Piot, Proc. IPAC'10, Kyoto, Japan, (23-28 May 2010), p. 4316.
- [4] T. Maxwell, PhD Thesis (NIU, 2012)
- [5] T. Arkan et al., Proc. LINAC'10, Tsukuba, Japan, September 2010
- [6] C. Baffes et al., Proc. IPAC'12 (New Orleans, USA)
- [7] J. Steimel, et al., Proc. IPAC'12 (New Orleans, USA), p.3877
- [8] E. Vogel, *et al.*, "Test and Commissioning of the Third Harmonic RF System for FLASH," IPAC10, Kyoto, Japan, THPD003
- [9] C. R. Prokop, P. Piot, and M. Church, "Beam dynamics simulation for a low-energy bunch compressor at ASTA", Fermilab technical memo FNAL-TM-2533-APC (2012).

## **7.0 Scientific Opportunities at ASTA**

### **7.1 Overview of Research Thrusts**

As described above, the unique features and capabilities of ASTA will allow the exploration of a wide range of advanced accelerator R&D topics. In this section we provide an overview of the major research thrusts.

#### **7.1.1 Accelerator R&D for Particle Physics at the Intensity and Energy Frontiers**

The combination of a state-of-the-art superconducting linear accelerator and a flexible storage ring enables a broad research program directed at the particle physics accelerators of the future. The proposed research program includes:

- Demonstration of technology and beam parameters for the Project X pulsed linac
- Investigation of acceleration and cooling of carbon-based crystal structures for muon accelerators
- Demonstration of technology and beam parameters of an ILC RF-unit
- Plasma-wakes in long bunch-trains
- Test of non-linear, but integrable, accelerator lattices (the Integrable Optics Test Accelerator) which have the potential to shift the paradigm of future circular accelerator design
- Test of Optical Stochastic Cooling
- Test of space charge compensation using an electron lens
- Measurement of the electron wave function

#### **7.1.2 Accelerator R&D for Stewardship and Applications**

With its high energy, high brightness, high repetition rate, and the capability of emittance manipulations built-in to the facility design, ASTA is an ideal platform for exploring novel approaches for producing bright photon beams and gamma rays. Its capabilities have captured considerable interest in the community, resulting in a very broad range of proposals. The proposed research program includes:

- High brightness X-ray channeling as a compact x-ray radiation source
- Advanced phase-space manipulations
- Demonstration of techniques to generate and manipulate ultra-low emittance beams for future hard X-ray free-electron lasers
- Development and test of a beam-beam kicker
- Feasibility of an XUV FEL oscillator
- Production of narrow-band gamma-rays
- Inverse Compton scattering gamma-ray source

- Attosecond VUV pulses via space-charge driven amplification of shot-noise density fluctuations
- Laser-induced microbunching studies with high micropulse-repetition rate electron beams
- Coherent diffraction radiation measurements of bunch length
- Non-intercepting optical diffraction radiation diagnostics
- Beam dynamics for the Matter-Radiation Interaction at the Extreme (MARIE) Project
- Flat-beam-driven dielectric-wakefield acceleration in slab structures

Subsequent sections in this proposal explore these research thrusts in greater detail.

## **7.2 Accelerator R&D Opportunities at ASTA: Toward HEP Discovery Science at the Intensity and Energy Frontiers**

### **7.2.1 Demonstration of High Power High Gradient SRF Cryomodules with Intense Beams**

The ASTA facility will be a unique test bed to carry out studies of high power, high gradient SRF cryomodules with high intensity beams. There are no other test facilities in the world where this research can be carried out. These studies are all critical to determining cavity configurations for Project X, for the ILC, and for the NGLS. In particular, whether HOM damping will be required and ramifications of long-pulse operation in the pulsed linac of Project X are key questions that need to be answered.

#### **7.2.1.1 ILC cavity HOM studies**

*HOM spectrum, trapped modes and effects of HOM excitation to cryogenic losses*

High Order Modes (HOMs) is an issue for most superconducting accelerators: because of a beam interaction with the HOMs their resonant excitation is possible which in turn may lead to additional cryogenic loss in a cavity and emittance dilution. Transverse collective instabilities, beam break-up (BBU) may result because of HOM excitation as well. For ion and proton machines, or accelerators with the beam recirculation longitudinal collective instabilities may be possible. Some of the HOMs may be trapped in multi-cell cavities having high loaded Q that may lead to the HOM excitation at high beam amplitude or long pulse trains. Careful measurements of the HOM excitation in a ILC-type cavity of ASTA, investigation of resonance HOM excitation and its consequences, comparing these measurements to the computer models will provide valuable information for future superconducting accelerators.

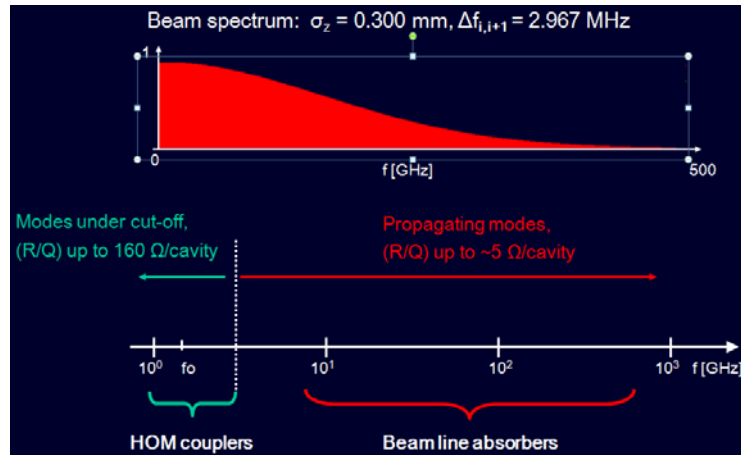


Figure 1: High order modes in ILC (J. Sekutowicz, DESY)

### *Lorentz Force Detuning for the HOM's*

Lorentz force detuning is well investigated for the operating modes in an ILC-type of the cavity. However, there is no any systematic investigation of the Lorentz force detuning for HOMs. These investigations are important for future superconducting accelerators, especially operating in pulsed regime.

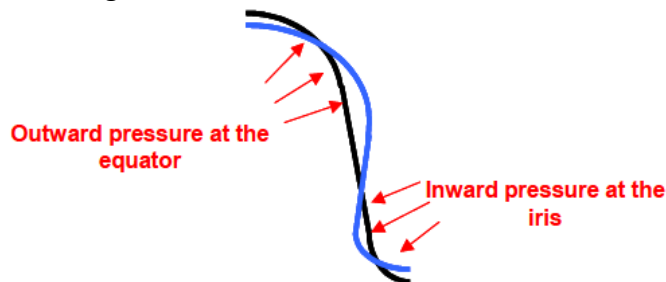


Figure 2: Illustration of cell deformation for the Lorentz force detuning.

### *Range of detuning of the HOM modes due to plastic deformation*

Special experiments performed at Fermilab Horizontal Test Stand (HTS) with the ILS-type 9-cell cavity, showed that the HOM spectrum changes after detuning of the operating mode and tuning it back. This change is caused by small residual plastic deformations. It leads to a possible conclusion that in a pulse accelerator like ILC, where a special system provides the operating mode stabilization in presence of Lorentz force, the HOM spectrum may change from pulse to pulse, decreasing the probability of resonant HOM excitation compared to CW machines. This effect is not investigated yet. SC system of a linear accelerator of ASTA may be used for such investigations, which in turn, are very useful for future long – pulse accelerators such as Project X.

| f, MHz   | $\Delta f$ , kHz | $\delta f$ , Hz | Passband    |
|----------|------------------|-----------------|-------------|
| 1300     | 90               | 0               | 1Monopole   |
| 1600.093 | -218             | 360             | 1Dipole     |
| 1604.536 | -215             | 240             | 1Dipole     |
| 1607.951 | -214             | 360             | 1Dipole     |
| 1612.189 | -210             | 360             | 1Dipole     |
| 1621.344 | -211             | 240             | 1Dipole     |
| 1625.458 | -208             | 370             | 1Dipole     |
| 1830.836 | -185             | 370             | 2Dipole     |
| 1859.882 | -36              | 120             | 2Dipole     |
| 2298.807 | -278             | 480             | 1Quadrupole |
| 2299.346 | -278             | 490             | 1Quadrupole |
| 2372.333 | -224             | 490             | 2Monopole   |
| 2377.333 | -221             | 490             | 2Monopole   |
| 2383.575 | -213             | 240             | 2Monopole   |
| 2399.289 | -210             | 490             | 2Monopole   |

Figure 3: HOM frequency change  $\delta f$  after the operation mode detuning and tuning back by  $\Delta f$  (T. Khabiboulline, Fermilab)

*Long term stability of the HOM frequencies for cavity in cryostat*

During the operation in a nominal regime, the tuning system maintains the operating frequency. However, Lorentz forces and microphonics may be a reason of long-term changes of the frequencies of HOMs. It was never investigated carefully. It is proposed to carry out a detailed investigation of a long-term stability of HOM frequencies for a 1.3 GHz dressed ILC cavity in a cryomodule.

*Effect of HOM to the beam dynamics*

High-order modes excited in a cavity, may create the following problems for a beam dynamics:

Increase a beam transverse emittance, or even cause the beam deflection and losses, because of collective transverse instability, BBU. BBU may develop for ultra-relativistic beams, in contrast to klystron-type longitudinal collective instability, and may be investigated at ASTA.

Beam transverse and longitudinal emittance dilution caused by HOM resonance excitation. These effects may be investigated at ASTA, because it operates in pulse mode – it is not possible for CW operation for regular beam timing structure.

*Using HOM signal for measurements of beam position in cavity (HOM based BPM)*

Measurements of the dipole HOMs excited by the beam may be used for measurements of the cavity off set versus the beam axis. These experiments were performed successfully at DESY, with 1.3 GHz cavity, and with 3.9 GHz cavity. They showed that it is really possible to provide reliable and precise measurements using this technique.

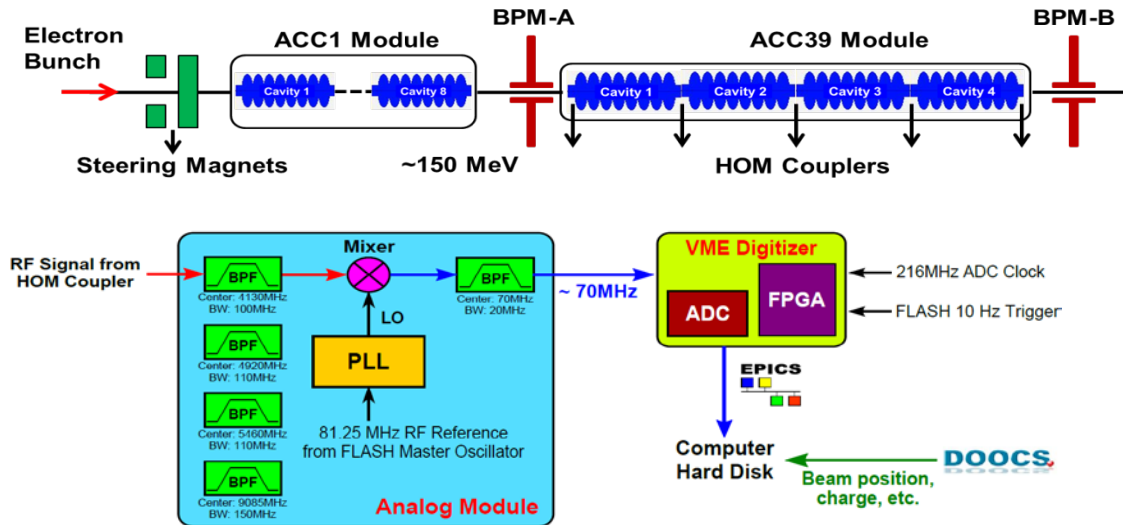


Figure 4: Schematic and electronics set up for cavity position measurement using HOMs at 3.9 GHz section (Pei Zhang, Nicoleta Baboi, Roger Jones, FLASH/DESY)

### Effect of cavity tilts

However, for collider operation, especially in the bunching system, not just cavity off-set is important, but also tilt of a cavity axis versus a beam axis, which may lead to significant emittance dilution. Special experiments may be done at ASTA in order to develop the technique to measure and correct for tilt.

#### 7.2.1.2 Studies of propagating high-frequency HOM's (wakefields)

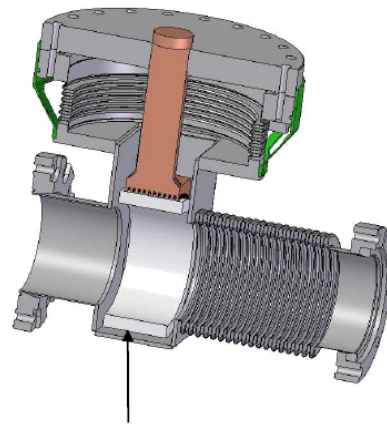
##### Cryo-losses

For short bunches (tens of microns) which is suitable not for ILC only, but for light source accelerators (NGLS, for example), the beam current spectrum is very wide, up to hundreds of GHz. These very high order modes may create additional cryo-losses. In order to prevent it, special HOM absorbers are to be developed and introduced.

##### Damping of the HOMs in absorber

However, design of efficient HOM absorbers requires careful investigation of very high order mode excitation in a chain of cavities along the linac, dissipation in the SC cavity walls,

radiation to the beam pipe and its interception by the absorbers. ASTA allows all these experiments.



Lossy ceramic (final choice CA137)

Figure 5: XFEL HOM absorber (J. Sekutowic, DESY).

*RF kick and Wakefields in cavity caused by RF and HOM couples (asymmetry)*

All RF cavities being axisymmetrical, have perturbations of the symmetry caused by manufacturing errors and, more seriously, by coupling elements (main power couplers, HOM couplers, etc). These perturbations may cause so-called RF kick and coupler wake, which may lead to significant emittance dilution, especially in a bunching systems, where the bunch is long.

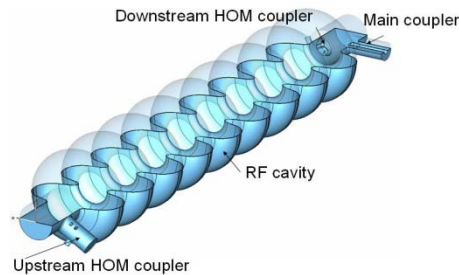


Figure 6: The ILC RF cavity with the main and HOM couplers.

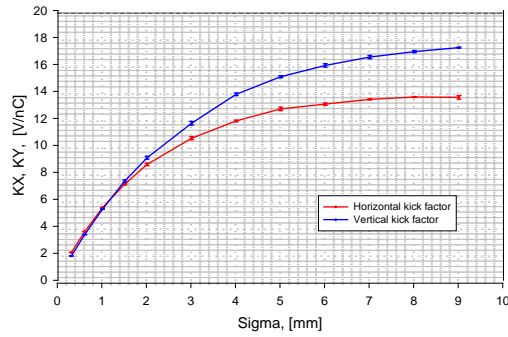


Figure 7: Horizontal and vertical wake kick-factors of the ILC type structure with couplers versus a bunch size (A. Lunin, Fermilab).

### 7.2.1.3 Lorentz Force Detuning Compensation (LFDC) studies

*LFD and microphonics studies for short (~1ms, ILC) and long pulse trains (8-30ms, Project X)*

It is proposed a detailed investigation of Lorentz force detuning compensation for short pulse, which suitable for ILC operation regime, and for a long pulse, which is essential for high-energy pulse part of the Project X. This work was already initiated at Fermilab, and impressive results are achieved already. However, further investigations are desired in order to achieve reliable operation of the pulsed linac of Project X.

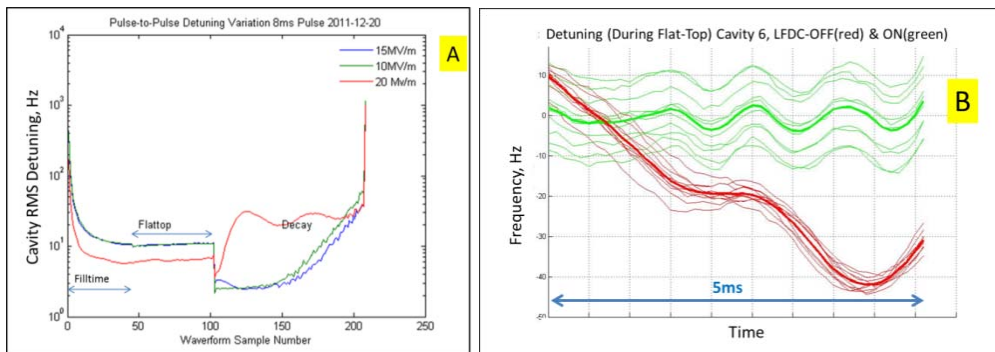


Figure 8: (A): Pulse-to-Pulse Detuning Variation (RMS Detuning) for  $E_{acc}=10; 15; 20\text{MV/m}$ . (B): Detuning (during 5ms Flat-Top) for the 10 RF pulses with LFDC system ON (green) and OFF (red). Thick line is average of 10 pulses. The gradient is  $10\text{MV/m}$ . (W. Schappert, Yu. Pischalnikov, Fermilab).

*Studies of sources of microphonics, spectrum, quantification of contribution from different sources and means to suppress microphonics*

Another issue which determines the resonant frequency stability of SC cavity is microphonics, i.e., frequency change caused by the cavity wall vibrations. These vibrations may have different causes (mechanical resonances, insufficient design of a Helium vessel and cryo system, etc.). It is shown at Cornell that the most serious reason of the microphonics is He pressure fluctuations. We propose detailed investigations of the reasons for the microphonics in ILC-type cryomodules, in order to quantify contributions from different sources, determine main reasons of microphonics, and thus, understand the means of the microphonics suppression. At Fermilab, work is already initiated, and good results have been achieved for SSR1 cavity.

*Microphonics due to cavity cross-talking*

Another important and poor-investigated issue is microphonics due to cavity cross – talk, i.e., a cavity vibration influencing the frequency of a neighboring cavity and other cavities in same cryo-module. Mechanical coupling of the cavities in a cryo-module may create additional difficulties for microphonics suppression and needs to be investigated.

*Effects of the CM ends to microphonics*

Mechanical coupling of a cavity to the environment depends strongly on the cavity position in a cryo-module. The end cavities are in a different position with different end constraints than the regular cavities. This may change microphonics amplitude and possibly create additional problems for their compensation.

**7.2.1.4 Field emission and Dark current**

*Spectrum, Energy, etc...*

Field emission may cause high losses in an SC cavity, and thus, seriously limit the acceleration gradient – SNS is a good example. Thus, investigation of the dark currents, the reasons, the energy spectrum, etc, is essential. ASTA allows experimental investigations of the dark currents, that is important for many projects of large SC accelerators.

**7.2.1.5 Cavity alignment**

*Effect of the cavity tilt on beam dynamics*

Experimental investigation of a cavity alignment – off-set and especially tilt is very important for large – scale accelerators. The cavity tilt provides the beam acceleration in

transverse direction and introduces momentum spread along the bunch, which in turn causes the emittance dilution. ASTA will allow one to carry out these measurements.

#### **7.2.1.6 Cavity gradient**

##### *Effect of CM ends to cavity gradient/degradation*

It is noticed (FLASH and SNS experience) that frequently the end cavities in a cryo-module provide less gradient than regular cavities. This limits the gradient of entire section. Sometimes degradation of the gradient in the end cavities takes place over time. We propose to investigate the reasons of the gradient limitation and degradation in the end cavities at ASTA cryomodules.

##### *LLRF and Gradient spread in CM*

Achieving design gradient 31MV/m on average is very challenging task for SRF cryomodules which will be properly addressed at ASTA. Cavity performance spread may lead to different RF filling behavior during the pulse for different cavities when fed by a single RF source. This needs especially designed LLRF systems in order to provide amplitude and phase stability of the average field "seen" by the different bunches in the beam pulse. Fermilab participates a long pulse experimental program at DESY, which has the goal to provide reliable operation of the linac for a long pulse when a number of cavities a fed by a single RF source. ASTA allows for such a program at Fermilab. There should be more time available at ASTA to work on this long pulse study as FLASH has only limited time available due to user operation.

#### **7.2.1.7 Effects of the CM end (cold to warm transition between cryomodules)**

##### *Contamination of the end cavities (long term effects)*

The end cavities in a cryo-module may be contaminated, which may in turn, cause long – term degradation. Investigation of the source of contamination may help to get rid of this problem.

##### *Field emission and cavity degradation*

Another effect is a field emission in the end cavities caused by contamination, which may influence all the cavities in cryo-module.

##### *Effect of thermal radiation from RT ends to cavities in CM*

The end cavities are exposed to the thermal radiation from room-temperature gaps between the cryo-modules, which may lead to additional cryo-losses.

ASTA allows for all these investigations and may clarify the issues with the end cavities and improve their performance in future SC linacs.

## **7.2.2 Integrable-optics test accelerator (IOTA) ring construction and operation**

### **7.2.2.1 Introduction**

What prevents us from building super-high intensity accelerators? The answer is case-specific, but it often points to one of the following phenomena: machine resonances, various tune shifts (and spreads), and instabilities. These three phenomena are interdependent in all present machines, which are built to have “linear” focusing optics (also called lattice). A path towards alleviating these phenomena can be opened by making accelerators nonlinear. This idea is not totally new: Orlov [1] and McMillan [2] have proposed initial ideas on nonlinear focusing systems for accelerators. However, practical implementations of such ideas proved elusive, until recently when Danilov and Nagaitsev proposed a solution for nonlinear integrable accelerator lattice that can be implemented with special magnets [3]. In this document we propose a proof-of-principle experiment for demonstration of the concept, and describe the design of machine for this demonstration – the Integrable Optics Test Accelerator (IOTA).

The ASTA facility will offer a unique opportunity to carry out the proposed research toward demonstration of the feasibility of the integrable optics technique. That research requires construction and operation of a dedicated storage ring (IOTA). It cannot be carried out anywhere else (e.g., at the existing storage rings) as it involves very special insertions (highly nonlinear magnets) which extend over a significant fraction of the ring circumference, special arrangements of the optics lattice and precise control of the elements (strength, positions, etc.).

### **7.2.2.2 Concept of nonlinear integrable optics**

#### **7.2.2.2.1 Nonlinear Integrable Optics and Potential**

Lattice design of all present accelerators incorporates dipole magnets to bend particle trajectory and quadrupoles to keep particles stable around the reference orbit. These are “linear” elements because the transverse force is proportional to the particle displacement,  $x$  and  $y$ . This linearity results (after the action-phase variable transformation) in a Hamiltonian of the following type:

$$H(J_1, J_2) = \nu_x J_1 + \nu_y J_2, \quad (1)$$

where  $\nu_x$  and  $\nu_y$  are betatron tunes and  $J_1$  and  $J_2$  are actions. This is an integrable Hamiltonian. The drawback of this Hamiltonian is that the betatron tunes are constant for all particles regardless of their action values. It has been known since early 1960-s that the

spread of betatron tunes is extremely beneficial for beam stability due to the so-called Landau damping. However, because the Hamiltonian (1) is linear, any attempt to add non-linear elements (sextupoles, octupoles) to the accelerator generally results in a reduction of its dynamic aperture, resonant behavior and particle loss. A breakthrough in understanding of stability of Hamiltonian systems, close to integrable, was made by Nekhoroshev [4]. He considered a perturbed Hamiltonian system:

$$H = h(J_1, J_2) + \varepsilon q(J_1, J_2, \theta_1, \theta_2), \tag{2}$$

where  $h$  and  $q$  are analytic functions and  $\varepsilon$  is a small perturbation parameter. He proved that under certain conditions on the function  $h$ , the perturbed system (2) remains stable for an exponentially long time. Functions  $h$  satisfying such conditions are called *steep* functions with quasi-convex and convex being the steepest. In general, the determination of steepness is quite complex. One example of a non-steep function is a linear Hamiltonian Eq. (1).

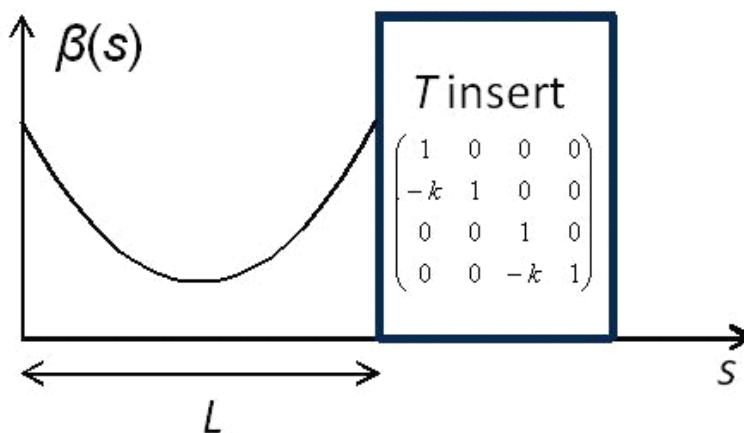


Figure 1. An element of periodicity: a drift space with equal beta-functions followed by a  $T$ -insert.

In Ref. [1] three examples of nonlinear accelerator lattices were proposed. Here we will concentrate on one of the lattices, which results in a steep (convex) Hamiltonian.

Consider an element of lattice periodicity consisting of two parts: (1) a drift space,  $L$ , with exactly equal horizontal and vertical beta-functions, followed by (2) an optics insert,  $T$ , which is comprised of linear elements and has the transfer matrix of a thin axially symmetric lens; see Figure 1.

Let us now introduce additional transverse magnetic field along the drift space  $L$ . The potential,  $V(x, y, s)$ , associated with this field satisfies the Laplace equation,  $\Delta V = 0$ .

Now we will make a normalized-variable substitution [3] to obtain the following Hamiltonian for a particle moving in the drift space  $L$  with an additional potential  $V$ :

$$H_N = \frac{p_{xN}^2 + p_{yN}^2}{2} + \frac{x_N^2 + y_N^2}{2} + U(x_N, y_N, \psi), \quad (3)$$

where

$$U(x_N, y_N, \psi) = \beta(\psi) V(x_N \sqrt{\beta(\psi)}, y_N \sqrt{\beta(\psi)}, s(\psi)), \quad (4)$$

and  $\psi$  is the "new time" variable defined as the betatron phase,

$$\psi' = \frac{1}{\beta(s)}. \quad (5)$$

The potential  $U$  in equation (3) can be chosen such that it is time-independent [1]. This results in a time-independent Hamiltonian (3). We will now choose a potential such that the Hamiltonian (3) possesses the second integral of motion. We will omit the subscript  $N$  from now on.

Consider potentials [5] that can be presented in elliptic coordinates in the following way

$$U(x, y) = \frac{f(\xi) + g(\eta)}{\xi^2 - \eta^2}, \quad (6)$$

where  $f$  and  $g$  are arbitrary functions,

$$\xi = \frac{\sqrt{(x+c)^2 + y^2} + \sqrt{(x-c)^2 + y^2}}{2c} \quad \eta = \frac{\sqrt{(x+c)^2 + y^2} - \sqrt{(x-c)^2 + y^2}}{2c} \quad (7)$$

are elliptic variables and  $c$  is an arbitrary constant.

The second integral of motion yields

$$I(x, y, p_x, p_y) = (xp_y - yp_x)^2 + c^2 p_x^2 + 2c^2 \frac{f(\xi)\eta^2 + g(\eta)\xi^2}{\xi^2 - \eta^2} \quad (8)$$

First, we would notice that the harmonic oscillator potential  $(x^2 + y^2)$  can be presented in the form of Eq. (6) with  $f_1(\xi) = c^2 \xi^2 (\xi^2 - 1)$  and  $g_1(\eta) = c^2 \eta^2 (1 - \eta^2)$ . Second, we have found the following family of potentials that satisfy the Laplace equation and, at the same time, can be presented in the form of Eq. (6):

$$f_2(\xi) = \xi \sqrt{\xi^2 - 1} (d + t \operatorname{acosh}(\xi)) \quad g_2(\eta) = \eta \sqrt{1 - \eta^2} (q + t \operatorname{acos}(\eta)), \quad (9)$$

where  $d$ ,  $q$ , and  $t$  are arbitrary constants. Thus, the total potential energy in Hamiltonian (3) is given by

$$U(x, y) = \frac{x^2}{2} + \frac{y^2}{2} + \frac{f_2(\xi) + g_2(\eta)}{\xi^2 - \eta^2}. \quad (10)$$

Of a particular interest is the potential with  $d = 0$  and  $q = \frac{\pi}{2}t$ , because its lowest multipole expansion term is a quadrupole. Figure 2 presents a contour plot of the potential energy Eq. (10) for  $c = 1$  and  $t = 0.4$ .

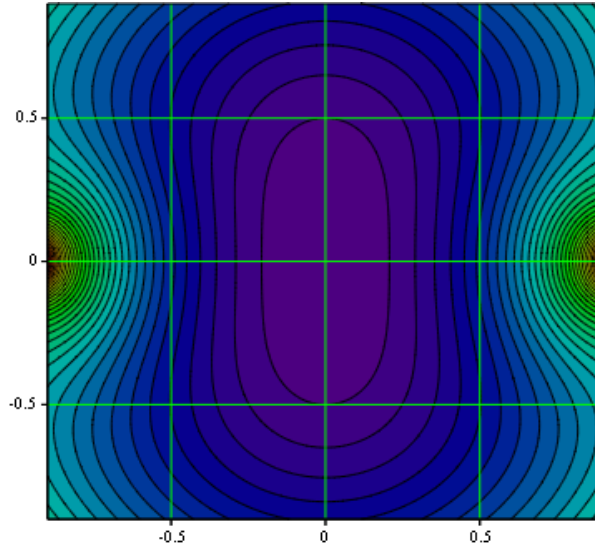


Figure 2: Contour plot of the potential energy Eq. (10) with  $c = 1$  and  $t = 0.4$ . The repulsive singularities are located at  $x = \pm c$  and  $y = 0$ .

The multipole expansion of this potential for  $c = 1$  is as follows:

$$U(x, y) \approx \frac{x^2}{2} + \frac{y^2}{2} + t \operatorname{Re} \left( (x+iy)^2 + \frac{2}{3}(x+iy)^4 + \frac{8}{15}(x+iy)^6 + \frac{16}{35}(x+iy)^8 + \dots \right) \quad (11)$$

where  $t$  is the magnitude of the nonlinear potential.

Since the 2D Hamiltonian with this potential has two analytic integrals of motion, it is integrable and thus can be expressed as an analytic function of actions:

$$H = h(J_1, J_2), \quad (12)$$

where

$$J_1 = \frac{1}{2\pi} \oint p_\eta d\eta \quad J_2 = \frac{1}{2\pi} \oint p_\xi d\xi \quad (13)$$

### 7.2.2.2 Maximum nonlinear tune shift

The potential (10) provides additional focusing in  $x$  for  $t > 0$  and defocusing in  $y$ . Thus, for a small-amplitude motion to be stable, one needs  $0 < t < 0.5$ . This corresponds to the following small-amplitude betatron frequencies,

$$\nu_1 = \nu_0 \sqrt{1+2t} \quad \nu_2 = \nu_0 \sqrt{1-2t} \quad , \quad (14)$$

where  $\nu_0$  is the unperturbed linear-motion betatron frequency. For arbitrary amplitudes the frequencies are obtained by

$$\nu_1(J_1, J_2) = \frac{\partial h}{\partial J_1} \quad \nu_2(J_1, J_2) = \frac{\partial h}{\partial J_2} \quad . \quad (15)$$

Figure 3 presents frequencies  $\nu_1(J_1, 0)$  and  $\nu_2(0, J_2)$ , normalized by  $\nu_0$  for  $t = 0.4$ .

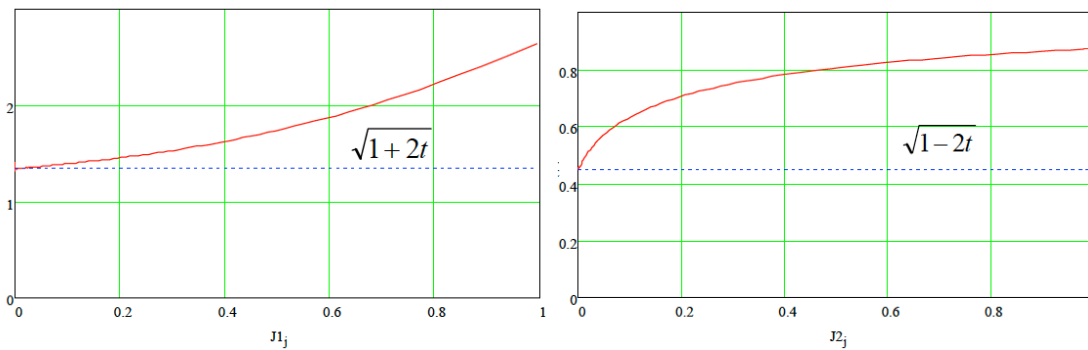


Figure 3: Betatron oscillation frequencies of the two modes - 1 (left) and 2 (right) normalized by  $\nu_0$  as functions of actions. Nonlinearity strength parameter  $t = 0.4$ .

The unperturbed linear motion tune  $\nu_0$  - the betatron phase advance over the drift space  $L$ , is limited to 0.5 (in units of  $2\pi$ ). The phase advance in T-insert must be a multiple of 0.5. This makes the full tune of one element of periodicity  $0.5+0.5n$ . Thus, the theoretical maximum attainable nonlinear tune shift per cell is  $\sim 0.5$  for mode 1 and  $\sim 0.25$  for mode 2. Expressed in terms of the full betatron tune per cell, this tune shift can reach 50% ( $0.5/(0.5+0.5)$ ).

Numerical simulations with single and multi particle tracking codes were carried out in order to determine the tune spread that can be achieved in a machine built according to the above recipe [6-8]. Various imperfections were taken into account, such as the perturbations of T-insert lattice, synchrotron oscillations, and other machine nonlinearities. In Figure 4 a result of one of the simulations is presented. The tune footprint obtained with Frequency Map Analysis [9] demonstrates that vertical tune spread exceeding 1 can be achieved and very little resonances are caused by imperfections. No dynamic aperture was observed in the system.

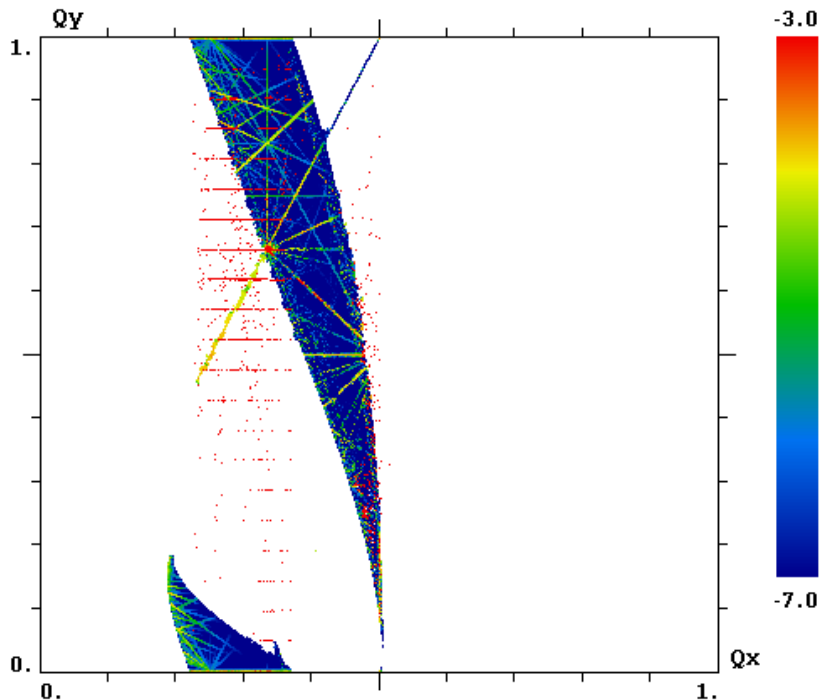


Figure 4: Beam tune footprint for  $\nu_0 = 0.3$ , four elements of periodicity,  $t = 0.4$ . Simulation with Lifetrac Frequency Map Analysis.

### 7.2.2.3 IOTA goals and scope

In Section 2 we demonstrated that using conventional and special nonlinear focusing magnets it is possible to construct an accelerator lattice, in which the betatron motion is strongly nonlinear yet stable. The strong nonlinearity of betatron motion would result in a significant spread of betatron tunes of particles within the bunch (up to 50% of the nominal tune), thus providing strong Landau damping of coherent instabilities.

The superconducting RF test facility at Fermilab (formerly NML) will provide electron beam with energies up to 750 MeV. The experimental area at the end of the linac will be located in a 20×15 m hall, which is large enough to house a small electron storage ring.

We propose to construct the Integrable Optics Test Accelerator (IOTA) ring, which would use the beam from the NML 1.3 GHz SRF linac with the goal of *demonstration of the possibility to achieve very large nonlinear tune shifts in a realistic accelerator design*. This proof-of-principle experiment would *only concentrate on the single-particle motion stability in the nonlinear integrable system*, leaving the studies of collective effects and attainment of high beam current to future research.

Research at IOTA will include experiments on the following topics:

- Achievement of large nonlinear tune shift/spread without degradation of dynamic aperture
- Suppression of strong lattice resonances (e.g. by crossing the integer resonance by part of the beam without intensity loss)
- Stability of nonlinear system to perturbations: chromatic effects, effect of synchrotron oscillations, lattice distortions
- Studies of different variants of nonlinear magnet design

In addition to the primary goal, the ring can accommodate other Advanced Accelerator R&D experiments and/or users. This is possible because only a portion of the ring circumference will be occupied with nonlinear magnets and otherwise the machine is a conventional low-energy storage ring. One of the AARD experiments incorporated in the current design of the ring is the Optical Stochastic Cooling.

#### **7.2.2.4 IOTA Design**

##### **7.2.2.4.1 Machine Lattice**

The machine lattice must satisfy the following design criteria:

- Be periodic, with the element of periodicity comprised of a drift space with equal beta-functions, and a focusing and bending block with the betatron phase advance in both planes equal to  $\pi$  (T-insert in Figure 1).
- The drift space must be long enough to accommodate practical nonlinear magnets. We set the minimum drift length to 2 m.
- The T-insert must be tunable to allow a wide range of phase advances (and beta-functions) in the drift space in order to study different betatron tune working points.
- It is preferable that the focusing block is achromatic in order to avoid strong coupling between the transverse and longitudinal degrees of freedom.
- The ring must have one long (5 m) straight section for the Optical Stochastic Cooling experiment.
- The machine must fit in the footprint of the experimental hall and be properly oriented with respect to the injection line.

In our design the ring is made of four cells. The cells are mirror-symmetric in pairs, and each consists of 8 quadrupoles and two dipole magnets bending by 30 and 60 degrees. With the betatron phase advance per cell of 0.8, this makes the total betatron tune of 3.2. Hence, in the extreme case the maximum tune shift generated by the nonlinear magnets may reach 1.6, meaning some particles in the bunch will cross an integer resonance.

This design provides 2 m insertions for the nonlinear magnets, two 1 m long straight sections for RF and other systems, and two 5 m sections – one for injection/extraction and

one for Optical Stochastic Cooling setup. The minimal number of quadrupole magnets required to implement an axially symmetric lens in a straight section is five. The large number of quadrupoles we use permits a wide range of tuning for the betatron tune, which can be varied between 2.4 and 3.6, and dispersion and momentum compaction.

Table 1 lists the main parameters of the machine. Figures 5, 6 show the machine layout in the experimental hall, and lattice functions of one cell.

Table 1: IOTA Ring Parameters

| Parameter                               | Value                       | Unit                              |
|---|-----------------------------|-----------------------------------|
| Beam Energy                             | 150                         | MeV                               |
| Circumference                           | 38.7                        | m                                 |
| Bending dipole field                    | 0.7                         | T                                 |
| RF voltage                              | 50                          | kV                                |
| Maximum $\beta$ -function               | 22                          | m                                 |
| Momentum compaction                     | 0.14                        |                                   |
| Betatron tune                           | $Q_x, Q_y=3.2$ (2.4 to 3.6) |                                   |
| Equilibrium transverse emittance r.m.s. | 0.06                        | $\pi\mu\text{m}$ (non-normalized) |
| Synchrotron radiation damping time      | 1.0                         | sec( $\sim 10^7$ turns)           |

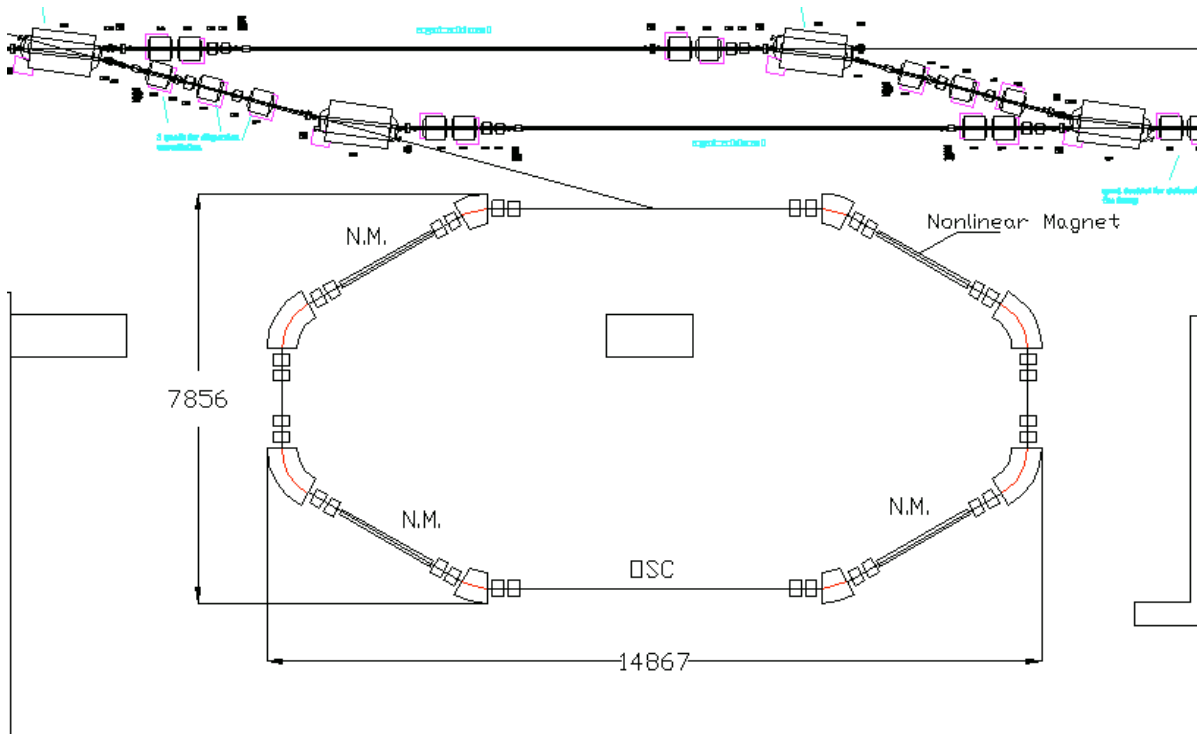


Figure 5: IOTA ring layout.

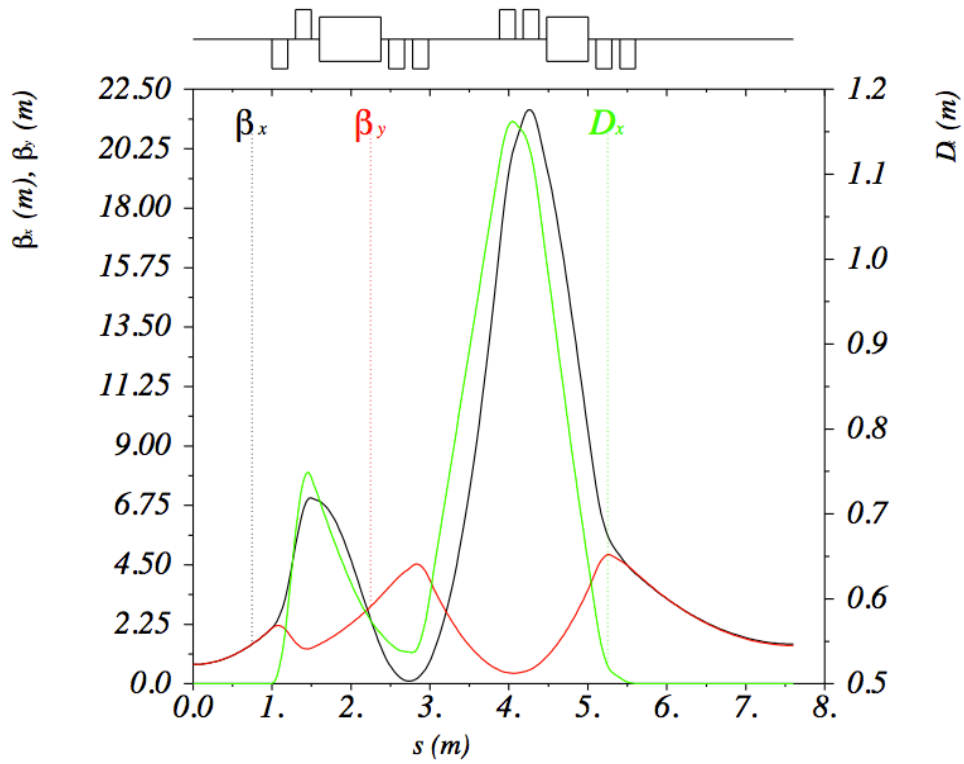


Figure 6: Lattice functions of the element of periodicity.

### 7.2.2.4.2 Nonlinear Magnets

The condition of the Hamiltonian time-independence requires that the nonlinear potential must *continuously* change along the length of the nonlinear section (Eq. 4). The potential is defined by two parameters: the strength parameter  $t$ , and the geometric parameter  $c$ , which represents the distance between the singularities, or the element aperture (Eq. 10). The geometric parameter  $c$  scales as the square root of  $\beta$ -function in the nonlinear straight section, and the strength parameter  $t$  scales as  $1/\beta$ . Since it's not practical to manufacture a magnet with complex varying aperture, we consider approximating the continuously varying potential with a number of thin magnets of constant aperture. Figure 7 shows the distribution of strength of the lowest (quadrupole) harmonic in 20 thin magnets.

The magnetic potential can be expanded into multipole series Eq. (11). However, this expansion is only valid inside the  $r = \sqrt{x^2 + y^2} < c$  circle. Vertical oscillation amplitudes  $y > c$  are essential for achievement of large tune spread. By proper shaping of the magnetic poles we were able to achieve good field quality in the region  $x < c, y < 2 \times c$  (Figure 8). The magnet can be optimized further to include fringe-field effects and extend the good field region.

In order to demonstrate the high tune spread within the beam, the transverse beam size must be comparable to the distance between the poles of the magnet. For the chosen ring energy and equilibrium emittance, the beam size  $\sigma_x, \sigma_y \approx 0.25$  mm, which would require impractically small transverse dimensions of the nonlinear elements. However, due to the very long damping time it is possible to “paint” a larger area with the small emittance linac beam. Hence, we considered nonlinear elements with the aperture  $2 \times c \approx 2$  cm.

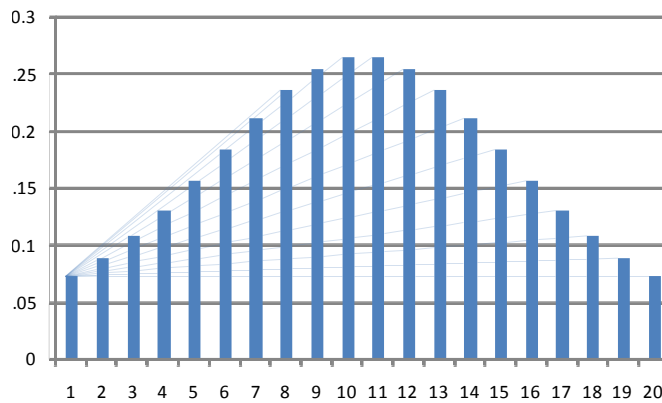


Figure 7: Distribution of quadrupole component (T/m) in the nonlinear magnet section.

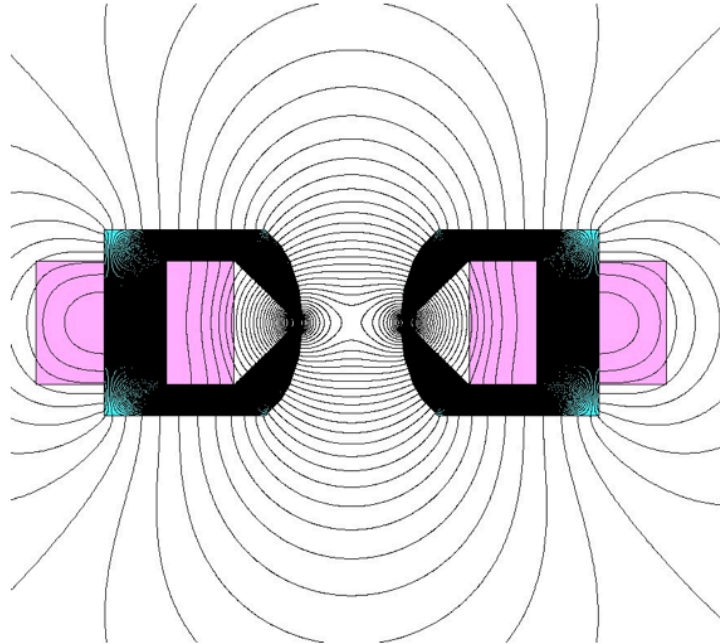


Figure 8: Cross-section of nonlinear magnet.

#### **7.2.2.4.3 Vacuum System**

Although studies of integrable optics require beam circulation only for 100,000 turns, other applications of the ring will demand beam lifetime of the order of 1 hour. This determines the specifications of the vacuum system, which must provide partial pressure of CO and H<sub>2</sub> of 10<sup>-7</sup> torr and 10<sup>-8</sup> for Ar. The Aluminum beam pipe will have round cross-section with 50 mm diameter in quadrupoles and dipole magnets, and elliptical shape 15×75 mm in the nonlinear magnet straight sections. Eight vacuum pumps will be attached to ports on the inside of dipole magnets.

#### **7.2.2.4.4 Beam Diagnostics**

Accurate tuning of the linear machine lattice is critical for proper functioning of the nonlinear integrable optics. The  $\beta$ -functions in the straight sections must be controlled to better than 5%, and tolerance on the betatron phase advance in the T-insert is 0.02. These requirements necessitate an extensive beam position monitoring system with 16 button-type pickups, capable of capturing the turn-by-turn beam position for 8-16 thousand turns with the precision of 100  $\mu$ m.

Additionally, the ports in vacuum chamber in dipole magnets will provide points for synchrotron light based diagnostics.

#### **7.2.2.4.5 RF System**

We plan to adopt the Project X 162 MHz copper cavity design with some modifications. The RF cavity parameters are listed in Table 2.

Table 2: RF Cavity Parameters

| Parameter         | Value             | Unit |
|-------------------|-------------------|------|
| Aperture diameter | 50                | mm   |
| Frequency         | 162.45            | MHz  |
| Q factor          | 30,877            |      |
| Shunt impedance   | $4.5 \times 10^6$ | Ohm  |
| Maximum voltage   | 50                | kV   |
| Power             | 0.56              | kW   |

### 7.2.2.5 Status and Schedule

As of the time of this document (2012), the machine design requirements are finalized. The layout was selected, and most numerical simulations of particle dynamics in the final lattice have been performed. Components of beam instrumentation and vacuum system have been procured. The technical specification on elements of magnetic system and vacuum chamber were ready by February, 2012.

An external review of IOTA has been organized by Fermilab's Accelerator Physics Center (APC) and took place at Fermilab on 02/23/2012. The review committee was chaired by Prof A. Seryi of John Adams Institute (UK).

The committee reviewed all aspects of the IOTA experiment, including:

- 1) theoretical foundations of the IOTA method
- 2) numerical computer simulation of the beam stability in IOTA
- 3) overall design and plan of the experiment
- 4) technical preparedness of the design of key components of IOTA
- 5) schedule of implementation, cost and resources
- 6) plan of beam studies and experiments beyond Phase I

Particular focus was on items 3 and 4 (magnets, vacuum, RF, injection, diagnostics, power supplies, mechanical support and alignment, beam dump, safety, controls and overall integration).

All presentations, summary report and committee recommendation are available at <https://indico.fnal.gov/conferenceDisplay.py?confid=5151>

The committee recommended to proceed with procurement of the longest lead items (magnets for IOTA ring) in FY12 in anticipation that the ring assembly will take place during 2013, and beam commissioning will start in 2014. The committee report is given below in Appendix.

We would like to thank V. Kashikhin, G. Romanov (FNAL) and I. Batalov (MIPT) for their contributions.

### 7.2.2.6 References

- [1] V. V. Vechev and Yu. F. Orlov, 1966 *J. Nucl. Energy, Part C Plasma Phys.* **8**, p. 717.
- [2] E. M. McMillan, in *Topics in Modern Physics. A Tribute to E. U. Condon*, edited by E. Britton and H. Odabasi (Colorado University Press, Boulder, 1971), pp. 219-244.
- [3] V. Danilov and S. Nagaitsev, *Phys. Rev. ST Accel. Beams* **13**, 084002 (2010).
- [4] N. Nekhoroshev, "Behaviour of Hamiltonian systems close to integrable", *Functional. Anal. Appl.* **5** (1971), 338–339
- [5] G. Darboux, "Sur un problème de mécanique", *Arch. Néerlandaises Sci.*, Vol. 6, 371–376 (1901).
- [6] S. Nagaitsev et al., in *Proceedings of HB2010*, Morschach, Switzerland (2010), TH01D01.
- [7] A. Valishev et al., in *Proceedings of PAC11*, New York, NY (2011), WEP070.
- [8] I. Batalov, A. Valishev, *Fermilab Beams-doc-3959* (2011).
- [9] D. Shatilov et al., *Phys. Rev. ST Accel. Beams* **14**, 014001 (2011).

### 7.2.3 Space Charge Compensation in High Intensity Circular Accelerators

We propose to explore a novel scheme of space-charge compensation that could lead a significant increase of the beam intensity for future accelerator-based high-energy physics experiments and other sciences.

Through its past success in electron cooling of high-energy antiprotons [1], beam-beam compensation using the electron lens [2], and controlled halo removal by hollow electron beams [3], Fermilab has gained extensive experience and resources in manipulating high-energy particle beams by means of well-controlled electrons. As the mission of US high energy physics program is pushing the Intensity Frontier, it is of great technical and scientific merit for the community if this remarkable tradition of Fermilab can be applied to overcome the beam intensity limit in the present accelerator technology. Hence, we propose to investigate a novel method of space-charge compensation to achieve very intense and stable beams in circular accelerators through trapping and controlling of the electrons generated from beam-induced residual gas ionization. The method has a great potential to improve performance of leading high-current proton accelerator facilities and experiments, such as LBNE with Project-X intensities, Mu2e and "g-2" after the intensity upgrades, compressor and accumulation rings envisioned in the Neutrino Factory and Muon Collider projects. The method may also offer a transformational technology for the next generation high-intensity proton sources, e.g., such as those needed for the Accelerator

## Driven Systems.

The main idea of this compensation method is based on the long-known fact that the negative effect of Coulomb repulsion can be mitigated if beams are made to pass through a plasma column of opposite charge. This idea has been successfully applied to transport high-current low-energy proton and  $H^-$  beams into the RFQ in many linacs. In circular machines, partial neutralization by ionized electrons was attempted with notable improvements in beam intensity, namely one order of magnitude higher than the space-charge limit. However, the beam-plasma system was subject to strong transverse electron-proton (e-p) instability. In principle, this difficulty can be overcome if protons and electrons are immersed in a longitudinal magnetic field which is a) strong enough to freeze the electron density distribution; b) strong enough to suppress the e-p instability; c) weak enough to allow positive ions to escape transversely, in addition to longitudinal draining; and d) uniform enough to avoid beta-beat excitations. In addition, we note that significant improvements have been made on the physics of non-neutral plasmas and on the stability of beam-plasma systems in plasma physics community over past decade, some of which could be readily adopted for the present project.

The scope of this proposal will be based on the resources and facilities available at Fermilab within the five year timeline. The existing ion source (proton and  $H^-$ ), LEBT system, and RFQ of High Intensity Neutrino Source (HINS) program will be reused as an injector for the ring with currents up to 20 mA and energy of 2.5 MeV. The newly proposed Integrable Optics Test Accelerator (IOTA) ring, which is now under construction at Fermilab with completion expected in 2014, will be used to accumulate protons through charge-exchange injection. The Tevatron electron lens system, a nonlinear element to be installed in IOTA ring, can be used to trap electrons for the initial experiments. The scientific program will consist of both extensive theoretical modeling, and installation and operation of the test accelerator, outlined as follows:

- Studies of the physics of electron column formation and the stability of beam-plasma system
- Measurements of electron accumulation and beam-plasma stability at HINS beamline
- Design and construction of charge-exchange injection system for IOTA ring
- Installation of HINS front-end (with  $H^-$  source) to ASTA hall
- Measurements of electron accumulation and beam-plasma stability at IOTA ring using the electron lens system
- Upgrade of the electron lens system with dedicated diagnostic and control equipment

The present proposal perfectly fits the main thrusts of the Fermilab's accelerator R&D plan, it will create lots of synergies with other programs as well. For example, once the IOTA ring stores low energy proton beams, combined effects of space-charge compensation and nonlinear integral optics could be readily studied.

The ASTA facility will offer unique opportunities to carry out the proposed research toward demonstration of the feasibility of the space-charge compensation methods, such as with electron columns, electron lenses, or in combination of the two with the elements of the integrable optics technique. That research requires a dedicated storage ring (IOTA) and its operation with protons. It cannot be carried out anywhere else as there are no existing proton storage rings or synchrotrons which can afford the installation of special insertions (columns, lenses, etc.), and offer special arrangements of the optics lattice and precise control of the insertion devices and the ring elements.

### **7.2.3.1 References**

- [1] S. Nagaitsev et al., Phys. Rev. Lett. 96, 044801 (2006)
- [2] V. Shiltsev et al., Phys. Rev. Lett. 99, 244801 (2007)
- [3] G. Stancari et al., Phys. Rev. Lett. 107, 084802 (2011)

### **7.2.4 Optical Stochastic Cooling Experiment at ASTA**

Besides the experiments on highly non-linear integrable optics, the 150 MeV electron storage ring IOTA at ASTA will be used to carry out a test of optical stochastic cooling (OSC) method. This method is novel approach to the beam dynamics paper and has potential serious implications for a range of heavier (than electron) particle accelerators, ranging from LHC and Muon Collider to other rings. The accelerator experts called for an experimental demonstration of OSC for a long time.

The experiment will have two phases: at the first step the cooling will be achieved without optical amplifier. It should introduce the damping rates higher than the cooling rates due to synchrotron radiation. At the second phase, an optical amplifier will be used.

The ASTA facility will offer unique opportunity to carry out the proposed research toward demonstration of the feasibility of the optical stochastic cooling technique. That research requires a dedicated storage ring (IOTA) and its operation with 100-150 MeV electrons. It cannot be carried out anywhere else as there are no existing electron storage rings in that energy range which can afford installation of special insertions (optical equipment, wigglers, etc.), and offer special arrangements of the optics lattice and precise control of the insertion devices and the ring elements. Previous attempts to identify such an existing facility were unsuccessful (e.g., the proposal to use MIT-Bates storage ring was found to be very expensive as the ring nominal energy and size were significantly beyond what was needed for the OSC demonstration).

### 7.2.4.1 Introduction

The stochastic cooling suggested by Simon Van der Meer [1,2] has been successfully used in a number of machines for particle cooling and accumulation. However it is not helpful for cooling of bunched beams in proton-(anti)proton colliders due to very high phase density of the bunches. In the case of optimal cooling the maximum damping rate can be estimated as:

$$\lambda \approx \frac{2W\sigma_s}{NC} ,$$

where  $W$  is the bandwidth of the system,  $N$  is the number of particles in the bunch,  $\sigma_s$  is the rms bunch length, and  $C$  is the machine circumference. For the LHC proton beam ( $\sigma_s = 9$  cm,  $C = 26.66$  km) and a system with one octave band and its upper boundary of 8 GHz one obtains  $\lambda^{-1} = 12000$  hour. An effective cooling requires faster damping rates by least 3 orders of magnitude. The OSC suggested by M. Zolotarev [3] can have a bandwidth of  $\sim 10^{14}$  Hz and, thus, suggests a way to achieve required damping rates. The basic principles of the OSC are similar to the normal (microwave) stochastic cooling but, in difference to it, it uses optical frequencies, allowing an increase of system bandwidth by 4 orders of magnitude.

In the OSC a particle radiates e.-m. radiation in the pickup wiggler. Then, the radiation amplified in an optical amplifier makes a longitudinal kick to the particle in the kicker wiggler as shown in Figure 1. Further we will call these wigglers pickup and kicker. A magnetic chicane is used to make space for an optical amplifier and to bring the particle and the radiation together in the kicker wiggler. In further consideration we assume that the path lengths of particle and radiation are adjusted so that the relative particle momentum change is equal to:

$$\delta p / p = -\kappa \sin(k \Delta s) . \tag{1}$$

Here  $k = 2\pi/\lambda$  is the radiation wave number, and  $\Delta s$  is the particle displacement on the way from the pickup wiggler to the kicker wiggler relative to the reference particle which obtains zero kick:

$$\Delta s = M_{51}x + M_{52}\theta_x + M_{56}(\Delta p / p) \tag{2}$$

Here  $M_{5n}$  are the elements of 6x6 transfer matrix from pickup to kicker,  $x$ ,  $\theta_x$  and  $\Delta p/p$  are the particle coordinate, angle and relative momentum deviation in the pickup.

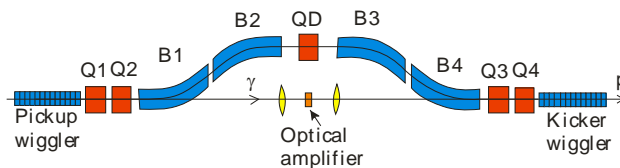


Figure 1: OSC schematic.

For small amplitude oscillations the horizontal and vertical cooling rates are [4]:

$$\begin{bmatrix} \lambda_x \\ \lambda_s \end{bmatrix} = \frac{k\kappa}{2} \begin{bmatrix} M_{56} - C\eta_{pk} \\ C\eta_{pk} \end{bmatrix}, \quad (3)$$

where  $\eta_{pk} = (M_{51}D_p + M_{52}D'_p + M_{56})/C$  is the partial momentum compaction determined so that for a particle without betatron oscillations and with momentum deviation  $\Delta p/p$  the longitudinal displacement relative to the reference particle on the way from pickup and kicker is equal to  $C\eta_{pk}\Delta p/p$ . Here we also assume that there is no x-y coupling. Introduction of x-y coupling outside the cooling area allows redistribution of horizontal damping rate into both transverse planes. The sum of damping rates,  $\Sigma\lambda_n = k\kappa M_{56}/2$ , does not depend on the beam optics outside of the cooling chicane.

An increase of betatron and synchrotron amplitudes results in a decrease of damping rates [4]:

$$\begin{aligned} \lambda_x(a_x, a_s) &= F_x(a_x, a_s)\lambda_x, \\ \lambda_s(a_x, a_s) &= F_s(a_x, a_s)\lambda_s, \end{aligned} \quad (4)$$

where the fudge factors are:

$$\begin{aligned} F_x(a_x, a_s) &= 2J_0(a_s)J_1(a_x)/a_x, \\ F_s(a_x, a_s) &= 2J_0(a_x)J_1(a_s)/a_s; \end{aligned} \quad (5)$$

and  $a_x$  and  $a_s$  are the amplitudes of longitudinal particle motion due to betatron and synchrotron oscillations expressed in the units of e.-m. wave phase:

$$\begin{aligned} a_x &= k\sqrt{\varepsilon_1(\beta_p M_{51}^2 - 2\alpha_p M_{51}M_{52} + (1 + \alpha_p^2)M_{52}^2)}, \\ a_p &= kC|\eta_{pk}|(\Delta p/p)_{\max}. \end{aligned} \quad (6)$$

Here  $\varepsilon_1$  is the Courant-Snyder invariant of a particle, and  $(\Delta p/p)_{\max}$  is its maximum momentum deviation. As one can see from Eqs. (4) and (5) the damping rate changes sign if any of amplitudes exceeds the first root of the Bessel function  $J_0(x)$ ,  $a_x, a_s > \mu_0 \approx 2.405$ .

The following conclusions can be drawn from Eqs. (3) and (6).  $M_{56}$  depends only on focusing inside the chicane, while  $\eta_{pk}$  additionally depends on the dispersion at the chicane beginning, *i.e.* on the optics in the rest of the ring. Consequently, the damping rates ratio,

$$\lambda_x / \lambda_s = M_{56} / C\eta_{pk} - 1 \quad (7)$$

and the longitudinal cooling range,

$$n_{\sigma_s} \equiv (\Delta p/p)_{\max} / \sigma_p = \mu_0 / |kC\eta_{pk}\sigma_p|, \quad (8)$$

depend on focusing and dispersion inside the chicane, but do not depend on the beta-function. Here  $\sigma_p$  is the relative rms momentum spread. In contrary, the transverse cooling range,

$$n_{\sigma_x} \equiv \frac{\varepsilon_{\max}}{\varepsilon} = \frac{\mu_0^2 / (k^2\varepsilon)}{\beta_p M_{51}^2 - 2\alpha_p M_{51}M_{52} + (1 + \alpha_p^2)M_{52}^2}, \quad (9)$$

does not depend on the dispersion but depends on the beta-function. Here  $\varepsilon$  is the rms momentum spread.

Below we consider two cooling schemes. The first one is passive cooling [5] where radiation is focused into the kicker wiggler but is not amplified; and the second one is active where an optical amplifier is used. Both of them have its advantages and drawbacks. In the case of passive cooling one does not need an amplifier and, consequently, can use higher optical frequencies and larger bandwidth which boost the gain. It also requires smaller path difference which considerably increases the cooling ranges,  $n_{os}$  and  $n_{ox}$ . In the case of active system one can reduce the length and magnetic field of the wigglers, but it requires an additional delay in the chicane to compensate a delay in the optical amplifier ( $\sim 5$  mm). Making an amplifier at required power and wavelength can be a challenging problem too.

#### 7.2.4.2 Beam Optics

The main parameters of the ring, called IOTA [6], are shown in the Table I. The OSC system will take one of four straight sections with length of  $\sim 5$  m. The beta-function and dispersion in the section are presented in Figure 2. The optics was build for 800 nm radiation where an optical amplification is a feasible task. The following limitations were taken into account in the optics design. The chicane should separate the radiation and the beam by 40 mm making a sufficiently large separation between the electron beam and optical amplifier. The cooling ranges,  $n_{os}$  and  $n_{ox}$ , (before the OSC is engaged) have to be large enough so that the major fraction of the beam would be cooled. The path length difference acquired by electron beam in the chicane has to be large enough to compensate delay in optical amplifier. Note that the rectangular dipoles do not produce horizontal focusing. Therefore in the absence of other focusing inside chicane the partial slip factor is equal to  $M_{56}/C$  and does not depend on the dispersion. Consequently, there is no transverse cooling. To achieve it a defocusing quad was introduced in the chicane center. The strength of this quad is limited by reduction of transverse cooling range,  $n_{ox}$ . That required sufficiently large dispersion in the chicane. The major parameters of the cooling section are presented in Table II.

Table I: Main Parameters of IOTA storage ring

|   |                       |
|---|-----------------------|
| Circumference   | 38.7 m                |
| Nominal beam energy                                     | 150 MeV               |
| Bending field   | 7 kG                  |
| Betatron tune   | 3.5 ÷ 7.2             |
| Maximum $\beta$ -function                               | 3 ÷ 9 m               |
| Transverse vertical emittance, non-normalized           | 3 nm r.m.s            |
| Rms momentum spread, $\sigma_p$                         | $1.5 \cdot 10^{-4}$   |
| SR damping rates (ampl.), $\lambda_s / \lambda_{\perp}$ | 4 / 2 s <sup>-1</sup> |

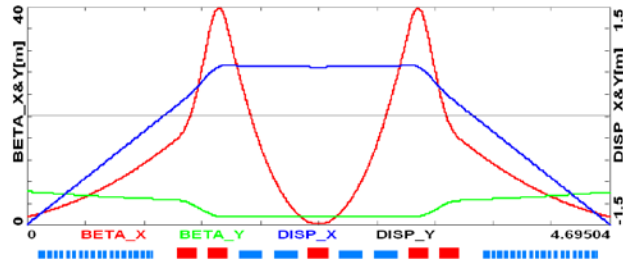


Figure 2: Optics functions in the OSC section.

Table II: Major parameters of chicane beam optics

|  |         |
|--|---------|
| $M_{56}$                                     | 8.7 mm  |
| Cooling rates ratio, $\lambda_x/\lambda_s$   | 7.5     |
| Horizontal beam separation                   | 40 mm   |
| Delay in the chicane                         | 4.5 mm  |
| Cooling ranges (before OSC), $n_{ox}/n_{os}$ | 3.5 / 2 |
| Dipole magnetic field                        | 4 kG    |
| Dipole length                                | 18 cm   |
| Strength of central quad, $\int GdL$         | 1.52 kG |
| Strength of central quad, $\int GdL$         | 1.52 kG |

The rms emittance and momentum spread are comparatively large for the chosen wavelength of 800 nm. To accommodate it the optics was tuned to maximize the cooling ranges. In particular, we choose (1) the large cooling rates ratio to increase  $n_{os}$ , and (2) small beta-function in the chicane center (2 cm) to increase  $n_{ox}$ . That resulted in high sensitivity of cooling parameters. Simulations show that relative accuracies should be of  $\sim 1\%$  for horizontal beta-function,  $\sim 2$  cm for dispersion, and  $\sim 2\%$  for the focusing of central quadrupole (see Figure 3)

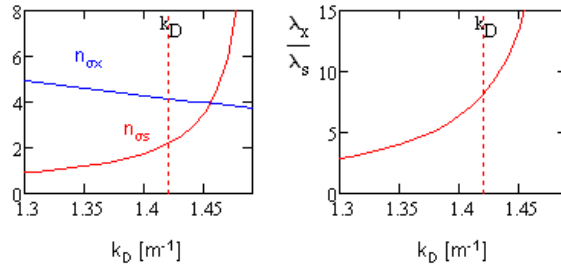


Figure 3: Dependencies of cooling ranges (left) and ratio of damping rates on focusing strength of central quadrupole.

### 7.2.4.3 Light optics

Let a particle to be moving in the flat undulator so that its coordinates depend on time as following:

$$\begin{aligned} v_x &= c\theta_e \sin \tau', & v_y &= 0, \\ v_z &= c \left( 1 - \frac{1}{2\gamma^2} - \frac{\theta_e^2}{2} \sin^2 \tau' \right), & \tau' &= \omega_u t' + \psi, \end{aligned} \quad (10)$$

where  $\gamma$  is the particle relativistic factor ( $\gamma \gg 1$ ), and  $\omega_u$  is the frequency of particle motion in the undulator.. Substituting velocities of Eq. (10) to the Liénard-Wiechert formula [7] for the horizontal component of electric field in the far zone one obtains:

$$\begin{aligned} E_x(r, t) &= 4e\omega_u \gamma^4 \theta_e \cos \tau' \times \\ & \frac{1 + \gamma^2 \left( \theta^2 (1 - 2\cos^2 \phi) - 2\theta\theta_e \sin \tau' \cos \phi - \theta_e^2 \sin^2 \tau' \right)}{cR \left( 1 + \gamma^2 \left( \theta^2 + 2\theta\theta_e \sin \tau' \cos \phi + \theta_e^2 \sin^2 \tau' \right) \right)^3}, \end{aligned} \quad (11)$$

where  $\theta$  and  $\phi$  are the angles for the vector from the radiation point,  $\mathbf{r}'$ , to the observation point,  $\mathbf{r}$ , in the polar coordinate system,  $R = |\mathbf{r} - \mathbf{r}'|$ , and  $t - t' = R/c$ . In further calculations we will be leaving the radiation in the first harmonic only,

$$\begin{aligned} E_\omega(r) &= \frac{\omega(\theta)}{\pi} \int_0^{2\pi/\omega(\theta)} E_x(r, t) e^{-i\omega t} dt, \\ \omega(\theta) &= 2\gamma^2 \omega_u / \left( 1 + \gamma^2 \left( \theta^2 + \theta_e^2 / 2 \right) \right), \end{aligned} \quad (12)$$

assuming that the radiation of higher harmonics is absorbed in the lenses and/or not amplified by optical amplifier. Then taking into account delay in the lens and applying Kirchhoff formula,

$$E(r'') = \frac{1}{2\pi ic} \int_S \frac{\omega(\theta) E_\omega(r)}{|r'' - r|} e^{i\omega|r'' - r|} ds, \quad (13)$$

one obtains the electric field in the focal point. For large acceptance lens,  $\theta_m \geq \theta_e + 3/\gamma$ , located in the middle of pickup-to-kicker distance the results of numerical integration can be interpolated by the following equation:

$$E_x = 4e\omega_u^2 \gamma^4 \theta_e F(\gamma\theta_e) / (3c^2), \quad (14)$$

$$F(K) \approx 1 / (1 + 2.15K^2 + 1.28K^4), \quad K \leq 4,$$

where  $K = \gamma\theta_e$  is the undulator parameter, and  $\theta_m$  is the lens angular size from the radiation point. Integrating the force along the kicker length one obtains the longitudinal kick amplitude:

$$c\delta p_{\max} \equiv \kappa c p = 2e^4 B_0^2 \gamma^2 L F(K) / (3m^2 c^4). \quad (15)$$

The bandwidth of the system is much more narrow ( $\leq 10\%$ ) if an optical amplifier is used. In this case the kick value is:

$$c\delta p_{\max} = \frac{2e^4 B_0^2 \gamma^4 L \theta_m^2}{m^2 c^4 (1 + K^2)^3} = \frac{2e^4 B_0^2 \gamma^4 L}{m^2 c^4 (1 + K^2)^3} \frac{\Delta\omega}{\omega}, \quad (16)$$

where in the second equality we assumed that  $\gamma^2 \Delta\theta_m^2 = (1 + K^2) \Delta\omega / \omega$ .

Above we assumed that the radiation coming out from pickup is focused in the particle location in the course of particle entire motion in the kicker. It can be achieved if the distance to the lens is much larger than the length of wiggler – the condition which is impossible to achieve in practice. A practical solution can be obtained with lens telescope which has the transfer matrix from the center of pickup to the center of kicker equal to  $\pm \mathbf{I}$ , where  $\mathbf{I}$  is the identity matrix. The simplest telescope has 3 lenses as shown in Figure 4. For symmetrically located lenses their focusing distances are:

$$F_1 = \frac{LL_1}{L + L_1}, \quad F_2 = \frac{L_1^2}{2(L + L_1)}. \quad (17)$$

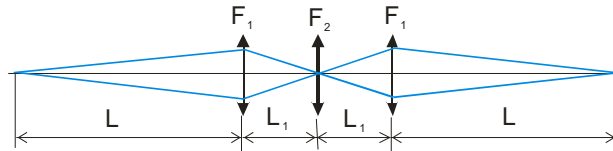


Figure 4: Light optics layout for passive cooling.

Table III presents main parameters of undulators, light optics and OSC damping rates for the passive and active OSC. The passive cooling requires about one octave band (0.8-1.6  $\mu\text{m}$ ). The wave packet lengthening looks satisfactory for 4.5 mm light delay in magnesium fluoride. However a suppression of transverse focusing chromaticity looks as an extremely challenging problem and needs additional study. Combination of glasses with normal and abnormal dispersions looks as a good direction for the study. A Ti:sapphire optical amplifier is considered as a good candidate capable to deliver  $\sim 20$  Db gain within the allocated signal delay. Technical details are presently under study.

Table III: Main parameters of OSC

|                                     |                            |
|-------------------------------------|----------------------------|
| Undulator parameter, K              | 1.5                        |
| Undulator period                    | 6.53 cm                    |
| Number of periods                   | 14                         |
| Total undulator length              | 0.915 m                    |
| Distance between undulators         | 3.6 m                      |
| Telescope length, $2L_1$            | 0.25 m                     |
| Telescope aperture, $2a$            | 40 mm                      |
| Lens focal distances, $F_1 / F_2$   | 116 / 4.3 mm               |
| Damping rates of passive OSC(x/y/s) | 100/100/25 s <sup>-1</sup> |
| Damp. rates 20 Db gain & 10% band   | 300/300/75 s <sup>-1</sup> |

#### 7.2.4.4 References

- [1] S. Van der Meer, "Stochastic damping of betatron oscillations", internal report CERN/ISR PO/72/31 (1972).
- [2] J. Bisognano and C. Leemann, "Stochastic Cooling" in 1981 Summer School on High En. Part. Accelerators, AIP Conf. Proceedings 87, Melville, NY, 1982, pp. 584-655.
- [3] M. S. Zolotarev and A. A. Zholents, Phys. Rev. E, **50**, 4, p. 3087 (1994).
- [4] V. Lebedev, p. 644, HB-2010, (2012).
- [5] A. Mikhailichenko, Phys. Rev. ST Accel. Beams **11**, 011302 (2008).
- [6] S. Nagaitsev, *et. al.*, p.16, IPAC-2012, (2012).
- [7] L. D. Landau, "Classical theory of fields", Nauka (1973).

### 7.2.5 Investigation of Acceleration and Cooling of Carbon-Based Crystal Structures for Muon Accelerators

#### 7.2.5.1 Objective

For the past decade, the HEP community has been greatly interested in muon accelerators since their low radiative losses enable particles to rapidly reach high energies. Complete development of a high gradient accelerator for an operational HEP  $\mu^+\mu^-$  collider [1], however, still faces various challenges [2]. On account of the small nucleus collision, the idea of using

atomic structures for muon acceleration has thus been widely investigated for many years. Recent work on radiative damping of channeled particle emittance has opened up the possibility of achieving both high luminosity and high energy in a crystal collider [3-6]. High gradient channeling of crystals offers a variety of opportunities for future accelerator R&D to accomplish high luminosity and high energy. Extending the scheme, we propose to develop an effective method for cooling and accelerating muons by using carbon-based nanostructures (CNT). The development of ultra-short pulse lasers, nanofabrication technology and a better experimental and theoretical understanding of high energy density effects in solids motivate us to examine the topic of a nano-channel accelerator. Large channels, wide acceptance angles, robust structural and thermal strengths, superconducting properties, exceptional capillarity, and high photon absorption make crystallographic nanostructures a unique alternative for muon accelerator application. Leading schemes for a future high energy  $\mu^+\mu^-$  collider rely on fast cooling and high gradient acceleration of short-lived muons. This project aims to prove that both processes can be integrated and achieved in the strong focusing environment of a nanostructure system. Practical demonstration of transverse cooling in a continuous focusing channel and verification of theoretically predicted cooling efficiencies are the first steps towards meeting the challenges of  $\mu^+\mu^-$  colliders. Furthermore, experimental demonstration of high-acceleration gradients around GeV/m promised by the high fields in a nanotube would make a muon accelerator a real possibility. We expect that successfully accomplishing the proposed missions will leverage current US muon collider R&D such as the Muon Accelerator Program (MAP) and Neutrino Factories.

The proposed research requires the highest available average power for electron beams (for muon production) and X-rays (for crystal excitation and damage studies) and the unique parameters of ASTA facility are the best fit to the needs of this proposal.

### **7.2.5.2 Technical Approach**

The density of charge carriers (conduction electrons) in solids  $n_0 \sim 10^{22-23} \text{ cm}^{-3}$  is significantly higher than what was considered above in plasma, and correspondingly, the longitudinal fields of up to 100 GeV/cm or 10 TV/m are possible. However, as particles in crystals escape from a driving field due to fast pitch-angle diffusion resulting from increased scattering rates, it was thus suggested that particles are accelerated along major crystallographic directions, which provide a channeling effect in combination with low emittance determined by an Angstrom-scale aperture of the atomic "tubes." In principle, a crystal channel can hold  $> 10^{13} \text{ V/cm}$  transverse and  $10^9 \text{ V/cm}$  longitudinal fields that are ideally applicable to fast muon cooling and acceleration. However, the major challenge of this x-ray channeling acceleration is that ultimate acceleration gradients  $\sim 10 \text{ TeV/m}$  might require relativistic intensities at hard x-ray regime ( $\hbar\omega \approx 40 \text{ keV}$ ), exceeding those conceivable for x-rays as of today [4], though x-ray lasers can efficiently excite solid plasma and accelerate particles inside a crystal channel waveguide. Moreover, only disposable crystal accelerators, e.g., in the form of fibers or films, are possible at such high externally excited fields which would exceed the ionization thresholds and destroy the periodic atomic structure of the crystal, so acceleration will take place only in a short time before full dissociation of the lattice [7].

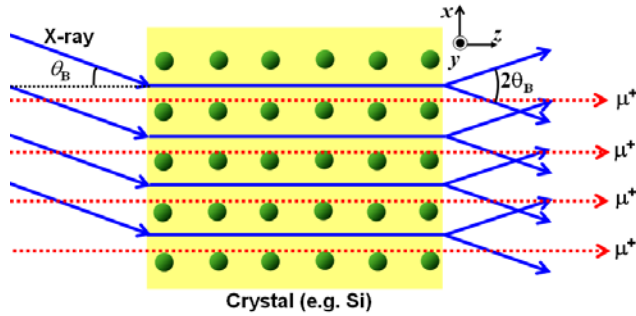


Fig. 1: Bormann anomalous transmission (BAT). When the x rays are injected at the Bragg angle, the Bormann effect takes place. Particle beams are injected along the crystal axis.

As nano-structures have a much wider range of flexibility, including superior physical strength, there were some efforts [8], [9] of replacing crystals with nano-structures for beam control such as collimation, bending, and refraction. Beyond the effort of these previous studies, we found that nanostructures have great potential to support fast muon cooling and acceleration via channeling interaction. In the channeling process (Fig. 1), the photon energy is taken at the hard x-ray range of  $\hbar\omega \approx mc^2\alpha$  and the linac structure is replaced by a crystal structure (e.g., silicon). Here the crystal axis provides the channel through which accelerated particles propagate with minimum scattering (channeling [10]) and the x rays are transmitted via the Bormann effect (anomalous transmission [11], [12]) when the x rays (wavelength  $\lambda$ ) are injected in the xz plane with a polarization in their plane into a crystal at the Bragg angle  $\theta_B$ ,  $\lambda/2b = \sin\theta_B$ . The row of lattice ions (perhaps with inner-shell electrons) constitutes the "waveguide" wall for x rays, while they also act as periodic irises to generate slow waves. A superlattice (in which the relative concentration  $c$  ranges from 0 to 1 over  $100 \text{ \AA}$  or longer in the longitudinal  $z$  direction) brings in an additional freedom in the crystal structure and provides a small Brillouin wave number  $k_s = 2\pi/s$  with  $s$  being the periodicity length. The x-ray light in the crystal channel walls becomes a slow wave and satisfies the high-energy acceleration condition,  $\omega/(k_z + k_s) = c$ , where  $\omega$  and  $k_z$  are the light frequency and longitudinal wave number [13].

The major challenge of this channeling acceleration is that:

- (1) Crystals (lattice constant of  $3 \sim 4 \text{ \AA}$ ) have efficient beam-wave coupling at very high x-ray energy ( $\sim 40 \text{ keV}$ ) with high diffraction orders, according to the Bormann transmission condition. This photon energy could be significantly lowered with a larger lattice constant.
- (2) In order to overcome losses of muon energy of  $\approx 10 \text{ MeV/cm}$ , the x-ray field must exceed  $E_x = 10^{11} \text{ V/cm}$ , corresponding to the power density of  $3 \times 10^{19} \text{ W/cm}^2$ . The required peak power for the electric field is  $3 \times 10^9 \text{ W}$  with the minimal size is  $L = 2 \times 10^3 a_B = 10^{-5} \text{ cm}$ . The energy losses of moving particles due to ionization, bremsstrahlung, and nuclear collisions

could be significantly reduced with increasing a lattice-to-lattice distance (reducing number of scatters/a unit cell).

- (3) Such high externally excited fields would exceed the ionization thresholds and destroy the periodic atomic structure of the crystal. It is well known that carbon-based nano-composites have excellent thermal and mechanical strength. In particular, the [chemical bonding](#) of carbon nanotubes (CNTs) is composed entirely of [sp<sup>2</sup> bonds](#), which are stronger than the [sp<sup>3</sup> bonds](#) found in [alkanes](#) and [diamond](#). CNTs are expected to be very good [thermal conductors](#) along the tube, exhibiting a property known as "[ballistic conduction](#)", but good insulators laterally to the tube axis. CNT has a room-temperature thermal conductivity along its axis of about 3500 W·m<sup>-1</sup>·K<sup>-1</sup> (copper: 385 W·m<sup>-1</sup>·K<sup>-1</sup>) The temperature stability of carbon nanotubes is estimated to be up to 2800 °C in a [vacuum](#) and about 750 °C in air.

Carbon nanostructures have various prospective advantages over crystals for muon acceleration such as wider channels (weaker de-channeling), broader beams (using nanotube ropes), wider acceptance angles (< 0.1 rad), lower minimum ion energies, 3D beam control over greater lengths, and in particular excellent thermal and mechanical strength, which are ideally fit to x-ray channeling acceleration and cooling application, plus beam extraction, steering, and collimation.

### **(1) CNT Survivability in X-ray Channeling Cooling and Acceleration Processes**

There are four possible energy sources capable of damaging a crystal undergoing channeling acceleration process (acceleration, laser, lattice ionization, and particle collision). As an acceleration gradient is proportional to a square root of electron density,  $n_0$ , and power proportional to  $n_0$ , channeling acceleration of 100 GeV/m accompanies impact of 10<sup>19</sup> W/cm<sup>3</sup> or 10<sup>5</sup> J/cm<sup>3</sup> to atomic layers. Crystals like silicon will sustain this energy for the order of 10 fs. Nano-second laser pulses deliver a 10<sup>12</sup> W/cm<sup>3</sup> power density in general and the temporal fracture threshold with < 0.1 mm skin depth is the order of 0.1 ns with 10<sup>13</sup> W/cm<sup>3</sup>. Lattice ionization threshold is 10<sup>15</sup> ~ 10<sup>16</sup> W/cm<sup>2</sup> with laser pulses. For high energy particle beams, crystals can endure 10<sup>11</sup> A/cm<sup>2</sup> current density for 10 fs. These damage time scales may not enable crystals to properly support sufficient energy gain before being destroyed. An accelerator structure should be strong enough to endure the ambient interaction energies for acceleration and relaxation times. Typical electron density of CNT is  $\sim 3 \times 10^{21}/\text{m}^3$ , ( $\omega_p \approx 3$  THz plasma frequency), so a CNT can endure 30 ps with the same level of impact, which is 3000 times longer than those of a silicon crystal. Within this time, the lattice remains sufficiently regular to allow x-ray channeling acceleration.

### **(2) Fast 6D Cooling**

Some previous theoretical results [14 – 16] on the radiative interaction of charged particles in a continuous focusing channel present an efficient method to damp the transverse emittance of the beam without diluting the longitudinal phase space significantly.

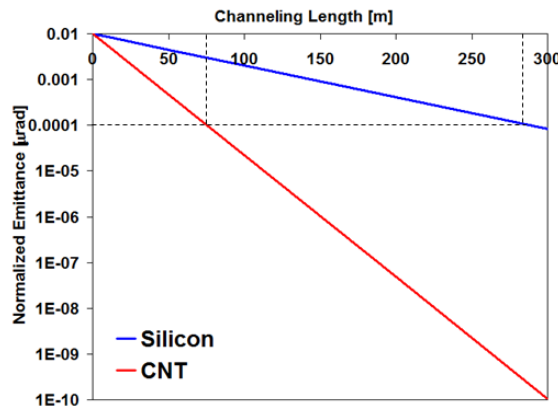


Fig. 2: Phase-space cooling efficiency vs. channeling distance of (a) silicon <110> and (b) armchair CNT.

The ionization energy loss [14] experienced by high energy channeling planes offers a fast muon cooling scheme. Relativistic muons passing through the channel lose energy uniformly in both the transverse and longitudinal directions. After passing through a short section of a channel ( $\Delta L \ll \Lambda$ :  $\Delta L$  is the crystal length and  $\Lambda$  is the characteristic damping length) muons are re-accelerated longitudinally to compensate for the lost longitudinal energy. Combining both processes (ionization energy loss and re-acceleration) leads to the transverse emittance shrinkage. For muon channeling in a dielectric channel, the dominant scattering process comes from elastic (Rutherford) muon scattering off the conduction electrons, which are present in the channel. The cooling efficiency of a crystal channel ( $L, \Lambda$ ) is normally expressed by the normalized transverse emittance evolution,  $\varepsilon_N = \varepsilon_N^0 e^{-L/\Lambda} + \Lambda \alpha (1 - e^{-L/\Lambda})$ . Figure 2 shows theoretical estimation of a <110> silicon crystal and single wall CNT (SWCNT) of armchair type under the same cooling condition. Assuming characteristic damping length,  $\Lambda$ , of 62.5 m, under the same cooling condition a CNT requires a 4 times shorter muon traveling distance,  $\sim 70$  m, to achieve the same normalized emittance. The strong focusing in a CNT channel results in the ultra small beta function, so it is quite feasible to decrease the transverse emittance of a muon beam by a few orders of magnitude. With the inter-planar electric fields of  $10^9$  V/cm, muon radiation length could be several kilometers. However, the extremely large transverse electric field ( $10^{13}$  V/cm) considerably decreases the length by strong radiation damping. In principle, high efficiency radiation cooling can be achieved even within several meters with the transverse electric field configuration. Furthermore, re-directing particles from one channel to the other by altering inter-planar trajectory can even further squeeze the muon beam within the smaller space. Therefore, the radiation damping can occur together with the ionization loss/re-acceleration, which will be highly effective for the muon cooling process.

### (3) X-ray channeling acceleration through nanotubes

As depicted in Fig. 3(a), X-ray photon energy for Borrmann anomalous transmission steeply decreases with increases of Bragg angle and crystal lattice constant. With increasing Bragg

angle, traveling photon modes of higher diffraction orders, which may have a decent longitudinal beam-wave synchronizing coupling and a good longitudinal group velocity, will lose transmission coupling efficiency into a crystal.

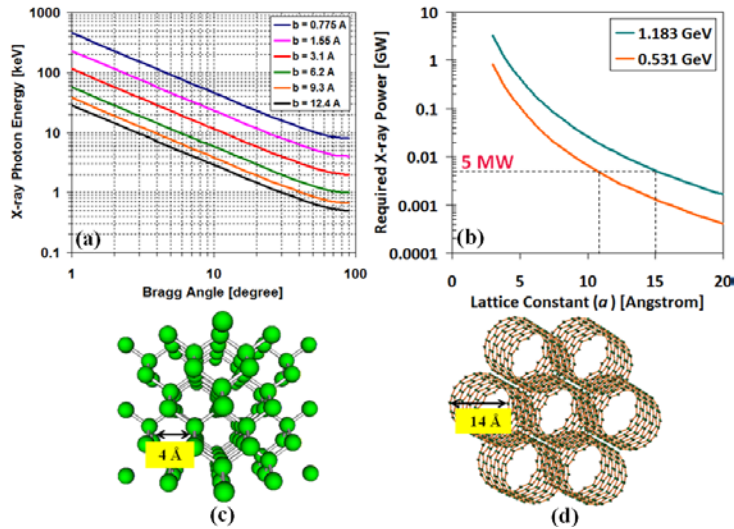


Fig. 3: (a) X-ray photon energy versus Bragg angle for Bormann Anomalous Transmission (BAT) with respect to lattice constants (b) minimum x-ray power versus lattice constant graph (c) front view of channels  $\langle 110 \rangle$  in silicon (d) entrance of a rope of SWCNT.

Therefore, increasing a lattice constant rather than an incident angle would be a better way to reduce an x-ray photon energy required for channeling acceleration. In Fig. 3(a), 40 keV photon energy for the 10<sup>th</sup> diffraction order with the lattice constant of 3.1 Å is lowered to 10 keV with 12.4 Å at the same angle ( $\sim 3$  degree), which would be more feasible with existing high energy X-ray radiation facilities. As shown in Figs. 3(c) and (d), a typical single-wall CNT has a few times larger unit cell dimension (tube radius), possibly lowering coupling photon energy for BAT coupling. The minimum x-ray power required to overcome intrinsic losses for channeling acceleration can be also significantly lowered. In order to overcome losses ( $\sim 10$  MeV/cm) of muon beams ( $\nu = 0.996c$ : 1.18 GeV,  $\nu = 0.98c$ : 0.53 GeV), while a silicon of 3 Å lattice constant (Fig. 3(c)) will need at least 3 GW x-ray laser with  $L (= 2 \times 10 \times a_B) = 10^{-5}$  cm:  $a_B =$  Bohr radius) spot size, a 14 Å wide CNT (Fig. 3(d)) will only require  $\sim 5$  MW under the same condition. Therefore, nanostructures can significantly mitigate the constraints of x-ray condition ( $< 10$  keV and  $5 < \text{MW}$ ). The idea is thus a promising alternative for high gradient acceleration as it makes the channeling accelerator viable with existing test facilities. Chemical synthesis has wide range of flexibility to fabricate tubes with different sizes, so the beam-wave synchronization at lower photon energies and diffraction orders will be readily controlled by changing tube-dimensions.

Figure 4 is the preliminary Finite-Difference-Time-Domain simulation with silicon crystal, showing guided traveling waves at the resonance condition of the 10<sup>th</sup> diffraction order (Si). The

transmission behavior in the simulation well agrees with theoretical prediction in that transmission intensity increases with the slab thickness. The simulation technique will be applied to BAT simulation of nanotubes.

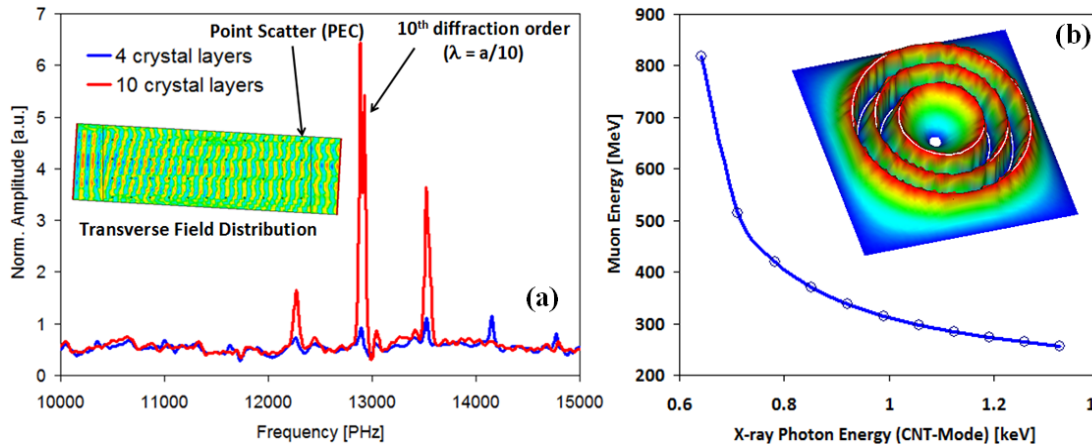


Fig. 4: (a) CST simulation of BAT with  $\langle 110 \rangle$  silicon at Bragg angle (b) synchronized muon versus x-ray energy graph in the CNT (inset: 3D electrostatic potential distribution of multiwall CNT).

Figure 4 (b) shows electrostatic potential distribution designed with the atomic potentials of a multiwall CNT with a carbon lattice constant (0.142 nm). In Figs. 4(b), the dispersion curve obtained from eigenmode simulations clearly indicates that X-ray photons (guided fundamental transverse mode:  $l = 0$ ) of  $\sim 0.65 - 1.35$  keV are synchronously coupled with muons of 250 – 830 MeV in a 1.4 nm wide nanotube. Numerically obtained static potential data will be transferred to the subsequent tracking and particle-in-cell (PIC) simulation codes. A broad range of multi-physics simulation modeling, including EM/optics/RF, particle tracking/beam optics, particle-in-cell (PIC), thermal/mechanical stresses, plasma/fluid dynamics, etc, will be performed to prove feasibility of nanotube for ultra-fast 6D cooling and TeV/m acceleration performance.

### 7.2.5.3 Experimental Plan for Feasibility Test

We also envision pursuing preliminary experiments of muon cooling and acceleration with a CNT sample, which will depend upon available muon and x-ray sources. Understanding a physical impact of high energy particles to nano-crystals is one of the most critical factors to estimate durability and cooling/acceleration dynamics of a CNT under high intensity and high energy channeling and acceleration conditions. The CNT beam collision test will be performed at this test area which utilizes a low-energy beam (50 MeV). A CNT film target will be collided with 50 MeV and 1.3 kA electron bunches. The beam-collided samples will be moved to NIU to analyze optical and electronic properties using microwave/THz transmission and DC resistance measurement techniques. The test will be followed by structural deformation analysis using the scanning electron microscope and X-ray diffraction that are currently available in NIU. The test

station will also be designed with a rotational stage, which will enable us to measure changes of CNT parameters dependent upon incident angle.

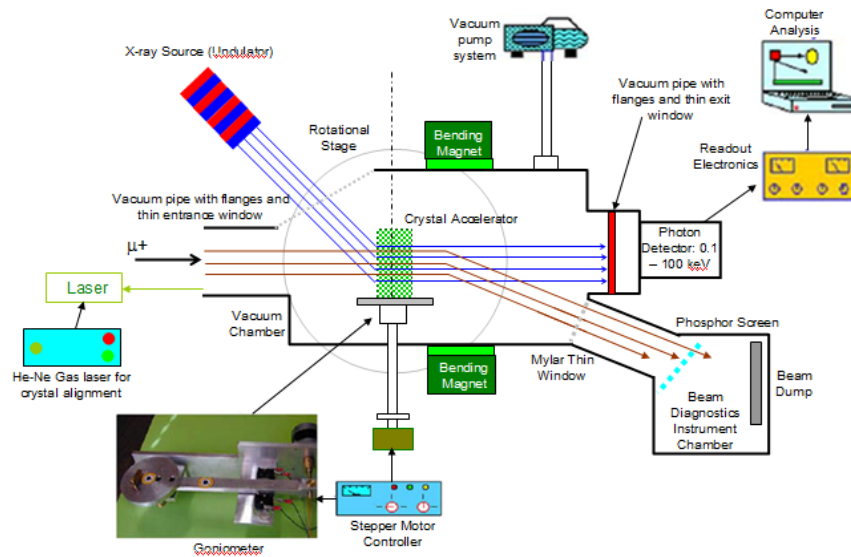


Fig. 5: Schematic layouts of muon cooling/acceleration test system.

A prompt procurement of the x-ray and muon sources will enable us to attempt experimental tests to prove theory and simulations. The first step is to measure initial and final emittances of CNTs. This way we can identify channeled and unchanneled particles on an event-by-event-basis. It is also possible to separate channeled and unchanneled muons by plotting their energy loss. The trigger will be provided by scintillation counters upstream, combined with a veto counter that rejects muons which do not intersect the crystal. A time-of-flight counter will be placed in a downstream position, to be used in concert with the timing pulse provided by the Fermilab beamlines. This will aid in particle identification since some positrons and pions will likely contaminate the beam. We will also detect predicted channeling radiation by surrounding the sample with CsI scintillation detectors, which are sensitive to x-rays. Direct modification of the beamline will provide a collimated beam of forward-decay muons at high intensity. In the same experimental chamber, acceleration of x-ray channeling will also be tested by measuring energy variation of muons channeling through an x-ray illuminated CNT sample at the entrance and exit of the system (Fig. 6). After interaction, the muon trajectory is deflected by bending magnets to beam dump in order to segregate a deflected x-ray beam from the muon beam. Optical energy of x-rays will be transferred to the muon beam with an efficiency of GeV per meter. A CNT array bundle would provide a GeV order of energy burst. Using a bending magnet in between drift chambers, we will measure the final energy of muons channeling through the tubes. The initial energy of each muon is provided by a spectrometer in the beamline. All the efforts to construct the test apparatus on the beam line and to perform experiments will require sophisticated system engineering and design optimization with available resources.

The project will consist of three phases across five years. In the first two years, we will perform a feasibility study of proposed concepts with analytic modeling and simulation analysis. Computer modeling analysis of CNT channeling, cooling, and acceleration will be extensively investigated in Phase-II with various measurements with prepared CNT samples. Experimental tests are planned in the fifth year of Phase-III with construction of a test beamline. The envisioned timeline resonates well with the commissioning schedule of the ASTA and other available facilities at Fermilab, which are potentially available for x-ray and muon productions. (Table. 1)

**(1) Phase-I Tasks**

The first priority in Phase-I is to develop theoretical models to characterize CNT properties and to theorize their particle interactions in nano-structures. A computational assessment of cooling and acceleration condition of carbon-based structures will be performed in Phase-I. Electronic energy band and atomic potential characteristics will be analyzed with solid state computational codes and optical properties and electrostatics of CNT structures will be investigated with various EM analysis codes. In this phase, CNT samples will be procured by nano-fabrication techniques such as CVD and/or PECVD in the NIU Microelectronic Research and Development Laboratory (MRDL) and with the other collaborators, which will be followed by microwave measurements (X-band and K-band).

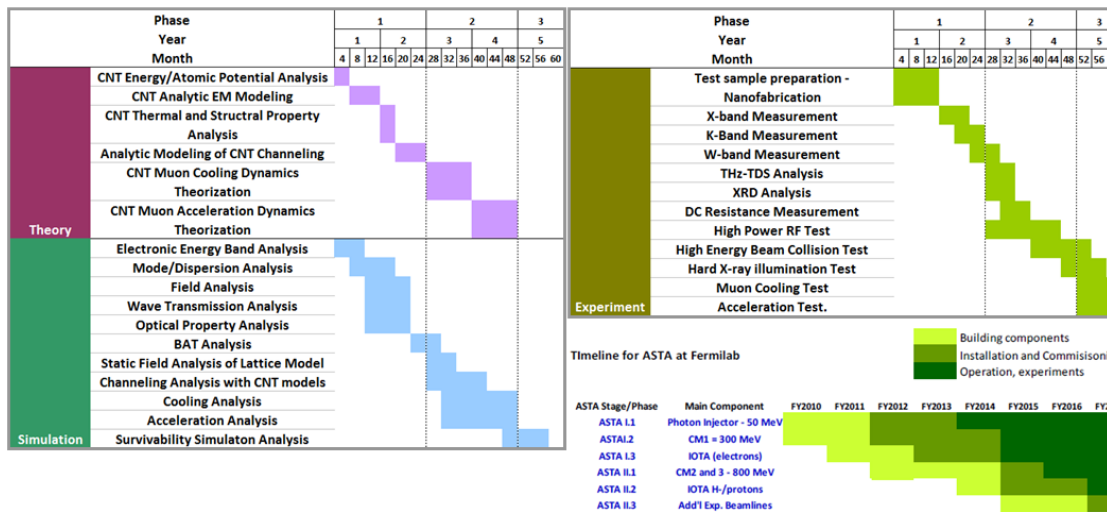


**Table. 1: Gantt Chart**

**(2) Phase-II Tasks**

In this phase, we will mainly focus on parametric assessment of cooling and acceleration conditions using theoretical models of *in-CNT* muon-photon interaction and advanced computer modeling techniques of electrostatics, including wave transmission, BAT phenomena, electrostatic field analysis, channeling, cooling, and acceleration of high energy particles. Our research team, including a post-doc and a graduate researcher, will develop a

comprehensive analysis tool to include physical implementation of plasmon/phonon excitation, cooling processes, ionization, bremsstrahlung radiation losses, and channeling particles. Currently, multi-physics simulation codes (VORPAL and CST) are accessible for tracking and PIC analyses of channeling particles. Ultimately, a collaborative effort will thus be to develop a fully integrated hyper-simulation platform capable of solving complex photon-muon interaction dynamics in nanostructure channels. Acceleration charge damage tests will be done with a 50 MeV beamline at ASTA, as described in Table-1. High frequency dielectric response will be characterized by signal reflection/transmission measurements using microwave Vector Network Analyzer and THz Time Domain Spectroscopy system, which will be followed by X-ray Diffraction analysis, DC resistance measurement, and high power microwave illumination test.

### **(3) Phase-III Tasks**

As scheduled in milestones of the ASTA at Fermilab, proposed R&D projects on x-ray and muon sources, if timely approved and commissioned, will enable us to pursue a high power X-ray illumination test and the following cooling and acceleration experiments in this phase. It is expected that a undulator with 0.01 – 0.1 % energy conversion efficiency will possibly create 10 keV level X-ray photons with 0.1 – 1 GW power range from electron beam bunches of 5 Hz/1 ms electron beam pulses with 1.3 kA peak current at ASTA. In this phase, muon cooling tests will be obtained from the measurement of initial and final emittances of channeled muons before and after a sample. Unchanneled and dechanneled muons will be separately counted from the primary beam in order to not contaminate the measured emittance. An available x-ray laser will deliver enough acceleration energy to nanostructures, which may provide a pulse of radially polarized light, which couples energy to the muon beam channeling through a sample. Optical energy will be transferred to the muon beam with an efficiency of > GeV per centimeter. Using a bending magnet in between drift chambers, we will measure the final energy of muons channeling through the crystal.

### **7.2.5.3 References**

- [1] S.Geer, *Annu. Rev. Nucl. Part. Sci.* 59:347–65 (2009)
- [2] Shiltsev V., *Mod. Phys. Lett. A* 25 567 (2010)
- [3] Dodin I, Fisch N *Phys. Plasmas* 15 103105 (2008)
- [4] Tajima T, Cavenago M *Phys. Rev. Lett.* 59 1440 (1987)
- [5] Chen P, Noble R *AIP Conf. Proc.* 398 273 (1997)
- [6] V.Shiltsev “High energy particle colliders: past 20 years, next 20 years and beyond”, arXiv:1205.3087 (2012)
- [7] P. Chen, R. Noble, *AIP Conf. Proc.* 398 273 (1997)
- [8] V. M. Biryukov, S. Bellucci, *Nuclear Instruments and Methods in Physics Research B* 234 (2005) 99–105
- [9] S. Bellucci, *Nuclear Instruments and Methods in Physics Research B* 234 (2005) 57–77

- [10] D. S. Gemmell, Rev. Mod. Phys. 46, 129 (1974); Channel ingedited ,by D. V. Morgan Wiley, London, 1973); Y. Ohtsuki, Charged Beam Interaction with Solids (Taylor and Francis, New York, 1983
- [11] B. W. Batterman and H. Cole, Rev. Mod. Phys. 36, 681 (1964)
- [12] P. O. Ewald, Fifty Years of X Ra-y Diffraction (International Union of Crystallography, Utrecht, 1962), 249
- [13] Biryukov V, Chesnokov Yu, Kotov V *Crystal Channeling and Its Application at High Energy Accelerators* (Springer-Verlag, Berlin, Heidelberg, 1997)
- [14] V.A. Ryabov. Nucl. Instr. and Methods B 90 ( 1994) 183, and references therein.
- [15] S.A. Bogacz and D.B. Cline, Muon acceleration and cooling in a strain modulated crystal channel, PTOC. Advanced Accelerator Workshop. Lake Geneva, June 1994.
- [16] Z. Huang, P. Chen and R.D. Ruth. Phys. Rev. Lett. 74( 10) ( 1995) 1759.

### 7.2.6 Electron Wave Function Size Measurements in IOTA Ring

The electron wave function size and its behavior in accelerators is a longstanding problem that does not have a solution yet. Simple quasiclassical estimates for the centroid motion were obtained long ago [1], but a theory for the wave function size has not been developed and it turned out to be too small to measure (see [2] and references therein). The reason for this could be that the electron wave function undergoes a continuous measurement process and its localization could be related to its collapse under acts of measurement. Or there are some other random processes that lead to the localization of the wave function. For next generations of electron machines it could be important to obtain insights into this problem – it may lead researchers to new physics of radiation, particle dynamics, etc.

The first dedicated experiments were started in Novosibirsk about two decades ago and described in [2, 3]. The experiments showed that the wave function of an electron in a storage ring is very localized, and its motion is similar to the motion of a classical particle with random kicks without any sign of phase space dilution due to potential (rf) well nonlinearities.

The experiments were performed in the VEPP-3 storage ring with a single circulating electron [3] and the light from an undulator that was detected by photomultipliers. The standard Brown-Twiss intensity interferometer scheme used a splitter to send the photons to two photomultipliers. The basic idea to measure the longitudinal wave function size was to detect two photons by different photomultipliers during one passage of an electron through the undulator and the rms difference in time, multiplied by velocity of light, was supposed to give the wave function size. Unfortunately, the photomultipliers were slow – their response time (called the dispersion in [3]) was around 160 ps. The signal time difference from two photomultipliers was well within this number, therefore it was concluded that the wave function size is much shorter than that resolution. This experiment characterized the fourth-order correlation function of the radiation field, and quantum

effects could be seen in it. Another high-order correlation experiment was the measurement of the photon arrival times during a long time interval. Fitting of amplitude and phase of synchrotron oscillation gave the electron trajectory in the longitudinal phase plane. The trajectory appeared to be continuous (with tens-picosecond precision) and chaotic, demonstrating the Brownian motion in a phase plane. In contrast to the classical Brownian motion, which may be predicted in principle by knowing the motion of molecules, surrounding the Brownian particle, the electron chaotic motion is fundamentally unpredictable (at least, according to the standard quantum theory), and gives us a rare example of the true random process.

The IOTA ring will have an undulator for the optical stochastic cooling experiments [4]. It is straightforward to repeat similar experiments with the VEPP-3 setup but with a much faster and advanced detection system – systems with a  $\sim$ psec resolution are under development by Fermilab, ANL and Univ. of Chicago now [5]. It corresponds to a 0.3-mm wave function size for electrons. If it is shorter than this we have to use or develop a different technique for the measurement. Having well-defined initial conditions and time structure, the radiation of a single electron may be a “standard candle” source for various kinds of quantum optics experiments with the high-order field correlation function, like, for example, quantum cryptography and teleportation. The experimental and theoretical investigation of the stationary state of the electron in a storage ring is useful for the development of non-perturbative methods of quantum electrodynamics, and, in general, the foundations of the quantum theory.

The ASTA facility will offer a unique opportunity to carry out the proposed measurement of the electron wave function size. That research requires a dedicated storage ring (IOTA) and its operation with 100-150 MeV electrons. It cannot be carried out anywhere else as there are no existing electron storage rings in that energy range which can afford installation of special insertions (wigglers, etc.), and which offer special instrumentation needed to perform such measurement. In addition, the high availability of IOTA for the experiment is extremely advantageous.

In summary, the proposed experiment with wave function measurements is practically an unknown territory with possibilities of scientific breakthroughs and the IOTA ring would be well suited to do these measurements.

#### **7.2.6.1 References**

- [1] M. Sands, Phys. Rev. 97 (1955) 470
- [2] N. Vinokurov, in Proceedings of Joint US-CERN-Japan-Russia accelerator school, World Scientific (1988) 108
- [3] T. Shaftan, PhD thesis, BINP, Novosibirsk (1997), in Russian
- [4] V. Lebedev, “Optical Stochastic Cooling Proposal”, this document.
- [5] <http://psec.uchicago.edu/>

## 7.2.7 LBNE Targetry Experiments at ASTA

### 7.2.7.1 Introduction

LBNE (the Long Baseline Neutrino Experiment) uses solid targets to convert high-energy protons into pions and kaons to produce neutrinos [1]. These targets are subject to severe thermomechanical shock and radiation damage from the beam. These two effects limit the lifetime of the target and the precision of the experiment. The target must maintain its shape, size, and density to produce a consistent neutrino beam. Variations on the order of a percent can be unacceptable. The two effects operate on different timescales: thermomechanical shock occurs within a single pulse and radiation damage accumulates over millions of pulses. Still, the two are related as radiation damage changes the physical properties of the material that determine whether it will fail under thermomechanical shock. LBNE is actively pursuing several different materials for the composition of the target and target assembly. Graphite and beryllium are candidates for the primary target material. Numerous materials may be used in the target assembly, including beryllium, titanium, aluminum, stainless steel, and ceramic. Choosing among these materials requires experimental validation.

The ASTA beam can simulate some of the aspects of the thermomechanical shock and radiation damage that the LBNE target will experience. There are three foreseen modes of how ASTA can be used for these studies:

- High strain rates induced by beam heating
- Beam-induced thermomechanical shock of previously irradiated materials
- Direct radiation damage of materials

For the first two, the ASTA electron beam can be used to simulate the thermomechanical shock of the LBNE proton beam. The parameters will not be identical, but comparable stress and strain rates can be achieved. For the third the  $H^-$  beam is likely best suited to induce radiation damage, though some can also be achieved with the electron beam. More detail follows in the below sections. The nominal LBNE beam parameters are listed in Table 1.

Table 1. Beam Parameters for LBNE.

|                                |                                      |
|--------------------------------|--------------------------------------|
| <b>Species</b>                 | Proton                               |
| <b>Energy</b>                  | 120 GeV                              |
| <b>Intensity</b>               | $4.9 \times 10^{13}$ protons         |
| <b>Pulse Length</b>            | 10 microseconds                      |
| <b>Repetition Rate</b>         | 0.8 Hz                               |
| <b>Size</b>                    | 1.3 mm RMS (horizontal and vertical) |
| <b>Power</b>                   | 700 kW                               |
| <b>Annual Beam</b>             | $\sim 6.5 \times 10^{20}$ protons    |
| <b>Instantaneous Dose Rate</b> | $5.2 \times 10^{-3}$ DPA/s           |
| <b>Average Dose Rate</b>       | $5.2 \times 10^{-8}$ DPA/s           |
| <b>Annual Dose</b>             | $\sim 1$ DPA/yr.                     |

### 7.2.7.2 High strain rates induced by beam heating

A central issue in the design of neutrino targets is whether they can withstand the thermomechanical shock of the beam impact. The central properties of the material are the strength (tensile/compressive), coefficient of thermal expansion, modulus of elasticity, specific heat, and energy deposition (determined by density, atomic number, and the beam properties). However, many of these parameters are valid only in the static limit. The rapidly pulsing nature of the particle beams will cause the material behavior to depart from that implied by the static material properties. Such departures are known as High Strain Rate (HSR) phenomena. HSR properties of materials are not well known, and are often measured only in idealized situations, not the heterogeneous situation of beam heating. Specifically, the tensile strength of beryllium could be as much as 40% greater for the strain rates relevant for LBNE [2].

For the LBNE, the goal will be to test candidate materials (chiefly graphite and beryllium) with comparable spatial and temporal profiles to that of the LBNE beam. The parameter space of total induced stress and strain rate will be explored to quantify the departure of material properties from static limits in regimes relevant to high-power targets. ASTA's capability to tune the pulse length and the focusing capabilities of the extraction line offer a wide area of coverage.

If the HSR effects can be established in a beam heating situation, it opens the door to building longer-lived targets. In particular, if beryllium's enhanced strength at high strain rate can be proven it becomes a more viable alternative to graphite. Beryllium is expected to experience radiation damage at a reduced rate as compared to graphite, and would thus have a longer lifetime. The static properties of typical graphite and beryllium are shown in Table 2.

Table 2. Static Properties of Graphite and Beryllium

|                                  | <b>Graphite (POCO ZXF- 5Q)</b> | <b>Beryllium (S- 65C)</b> |
|----------------------------------|--------------------------------|---------------------------|
| Apparent density                 | 1.81 g/cc                      | 1.82 g/cc                 |
| Compressive Strength             | 195 MPa                        | 260 MPa                   |
| Tensile Strength                 | 90 MPa                         | 370 MPa                   |
| Modulus of Elasticity            | 12.5 GPa                       | 310 GPa                   |
| Thermal Conductivity             | 70 W/m/K                       | 200 W/m/K                 |
| Coefficient of Thermal Expansion | 8.1 um/m/K                     | 10.7 um/m/K               |
| Specific Heat                    | 710 J/kg/K                     | 1770 J/kg/K               |

### 7.2.7.3 Beam-induced thermomechanical shock of previously irradiated materials

LBNE, as part of the RaDIATE collaboration [3], has amassed an inventory of accelerator materials that have been substantially irradiated at Fermilab and other locations. As a result of irradiation, it is expected that the material properties of the deviate from their un-irradiated values. This radiation damage is a potential failure mode for all high-power targets and must be investigated. At ASTA, these previously irradiated items can be tested under intense thermomechanical shock and the material properties investigated.

Most of these items are typical materials such as prototype targets and beam windows made of beryllium, tungsten, graphite, and other forms of carbon. They received substantial radiation dose, but often at reduced shock conditions. Some of these materials are activated, so transportation for study may prove difficult. For those materials stored at Fermilab, ASTA simplifies the issue of transport.

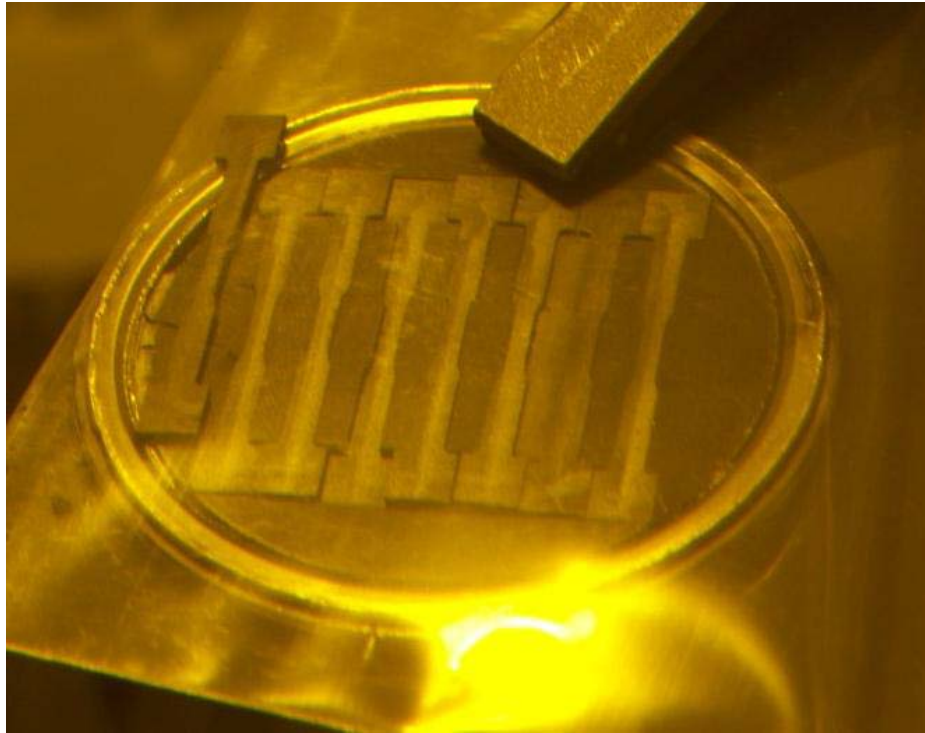


Figure 1: Graphite radiation damage samples irradiated in a previous beam test at the Brookhaven Linear Isotope Producer (BLIP).

#### ***7.2.7.4 Direct radiation damage of materials***

A portion of the RaDIATE collaboration allows the measurement of static material properties of very small irradiated samples. The role of ASTA here would be to produce a range of irradiated samples for this external testing. The nature of irradiation is relevant, and it is difficult to find a perfect proxy for any alternative beam. Still, some radiation effects can be simulated by the ASTA beams, specifically the H<sup>-</sup> (or proton) beam in addition the electron beam.

The ASTA beams will radiate the materials at various levels, with different beams and different irradiation conditions. Factors such as the temperature and environmental materials affect radiation damage. Joints between materials are a particular area of concern.

Comparing the various radiation techniques will be useful in understanding the radiation damage processes. Below are comments on three relevant mechanisms.

- **Ionization:** the ASTA electron beam is well-suited to induce bulk ionization which can rearrange the crystalline structure of materials and exacerbate corrosive effects. This is the most common form of irradiation, so there already exist substantial studies in this area; the other mechanisms are less well investigated.
- **Atomic Displacement:** the ASTA  $H^-$  or proton beam would be well-suited to induce atomic displacements (measured in DPAs – Displacements Per Atom). This is one of the central mechanisms of radiation damage relevant to high-energy beams. It can have a drastic effect on the properties of any material. The samples in this case would be rather thin, < 1 mm, because of the short range of MeV-scale protons in solid materials. However, this leads to much more concentrated production of DPAs. The electron beam is not very useful for this application. The  $H^-$  beam can be used, though the energy is only just above threshold. The coulomb barrier is 1-2 MeV for the relevant nuclei, so an enhanced  $H^-$  energy would be preferred.
- **Gas Production:** production of gasses (predominantly hydrogen and helium) is one of the unique challenges of high-energy particle irradiation. These gasses are created through spallation or other endothermic nuclear process. High-energy is needed to induce the spallation process or provide the extra energy to break up nuclei. These gasses can build up within bulk material leading to chemical changes and mechanical pressure contributing to failure. The  $H^-$  beam is only capable of producing helium in beryllium, more than 8 MeV would be required for carbon. The cross section will also be quite low at this energy. However, the  $H^-$  can be a tool for direct implantation of gas into a sample, which can be combined with general ionization and atomic displacement to make a more accurate proxy for high-energy irradiation. Helium implantation would be an attractive addition.

#### 7.2.7.5 References

- [1] C. D. Moore *et al.*, "Overview of the LBNE Neutrino Beam", PAC2011 -WEP248, FERMILAB-CONF-11-086-AD (2011).
- [2] Air Force Materials Laboratory "Mechanical Properties of Structural Grades of Beryllium at High Strain Rates", AFML-TR-75-168 (1975), [www.dtic.mil/cgi-bin/GetTRDoc?AD=ADA020076](http://www.dtic.mil/cgi-bin/GetTRDoc?AD=ADA020076).
- [3] RaDIATE (Radiation Damage In Accelerator Target Environments) Collaboration, <http://www-radiate.fnal.gov/index.html>.

### 7.2.8 A Tagged Photon Beam at ASTA for Detector R&D

The efficient detection of photons in the energy range 10 MeV – 100 MeV is a challenge for many experiments envisioned in the future at Fermilab. For instance, one of the most important backgrounds for a Project X experiment designed to measure the rate of  $K^0 \rightarrow \pi^0 \nu \bar{\nu}$  [1] is the decay  $K^0 \rightarrow \pi^0 \pi^0$  in which one  $\pi^0$  decays asymmetrically and the high energy photon is lost down the beamline. A related experiment, ORKA [2], which plans to run before Project X, will measure the rate of  $K^+ \rightarrow \pi^+ \nu \bar{\nu}$  using a stopped  $K^+$  beam. One of the most problematic backgrounds is the decay  $K^0 \rightarrow \pi^0 \pi^0$ , with an asymmetric  $\pi^0$  decay. In this case, the event kinematics ensures that the low energy gamma is at least 20 MeV. A tagged source of ~20 MeV photons would be an important resource during the development of instrumentation for these experiments.

Tagged bremsstrahlung photon beams have been used at electron accelerators for many years. The intensity of a tagged photon beam at ASTA would be limited by the requirement that the system operate in “singles mode.” As shown in the figure below, the spectrum of forward bremsstrahlung photons peaks at low energy. The rate of low energy photons needs to be kept low enough so that they do not create a significant background for measurements made with tagged high energy photons. An optimized tagger could require a customized magnetic spectrometer. However, it appears likely that a very inexpensive tagger could be designed using a standard ASTA dipole magnet and a small system of either scintillation counters or silicon detectors. During 50 MeV accelerator operation, this system could tag a modest, but useful, flux of photons in the 10-50 MeV range. A wider range of photon energies would become accessible with a 300 MeV electron beam.

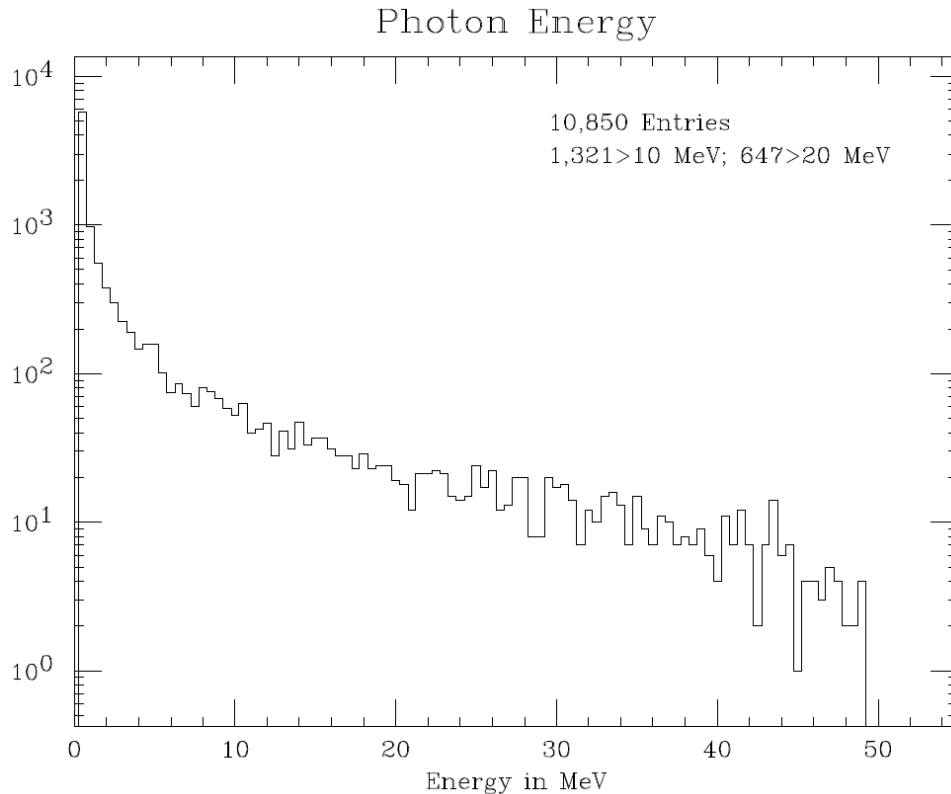


Figure 1. The energy distribution of photons produced into a forward 10mradian cone in a G4beamline [3] simulation of 5 million 50 MeV electrons passing through 20 microns of aluminum ( $\sim 2 \times 10^{-4}$  of a radiation length).

**References:**

- [1] June 2012 Project X Physics Study:  
<https://indico.fnal.gov/conferenceDisplay.py?confId=5276>  
"The Project X Kaon Physics Program," accessible from the Project X web site:  
<https://indico.fnal.gov/getFile.py/access?resId=1&materialId=0&confId=3579>
- [2] Fermilab proposal P1021, "ORKA: Measurement of the  $K^+ \rightarrow \pi^+ \nu \bar{\nu}$  Decay at Fermilab"  
<https://projects-docdb.fnal.gov:440/cgi-bin/ShowDocument?docid=1365>.
- [3] G4beamline:  
<http://www.muonsinc.com/muons3/tiki-index.php?page=G4beamline>

## 7.2.9 Applications of Inverse Compton Scattered Photons

### 7.2.9.1 Measurement of Nuclear Processes Important to Astrophysics

The  $^{12}\text{C}(\alpha,\gamma)^{16}\text{O}$  triple reaction is a critical gateway process in stellar evolution for the production of elements heavier than oxygen and is also important in the transition from helium burning to nova ignition conditions. [1,2,3,4]. Understanding of this process has been described by W. Fowler in his Nobel acceptance speech as the “Holy Grail” of nuclear astrophysics [5]. The dynamics of this reaction can be studied in the laboratory through the photon induced reverse reaction  $^{16}\text{O}(\gamma,\alpha)^{12}\text{C}$  with gamma energies in the 8.7-10.0 MeV range on an oxygen target, where the expected cross section is very small, less than 0.5 nb [6]. The potential extreme brilliance of photons produced at ASTA through Inverse Compton Scattering (ICS) in this energy range enables consideration of experiment configurations that could access the tiny  $^{16}\text{O}(\gamma,\alpha)^{12}\text{C}$  cross section with high signal/background [6,7].

Inverse Compton scattering has been used previously at a number of electron storage ring facilities to pursue these  $(\gamma,\alpha)$  measurements where the circulating electron currents approach 100 mA and the laser power is modest. One clear advantage of the ASTA ICS concept is that a relatively low electron beam current is planned while the laser power would be large because it is effectively amplified with a recirculating cavity. This is a tremendous advantage for very low cross section measurements such as those important to nuclear astrophysics since the background from beam electron bremsstrahlung on residual gas can be relatively large in a high current storage ring. This class of background is expected to be reduced by several orders of magnitude with the ASTA ICS concept.

| Electron drive beam energy | Peak ICS photon energy with YAG (1064nm) laser |
|----------------------------|--|
| 700 MeV                    | 8.7 MeV  |
| 750 MeV                    | 10.0 MeV                                       |
| 800 MeV                    | 11.4 MeV                                       |
| 918 MeV                    | 15.0 MeV                                       |

Table 1. Peak photon beam energies achievable with YAG laser photons (1064 nm, 1.17eV photons) Inverse Compton Scattering (ICS) from the ASTA electron drive beam.

### 7.2.9.2 R&D toward a next generation photo-fission source of isotopes.

The practical production of important nuclear isotopes through photo-fission with an electron bremsstrahlung photon source was discussed by W. Diamond in 1999 [8]. This seminal concept and subsequent work has led to the design and construction of the ARIEL photo-fission facility [9] at TRIUMF, where commissioning running is expected to commence in 2014. The photo-fission cross section for the actinides peaks at 12-15 MeV, and an ICS source tuned in the 10-17

MeV band could in principle provide a very efficient mechanism to produce photo-fission isotopes [10]. The potential extreme brilliance of an ASTA ICS source could provide correspondingly high yields of photo-fission isotopes. R&D at ASTA in the near future is timely toward consideration and conceptual design of a next generation ICS photo-fission facility, which could motivate a modest upgrade of the ASTA facility to reach ICS photon energies in the 10-17 MeV range.

**References:**

- [1] Rauscher, T., & Thielemann, F.-K. 2000, *At. Data Nucl. Data Tables*, 75, 1
- [2] Wallerstein, G., et al. 1997, *Rev. Mod. Phys.*, 69, 995
- [3] Weaver, T. A., & Woosley, S. E. 1993, *Phys. Rep.*, 227, 65
- [4] Woosley, S. E., & Weaver, T. A. 1995, *ApJS*, 101, 181
- [5] W.A. Fowler, *Rev. Modern Phys.* 56 (1984) 149.
- [6] Weller et al, *Progress in Particle and Nuclear Physics* 62 (2009) 257303
- [7] Personal communication, R. Holt (ANL), A. Sonnenschein (FNAL).
- [8] W. Diamond, *Nuclear Instruments and Methods in Physics Research A* 432 (1999) 471-482
- [9] ARIEL photo-fission facility at TRIUMF (<http://www.triumf.ca/ariel>)
- [10] Personal communication, L. Merminga (TRIUMF).

## 7.3 Accelerator R&D Opportunities at ASTA: Stewardship and Applications

### 7.3.1 High-brightness X-ray channeling radiation source

The quest for short-wavelength compact light source has been driven by applications ranging from fundamental science to homeland security. Recently, Vanderbilt and Northern Illinois University received funding to work on the development of a compact X-ray radiation source. The proposal aims at producing X-rays using a 40-MeV electron beam. A proof-of-principle experiment is foreseen in the ASTA photoinjector area. This project aims at producing X-rays at 80 KeV with high-average spectral brilliance. The proposal leverages on the ASTA's pulse-train format capabilities. Conversely, the possibility of operating field-emission cathode in the ASTA rf gun would provide a bunch train with a 1.3-GHz intra-bunch frequency. Such high-repetition rate train could be used to, e.g., explore high-order-mode excitation in the ASTA superconducting linac in a new regime. In addition, the exquisitely small emittance projected from the field-emission source will move RF-accelerator science into a regime where it has never played a role before. New diagnostics will be needed even to explore this region, and new effects will probably be discovered. Extension from a single field-emitter to an array will increase the total current, and used together with the beam-manipulation developments discussed in the following section may play a role in the development of coherent light sources. Thus, as an extra benefit, the channeling-radiation project will advance the basic objective of ASTA as an accelerator research tool. A major advantage of ASTA is its capability of supporting an X-ray source with high-average spectral brilliance. This section is based on the proposed concept detailed in Ref. [1].

#### 7.3.1.1 Introduction: Channeling radiation as a ultra-bright X-ray source

In a crystal, the ions in each crystal plane form a sheet of positive charge. When a relativistic electron travels through the crystal parallel to the crystal plane, Lorentz contraction increases the charge density by the factor  $\gamma$  and the electron oscillates about the crystal plane in quantum states normal to the plane, as depicted in Figure 1. Radiation from transitions between the quantum states is called channeling radiation. Channeling radiation was predicted theoretically by Kumakhov [2] in 1974, and experimentally observed by Terhune and Pantell [3] in 1975. Since then, there has been extensive theoretical and experimental investigation of channeling radiation, and theory and experiment are in good agreement.

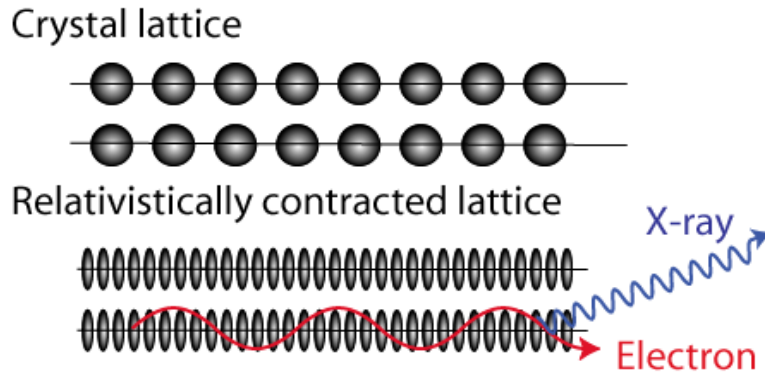


Figure 1: Mechanism of channeling radiation production (from Ref. [1]).

The transverse forces experienced by an electron traveling along a crystal plane are comparable to those in a  $10^4$ -T magnetic undulator or a 1-TW laser undulator focused to a 10- $\mu\text{m}$  spot. The equivalent “undulator period” is on the order of 0.1  $\mu\text{m}$ . The coherence length of the crystal “undulator” is limited by scattering to the order of 1  $\mu\text{m}$ , so the effective number of “undulator periods” in channeling radiation is on the order of 10. The photon yield is more than 10 photons per electron at high energy (GeV), but on the order of  $10^{-4}$  photons per electron in the X-ray region [4]. The channeling-radiation peaks are typically an order of magnitude above the bremsstrahlung background [5]. The advantages of a channeling radiation source are clear. Compared with a conventional undulator, channeling radiation requires only a 40-MeV electron beam, rather than a 10-GeV beam to reach the hard X-ray region. Compared with a laser undulator, a channeling radiation source comprises a small diamond chip rather than a complex laser system circulating a kilowatt of laser power.

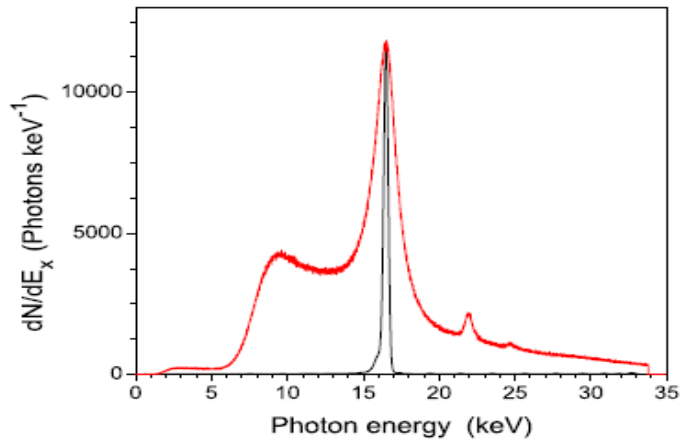


Figure 2: Observed spectrum of channeling radiation for transitions in (110) plane of diamond crystal at an electron energy of 14.6 MeV. Red: natural spectrum; black, monochromatized by Bragg reflection to remove the wings of the CR line and the Bremsstrahlung background. (Figure from Ref. [6]).

For electrons channeling in diamond, the best available measurements are those of Azadegan [6]. A typical channeling radiation spectrum is illustrated in Figure 2. The radiation is forward directed in a cone of angle  $1/\gamma$ , and Doppler shifted by the factor  $2\gamma$ . Including the Lorentz contraction of the crystal lattice, the photon energy scales roughly as  $\gamma^{1.7}$ , and spans the X-ray and gamma ray regions. For the  $1 \rightarrow 0$  transition in (110) diamond, the photon energy may be tuned from 10 to 80 keV by varying the electron energy. For a 30-MeV electron incident on a 42.5-micron thick diamond crystal, the yield on the  $1 \rightarrow 0$  transition corresponds to about 0.028 photons-steradian-keV in a line 3-keV wide centered near 56 keV [6]. In conventional units, this corresponds to  $10^{-9}$  photons-mrad<sup>2</sup>-0.1% bandwidth per electron.

The spectral brilliance of the X-radiation depends on how tightly the electron beam can be focused, and this depends on the emittance of the beam. At the radiation source ELBE, in Dresden, a high-intensity channeling radiation source has been developed using a high-brightness electron beam incident on a diamond crystal [4]. Diamond is the best material for this application owing to its high thermal conductivity [7]. The normalized emittance of the beam after aperturing was 3  $\mu\text{m}$  rms at an average current of 100  $\mu\text{A}$  [8], which corresponds to a peak brightness on the order of  $10^9$  A/m<sup>2</sup>-sterad. The beam was focused to a mm-size spot on the diamond. As much as  $10^{11}$  photons/s were obtained in a 10% bandwidth, which corresponds roughly to an average spectral brilliance on the order of  $10^6$  photons/s-mm<sup>2</sup>-mrad<sup>2</sup>-0.1% bandwidth.

The innovation being pursued by the Vanderbilt/NIU group is to use a single field-emitting tip as the current source, in place of the gridded thermionic gun used at ELBE. Simulations

of a single-tip field emitter yield a normalized emittance of 1.3 nm [9], which is an improvement of three orders of magnitude over the ELBE thermionic gun. In experiments at Vanderbilt, we have observed more than 10  $\mu\text{A}$  average current from a single field-emitting tip [10] with brightness approaching the quantum limit [11]. The current was limited by damage to the anode, which was in close proximity. The ultimate performance of diamond tips has yet to be determined. By using a single tip it may be possible to improve the transverse brightness of the electron beam by as much as six orders of magnitude, with a corresponding improvement of the spectral brilliance of the X-ray beam. The absolute emittance of the beam from a single tip, extrapolated to 30 MeV, is  $\sim 40$  pm. If we focus this at the critical angle for channeling radiation in diamond (about 1 mrad), we get a spot diameter of 40 nm; the spectral brilliance of the X-ray beam is then  $10^{12}$  photons/s-mm<sup>2</sup>-mrad<sup>2</sup>-0.1% bandwidth at an average current of 200 nA.

### **7.3.1.2 Production of X-rays at ASTA: Challenges & Methods**

The beam must be accelerated to high energy ( $\sim 30$ -50 MeV) to create hard X-rays. At ASTA, the first-stage acceleration will occur in the rf-gun to energies up to 4-5 MeV and further acceleration to 40 MeV will happen in CAV1 and CAV2 cavities. We currently envision the field-emitter cathode to be mounted on the tip of the inner conductor of a coaxial line. The coaxial line will be driven by 1.3 and 3.9-GHz signals with solid-state amplifiers to bias the gate electrode and gate the field emission over duration shorter than the rf gun's fundamental period. Calculations indicate that such a biasing scheme will generate bunches with duration of approximately 20 ps [12]. Preserving the ultra-low transverse emittances produced by the tip after subsequent acceleration and manipulation will be challenging. Chromatic aberrations due to energy spread in the beam; emittance dilution due to nonlinearity in the rf fields, geometric aberrations in the electron beam transport lines, and collective effects can be mitigated according to start-to-end numerical simulations [13]. Numerical simulations performed for the ASTA configuration are summarized in Figures 3 and 4. The simulated electron-beam parameters represent two orders of magnitude increase in electron beam quality. Other degrading effects which to date have been unnoticed, may also become important. One concern, for instance, is the extent to which Coulomb collisions at low energies (Boersch effect) will contribute to phase-space dilution [14].

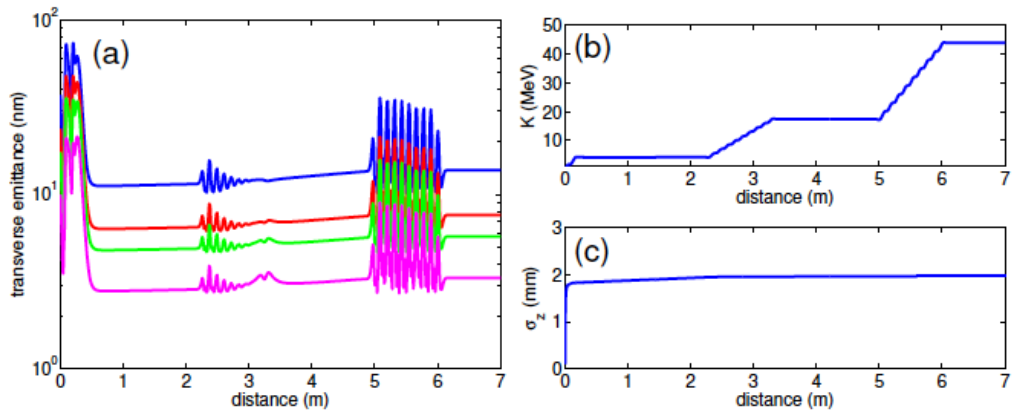


Figure 3: Transverse emittance (a), kinetic energy (b) and bunch length (c) evolution along the ASTA photoinjector accelerating section [comprising the RF gun ( $0 < z < 30$  cm), CAV1 ( $2.2 < z < 3.2$  m) and CAV2 ( $5 < z < 6$  m)]. The magenta, green, red and blue traces in plot (a) correspond to emittance respectively computed for the 85, 90, 95, and 100-percentile of the particle distribution (from Ref. [13]).

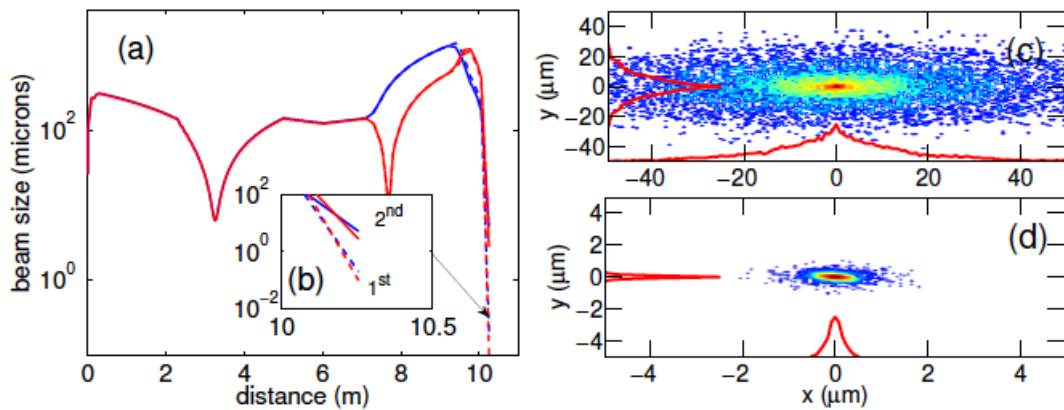


Figure 4: Horizontal (blue) and vertical (red) rms beam size evolution along the ASTA photoinjector beamline up to location of the diamond crystal (a). The solid and dashed line corresponds respectively to second- ("2<sup>nd</sup>") and first-order "1<sup>st</sup>") particle-tracking simulations and inset (b) shows the rms beam sizes in the vicinity of the crystal. Density plots (c) and (d) are respectively the beam transverse density at the crystal location obtained from second and first order calculations. The red traces in plots (c) and (d) are the corresponding horizontal and vertical projections (from Ref. [13]).

Because the x-rays are produced by the interaction of the electron beam with the crystal, the maximum current of the electron beam is limited by heating of, and radiation damage to, the crystal. Measurements and computations show that for diamond at room temperature the effects of heating are acceptable up to a few mA of beam current, so this

will not be a limitation even for cw operation [7]. Measurements show that radiation damage becomes significant above a total beam fluence on the order of a few C per square centimeter. Thus, the 40-nm focal spot is destroyed in about 100  $\mu$ s. The crystal must be moved at about 1 mm/s, and the crystal is destroyed at the rate of 0.1 square millimeters per hour at 100% duty factor. At the 1-percent duty factor of ASTA, the diamond consumption rate will be much smaller.

### 7.3.1.3 Experimental plans at ASTA

The production of channeling radiation will use the  $\sim$ 40-MeV beam produced by ASTA; see Figure 5. We plan to install the channeling radiation crystal downstream of a set of quadrupole magnets and just upstream of the first dipole of a chicane bunch compressor. This configuration will enable us to focus the beam on the crystal and separate the electron beam from the X-rays using the first dipole. In the straight-ahead line we plan on installing the energy-resolved CdTe detector needed to characterize the X-ray radiation.

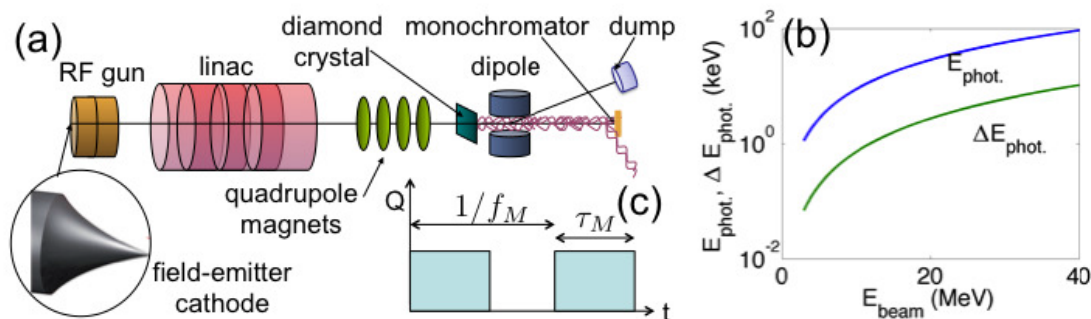


Figure 5. The layout of the X-ray channeling radiation source experiment in the 40-MeV area of ASTA (from Ref. [13]).

To minimize the risk, the approach will be staged. First the coaxial cathode holder will be developed and tested at the HBESL facility where the generation of field-emitted bunched beam will be demonstrated. Upon successful completion of this experiment the coaxial-line cathode holder will be installed at the ASTA. Because of the similarities between the HBESL and ASTA rf guns, we expect that the field-emitted cathode holder and associated subsystems developed during the test at HBESL will be integrally reusable without major changes. In parallel and independently from the success of the field-emission source R&D, we will use the nominal electron beam produced via photoemission to gain experience with producing and detecting X-rays from channeling radiation. It is expected that nanometer-level transverse emittance could also be produced by photoemission from the nominal Cesium-Telluride cathode using very small transverse laser spot [15]. Generation and characterization of ultra-low-emittance beams will be attempted during early commissioning of the ASTA photoinjector.

### 7.3.1.4 Other spin-off opportunities

The demonstration of the generation of bunched beam from field emission could find other applications especially since the principle could be applied to a field-emitter array cathode instead of a single-tip field emitter. The latter could produce much higher charge per bunch. For instance, if operated over the full duration of the macropulse, the total number of field-emitted bunches would be  $1.3 \times 10^6$ . Assuming a charge per bunch of 1 pC, this would result in a 1 mC charge within the entire macropulse. This type of unprecedented bunch format could be used to investigate high-order mode excitation in the TESLA cavity or mimic the charge per macropulse anticipated in high-intensity linacs (e.g. Project X) proposal. In addition, the generation and acceleration of electron beams with exquisitely small emittance will extend accelerator technology to a new level. Alternatively a photo-field-emission cathode could be used and attosecond manipulation of the emitted bunches could be anticipated [16] thereby enabling new regimes for planned experiments in advanced acceleration technique or development of novel compact X-ray sources capitalizing on advanced phase space manipulations pioneered at Fermilab.

### 7.3.1.5 References

- [1] C. Brau, B. Choi, J. Jarvis, J. W. Lewellen and P. Piot, *Synchrotron Radiation News*, 25: 1-20 (2012); online at <http://dx.doi.org/10.1080/08940886.2012.645419>.
- [2] M. A. Kumakhov, *Phys. Lett. A* **57**, 17 (1976).
- [3] R. W. Terhune and R. H. Pantell, *Appl. Phys. Lett.* **30**, 265 (1977).
- [4] W. Wagner, B. Azadegan, M. Sobiella, J. Steiner, K. Zeil, and J. Pawelke, *Nucl. Instrum. Meth. B* **266**, 327 (2008).
- [5] M. A. Kumakhov, *International Conference on Charged and Neutral Particles Channeling Phenomena*, edited by S. B. Dabagov.
- [6] B. Azadegan, Ph.D. thesis, Technische Universität Dresden, 2007.
- [7] C. K. Gary, R. H. Pantell, M. Ozcan, M. A. Piestrup, and D. G. Boyers, *J. Appl. Phys.* **70**, 2995 (1991).
- [8] W. Neubert, B. Azadegan, W. Enghardt, K. Heidel, J. Pawelke, W. Wagner, *Nucl. Instrum. Meth. B* **254**, 319 (2006).
- [9] C. Brau, Private communication (2011)
- [10] J. D. Jarvis, H. L. Andrews, C. A. Brau, B.-K. Choi, J. Davidson, W.-P. Kang, and Y.-M. Wong, *J. Vac. Sci. Technol. B* **27**, 2264 (2009).
- [11] J. D. Jarvis, H. L. Andrews, B. Ivanov, C. L. Stewart, N. de Jonge, E. C. Heeres, W.-P. Kang, Y.-M. Wong, J. L. Davidson, and C. A. Brau, *J. Appl. Phys.* **108**, 094322 (2010).
- [12] J. W. Lewellen and J. Noonan, *Phys. Rev ST Accel. Beams* **8**, 033502 (2005).
- [13] P. Piot, C.A. Brau, W. E. Gabella, B. K. Choi, J. D. Jarvis, J. W. Lewellen, M. Mendenhall, D. Mihalcea, Fermilab preprint fermilab-conf-12-425-apc; to appear in the Proceedings of the 2012 Advanced Accelerator Concept Workshop (AAC12), Austin TX, June 10-15, 2012.

[14] H. Boersh, Zeit. Physik, **139**, 115-146 (1954).

[15] R. K. Li, K. G. Roberts, C. M. Scoby, H. To, and P. Musumeci, Phys. Rev. ST Accel. Beams **15**, 090702 (2012).

[16] M. Krueger, M. Schenk, and P. Hommelhoff, Nature **475**, 77 (2011).

## **7.3.2 Advanced phase space manipulations**

### ***7.3.2.1 Transformative applications of advanced phase space manipulations***

Over the last decade, Fermilab has pioneered the experimental development of advanced phase space manipulations at the A0 photoinjector test facility. These manipulations include the generation of “flat” beams with high transverse-emittance ratio [1,2,3,4] and the emittances exchange between the horizontal and longitudinal degrees of freedom [5,6]. The beamline used for the latter experiment was also shown to be capable of producing arbitrary-shaped current profile including the production of sub-picosecond bunch trains with variable spacing as needed to produce, e.g., tunable coherent radiation [7,8]. The combination of these two manipulations could enable the arbitrary repartitioning of emittances between the three degrees of freedom [9,10]. Given the local expertise, this type of experiments will be resumed at ASTA with the end goal of pushing their limits to new frontiers and possibly utilizing these phase-space-manipulation concepts to advance the performances of accelerator-based light sources or new acceleration concepts.

Advanced phase space transformation techniques (flat beam generation, emittance exchange and temporal pulse shaping) could have transformative applications to advanced accelerator science. At ASTA some of these transformations were included in the baseline design (e.g. flat beam in the photoinjector) and will be readily available to user. Most of the components and expertise required to assemble others phase space manipulation methods, e.g. emittance exchange, are available. The availability of these manipulation techniques to carry experiment is unique to the ASTA facility and, when combined with the high-repetition rate, could be utilized to investigate, e.g., dynamical effect in plasma-wakefield accelerators.

### 7.3.2.2 Flat beam transformation

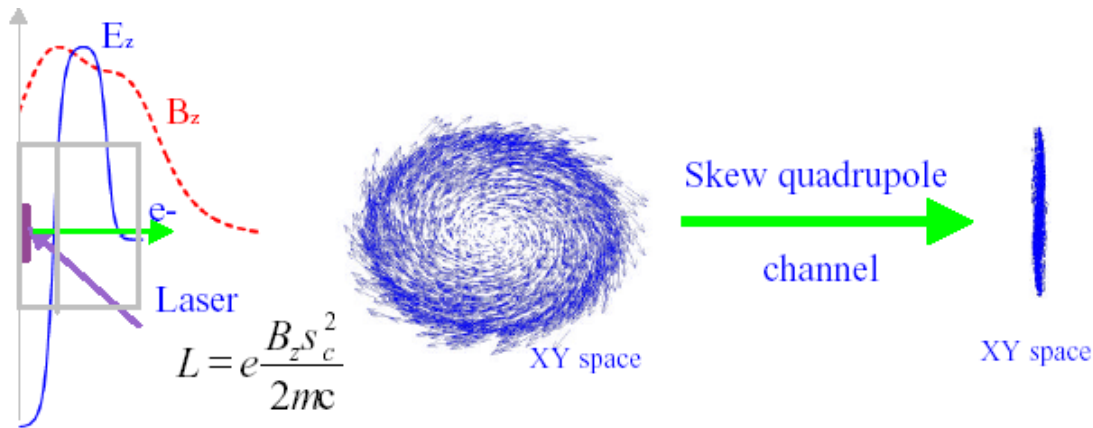


Figure 1. The round-to-flat beam transformation. The beam is produced in an rf gun (left), wherein the axial magnetic field is non-zero, thereby imparting a nonzero canonical angular momentum. Upon exit from the gun and the magnetic field, the canonical angular momentum is converted into kinetic angular momentum (middle). The angular momentum is removed by applying a torque on the beam using a system composed of three skew-quadrupole magnets. The beam is thereby made flat (right).

Under normal conditions, the electron beams generated in a photoinjector are round due to the cylindrical symmetry of the photocathode drive-laser as well as the rf acceleration and solenoidal focusing system. Several factors drive the bulk properties of an electron beam, such as space-charge, beam emittance and angular momentum. An electron beam in thermal motion inside a cathode is born into a region with an axial magnetic field  $\mathbf{B}$ , suddenly acquiring canonical angular momentum. The beam is then brought into a field-free region, and the kinetic angular momentum is removed by a set of three skew-quadrupole magnets. In this process the initially equal emittances are partitioned into unequal emittances ( $\gamma\mathcal{E}_+$ ,  $\gamma\mathcal{E}_-$ ), preserving the product:  $\gamma\mathcal{E}_x \times \gamma\mathcal{E}_y = \gamma\mathcal{E}_+ \times \gamma\mathcal{E}_-$ ; see Figure 1.

An unequal partitioning of equal emittances is not possible in a symplectic process; in a symplectic process the emittances in different directions can either remain the same or be exchanged among themselves. The flat-beam technique circumvents this limitation because the process of beam birth in a magnetic field is non-symplectic. The expected flat beam transverse emittances are [11]:

$$\gamma\mathcal{E}_{\pm} = \left[ (\gamma\mathcal{E})^2 + (\gamma\Lambda)^2 \right]^{1/2} \pm \gamma\Lambda \xrightarrow{\gamma L \gg \gamma\mathcal{E}} \begin{cases} 2\gamma\Lambda \\ \gamma\mathcal{E} \\ 2\Lambda\gamma \end{cases}$$

where  $\Lambda$  is related to the beam's mean canonical angular momentum. The emittance ratio after the round-to-flat-beam transformation is given by

$$\frac{\varepsilon_+}{\varepsilon_-} \approx \left( \frac{2\gamma\Lambda}{\gamma\varepsilon} \right)^2 = \left( \frac{eB(\sigma_c)^2}{mc\gamma\varepsilon} \right)^2 \gg 1,$$

where  $e$  is the electron charge,  $m$  is the electron mass,  $c$  is the speed of light, and  $\sigma_c$  is the transverse rms beam size of the laser on the photocathode.

The flat-beam technique was experimentally demonstrated at Fermilab's A0 Photoinjector [4] where an emittance ratio of  $\sim 100$  was achieved; see Figure 2.

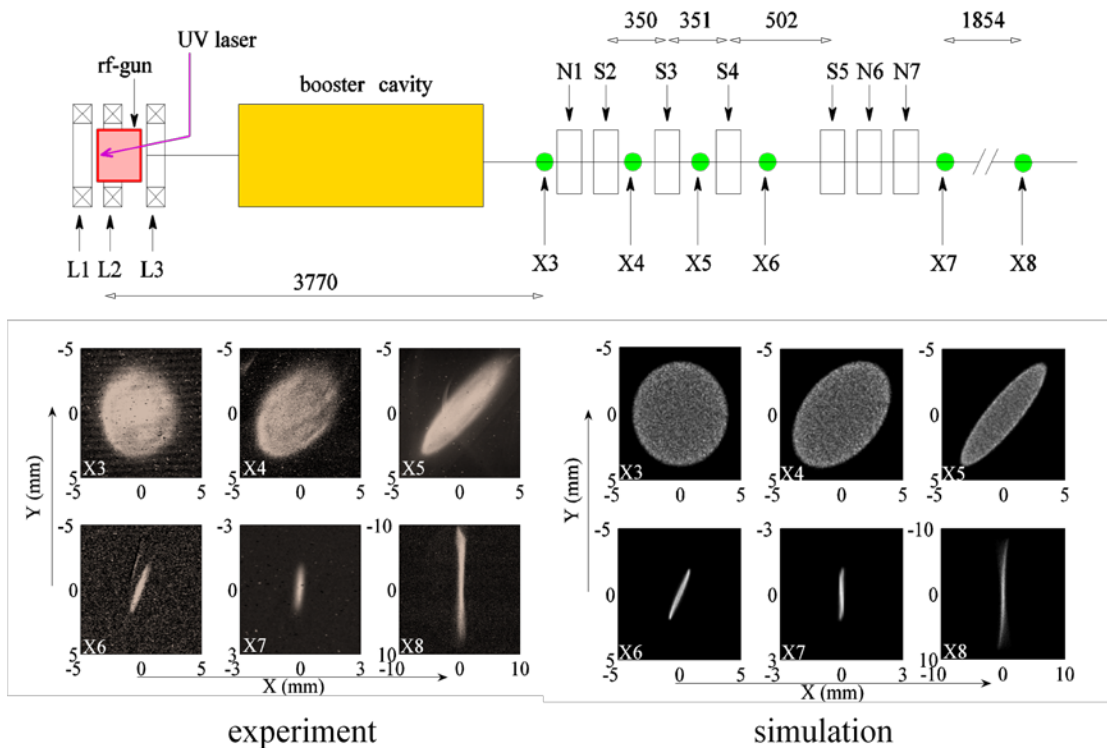


Figure 2: The round-to-flat beam transformation experiment at A0 photoinjector (from Ref.[3]). Top: experimental configuration (the labels “X”, “N”, “S” respectively represent the locations of diagnostics, normal and skew quadrupole magnets). Bottom: transverse measured (left) and simulated (right) beam density at different axial locations along the accelerator beamline.

The ASTA photoinjector incorporates a set of three skew-quadrupole magnets, a round-to-flat-beam transformer (RFBT), to possibly convert an incoming magnetized round beam into a flat beam. Furthermore, the solenoidal lenses surrounding the rf gun can be axially moved. The bucking solenoid on the rf-gun was designed to provide a large axial field on the photocathode surface. Therefore, by properly positioning the solenoidal lenses and setting their currents, the axial magnetic field on the photocathode can be tuned from zero to

thousands of Gauss. At bunch charge of 1.0 nC and beam energy of 40 MeV, the normalized emittance is optimized around  $\varepsilon_{\perp}^n = 2.3 \mu\text{m}$  [12]. This includes the thermal emittance which is about  $0.85 \mu\text{m}$  for a residual kinetic energy of 0.55 eV from CsTe cathode. Considering the case of a 1000-G axial magnetic field on the photocathode would result in a normalized angular momentum  $\gamma L = 29.64 \mu\text{m}$ ; then the achievable flat-beam transverse normalized emittances partition is  $(\gamma\varepsilon_-, \gamma\varepsilon_+) \approx (0.1, 59.4) \mu\text{m}$  corresponding to an emittance ratio of  $\sim 600$ . The small emittance will be challenging to measure with the standard multislit method but should be properly diagnosed with the quadrupole scan method. Accelerating these flat beams to 250 MeV while preserving the small emittance will also present interesting challenges and remains to be demonstrated.

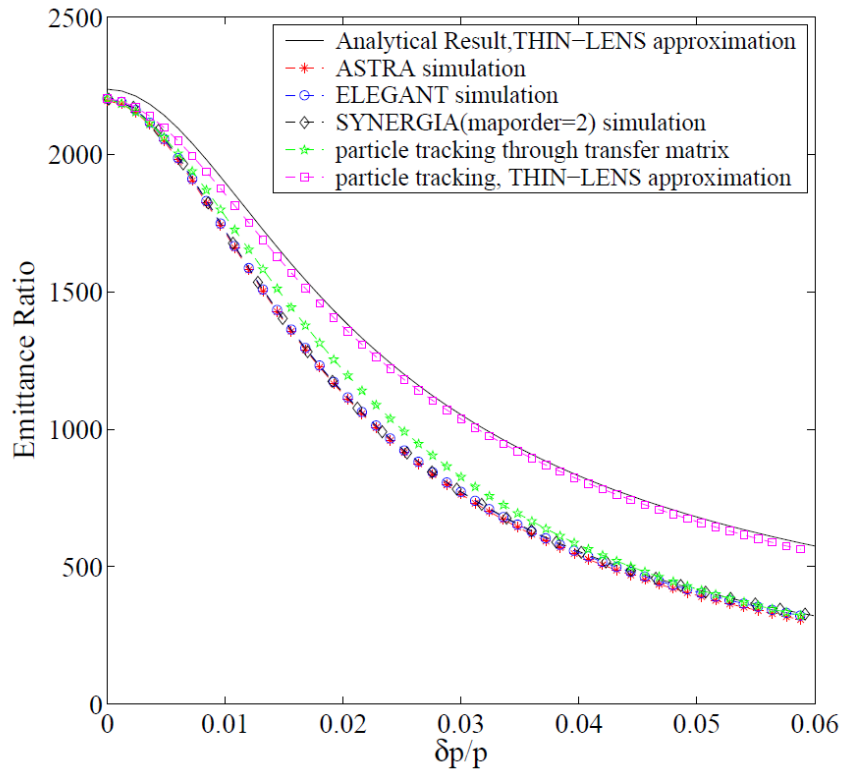


Figure 3: The Impact of chromatic aberrations on the RFTB insertion.

Finally, compressing the produced flat beam could provide exciting opportunities: compressed flat beam can be used for image charge undulators. In addition, flat beams could also provide a way to mitigate deleterious effects in magnetic chicane bunch compressor. A full compression in the injector bunch compressor (BC1) requires the longitudinal phase space to be chirped with a chirp given by  $\frac{\partial\delta}{\partial z} = -\frac{1}{R_{56}}$  where  $R_{56} \approx -0.2 \text{ m}$  is the momentum compaction associated to BC1. Therefore the required chirp will only be  $\partial\delta/\partial z \approx 5 \text{ m}^{-1}$  corresponding to a rms relative momentum spread of  $\sigma_{\delta} \approx \sigma_z(\partial\delta/\partial z) \leq 1\%$  for

typical bunch length expected downstream of the 2<sup>nd</sup> accelerating cavity (CAV2). This fractional energy spread value should result in manageable chromatic aberrations in the round-to-flat beam transformer that should not significantly deteriorate the emittance ratio; see Figure 3. This would be a significant improvement over the flat beam experiment carried at the A0 photoinjector where the low momentum compaction imposed large energy spread.

### 7.3.2.3 Transverse-to-longitudinal phase space exchange

The transverse and longitudinal phase space coordinate can be exchanged by a beamline composed of a deflecting cavity operating on the TM<sub>110</sub> flanked by two dispersive sections. A simple implementation of such a beamline is the “double-dogleg configuration” where two dispersive sections are simple doglegs composed of two dipoles; see Figure 4.

In such a configuration the condition for phase space exchange is that the normalized deflecting strength of the cavity satisfies  $\kappa = -1/\eta$ . When this condition is fulfilled and under the thin lens approximation, the horizontal and longitudinal phase space coordinates  $(x, x', z, \delta)$  before and after the EEX are related via the transfer matrix of the double dogleg beamline as follows:

$$\begin{pmatrix} x \\ x' \\ z \\ \delta \end{pmatrix}_{out} = \begin{pmatrix} 0 & 0 & \frac{L+S}{\alpha L} & \alpha S \\ 0 & 0 & \frac{1}{\alpha L} & \alpha \\ \alpha & \alpha S & 0 & 0 \\ \frac{1}{\alpha L} & \frac{L+S}{\alpha L} & 0 & 0 \end{pmatrix} \begin{pmatrix} x \\ x' \\ z \\ \delta \end{pmatrix}_{in}$$

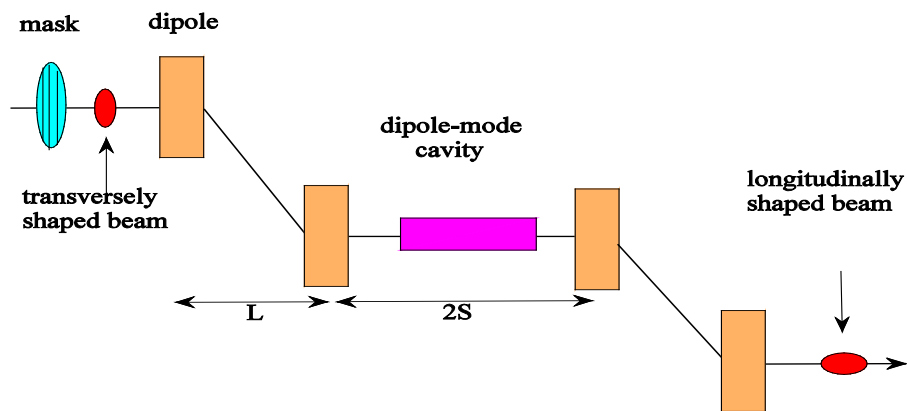


Figure 4: The Impact of chromatic aberrations on the RFTB insertion.

Since this beamline exchanges the phase space coordinates, it also swaps the transverse and horizontal emittances. In fact this was the initial motivation for developing such types of beamline [13]. A proof-of-principle experiment demonstrating the exchange of transverse and longitudinal emittances was carried at the A0 photoinjector [6]. It was later realized that this phase space exchange beamline could also be used as current shaper [14] and proof-of-principle experiment was carried at the A0 photoinjector; see Figure 5. A byproduct of this experiment was the generation of narrowband THz coherent transition radiation. The radiation was shown to have a 20-25 % FWHM relative bandwidth and was tunable over the 0.4-0.9 THz range. These experiments were limited by the mask used to produce a transversely-segmented beam (the mask was indeed optimized to measure the beam emittance). At the A0 photoinjector, the deflecting cavity used was a LN<sub>2</sub>-cooled normal conducting cavity composed of five elliptical cells following the design of a superconducting cavity developed for kaon separation [15].

We plan on continuing phase space exchange experiments at ASTA. Several avenues to improve over the series of experiments performed at the A0 photoinjector are under consideration. The overarching goals of this “second generation” phase space exchange experiments are:

1. to improve the performance of the first generation phase space exchange experiment, and
2. to find beamline configuration that would be more practical.

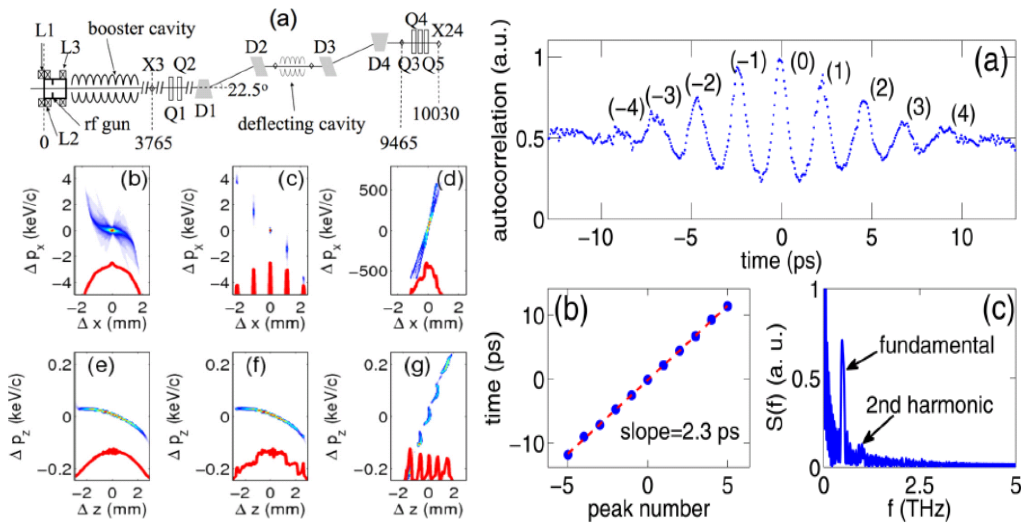


Figure 5: Left figures: (a) experimental configuration and simulated transverse (b,c,d) and longitudinal (e,f,g) phase spaces before (b,e) and after (c,f) the multi-slit mask and downstream (d,g) of the emittance-exchanger beamline. Right figure: typical autocorrelation of transition radiation (a) and corresponding peak separation (b) and frequency analysis (c).

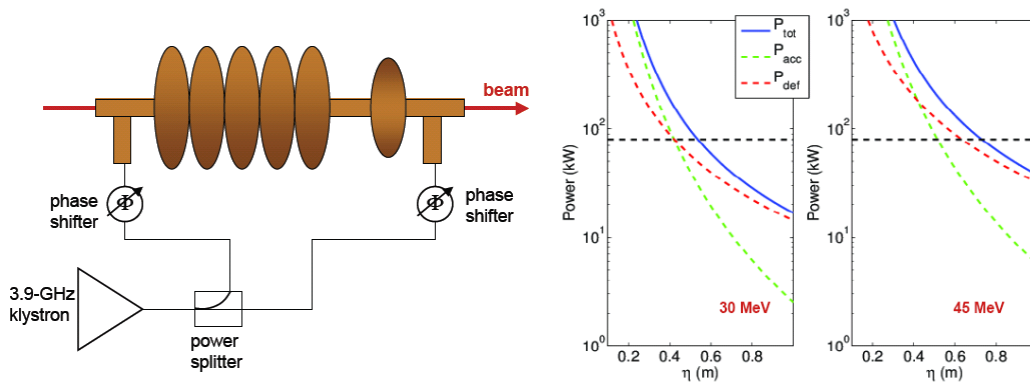


Figure 6: The “thin-lens” deflecting cavity consisting of a five-cell TM110 cavity followed by a single-cell TM010 cavity (left). Requirements on klystron power for ideal longitudinal to transverse phase space exchange as a function of the dispersion value at the cavity location. The calculations are performed for a 3.9-GHz klystron feeding an LN<sub>2</sub>-cooled system. The horizontal black line corresponds to the maximum power available from the available klystron.

Item (1) consists in improving the diagnostics downstream of the phase space exchanger beamline (the A0 experiment did not have any viable longitudinal phase space diagnostics which precluded a direct measurement of the final longitudinal emittance) and possibly considering an “hybrid” deflecting cavity that will also have a 6<sup>th</sup> cell operating on the TM<sub>010</sub> mode. The latter improvement was shown to cancel some aberration associated the realistic (and not thin lens model) of deflecting cavities [16]. The current 3.9-GHz rf system should be able to drive such a hybrid cavity provided the dispersion at the cavity is close to 0.8 m (for a 40-MeV beam); see Figure 6. One option would consist in installing a double-dogleg beamline in the 40-MeV experimental area; see Figure 7. However due to the limited 3.9-GHz klystron power (80 kW), the use of a LN2-cooled deflecting cavity forces us to increase the dispersion in order to lessen the deflecting strength required for full phase space exchange. In current layout, the dipole magnets in each dogleg are separated by 1.07m and the distance between the two center dipole is 1.99 m. Each dipole bends the beam by 22.5° while each dogleg generates a dispersion of 44 cm. The beamline was modeled using General Particle Tracer with 3D space-charge effects included for a 250 pC and 40 MeV electron bunch. The design is in essence very similar to the setup used at the A0 photoinjector but would include better diagnostics. In addition it could support experiment aiming at repartitioning the emittances within the three degrees of freedom. In such experiments, the flat beam transform would be used to create a flat incoming beam and the phase space exchange would exchange the horizontal and longitudinal emittances. This versatility would allow for parametric studies of the phase space exchange mechanism. Finally the beamline could also support more advanced current shaping technique. Using triangular mask (or shaping the transverse profile of the laser on the photocathode) could be used to produce ramped bunches which have extremely important applications in beam driven wakefield acceleration technique as they enhance the transformer ratio.

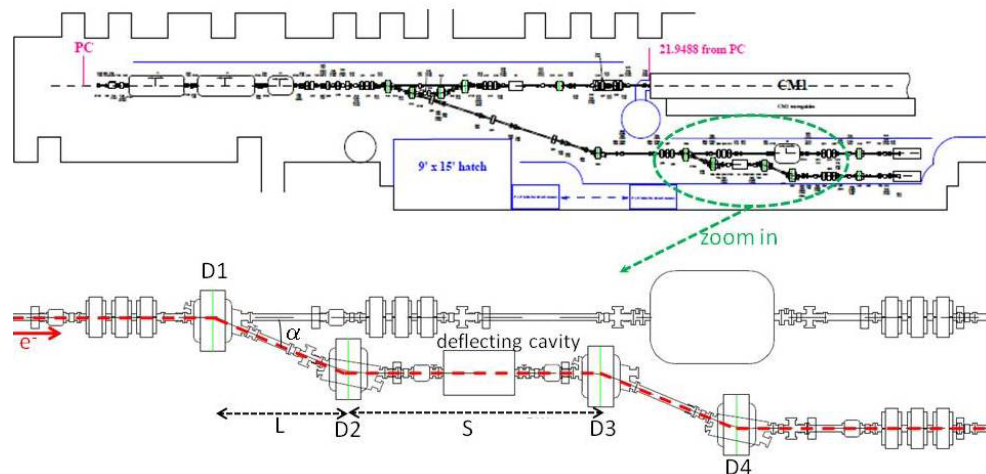


Figure 7: The NML injector and double dogleg beamline for transverse-to-longitudinal phase space exchange.

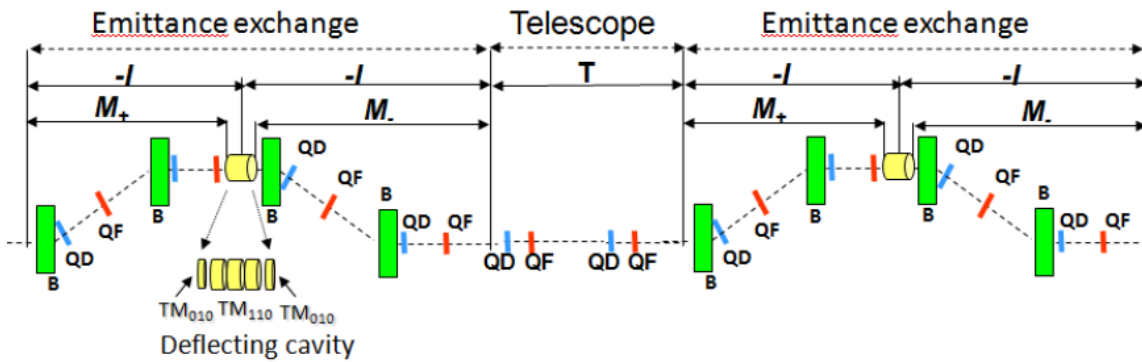


Figure 8. A possible configuration for a double phase space exchange [from Ref. 16].

Beside the double-dogleg beamline, other configurations are also possible, such as the magnetic chicane with quadrupoles inserted between the dipole. This latter setup has the main advantage of not translating the beam direction and could be a more suitable configuration for a higher energy phase space exchanger. It could also open the exploration of trade off between dispersion and deflecting strength. Numerical simulations are currently underway to explore possible layouts at ASTA.

#### 7.3.2.4 Transverse-to-longitudinal phase space exchange at ~700 MeV

The chicane-type configuration described in the previous section could form the basis for a phase space exchange beamline downstream of the accelerating section. It was recently suggested by A. Zholents that using two phase space exchangers back to back separated by an appropriate optical lattice could be used to perform the current shaping described above; see Figure 8. The shaper would be located between the two emittance exchangers.

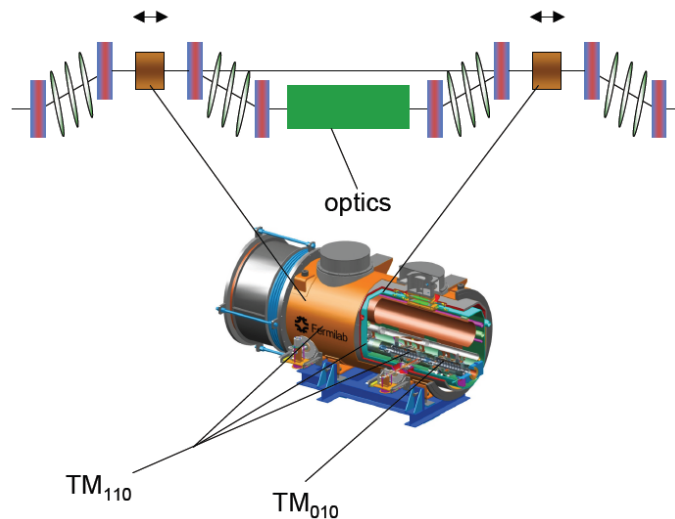


Figure 9. A possible configuration for a 3.9 GHz deflecting/accelerating hybrid SRF structure for a double phase space exchanger in the high energy beamline of ASTA.

The overall advantage of such a “double phase space exchanger” configuration compared to a single phase space exchanger is that it lets the transverse emittances untouched (under linear optics). Another important application of the double phase space exchanger scheme is to compress the beam without requiring an incoming energy correlation along the bunch. This is achieved by inserting a telescope between the two phase space exchanger, thus a bunch can be compressed without energy chirp as needed in a conventional chicane-type bunch compressor. Therefore the beam can be impressed after it goes through all the acceleration sections, thus avoid the collective effects associated with high peak current in the linac. The new double EEX bunch compressor can also be used for frequency up-conversion of the energy modulation provide by the laser interaction with electron beam, thus can possibly seeding a free-electron laser at a significantly higher harmonics; or it can also be used to do frequency down-conversion for generation of THz radiation.

The design of such a double EEX beamline would require a detailed study. From first order-of-magnitude analysis, LN<sub>2</sub>-cooled cavities would put a high demands (several MW) on the klystrons. Thus it is natural to consider a SRF system operating at 3.9 GHz similar to the system developed at Fermilab for kaon separation and longitudinal phase space linearization of the FLASH accelerator at DESY. A possible configuration is diagrammed in Figure 9.

### 7.3.2.5 References

- [1] D. A. Edwards, et al., "Status of the flat electron-beam production", Proceedings of the 2001 Particle Accelerator Conference, Chicago, p. 73 (2001).

- [2] Y.-E Sun, "Angular-momentum-dominated electron beams and flat-beam generation", PhD Dissertation, University of Chicago (May 2005).
- [3] Y.-E Sun et al., Phys. Rev. ST Accel. Beams 7, 123501 (2004).
- [4] P. Piot, Y.-E Sun, and K.-J. Kim, Phys. Rev. ST Accel. Beams 9, 031001 (2006).
- [5] T. Koeth, PhD Dissertation, "An Observation of a Transverse to Longitudinal Emittance Exchange at the Fermilab A0 Photoinjector" Rutgers University (May 2009).
- [6] J. Ruan, et al., Phys. Rev. Lett. 106, 244801 (2011).
- [7] Y.-E Sun et al., Phys. Rev. Lett. 105, 234801 (2010).
- [8] P. Piot, et al., Appl. Phys. Lett. 98, 261501 (2011).
- [9] N. Yampolski, et al., "Controlling Electron-Beam Emittance Partitioning for Future X- Ray Light Sources", preprint arXiv:1010.1558 (2010)
- [10] P. Emma, Z. Huang, K.-J. Kim, and P. Piot, Phys. Rev. ST Accel. Beams 9, 100702 (2006).
- [11] K.-J. Kim, Phys. Rev. ST Accel. Beams 6, 104002 (2003).
- [12] P. Piot, Proc. IPAC'10, Kyoto, Japan, (23-28 May 2010), p. 4316.
- [13] M. Cornacchia and P. Emma, Phys. Rev. ST Accel. Beams 5, 084001 (2002).
- [14] P. Piot, et al., Phys. Rev. ST Accel. Beams 14, 022801 (2011).
- [15] M. McAshan and R. Wanzenberg, report FERMILAB-TM-2144 (2001).
- [16] A. A. Zholents and M. S. Zolotorev, "A New Type of Bunch Compressor and Seeding of a Short Wave Length Coherent Radiation", report ANL/APS/LS-327 (2011).

### **7.3.3 Demonstration of techniques to generate and manipulate ultra-low emittance beams for future hard X-ray free-electron lasers**

#### **7.3.3.1 Abstract**

Next generation X-ray free-electron lasers (XFELs) will require significantly lower emittances than currently achievable to reach sub-Angstrom wavelengths. For example, the XFEL proposed for the Los Alamos Matter-Radiation Interactions in Extremes (MaRIE) experimental facility [1] will require 100-pC to 250-pC electron bunches with transverse emittances of about 0.15  $\mu\text{m}$  to produce 42 keV photons. New beam-based seeding schemes have additionally been proposed to provide narrow X-ray bandwidth and enhanced longitudinal coherence, also of potential use for MaRIE. The Advanced Superconducting Test Accelerator (ASTA) offers promise as a unique test bed to test and demonstrate emerging new concepts that may lead to meeting these types of requirements. Specifically, ASTA can be used to demonstrate novel emittance partitioning schemes, test compressed harmonic generation (CHG) schemes, and verify our current understanding of coherent synchrotron radiation (CSR) and to benchmark CSR simulation models.

### 7.3.3.2 Two-stage emittance partitioning

The technological limit on generating hard X-ray radiation is mainly determined by the availability of transversely bright electron beams. In order for an FEL to lase optimally, the normalized transverse beam emittance must be small,  $\varepsilon_n \leq \beta\gamma\lambda_{x-ray}/4\pi$ , to ensure overlap between the electron and X-ray phase spaces, where  $\beta$  and  $\gamma$  are the beam's velocity normalized to the speed of light  $c$  and its relativistic factor, respectively, and  $\lambda_{x-ray}$  is the X-ray wavelength. This condition is easier to satisfy at higher beam energies and this approach was used to design Linac Coherent Light Source (LCLS) [2] which generates 8 keV photons using a 14 GeV electron beam.

The next generation of hard X-ray FELs, producing photons well above 10 keV, cannot use the same approach due to increased beam energy spread caused by the single-particle synchrotron radiation at high energies. At the end of an undulator, this spread is equal to

$$\frac{\Delta E_{rms}}{E} = \sqrt{\frac{55}{48\sqrt{3}}} \sqrt{\frac{\hbar e^5 B^3}{4\pi\varepsilon_0 m^5 c^6}} \gamma L^{1/2},$$

where  $B$  is the rms undulator field strength,  $L$  is the undulator length, and  $e$ ,  $m$ ,  $\hbar$  and  $\varepsilon_0$  are the electron charge, electron mass, normalized Planck's constant, and free-space permittivity. FEL performance is degraded when the total beam energy spread is greater than the gain parameter. Estimates for generating 50-keV photons (with a 100-meter long undulator with a 2.4-cm period and a 1-T rms field, driven by a 3.4-kA beam) show that the beam energy is limited to about 20 GeV. At this energy both the induced energy spread and the FEL gain parameter are close to 0.015% and the FEL efficiency rapidly drops at higher energies. This limitation on the beam energy puts a constraint on the normalized transverse beam emittance. Numerical simulations for this case indicate that emittances as high as 0.15  $\mu\text{m}$  are marginally acceptable (these transverse emittances are about a factor of two more relaxed than the optimal constraint, with some corresponding loss of efficiency), and with performance degrading significantly as the emittance is increased above that. In contrast, the longitudinal emittance for a 150-fsec bunch and 0.01% energy spread can be as high as 180  $\mu\text{m}$ . A 250-pC electron bunch produced with currently available high-brightness photoinjectors would typically have normalized beam emittances  $\varepsilon_{x,n}/\varepsilon_{y,n}/\varepsilon_{z,n}$  of 0.5/0.5/1  $\mu\text{m}$ , with a total phase-space volume of 0.25  $\mu\text{m}^3$ . At the same time, the electron bunch required for a 50 keV XFEL must have normalized beam emittances not exceeding  $\varepsilon_{x,n}/\varepsilon_{y,n}/\varepsilon_{z,n}$  of 0.15/0.15/25, with a total phase-space volume of 0.6  $\mu\text{m}^3$ . Therefore, currently available photoinjectors can generate bunches with sufficiently small phase-space volumes, but the partitioning of this phase space into longitudinal and transverse emittances is not ideal.

These considerations have led to the proposal of two-stage emittance partitioning schemes [3] which can be demonstrated for the first time at ASTA. The overall concept is shown in Figure 1.

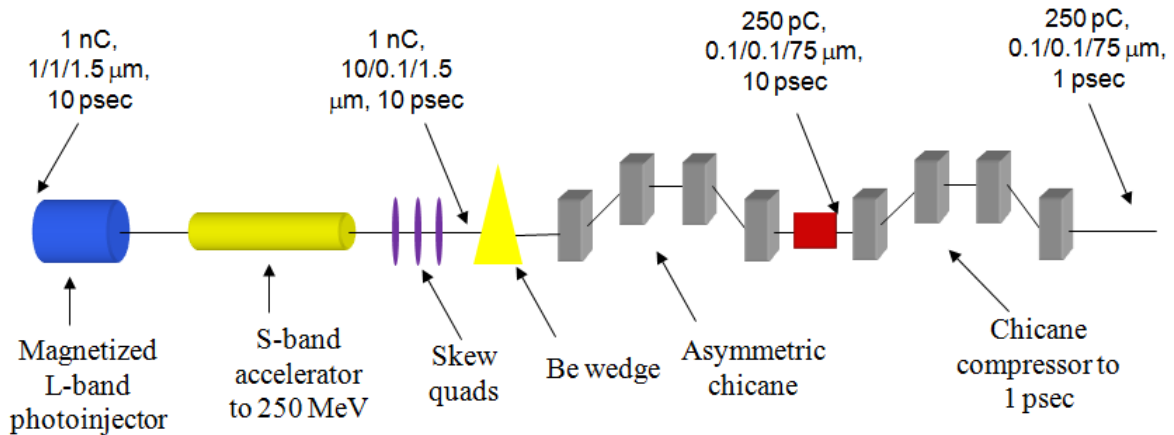


Figure 1: Overview of a two-stage emittance-partitioning scheme capable of producing an ultra-low transverse emittance beam.

A magnetized photoinjector (where the axial field at the cathode is non-zero) can lead to highly asymmetric transverse emittances, that can be recovered with a flat-beam transform (FBT), shown ideally here at 250 MeV. The larger transverse emittance (here 10 μm horizontally) can be reduced at the expense of the axial emittance by using an element to generate a horizontal-axial coupling. A wedge-shaped piece of beryllium is shown as this element. This element should not be linearly symplectic in order to change the beam's eigen-emittances. In other words, while we can always define a linear part of the beam transformation across this element  $R$  (from the quadratic part of the Hamiltonian obtained by expanding about a trajectory), the rms eigen-emittances are no longer necessarily conserved because  $\sigma_f \neq R\sigma_i R^T$  if the Hamiltonian is higher order in phase space variables.

Although a wedge is one possible non-symplectic element, a canted undulator and inverse Compton scattering are other possibilities. For a canted undulator, the undulator gap varies horizontally across the beam, leading to an energy loss due to incoherent synchrotron radiation emission correlated with horizontal position. Alternatively, an offset high-power laser can lead to an equivalent correlated energy loss due to inverse Compton scattered photons. A wedge is the simplest version for demonstrating this concept, and can be used at energies as low as 50 MeV, and with ASTA parameters. Remarkably, the eigen-emittances formed through this scheme can be recovered with a simple dogleg or asymmetric chicane.

Figure 2 shows numerical simulations illustrating features of this concept. These two figures

below show the eigen-emittances produced from a magnetized LCLS injector, through the first two traveling-wave structures (here to a total energy of 100 MeV).

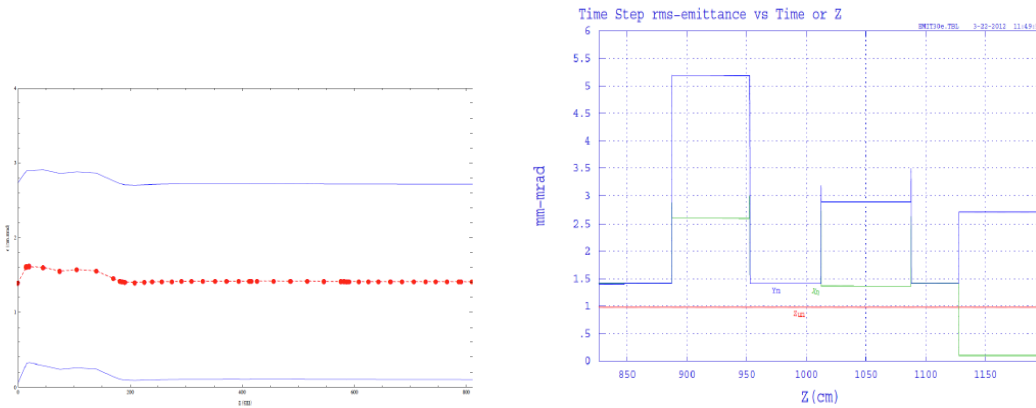


Figure 2: Evolution of the eigen (blue traces) and physical (red trace) emittances in the LCLS photoinjector (left). Emittance evolution along the RFB converter (right).

The red lines in the above left figure are the physical emittances (about 1.35 mm), and the blue lines are the eigen-emittances (about 0.1 and 2.7 μm respectively). The emittance evolution in the FBT section is shown in the above right figure, and the eigen-emittances are recovered as the physical emittances, at the levels of 0.1 and 2.7 μm. There was 605G on the cathode for this simulation and the final product of the emittances is within 10% of the optimized emittances for the unmagnetized case.

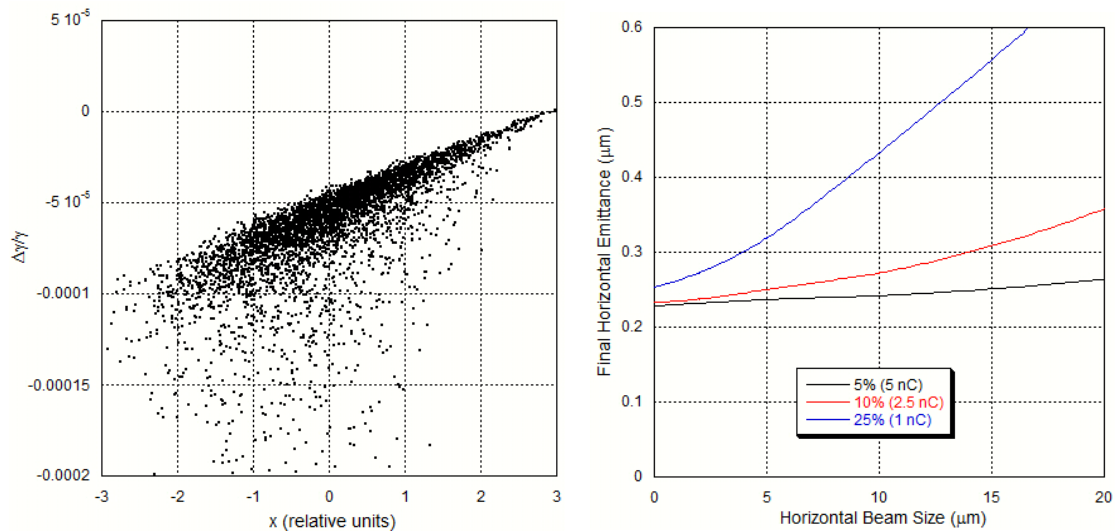


Figure 3. Energy-position correlation downstream of the wedge (left) and final horizontal emittance downstream of the asymmetric chicane (see Figure 1).

Figure 3 shows the basic concept of the second stage. After transmission through the wedge, an energy deviation is generated that is correlated with horizontal position, as shown in the above left figure. The dispersion of the dogleg or asymmetric chicane is adjusted so the energy-horizontal slew is rotated vertically, thereby decreasing the beam's horizontal size. The final normalized eigen-emittances are then (where  $\varepsilon_{n+}$  becomes  $\varepsilon_{z,n}$  and  $\varepsilon_{n-}$  becomes  $\varepsilon_{x,n}$ ):

$$\varepsilon_{n+} = \gamma\beta \left( \frac{\Delta\gamma}{\gamma} \right)_{slew} \sigma_z \quad \text{and} \quad \varepsilon_{n-} = \gamma\beta \frac{\left( \left( \frac{\Delta\gamma}{\gamma} \right)_{ind}^2 + \left( \frac{\Delta\gamma}{\gamma} \right)_{int}^2 \right)^{1/2}}{\left( \frac{\Delta\gamma}{\gamma} \right)_{slew}} \left( \varepsilon_{x,ind}^2 + \varepsilon_{x,int}^2 \right)^{1/2}$$

where here we have included the effects of both the intrinsic (*int*) beam emittance and energy spread as well as those induced (*ind*) by the interaction with the wedge. Due to these effects on the beam from the wedge, it is best to consider a larger initial bunch charge (even though that increases the initial emittances from the FBT) and to make the final 250 pC bunch charge from best 10% to 25% of the initial bunch charge (shown in the above right figure).

Preliminary estimates indicate that a 2.5 nC ASTA bunch can produce a 250 pC bunch with a product of transverse emittances about an order of magnitude smaller than starting with an optimized 250 pC bunch.

### 7.3.3.3 Compressed harmonic generation in double emittance exchangers

Theoretically, compressed harmonic generation (CHG) preserves harmonic seeding on a bunch better than other schemes like high-gain harmonic generation (HG) and even echo-enabled harmonic generation (EEHG) [4]. Conceptually, CHG is like the compression of an accordion bellows, where the modulation structure is the same as before, except the length scale has been compressed. Ratner [5] has proposed a multiple chicane based scheme, shown in Figure 4.

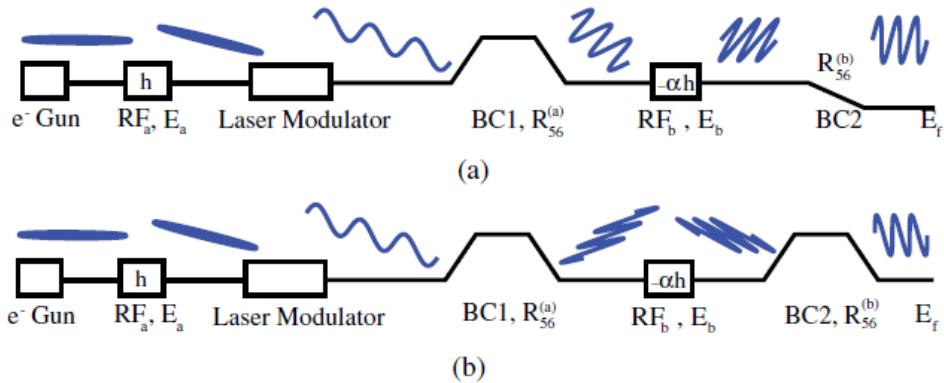


Figure 4. Principle of compressed harmonic generation (CHG).

Due to the simplicity of chicane compression, a relatively complex scheme has to be employed (otherwise the slight high-frequency modulation put on the beam gets dwarfed by the larger energy slew for the gross compression of the bunch).

A promising CHG scheme has been proposed by both Carlsten [6] and Zholents [7], where a double emittance exchanger (DEEX) is used to compress a bunch with an initial sinusoidal modulation on it. Such an architecture is diagrammed in Figure 5.

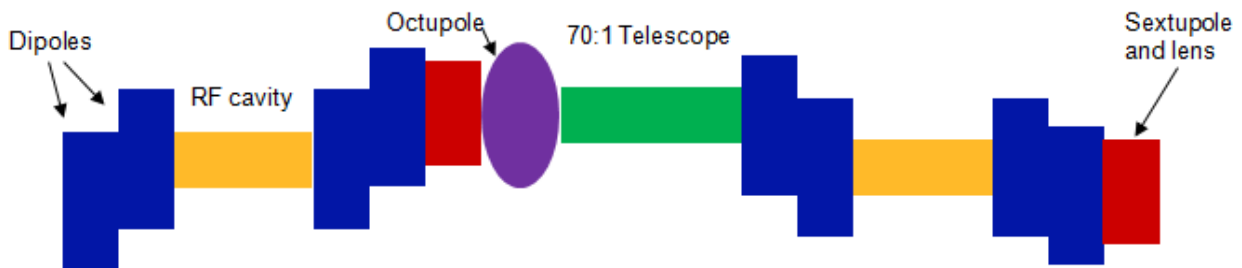


Figure 5. Principle of compressed harmonic generation (CHG) using a double-emittance-exchanger (DEEX) beamline.

ELEGANT simulations not only show that such a compressor can be used to compress a beam without emittance growth, but that the optics in between the EEXs can also be used to straighten out the curvature induced from the beam's wakefields in the longitudinal phase space, shown in Figure 6 for a nominal 1 GeV compression design.

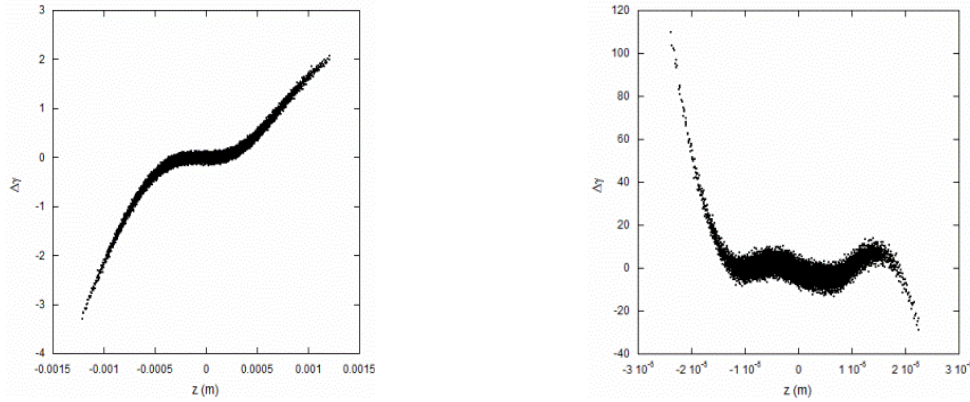


Figure 6. Longitudinal phase space before and after compression in a double emittance-exchange beamline.

Of particular importance for a CHG design is that the final axial position of a particle only depends the initial axial position, and nonlinear effects are negligible. Various designs have been proposed and modeled, and the high energy ASTA beam would lead to a compelling demonstration of one or more optimized designs.

### 7.3.3.4 Studies of CSR fields enhancement due to beam microbunching

CSR studies using exact particle fields (instead of the ultra-relativistic 1-D approximation) indicate that microbunching in beams result in much stronger energy-dependent CSR fields as compared to beams without bunching [8], see Figure 7.

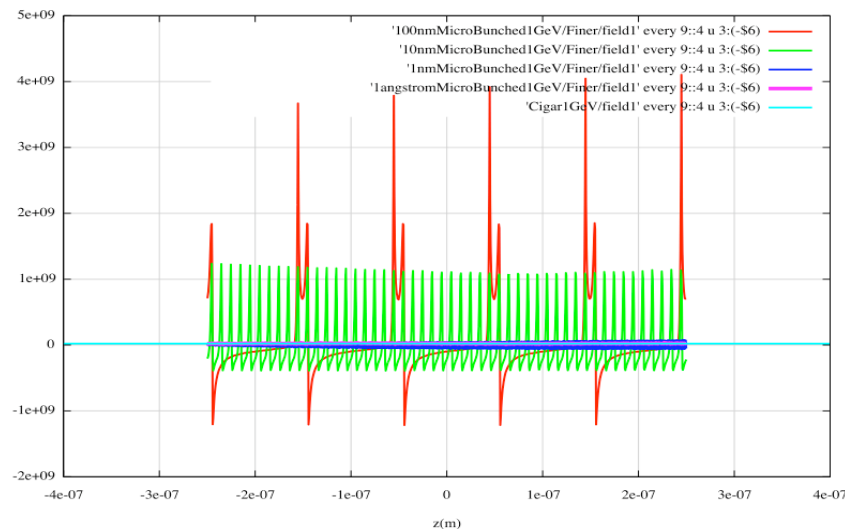


Figure 7. CSR electric field (vertical axis is in V/m) over a small fraction of the electron bunch.

For this 1 GeV case, the peak CSR field from 100-nm microbunching (shown by the orange curve above) is nearly two orders of magnitude larger than the field for an unbunched Gaussian beam (shown by the light blue curve). This effect is expected to result in an additional energy-dependent growth of the microbunching instability which may significantly increase the beam energy spread and emittance in bunch compressors. Moreover, beam-based seeding schemes for FELs may be affected by this mechanism resulting in increased beam energy spread or increased bandwidth of the microbunching (this is why the CHG scheme described above uses an energy modulation but not a current modulation).

Experimental studies of this effect can be performed at the ASTA facility. An upstream masked EEX optics can be used to create a longitudinally bunched beam in a controlled manner, as demonstrated earlier at Fermilab [9]. Specifically, the radiated power and power spectrum of the synchrotron radiation will provide enough information to determine if this enhanced CSR radiation exists, and will help benchmark numerical models used for simulating the microbunch instability.

The CSR radiation power is expected to scale quadratically with the bunch charge since CSR fields and beam current scale linearly with the total charge. In this way it will be possible to separate contributions from CSR and single-particle radiation from the total radiated power. Additionally, CSR generated by a microbunched beam is expected to be observed in two frequency domains determined by the wavelength of the microbunching and the rms bunch length. Therefore, it will be possible to determine whether beam microbunching significantly increases the effect of CSR on beam energy losses as the bunch charge and the microbunching wavelength can be varied separately from each other, which significantly simplifies the calibration of these measurements.

#### 7.3.3.5 References

- [1] <http://marie.lanl.gov>
- [2] P. Emma, et al, *Nature Photonics* **4**, 641 (2010).
- [3] B. E. Carlsten et al, "Two-stage generation of beam correlations in electron beams to establish low transverse beam emittances," submitted to *Physical Review Special Topics – Accelerators and Beams*, 2011.
- [4] N. A. Yampolsky, "Description of modulated beam dynamics," submitted to *Physical Review Special Topics – Accelerators and Beams*, 2012.
- [5] D. Ratner, A. Chao, and Z. Huang, *Phys. Rev. ST Accel. Beams*, **14**, 020701 (2011).
- [6] B. E. Carlsten, K. A. Bishofberger, S. J. Russell, and N. A. Yampolsky, *Phys. Rev. ST Accel. Beams*, **14**, 084403 (2011).
- [7] A. Zholents and M. Zolotarev, "Emittance exchange and bunch compression," presentation to the 2011 Particle Accelerator Conference, New York (2011).
- [8] B. Carlsten, et al, "Three-dimensional coherent synchrotron radiation calculations," presentation to the 50<sup>th</sup> ICFA Advanced Beam Dynamics Workshop on Energy Recovery

Linacs, presentation available at

[http://erl2011.kek.jp/author\\_information/oral/index.html](http://erl2011.kek.jp/author_information/oral/index.html).

[9] Y.-E. Sun, et al, *Phys. Rev. Lett.*, **105**, 234801 (2010).

## 7.3.4 Beam-beam kicker for electron-ion collider

### 7.3.4.1 Letter of Intent

August 14, 2012

Dr. Vladimir Shiltsev, Director  
Accelerator Physics Center  
Fermi National Accelerator Facility

Dear Vladimir,

As you know, Jefferson Laboratory is conducting study of possibilities for future high luminosity polarized Medium Energy Electron-Ion Collider (MEIC) at JLab: [see Ref.[1] or [http://casa.jlab.org/meic/files/MEIC\\_Report.pdf](http://casa.jlab.org/meic/files/MEIC_Report.pdf)].

Crab-crossing beams of low charge very short (up to 5 - 10 mm) bunches at high repetition rate (up to .75 - 1.5 GHz) is the luminosity concept. Collider design includes use of ERL-based Electron Cooling for 20 - 100 GeV hadron beam. In order to reduce the required electron current in ERL, the cooler scheme is complemented with a Circulator-cooler ring (CCR) operated by a fast kicker in a CW mode. Creation of fast kicker of raise time in range of a fraction of ns is the central challenge of the CCR and cooler design.

As a clearly envisioned and promising version of such a kicker, we considering your kicker beam idea you proposed in 90s [2]. As an adjustment for more efficiency of your concept, we consider implementation of round to flat transformations of both beams in the kick sections. The imagined scheme is described in more detail and illustrated in numbers in the attached note.

It is our understanding that, in order to proceed firmly with these developments toward a viable cooler design and creation of a test device, we have to incorporate and rely essentially on collaboration with professionals of Fermi Laboratory and, specifically, with you and your Accelerator Physics Center which has experts and experience over many aspects of the related beam physics and techniques. I also would like to add that, our cooperation certainly could be extended to the joint efforts on whole the cooler design, building and tests for MEIC and other facilities with high energy hadron beams.

I would appreciate very much your reply, would you and your colleagues been interested in the subjects and cooperative work in these directions.

If you find it timely to start with connections on the matters, I can suggest the following names (CASA members) for communications:

Dr. Yuhong Zhang  
MEIC Project Manager. [Yzhang@jlab.org](mailto:Yzhang@jlab.org)

Dr. Eduard Nissen.  
["Nissen@jlab.org"](mailto:Nissen@jlab.org)

Dr. Geoff Krafft,  
 CASA Director. [Krafft@jlab.org](mailto:Krafft@jlab.org)

Prof. Y. Derbenev  
 Scientist, [derbenev@jlab.org](mailto:derbenev@jlab.org)

### 7.3.4.2 Beam-Beam Kicker

An innovative idea recently under active investigation for MEIC project [1] utilizes a non-relativistic sheet beam for providing transverse kicking to a flat electron bunch [3]. This idea of a beam-beam kicker was first proposed by Shiltsev [3] for two round Gaussian beams. Here we consider a case of two flat beams as shown in Figure 1, though analytical treatments for these two cases are quite similar. We present here final results plus considerations of cooling electron bunch requirement in order to have an effective kicker scheme. Two technical issues will be also briefly discussed.

Since the target flat (cooling) beam is moving at the speed of light, it passes through the non-relativistic kicking flat beam in a period of time determined by the length of the kicker beam  $l_k$ . We consider ejection/injection of cooling bunches in the horizontal plane by kicks in  $x$ -direction, so both beams should be flattened in the kick sections to have a small horizontal size while relatively large the vertical sizes. This can be achieved by use of magnetized beams and performing flattening gymnastics, specific for each of two beams. At a close distance to the kicking beam, an electron in the target beam receives an instant horizontal angle kick determined by integration of the transverse force over that passing time

$$\theta_k = \frac{2\pi N_k r_e}{\gamma l_{yk}}$$

under conditions

$$\theta_x \ll \theta_k$$

and

$$\sigma_x, \sigma_y, h \ll l_{yk}$$

where  $N_k$  and  $h$  are number of electrons and vertical size of the kicker bunch,  $\theta_x$  and  $\theta_y$  is the angle spread and transverse size of the cooling bunch in horizontal plane,  $\gamma$  is its Lorentz factor, and  $r_e$  is the electron classical radius.

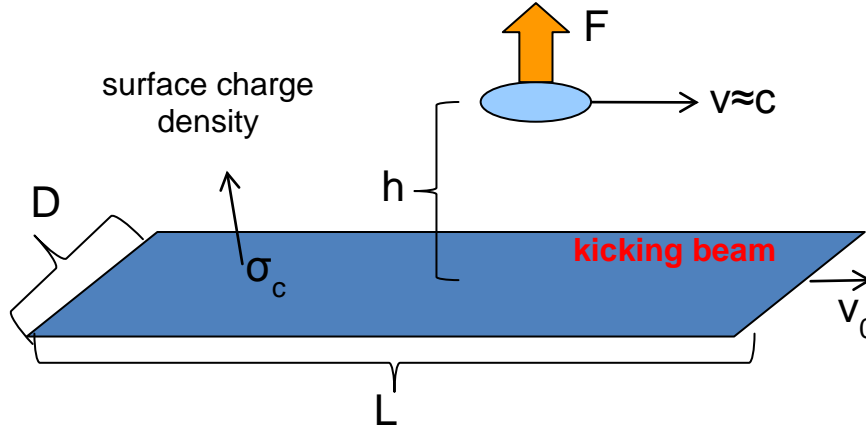


Figure 1. A schematic drawing of a fast beam-beam kicker

In order to reduce the required kick, the cooling beam should have a small horizontal emittance and possibly large horizontal beta function at the kicker section. Combining this with the flatness condition, we find the following requirements to the cooling beam:

$$\theta_k \gg \sqrt{\frac{\epsilon_x}{\gamma\beta_x}} \rightarrow \frac{2\pi N_k r_e}{\gamma l_{yk}} \gg \sqrt{\frac{\epsilon_x}{\gamma\beta_x}}$$

$$\sigma_y = \kappa l_{yk}; \quad \kappa \ll 1$$

$$\sigma_x = \sqrt{\frac{\epsilon_x}{\gamma} \beta_x} \ll l_{yk} = \frac{1}{\kappa} \sqrt{\frac{\epsilon_y}{\gamma} \beta_y}$$

Table 1 summarizes the design parameters for a beam-beam kicker for the ELIC CR cooler design. It should be noted that, with 100 to 300 revolutions of cooling electron bunches in the CR, the repetition frequency of the kicking beam can be a factor of 100 to 300 smaller than the repetition rate of the CW cooling beam.

### 7.3.4.3 Making of a Flat Kicker Beam

A flat kicker beam can be produced utilizing a grid-operated DC (thermionic) electron gun with a round magnetized cathode. While maintaining the beam in solenoid, one can impose a constant quadrupole field that causes beam shrinking in one plane while enlarging in the other plane due to the drift motion of particles. The process should be adiabatic relative to the particles' cyclotron motion in the solenoid [3]. The beam current density could be specifically profiled at the cathode to create uniform distribution in a homogenous field in a direction transverse to in the "plane" of flattened beam.

### 7.3.4.4 Obtaining a Flat Cooling Beam

While the magnetized state of a cooling beam is transplanted from the gun to the solenoids in the cooling section, the beam can be made flat at a kicker section of the circulator ring applying round-to-flat beam transformation proposed for an angular momentum dominated beam [4]. Such transformation can be performed by a special group of skew-quadrupoles matched with optics of the circulator ring. This will create flat beam with two very different emittances [4-6]:

$$\frac{\epsilon_x}{\epsilon_y} = \frac{\epsilon_c}{\epsilon_d} = \frac{r_c^2}{a_0^2}$$

here  $r_c$  and  $a_0$  are the characteristic cyclotron radii of electrons and beam area radii in solenoid of cooling section, respectively.

Table 1. Design parameters for MEIC beam-beam kicker

|                              |      |         |
|------------------------------|------|---------|
| Circulating beam energy      | MeV  | 33      |
| Kicking beam energy          | MeV  | ~0.3    |
| Kicking Repetition frequency | MHz  | 5 – 15  |
| Kicking angle                | mrad | 0.2     |
| Kicking bunch length         | cm   | 10 – 20 |
| Kicking bunch width          | cm   | 0.5     |
| Kicking bunch charge         | nC   | 2       |

### 7.3.4.5 Uniqueness of ASTA

The beam-beam kicker concepts proposed aim at demonstrating the deflection of a flat beam using a non-relativistic sheet beam at MHz repetition rate. The availability of bunch trains with comparable intra-bunch frequency along with the round to flat beam transformation make ASTA uniquely suited to carry out the beam-beam kicker experiments.

### 7.3.4.6 References

- [1] S. Abeyratne, et al, "Science Requirements and Conceptual Design for a Polarized Medium Energy Electron-Ion Collider at Jefferson Lab" (JLAB, 2012), [http://casa.jlab.org/meic/files/MEIC\\_Report\\_20120810\\_rev1-2-5.pdf](http://casa.jlab.org/meic/files/MEIC_Report_20120810_rev1-2-5.pdf)
- [2] V. Shiltsev, NIM, A374 (1996) 137
- [3] Ya. Derbenev and Y. Zhang, "Electron Cooling For Electron-Ion Collider at JLab", Proc. of Proc. of COOL 09, Lanzhou, China, 10-14 Sept. 2009.
- [4] Ya. Derbenev, University of Michigan Report No. UM-HE-98-04, 1998.
- [5] A. Burov, S. Nagaitsev, and Ya. Derbenev, Phys. Rev. E **66**, 016503 (2002)
- [6] Y.-E Sun, et al, "Generation of angular-momentum-dominated electron beams from a photoinjector", Phys. Rev. ST Accel. Beams **7**, 123501 (2004)

## 7.3.5 Feasibility of an XUV FEL Oscillator at ASTA

### 7.3.5.1 Abstract

The ultrabright electron beam with a micropulse repetition rate of 3 MHz and GeV-scale energy of the Advanced Superconducting Test Accelerator (ASTA) facility could enable the *first* XUV free electron laser oscillator (FEL) experiments. The ultrabright beam will provide sufficient gain to compensate for reduced mirror reflectances in the VUV-XUV regimes, the micropulse repetition rate will support an oscillator configuration, the SRF linac will provide energy stability, and the eventual GeV-scale energy will provide the resonance condition in the XUV. Concepts based on combining such beams with a suitable undulator and optical resonator cavity for an FEL are described. In addition preliminary single-pass studies using undulator radiation (UR) as a nonintercepting diagnostics technique for bright electron beams are presented. Initial studies at visible wavelengths would be done for 125-MeV electron beams using an undulator with period of 4-5 cm, magnetic structure length of 4.5 m, and tunable field parameter,  $K$ . Standard time-resolved imaging techniques would be employed to evaluate beam size, position, emittance, bunch length, phase, and energy during the macropulse. Extension of the techniques to higher energy beams using the corresponding UV and VUV UR will also be described.

### 7.3.5.2 Introduction

One of the exciting challenges of the present-day and proposed superconducting linear accelerators with concomitant high-power beams is identification of unique new applications for those beams. The high-power electron beams for the Advanced Superconducting Test Accelerator (ASTA) facility involve up to 3000 micropulses at a 3 MHz repetition rate with up to 3.2 nC per micropulse in a 1-ms macropulse in the ILC-like mode [1]. With beam energies projected from 45 to 800 MeV, various beam dynamics issues will be addressed, but it is proposed such a beam in a lower-charge and low-emittance mode

could also uniquely drive the *first* extreme ultraviolet (XUV or EUV) free-electron laser (FEL) oscillator experiments. These anticipated transform-limited photon pulses in wavelength and pulse length would address issues of limited bandwidth inherent to the self-amplified spontaneous emission (SASE) FELs that start from noise and should be competitive with seeded FELs as discussed in a recent LBNL-SLAC workshop [2]. An existing undulator is combined with a previously suggested ring resonator optical configuration [3,4] or a concentric cavity optical configuration that in principle could fit the FELO in the ASTA tunnel. Preliminary estimates are reported for the FEL oscillator power saturation at 42 nm and 13.4 nm with scaling to shorter wavelengths with higher beam energies and shorter period undulators.

In preparation for the multi-pass FEL tests, single-pass experiments are also proposed that provide the non-intercepting diagnostics of the beam size, emittance, energy, bunch length, and phase. The acquisition of a comprehensive set of electron beam properties from a linear accelerator based on undulator radiation (UR) emitted from a 5-m long device was demonstrated over two decades ago on a visible wavelength free-electron laser (FEL) [5] driven by a pulse train of 100- $\mu$ s extent. Comparable investigations were performed using x rays with a dedicated diagnostics undulator on two storage ring projects [6,7]. The high-power electron beams of the ASTA facility with beam energies projected from 45 to 800 MeV will need non-intercepting diagnostics. Besides the rf BPMs, optical synchrotron radiation (OSR), and optical diffraction radiation (ODR) techniques already considered, I propose the use of the properties of undulator radiation for electron-beam diagnostics from a dedicated device with a nominal period of 4-5 cm, a tunable field parameter  $K$ , and a length of several meters. One proposes time resolving the e-beam properties within the macropulse by viewing the undulator radiation with standard electronic-shuttered CCDs or gated ICCD's (size and position) and a synchroscan streak camera coupled to an optical spectrometer (energy, bunch length, and phase). The feasibility of extending such techniques in the visible regime at a beam energy of 100-125 MeV into the UV and VUV regimes with beam energies of 250 and 500 MeV will be presented.

After discussion of the single-pass mode aspects, I introduce considerations of taking full advantage of the ASTA electron beam's 3-MHz micropulse repetition rate and 6-dimensional ultrabright beam quality to drive the first XUV FEL oscillator using an on-axis concentric optical cavity or a ring resonator optical configuration. This would be a unique opportunity to shatter the existing short-wavelength record of 176 nm in an FEL oscillator [8], and such a demonstration would impact the designs of the next generation of light sources.

The proposal to push the FEL oscillator concept to shorter VUV wavelengths requires a high-repetition rate to enable build-up of the radiation field within the FEL oscillator cavity. The 3-MHz, 1-ms bunch length train available only at ASTA and the anticipated single-bunch brightness are shown to be adequate to drive a short-wavelength FEL oscillator. The availability of such a high-average-brightness electron beam is unique to ASTA.

### 7.3.5.3 Conceptual Aspects of Undulator Radiation

The propagation of the electron beam through the alternating magnetic fields of an undulator results in electron beam trajectory oscillations and the generation of co-propagating photons as schematically shown in Figure 1. This is initially through the spontaneous emission radiation (SER) process, but under the right conditions in a long undulator a favorable instability evolves, and the electron beam is microbunched at the resonant wavelength leading to a self-amplified spontaneous emission (SASE) FEL. This intrinsic SASE-induced microbunching (SIM) is fundamental to all SASE FELs and analogous microbunching occurs in all FELs. For a planar undulator, the radiation generation process on axis is governed by the resonance condition:

$$\lambda = \lambda_u (1 + K^2/2)/2n\gamma^2, \quad \text{Eq. 1}$$

where  $\lambda$  is the UR wavelength,  $\lambda_u$  is the undulator period,  $K = e B_0 \lambda_u / 2\pi mc = 0.934 \lambda_u$  (cm)  $B_0$  (T) is the undulator field strength parameter ( $B_0$  is the magnetic field in the gap,  $e$  and  $m$  are the electron charge and mass, and  $c$  is the speed of light),  $n$  is the harmonic number, and  $\gamma$  is the relativistic Lorentz factor.

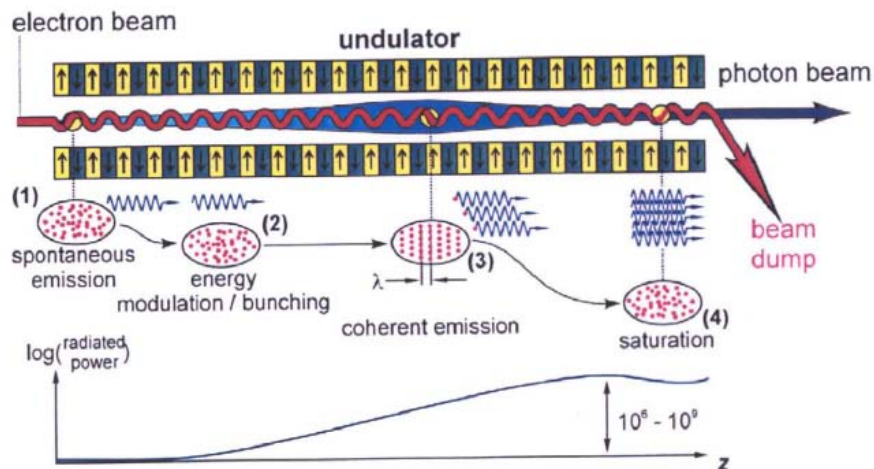


Figure 1: Schematic of the generation of undulator radiation for SER and SASE mechanisms [9].

Additionally, it has been calculated that there is coupling strength for energy exchange between the copropagating electrons and the photon fields at the third harmonic of the planar undulators as shown in Figure 2 from reference [10]. The coupling coefficients  $JJ_n$  for  $n=1,3,5$  versus  $K$  are reasonable, although with a rapid decrease in their values below  $K=1.5$  for  $n=3,5$ . This indicates that the generation and measurement of these harmonics may in some cases be advantageous, particularly if the goal is to reach shorter wavelengths for a given beam energy.

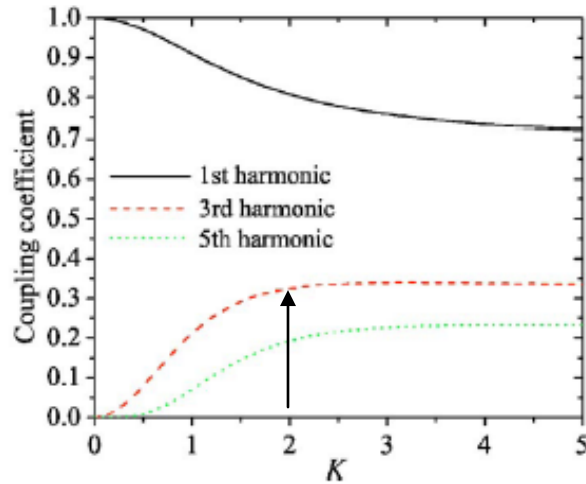


Figure 2: Coupling coefficients for odd harmonics for a planar wiggler as a function of  $K$ . The  $\gamma=500$  case with  $K=1.8$  is indicated by the arrow. [10]

#### 7.3.5.4 Proposed Studies

The ASTA linac (see Fig. 4, Sec. 8.2.3) with photocathode (PC) rf gun, two booster L-band SRF accelerators (CC1 and CC2), and beamline will provide 40- to 50-MeV beams before the chicane, and an additional acceleration capability up to a total of 800 MeV will eventually be installed in the form of three cryomodules with eight 9-cell cavities with average gradient of up to 31 MV/m after the chicane. The phase of the CC2 section can be adjusted to energy chirp the beam entering the chicane to vary bunch-length compression. Maximizing the FIR coherent transition radiation (CTR) in a detector after the chicane will be used as the signature of generating the shortest bunch lengths. Micropulse charges of 20 to 3200 pC will be used typically. The nominal pulse format for high power ILC-like beam is 3.2 nC per micropulse at 3 MHz for 1 ms, and the macropulse repetition rate will be 5 Hz. As schematically shown in Figure 3, this aspect is unique for test facilities in the USA and highly relevant to the next generation of FELs as will be discussed later in this paper. Basic applications of an undulator with ASTA beams are next described with the most significant being the feasibility of an XUV or EUV FEL oscillator being driven by such beams.

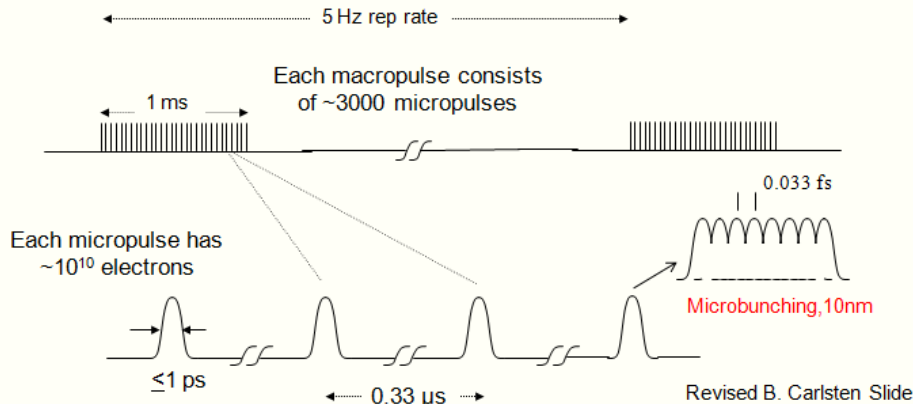


Figure 3: Schematic of the ASTA pulse structure showing the key time scales from ms to  $\mu$ s to ps to fs.

### 7.3.5.5 Application 1: Diagnostics Undulator

Initially single-pass operations with an undulator would enable the use of UR properties for deducing time-resolved electron beam properties. The base image size and position will be seen in the UR spot size and transverse position (although the size will have depth-of-focus issues to address. A telescope with limited depth of focus may be used to emphasize a shorter  $z$  length within the undulator's 4.5 m length.) The central wavelength of the emission is directly correlated with electron-beam energy, and the bandwidth from the UR will be about  $1/nN$  (where  $n$  is the harmonic number and  $N$  is the number of periods) or 1% for 100 periods at the fundamental and 0.3% at the third harmonic. Signal strengths should allow tracking of a subset of the micropulses with standard imaging. The UR pulse length would be measured with the UV-visible C5680 streak camera, and this pulse length should be correlated with the electron beam bunch length subject to some narrowing when there is SASE gain. The synchroscan streak camera will also allow tracking of the relative phase within the macropulse of sets of micropulses to about 200 fs. At this time we anticipate one would provide optical transport for the signals to the high energy end laser lab where a small diagnostics suite of CCD camera, ICCD camera, streak camera, and optical spectrometer would be available on an optics table for characterizing the UR properties and the deduced electron-beam properties. Initial detection could be in the tunnel with local camera stations or detectors.

It is proposed to start studies during the commissioning of the first cryomodule at a beam energy of 125 MeV. As shown in Table 1 with the 5-cm period and the magnetic gap adjusted for  $K=1.2$ , the fundamental UR would be at 680 nm with a third harmonic at 226 nm. One could track the beam at higher energies by reducing the gap and increasing the  $K$  value so that the resonance condition remains in the visible-UV regime to simplify the early tests. One can also consider 150-, 200-, and 250- MeV cases as given in Table 1. At 150 MeV the e-beam energy and bunch length via the central wavelength and pulse length of the UR,

respectively, could be evaluated prior to injection of beam into the Integrable Optics Test Accelerator (IOTA) ring since the transport lines separate the paths at the high-energy end.

Table 1: Summary of possible SER/UR estimated wavelengths predicted with a 5-cm period undulator following the cryomodule(s) at ASTA at 125 MeV and higher electron-beam energies. The last row is for a SC undulator with shorter period built for the ILC R&D program in England [13].

| Phase # | Beam Energy (MeV) | Undulator Fundamental (nm) | Period (cm), $K$ | Undulator Radiation Harmonics (nm) 3, 5 |
|---------|-------------------|----------------------------|------------------|---|
| 1       | 125               | 680                        | 5.0, 1.2         | 226                                     |
| 1       | 150               | 472                        | 5.0, 1.2         | 157                                     |
|         | 200               | 265                        | 5.0, 1.2         | 88                                      |
| 1       | 250               | 170                        | 5.0, 1.2         | 57                                      |
| 1       | 250               | 262                        | 5.0, 1.8         | 87                                      |
| 2       | 500               | 42                         | 5.0, 1.2         | 14, 8.3                                 |
| 3       | 800               | 16                         | 5.0, 1.2         | 5.3                                     |
| 3       | 800               | 13.7                       | 5.0, 0.9         | ---                                     |
| 4       | 900               | 3                          | 1.1, 0.9         | ---                                     |

At these wavelengths and for the expected beam quality, the gain length should be sub-meter so sufficient SASE-induced microbunching should also occur in the 4.5-m length that could be accessed by demonstrated coherent optical transition radiation (COTR) techniques [11]. In the past these have allowed evaluation and adjusting of the critical electron-beam-photon-beam overlap [12].

In Phase 2 with two cryomodules and a beam energy of 500 MeV, one would need VUV diagnostics since the resonance condition for the fundamental would be at  $\sim 42$  nm with the third harmonic at 14 nm and the fifth at 8.3 nm. An available in-vacuum flange-mounted 40-mm diameter microchannel plate (MCP) manufactured by BURLE Electro-Optics has been identified as a candidate 2D imager that has sensitivity from 1 eV to 50 keV. The output P43 phosphor would be viewed by a standard CCD camera, and two-dimensional images of the VUV UR angular distribution (and CVUVTR if one can block VUV UR) could be recorded. These should indicate laser/e-beam angular overlap which has been shown to impact SIM and FEL gain [12]. The bunch length and phase information could be tracked by collaborating with Dr. B. Yang on use of ANL's Hamamatsu VUV-X-ray streak camera mainframe with FNAL's M5676 synchroscan units tuned to 81.25 MHz. The intrinsic time resolution will not be as good as in the visible regime ( $\sigma < 1$  ps), but the flexibility for sub-macropulse studies would be maintained as well as system phase stability.

Implementation of such a streak camera with a VUV spectrometer is also possible in principle.

Evaluation of the LBNL multilayer metal mirrors at various VUV-XUV wavelengths, and testing of their robustness to photon-beam pulse trains would be of interest. The multilayer mirrors would be located after the downstream dipole to eliminate e-beam bombardment. Development of VUV filtering schemes would also be tested. More detailed harmonic information should be obtained by use of imaging spectrometers in the UV and VUV (McPherson spectrometer version has a series of gratings to use and an imaging array for display). There also may be e-beam emittance effects detectable in the relative harmonic intensities and/or the spectral widths.

#### **7.3.5.6 Application 2: XUV FEL Oscillator**

In a separate proposal section (7.3.8) the possibility of laser-induced microbunching and high gain harmonic generation (HG) FEL R&D at ASTA was explored [14]. In principle the 4.5-m long undulator could be the radiator for seeded FEL tests at 40-50 nm (but probably would not reach saturation). This would require an upstream modulator and chicane to be installed with the appropriate parameters. This is under evaluation, but we will defer further discussion of this aspect here in favor of the more intriguing application: the investigation of a VUV-XUV FEL oscillator configuration. The ASTA pulse train at 3 MHz with a bright electron beam of nominal transverse emittances of  $2 \pi$  mm mrad, peak current of 300 to 800 A, GeV-scale energy, energy spread of  $5 \times 10^{-4}$  provides the enabling technology. Over two decades ago numerical studies using a ring resonator optical configuration were executed at Los Alamos with the FEL 3D simulation code, FELEX, in the VUV and XUV regimes [3]. This relied on two grazing incidence mirrors on-axis and two off-axis multifaceted mirrors (with 6 facets each) to obtain the individual mirror reflectivities needed in the XUV. This is schematically shown in Figure 4. They considered operations at 100, 50, 12, and 4 nm. At the time their 90% normalized emittance numbers, which I interpret as 4-sigma values, varied from 31 to  $10 \pi$  mm mrad (the latter being viewed as speculative at that time, but critical for the 4-nm case). They were using a photo-injected gun and normal conducting L-band rf linac in the plan with 8 nC per micropulse of 20 ps duration and transverse emittances of about  $25 \pi$  mm mrad [4]. At this time, one can expect to surpass at ASTA even their emittance speculations, albeit with lower charge per micropulse. Although they considered a 1.6-cm-period undulator with low  $K$  value, we can use higher energies than their 261 MeV to reach the resonance conditions in the 40-50 nm regime with only two cryomodules installed. One notes initial gain length evaluations could be done empirically in the single-pass mode before the final design, and a test of the resonator optical path tuning could be initiated with UV-Visible light with only one cryomodule operating.

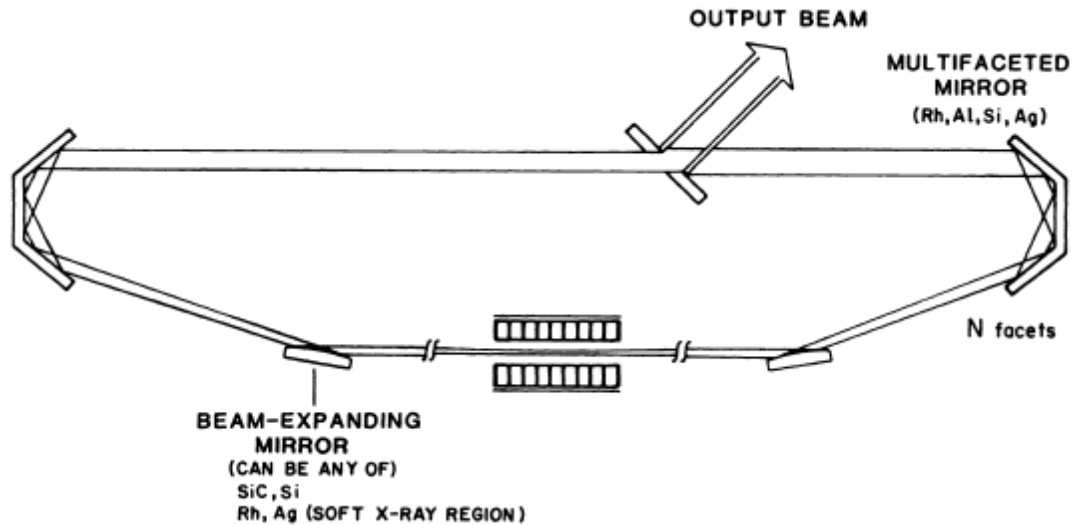


Figure 4: A schematic of the ring optical resonator for an XUV FEL oscillator using multifaceted mirrors and on-axis beam-expanding mirrors [3].

One can also consider, in principle, an on-axis concentric optical cavity based on two mirrors with  $z$  separation of 50 m (100 m roundtrip) with photons striking at 90 degrees to the surface of the multilayer metal mirrors. If each mirror has  $\sim 70\%$  reflectivity as reported for multilayer metal mirrors at LBNL in the XUV regime, the expected gain should exceed the losses. Examples at shorter wavelengths with Mo/Be and Mo/Si multilayers are shown in Figure 5, and the second case is at the key lithography wavelength of 13.4 nm. Some focusing element would still be needed to provide a Rayleigh range of about 2.2 m for the optical mode. Key issues of spherical aberrations and thermal distortions of the mirrors would be common for all of the designs since absorption of energy is expected in the mirrors. These issues may determine whether a simple concentric cavity would be actually practical.

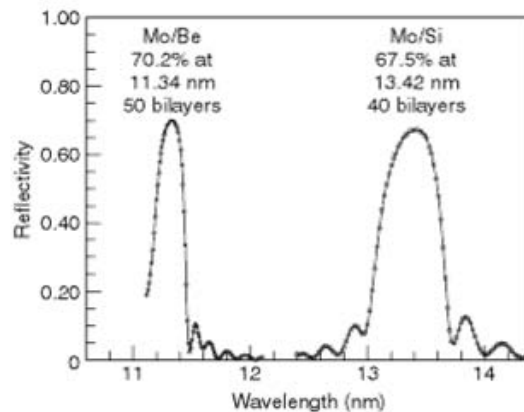


Figure 5: Examples of the reflectivities for multilayer metal mirrors with the incidence angle of 90 degrees to the surface. X-ray Data Booklet, Section 4.1, James H. Underwood, CXRO-LBNL website.

In the ring resonator mode the resonator plane would be vertical (horizontal) so the circulating UR would pass just above (or left side of) the undulator. For a 100-m path length resonator, we would need one optical pass to time with the 100-m spacing of the electron beam micropulses at 3 MHz (alternatively, one optical pass of 50 m length for a 6-MHz micropulse rate). A single optical pass is definitely preferred so use of the full 50 m in z in the tunnel should be considered. The z length in the beam line would be about 46 m with 2-m distances to the respective off-axis mirrors. In the concentric cavity mode, only two on-axis mirrors are used. A chicane (not shown) could be used to transport the e beam around the left end on-axis mirror location in either case. Figure 6 shows the ring resonator with z-footprint of about 23 m and 50-m optical path (invoking the 6-MHz rate) as it might fit into one high-energy AARD test area. Note this area is about 42 m downstream of the end of cryomodule 3 and where the chicane might be positioned for the 50-m spacing. (The initial Los Alamos design with two grazers and two multifaceted mirrors is only a little longer at 29.5 m in z for a 60-m round trip path) Simplistically, the gain,  $G$ , should satisfy the relation  $(1+G)(\text{Total reflectivity}) > 1$  so we need about three gain lengths in the undulator in this case [15]. Based on our previous calculations for SASE gain lengths of about 1 m at 26-40 nm with a different undulator with 3.3-cm period [16], the 4.5-m undulator length should be enough to reach the needed gain and reach saturation in a few hundred passes. Output power coupling of FEL photons was previously proposed by a scraper mirror in one arm of the transport or by a mm-radius hole in one of the mirrors [3, 17].

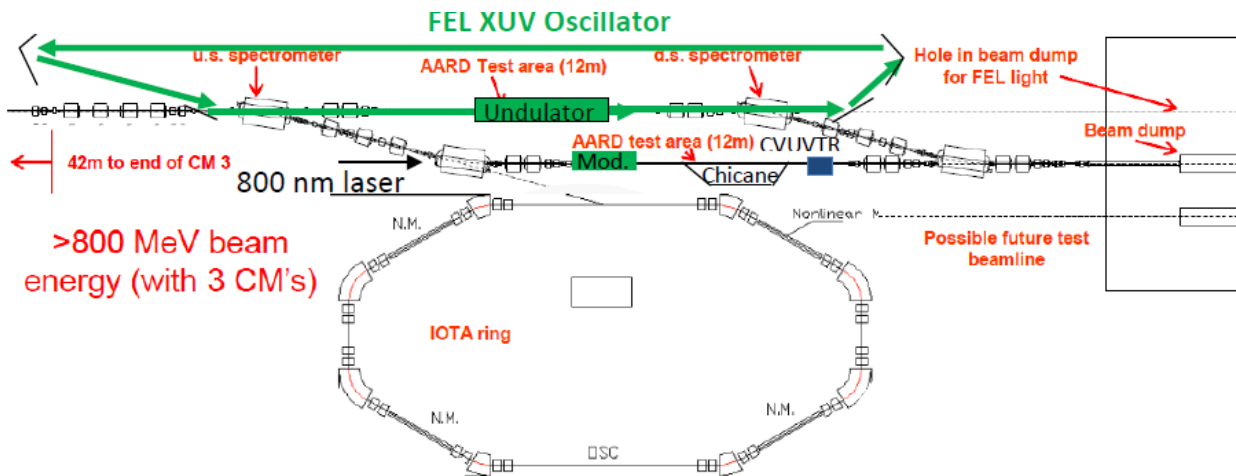


Figure 6: Schematic of the experiment layout in one high-energy AARD test area at ASTA for the undulator and XUV FEL oscillator. In the ring resonator mode the resonator plane would be vertical so the circulating UR would pass just above the undulator as if the green arrows in this figure are a side view.

The above are rough estimates so I recently requested modeling of the oscillator properties and parameter dependencies with an existing 1-D particle tracking code with support for oscillators at LBNL. The initial calculations were to be followed by GINGER-based simulations for a subset of conditions as performed at LBNL. The LANL paper had reported a 50-nm FEL case with just a 5-m undulator length [3] so this regime is where we started. The

ASTA 42-nm case at 500 MeV beam energy was just evaluated by M. Reinsch (LBNL), and the results are shown in Figure 7 for a 400-A peak-current value. The cavity was approximated with four reflections with a net power reflectance of  $(0.7)^4$ . This was a compromise on a single-pass ring resonator estimate. The Beta value assumed was 5 m for the electrons at the undulator. The encouraging results show power gain of  $10^5$  in 62 passes and saturation after about 100 passes for the 400-A case. The power saturates even sooner for 500- and 600-A cases. The gain length was computed at 1.0 to 1.2 m in the exponential growth regime so the 4.5 m undulator length was needed. The issues of mirror quality, thermal distortions, and mirror damage need also to be addressed. Perhaps the old FELEX code can be used to assess the former issue and newer codes the latter. There is expected to be relevant expertise at LBNL for XUV mirror robustness issues, and the newer mirror cooling techniques may be needed.

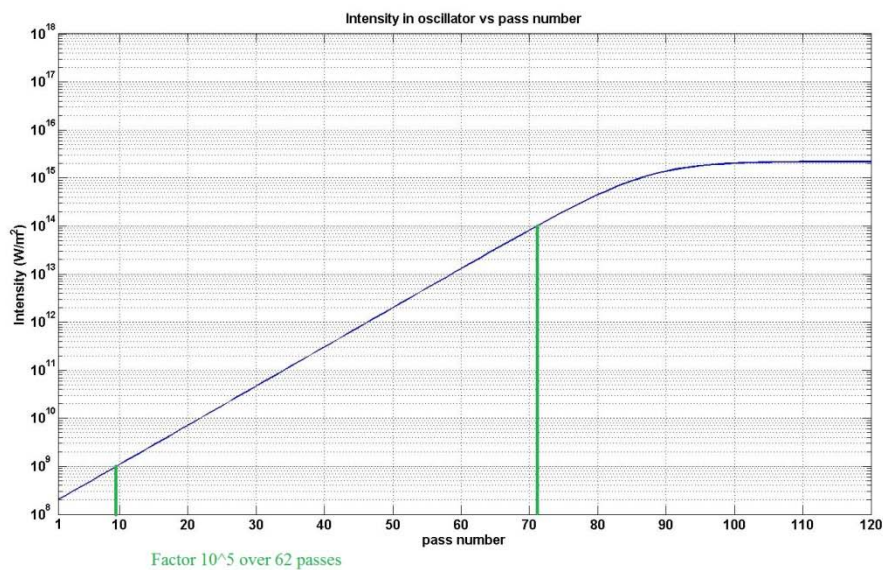


Figure 7: Preliminary FEL oscillator calculational results at 42 nm, using 400 A and 500 MeV beam based on the 1-D particle tracking code with support for oscillators at LBNL. (courtesy of M. Reinsch)

More recently the first GINGER simulations for oscillator cases with projected ASTA beam parameters have been run at LBNL in consultation with M. Reinsch. These calculations were done using the 4.5-m undulator length. After discussion with optics experts at LBNL, surprisingly the solutions for longer wavelengths of 40-50 nm with multilayer mirrors are estimated at only 40-50% reflectivity as compared to their reported 68% value at 13.4 nm. It appears that in this full simulation shown in Figure 8, the effective gain length is less optimistic than the 1-D code, but one still can reach output power saturation at 40 nm and 13.4 nm in the concentric cavity cases invoking 50% and 68% reflectance, respectively, at 90 degrees using multilayer metal mirrors. This would occur after about 300 passes in the potential 3000-micropulse train with an 800-A peak current for 13.4 nm as shown in Figure 8b. These are only one example of the over 20 diagnostics plots from the simulations for each case. The multifacet mirror concept with comparable net reflectances may thus be the primary solution for broadband tunability of the FEL. In general, photon optics development

for high reflectivity and at high power remains a critical R&D topic that is ongoing at different light source and laser laboratories.

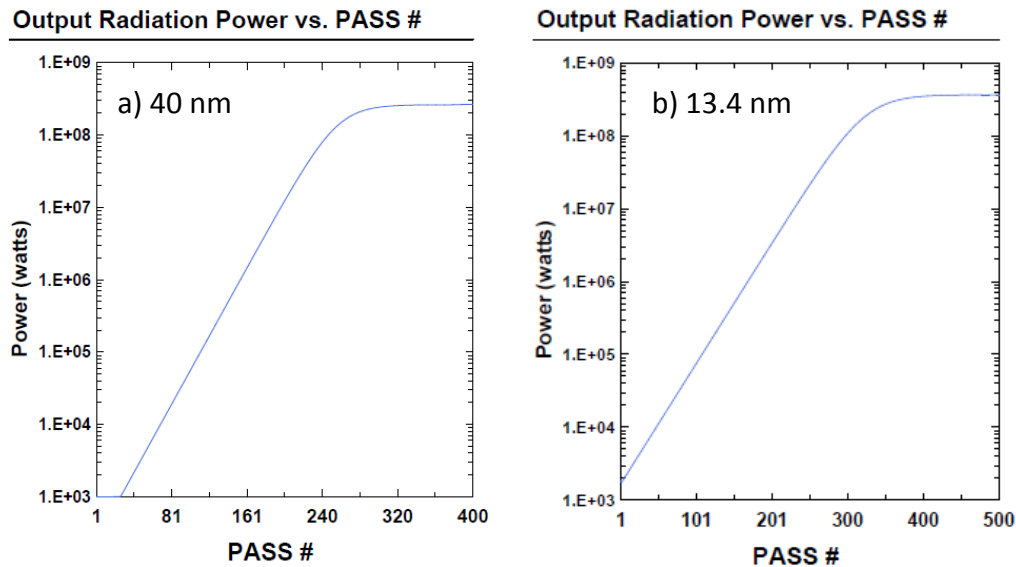


Figure 8: Initial GINGER simulations for output power saturation at the fundamental wavelength of a) 40.0 nm and b) 13.4-nm for a concentric cavity with multilayer mirror reflectances of 50 % and 68%, respectively. Peak currents of 700 A at 470 MeV and 800 A at 800 MeV were used with N=90 periods. The output power growth with pass number is shown. (courtesy of M. Reinsch)

There is a significant opportunity for this FEL oscillator R&D that can uniquely be done at ASTA. It is one possible configuration of the next generation of light sources with the potentially narrower bandwidths (transform limited) needed by some science cases, and should complement the seeded and self-seeded FEL configurations. Demonstration of an FEL oscillator at even 40-50 nm would shatter the existing world record of ~180 nm [8]. With higher energies and shorter period undulators the few-nm regime should be attainable in principle as roughly scaled in the Phases 3 and 4 of Table 1, assuming the ring resonator concept with multifaceted mirrors is viable and/or cooled mirrors are used.

### 7.3.5.7 Practical Considerations

The two investigation areas provide a compelling case for consideration of installing such an undulator in ASTA. We currently have an option for the U5.0 undulator device [18] that is being retired from the ALS storage ring in January 2013. There are some practical considerations, however, mostly driven by the labeled weight of 47,000 lbs which is close to the NML crane's 25-ton capacity. The undulator has a 5.0-cm period, 4.5-m magnetic structure length, a maximum field strength of 0.87 T at 1.4-cm gap, and a remotely controlled adjustable gap from 1.4 to 21.4 cm leading to a range of  $K$  values. The strong back and the specification to have the device's gap constant to about 50  $\mu\text{m}$  over the 4.5 m length leads to the very substantial support structure. Its total height is 2.4 m as compared to the ASTA tunnel height of 3.2 m (10.5 ft). The vacuum chamber is 5.1 m flange to flange

and has an antechamber. As staged at ALS, the beamline centerline is at ~55 inches, higher than our ASTA beamline center of 48 inches. There appears in reference [18] to be a base plate under the frame of about 15 in. height that might be shortened. These should be evaluated for modification, or we have to shift the beam trajectory upward with a dogleg in this area. Two photographs of the device in situ from M. Wendt's visit to LBNL in April 2012 are shown in Figure 9, and initial device characterizations were previously reported [19]. I don't believe there are any diagnostics or quadrupoles embedded within the structure's length. The mechanical, vacuum, and gap control aspects should be still evaluated by experts at FNAL.



Figure 9: Photographs of the ALS U5.0 Undulator in the storage ring in April 2012.

Also, the estimated cost for a 1-m length permanent magnet device, 2-cm period, and with fixed gap from a vendor (as I recall) was \$125 K with a 12-15 month lead time based on discussions with undulator-cognizant staff at ANL and LBNL in 2011. The permanent magnets themselves have been on a 12-month lead time from Japan for many months. There is a flexible magnet design with 2.4-cm period at Cornell [20], but at the moment no 4.5-m-long device to borrow. The ALS U5.0 option costs FNAL the shipping, installation, and controls time, but the device replacement value is over \$1M (vendor's replacement estimate provided at FEL12). In the present budget climate, an undulator in hand is worth two elsewhere.....or priceless.

#### **7.3.5.8 Summary**

In summary, we have described applications at ASTA of a 5-cm period undulator with 4.5-m length *and* tunable magnetic gap including: 1) non-intercepting e-beam diagnostics using UR during commissioning of the first cryomodule and 2) the magnetic structure for the *first* XUV FEL oscillator in the world. Although the ALS device may not be optimized for each application, its presence would jump start photon-related research at ASTA and support initial FEL oscillator tests at ~40 nm and perhaps 13.4 nm later. In the future, use of shorter period (1.8 cm) permanent magnet devices or existing 1.1-cm-period SC devices and higher beam energies would allow us to push to few-nm wavelengths and soft x-rays which should

be of interest to the next-generation-of-light-source strategies (and consequently DOE/HEP, DOE/BES, and the National Science Foundation). The experiments should drive mirror technology implementations, XUV detector development, and preliminary basic science experiments that need transform-limited coherent photon sources of sub-ps duration as consistent with the identified mission needs of DOE. This would be a highly leveraged test program since the major infrastructure of the SRF linac is assumed as given and an undulator transfer negotiation is underway. The oscillator cavity and some detectors are the incremental costs and estimated as a fraction of the replacement value of the undulator. Finally, we note that FEL technology has been proposed recently at the Higgs Factory Workshop [21] as a possible high power photon source (when combined with Compton back scattering from 80-GeV electrons) for future gamma-gamma colliders. Exploration of parameter spaces available with the SRF-linac-driven FEL configurations with the 1-ms pulse train could be initiated.

#### **7.3.5.9 Acknowledgements**

The author acknowledges discussions with: M. Wendt, M. Church, H. Edwards, S. Nagaitsev, and S. Henderson of FNAL on the ASTA facility and the AARD program; R. Lindberg (ANL), M. Reinsch (LBNL) and J. C. Goldstein (LANL, retired) on FEL oscillators; and J. Ruan of FNAL on UV-Visible optical considerations.

Notes: Installation of 1-3 cryomodules assumed with transport of beam to the high energy beam dump. The details of the soon-to-be-retired ALS U5.0 undulator's transfer to FNAL are ongoing. The mirror chambers are estimated at \$25k each for single mirrors with piezo adjustments for the initial concentric UV case. The ring resonator with multifacet mirrors needs further evaluations. A diagnostics suite would also be needed, but initially an existing in-vacuum MCP with standard camera, and YAG:Ce or LYSO:Ce scintillator crystals with photo detectors could be used. A VUV-XUV spectrometer would be needed to evaluate laser performance.

#### **7.3.5.10 References**

- [1] Sergei Nagaitsev, "ILC-TA at NML", ILC-TA Workshop at Fermilab, November 2006; J. Leibfritz, "Status of Plans for a Superconducting RF Test Facility at Fermilab", Proc. of IPAC12, May 2012.
- [2] "Realizing the Potential of Seeded Soft X-ray FELs Workshop", hosted by LBNL and SLAC, Berkeley CA, Oct. 26-28, 2011.
- [3] B.E. Newman et al., SPIE Vol. 1552, 154 (1991).
- [4] John C. Goldstein, Brian. D. McVey, and Brian E. Newman, Nucl. Instr. and Methods in Phys. Research A296, 288 (1990); B.E. Carlsten, Nucl. Instr. and Methods in Phys. Research A285, 313 (1989).
- [5] Alex H. Lumpkin, Nucl. Instr. and Methods in Phys. Research A296, 134-143 (1990).
- [6] E. Tarazona and P. Ellaume, Rev. of Sci. Instrum. **66**, 1974 (1995).

- [7] Alex H. Lumpkin and Bingxin Yang, Phys. Rev. Letters, Vol. 82, No. 18, May 3, 1999, pp. 3605-3608.
- [8] F. Curbis et al., Proc. of the 27<sup>th</sup> FEL Conference, 473, JACoW econf, (2005).
- [9] Based on D. Moncton slide at the WIFEL Workshop in Oct. 2007 and the original paper by R. Bonifacio, C. Pellegrini, and L. Narducci, Opt. Commun. 50,373 (1984).
- [10] P. Musumeci, C. Pellegrini, and J.B. Rosenzweig, Phys. Rev. E **72**, 016501 (2005).
- [11] A.H. Lumpkin et al., PRL **88**, 234801, (2002).
- [12] A. H. Lumpkin et al., Proceedings of the 25<sup>th</sup> FEL Conference, Tsukuba, Japan, Sept. 8-12, 2003, NIMA 528, pp. 179-183 (2004).
- [13] E. Baynham et al., Proc. of PAC09, WE2RAIO1 (2009).
- [14] A. H. Lumpkin, J. Ruan, J. M. Byrd, and R. Wilcox, "Potential for Critical Laser-Induced Microbunching Studies with the High-Micropulse-Repetition Rate Electron Beams at ASTA", DocDB Fermilab Dec. 2011.
- [15] R. Lindberg (private communication, June 2012).
- [16] A.H. Lumpkin, M. Church, H. Edwards, S. Nagaitsev, and M. Wendt, "Considerations on Fermilab's Superconducting Test Linac for an EUV/Soft X-ray SASE FEL", Proc. of FEL10, JACoW, (2010).
- [17] Neil Thompson et al., "The 4GLS VUV-FEL", 29-03-07.
- [18] E. Hoyer et al., Rev, Sci. Instrum. 63 (1), 359 (1992). This paper describes the ALS U5.0 undulator design.
- [19] P. Heimann et al., Rev, Sci. Instrum. 66 (2), 1885 (1995).
- [20] A. Temnykh, Proc. of PAC09, MO6PFP084, 324, JaCoW (2009).
- [21] T. Raubenheimer, "SLC and NLC -type Higgs Factory", Higgs Factory Workshop, FNAL, Nov. 14-16, 2012.

## 7.3.6 Production of Narrow Band Gamma-Rays

### 7.3.6.1 Letter of Intent

October 10, 2011

Stuart Henderson  
Vladimir Shiltsev  
Fermilab

Dear Stuart and Vladimir:

This is an expression of our interest to do an experiment using the proposed electron beam at the New Muon Lab.

With support from Pacific Northwest National Laboratory and in collaboration with colleagues at that lab, Muons, Inc. is developing a system that will produce gamma rays with tunable energy and narrow energy spread. We have developed innovative design concepts and carried out extensive simulations in pursuit of this goal. Three papers at IPAC'10 in Kyoto described aspects of that work.

Such a system would be very useful for scanning cargo containers for the presence of dangerous contents such as fissile material. If fissile material is present, photo-fission reactions would provide a telltale signal. That application is the primary motivation for this work. Such a source of gamma rays may also be very useful for other applications in pure and applied physics.

The basic idea is to use the annihilation in flight of nearly mono-energetic positrons. The system concepts are described in detail in the accompanying summary paper. Briefly, the positrons are produced by an electron beam impinging on a high-Z target at the entrance of a dipole in which a 180-degree bend generates a dispersed horizontal focus. At that point, along the same face of the dipole, a low-Z wedge is used to render the positrons roughly mono-energetic. Another dipole separates the positron beam from backgrounds produced in the wedge, after which the positrons annihilate in flight in a thin low-Z converter plate.

The next step in the development of these concepts is to carry out a proof-of-principle experiment. We are in the process of designing such an experiment; measurements are needed to validate our simulations and to characterize the performance of a prototype system. The ideal electron beam energy is 100 MeV. The experiment will emphasize the production of gamma rays at 10 MeV. The scheduling is flexible; we believe we can be ready in two or three years. A considerable advantage of doing the experiment at Fermilab is that many of our staff are already familiar with our Fermilab colleagues and with the excellent support that Fermilab provides to experimenters.

Sincerely,

Charles M. Ankenbrandt  
Muons, Inc.

### 7.3.6.2 Description

This experiment has been proposed by Muons, Inc., an SBIR company. Basic concept is shown in Figure 1.

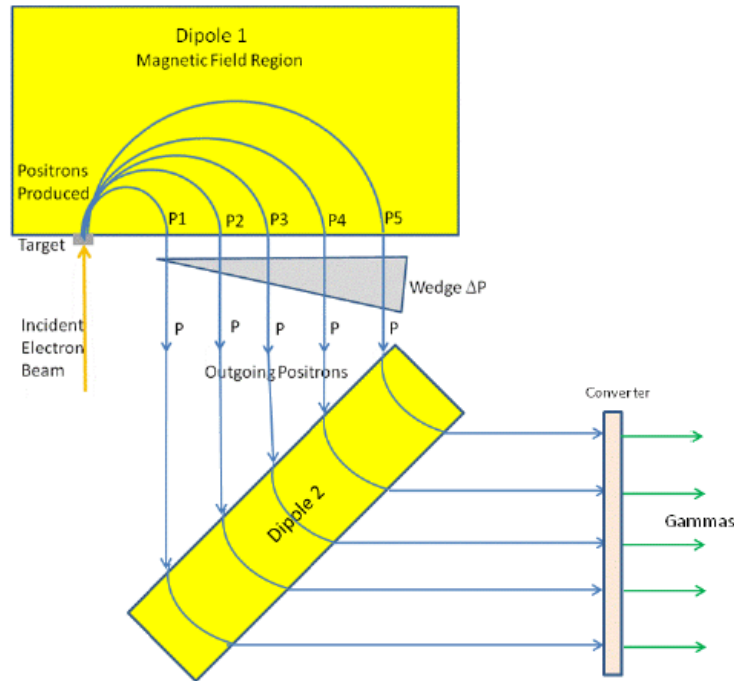


Figure 1. Concept for producing narrow band gamma-rays

"Project Gamma" has been developed under a contract with Pacific Northwest National Lab. A Preliminary Conceptual Design Document for a proof-of-principle experiment has been completed in 2012 and published [1]. It includes results of a complete end-to-end simulation of the system. More detail could be provided by request.

Generating narrowband gamma-rays with large photon fluxes would significantly improve stand-off inspection of cargos for fissile material. The proposed experiment would use the 100-MeV high-repetition rate electron bunch available through partial acceleration in ACC1 of ASTA to test a novel scheme for production of large-flux narrowband gamma-ray beams. The repetition rate and train-duration capability provided at ASTA is critical to this experiment.

Muons Inc. has submitted an expression of interest to Fermilab.

### 7.3.6.3 References:

- [1] R. J. Abrams, et al, "Conceptual design of a positron-annihilation system for generation of quasi-monochromatic gamma rays", Proc. of IPAC-2012 (New Orleans, USA, 2012), p.1476.

### 7.3.7 Inverse Compton Scattering Gamma-Ray Source at ASTA

Inverse Compton Scattering (ICS) is a process, in which an intense laser beam of optical light scatters off of a relativistic electron beam (Figure 1), forming a directional beam of photons up-shifted in energy via relativistic Doppler effect by a factor of  $4\gamma^2$ . The process is accurately characterized by the classical Thomson cross section for a wide range of output gamma energies (up to 100s of MeV), while the source brightness scales as  $\gamma^5$ , due to quadratic growth of photon energy, quadratic narrowing of the opening angle and linear reduction in the e-beam source area. As a consequence, in the medium energy range ( $\sim 10$  MeV), the ICS is a very efficient method to generate a high flux, narrow bandwidth, directional and tunable gamma-rays.

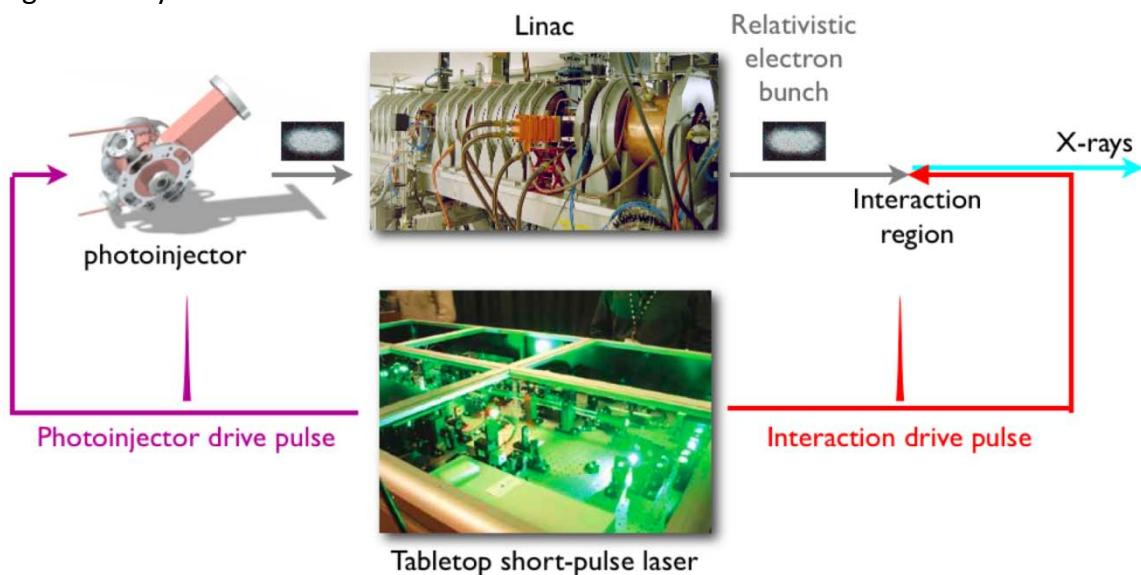


Figure 1. Pictorial diagram of the Inverse Compton Scattering process

This unique electron beam parameters space of the Advanced Superconducting Test Accelerator (ASTA) facility at Fermilab offers a possibility to develop an ICS gamma ray source of very high peak and average brightness (Figure 2).

Head-on collisions of a relativistic high-repetition rate electron beam available at ASTA with a high-repetition laser pulse could produce gamma rays with large flux for homeland

security and scientific applications. The availability of laser-produced high-repetition rate electron bunches at ASTA with unique average power and the highest average and peak brightness make this facility the best choice for the proposed ICS experiment.

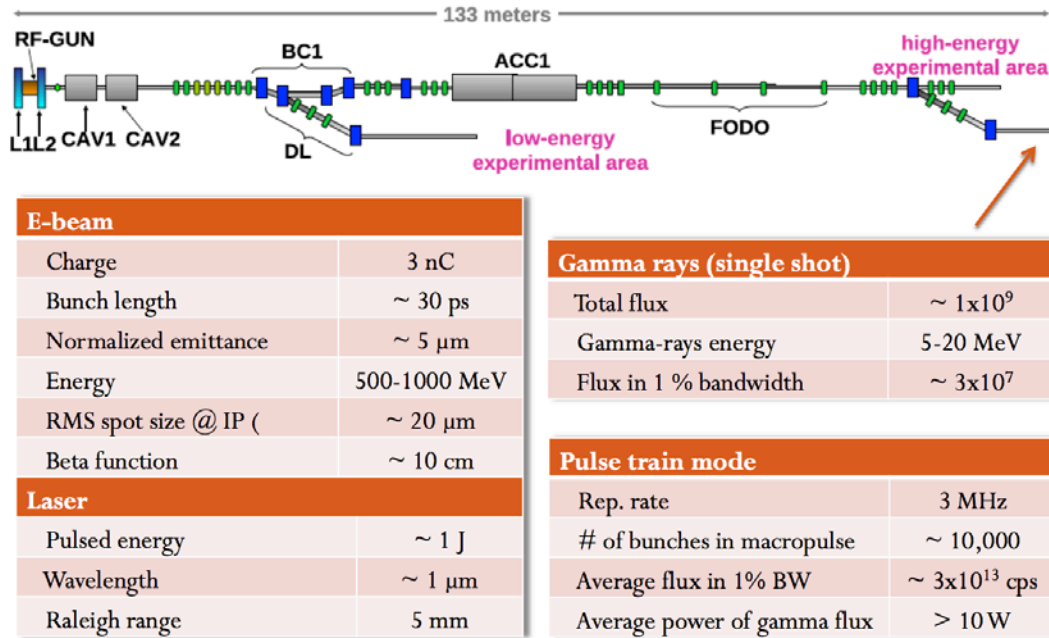


Figure 2. ASTA schematics showing location of the ICS gamma-ray source, and characteristic parameters of such source evaluated at preliminary working point (before thorough optimization).

With such parameters ASTA ICS gamma-ray source will feature an unprecedented peak brilliance: in excess of  $10^{23}$  photons/s.1%BW-mm<sup>2</sup>-mrad<sup>2</sup> at 10 MeV, at least 4 orders of magnitude above the brilliance presently achieved anywhere else, and in line with the most ambitious projects presently in the planning stage (Fig 3).

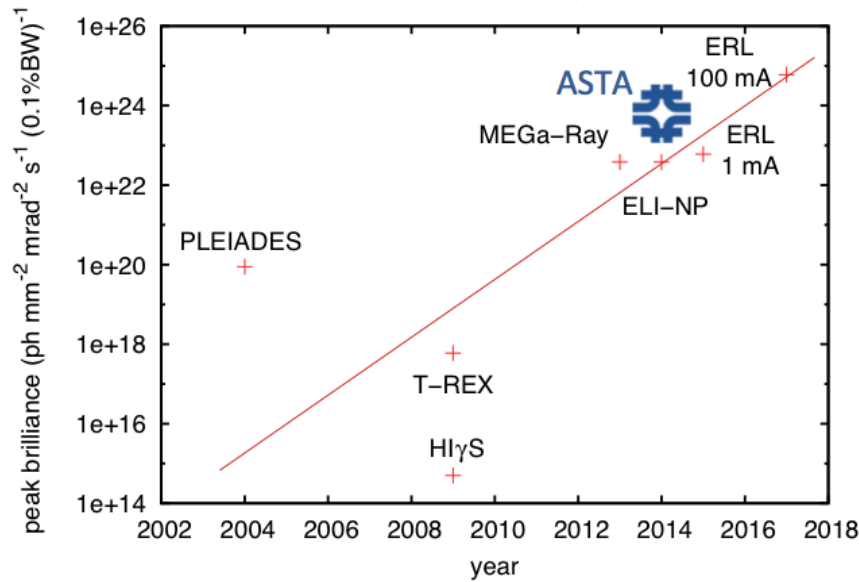


Figure 3. Comparison of the proposed source at ASTA to other existing and planned ICS gamma-ray sources normalized to 10 MeV (adapted from *D. Habs and U. Köster, Applied Physics B 103, 2011*)

Such capabilities will enable wide range of novel applications, including probing the properties of nuclear matter and nuclear physics research, synthesis of rare medical isotopes, and development of novel techniques of non-destructive testing for industrial and homeland security needs.

In fundamental nuclear physics research, high brilliance gamma-ray source can be utilized for studies of the photo-nuclear interactions, nuclear resonance fluorescence and spectroscopy, and studying a dynamics of intense gamma rays in materials. The latter is of particular interest in view of recent discovery of gamma rays refractive behavior [1], which may become a foundation for gamma ray optics development.

In addition there is strong interest in photo-nuclear synthesis of medical isotopes. In particular it was discussed in recent publications, that many specific action isotopes could be uniquely synthesized with photo-nuclear excitations by monochromatic gamma-rays. With the high flux gamma rays ASTA facility may attract a significant interest from drug discovery and biotech communities.

Other important applications of tunable gamma ray beams include remote detection of concealed special nuclear materials, characterization of the nuclear waste, non-destructive testing of bridges and other civil construction elements, as well as high fidelity industrial components and systems.

Finally, being the first of its kind gamma ray light source, ASTA ICS could also be a test bed of systems, components and advanced technologies necessary to develop commercially viable, compact, stand-alone ICS sources for medical and industrial applications.

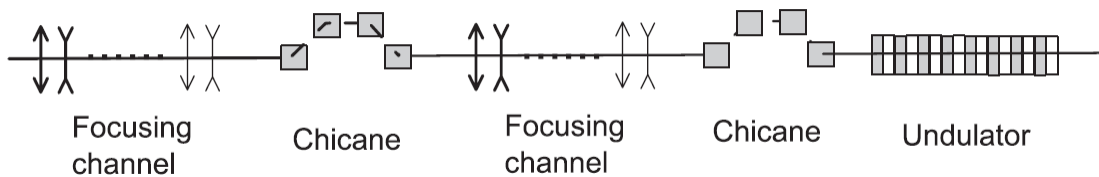
### 7.3.7.1 References:

[1] D. Habs *et. al.* , Phys. Rev. Lett. **108**, 184802, 2012.

## 7.3.8 Attosecond vacuum-ultraviolet pulses via space-charge-driven amplification of shot-noise density fluctuations

Over the past years, micro-bunching instabilities developing in high-brightness linear accelerator has received much attention as it hampers the performances of short-wavelength free-electron lasers. Such an instability develops due to the bunch self-interaction via longitudinal space charge and coherent synchrotron radiation. The micro-bunching effect has also been observed in standard beam diagnostics based on optical transition radiation.

Recently, it was proposed to control this instability to produce broadband radiation in the vacuum ultraviolet with attosecond durations.



In the proposed scheme a series of longitudinal space charge amplifier (LSCA) modules are used; see Figure above. A LSCA module consists of a transversely focusing channel that act as a longitudinal drift followed by a magnetic chicane. In the longitudinal drift, energy modulations produced by the longitudinal space charge field accumulates. In the chicane these energy modulations are converted into density (current) modulations. One can associate a gain per LSCA module defined as the ratio of input over output density modulations. Several LCSA modules are consecutively used until the final modulation is on the order of unity. In the latter case the bunch current is fragmented and can radiates coherently at wavelength comparable to the characteristic size of the beamlets.

Dohlus, et al. [1] provide a prescription for designing a system operating in the LSCA regime. Under optimum design, the typical gain of one LSCA module is

$$G \approx \frac{1}{\gamma\sigma_\delta} \sqrt{\frac{\mathcal{I}_A}{I}},$$

where  $\gamma$ ,  $\sigma_\delta$ ,  $I$ , and  $\mathcal{I}_A$  are respectively the beam's Lorentz factor, rms intrinsic (uncorrelated) fractional momentum spread and peak current, and the Alfen current (17 kA). For the anticipated beam parameters at ASTA, gain values in excess of 10 are expected.. The optimum gain assumes the LSCA module is optimized to amplify density modulations with wavelength  $\lambda \approx 2\pi\sigma_\perp/\gamma$  where  $\sigma_\perp$  is the average rms transverse beam size in the longitudinal drift space.

Considering the case of ASTA in its operating phase II [E~500 MeV ( $\gamma \approx 1000$ )] and focusing the beam to 50  $\mu\text{m}$  could result in density modulations with a wavelength on the order of 300 nm (this is the near-ultraviolet region of the spectrum but varying the beam size could also provide amplification from the vacuum ultraviolet to the optical regime -- the latter might be beneficial for experimental purpose especially while trying to understand the gain mechanism of an LCSA module). In order to enable the production of small transverse beam sizes we consider a FODO cell with average betatron function  $\bar{\beta} = 2L/\sin \mu = 2$  m where the half-length of the FODO cell and the betatron phase advance are respectively  $L=1$  m and  $\mu = \pi/2$ . The total drift length of the LSCA should be  $D \approx \gamma^2 \frac{\lambda}{2\pi} \sqrt{\frac{\mathcal{I}_A}{I}} \sim 6$  m which corresponds to 3 FODO cells. Finally, the optimum momentum compaction for the magnetic chicane is given by  $R_{56} \approx \lambda/(2\pi\sigma_\delta)$ . Achieving a net gain of 100 would conservatively require the cascading of three LSCA modules totaling a length of ~20 m (well within the real estate available during the phase II or III of ASTA).

A possible lattice for a cascaded LSCA will need to be located downstream of ACC2. Upstream and downstream of the FODO channel, matching telescopes will respectively match the incoming beam's Courant-Snyder parameters into the FODO channel and match the outgoing parameters into the spectrometer beamline. The needed three magnetic chicanes could be inserted within half the length of a FODO cell (i.e. between two consecutive quadrupole magnets) as the typical required momentum compaction values are on the order of a few mm maximum. Since these chicanes will not significantly perturb the lattice, one could practically envision a 20-m long FODO channel with chicanes inserted every 3-4 cells.

Finally, it is worth mentioning that as ASTA energy increases, the system could be scaled to micro-bunch at smaller wavelengths and eventually produces radiation in the vacuum ultraviolet regime (e.g. once ACC3 is installed). In addition, the present phase I configuration already include a FODO channel with average betatron function of 40 m this should amplify wavelengths in the THz regime and could therefore provide a first set of data on the experimental feasibility of the suggested scheme.

This proposal aims at testing an inexpensive method for generating XUV pulses based on the development of a space-charge instability in a cold beam. The method is very well suited to the early phases of ASTA (with one cryomodule) as it would benefit from the long drift sections. In addition, the high repetition rate will provide higher radiation power. The combination of these two features is not available at any other facilities.

[1] "[Generation of attosecond soft x-ray pulses in a longitudinal space charge amplifier](#)" M. Dohlus, E. A. Schneidmiller, and M. V. Yurkov, *Phys. Rev. ST Accel. Beams* **14**, 090702 (2011).

### **7.3.9 Potential for Critical Laser-Induced Microbunching Studies with the High-Micropulse-Repetition-Rate Electron beams at ASTA**

#### **7.3.9.1 Abstract**

Investigations of the laser-induced microbunching as it is related to time-sliced electron-beam diagnostics and high-gain-harmonic generation (HG) free-electron lasers using bright electron beams are proposed for the ASTA facility. Initial tests at 40-50 MeV with an amplified 800-nm seed laser beam co-propagating with the electron beam through a short undulator (or modulator) tuned for the resonance condition followed by transport through a subsequent chicane will result in energy modulation and z-density modulation (microbunching), respectively. The latter microbunching will result in generation of coherent optical or UV transition radiation (COTR, CUVTR) at a metal converter screen which can reveal slice beam size, centroid, and energy spread. Additionally, direct assessment of the microbunching factors related to HG by measurement of the COTR intensity and harmonic content after the chicane as a function of seed laser power and beam parameters will be done. These experiments will be performed using the ASTA 1-MHz-rate micropulse train for up to 1ms which is unique to test facilities in the USA.

#### **7.3.9.2 Introduction**

We have identified critical aspects of laser-induced microbunching (LIM) to be explored at the Advanced Superconducting Test Accelerator (ASTA) which relate directly to time-sliced electron-beam diagnostics and seeded free-electron laser (FEL) issues. In the first category the capability of evaluating the electron beam parameters such as beam size, centroid, and energy spread as well as the microbunching factors in sub-ps time slices should be possible by imaging the LIM coherent optical and UV transition radiation (COTR, CUVTR). In the second category, enhanced performance in gain length, spectral bandwidth, central wavelength stability, etc. of free-electron lasers (FELs) can be obtained by seeding the FEL either with electron beam microbunching at the resonant wavelength as in the case of high

gain harmonic generation (HGHG), cascaded HGHG, and echo-enhanced harmonic generation (EEHG) [1-3] or by generating a photon beam at short wavelengths such as from a plasma as in high harmonic generation (HHG)[4]. These seeding processes are initiated by co-propagating a laser beam with the electron beam through a short undulator (modulator) tuned to the seed wavelength to generate an energy modulation which is then converted to a z density modulation (microbunching) in a dispersive section such as a chicane. It has been found that the electron beam is also microbunched at the harmonics of the laser fundamental after the chicane, and the radiator undulator is tuned to one of them for the FEL [1]. Yu et al. have reported lasing on the 3<sup>rd</sup> harmonic of the laser fundamental of 800 nm, and FERMI@Elettra staff have reported recent HGHG results out to the 13<sup>th</sup> harmonic of 266 nm [5]. The direct measurement of the microbunching by looking at the coherent optical and UV transition radiation (COTR) was first done in a SASE FEL [6], but microbunching generated by LIM has rarely been measured [7]. Moreover, high harmonic content has not been directly observed, but it has been deduced from the HGHG radiator results [8]. Direct microbunching measurements have been proposed on the SDUV FEL in Shanghai [9], and discussions are underway with FERMI@elettra staff for VUV tests on their HGHG FEL. Elucidating the harmonic content, optimizing it, and benchmarking codes would be critical to present and future short wavelength (VUV-soft x-ray) FEL projects based on HGHG or EEHG. Only ASTA has the high-micropulse-repetition rate (1 MHz for 1 ms) beam such as proposed for the next generation of FELs [10], albeit with higher duty factor for the latter.

Our emphasis in this report is on the use of COTR (ultimately CVUVTR) as a direct microbunching diagnostic with the potential for time-resolved electron beam diagnostics and for benchmarking relevant FEL codes. As context, we point out that there are at least three mechanisms for generating optical-regime microbunching (which can be extended to the VUV) in an electron beam:

1. longitudinal-space-charge-induced microbunching (LSCIM): This mechanism has been suggested by Saldin et al. [11] to contribute more in the visible wavelength regime than coherent synchrotron radiation (CSR) or wakefields. This effect can be considered as starting from shot noise in the charge distribution that couples through the longitudinal impedance of the transport line and linac into an energy modulation. This energy modulation will become a z-density modulation, or microbunching, after bunch compression in a chicane (or other  $R_{56}$  lattice point) [12]. It is generally a broadband effect in wavelength, and most of the gain is in the FIR (>10- $\mu$ m regime). However, we have the LCLS/SLAC [13], APS/ANL [14], FLASH/DESY [15], and FERMI@Elettra [16] results on COTR in the OTR images and even scintillator screens. Spatially localized enhancements of 10-10,000 at visible wavelengths have been reported which prevent using the standard beam profiling techniques with optical beam images.

2. laser-induced microbunching (LIM): a) where an external laser beam is injected into the beamline so it copropagates with the electron beam through a short undulator (the modulator) which interaction modulates the beam energy that then becomes a z-density

modulation after a dispersive element such as in a chicane and b) where the seeding of an FEL with an external laser or harmonic at the long radiator undulator itself. The former results in narrowband microbunching and is used to prebunch or seed the beam for the FEL, and the latter is used as input to an FEL amplifier. The main objective of these proposed studies is measuring LIM.

3. SASE-induced microbunching (SIM) which is the fundamental mechanism of the self-amplified spontaneous emission (SASE) FEL process starts from noise when the SASE photon fields acting with the undulator fields on the electrons result in the growth of electron beam microbunching and concomitant exponential growth of SASE light at the resonant wavelength and harmonics. This is a narrowband effect. We note evidence for the LSCIM from the linac providing prebunched beam on experiments in the APS visible SASE FEL [17]. This demonstration actually links to the HGHG process via the principle of a prebunched beam's enabling FEL startup, as opposed to startup from noise as in a SASE FEL. Historically, LSCIM and SIM COTR were modeled after the first experiments, but in the LIM case we have more modeling in place before extensive experiments have been performed. We also expect to take advantage of techniques developed for the earlier modes.

This proposal would interact the electron beam with laser inside an undulator to produce microbunching structure for the electron beam at harmonic frequency of the laser frequency. The microbunched beam is then expected to produce ultraviolet radiation. In the US, only ASTA has the pulse train to test the technique at 3 MHz as needed, as well as the low energy jitter of an SC linac to enable generation and averaging of higher harmonics to greatly improve the signal-to-noise ratio and significantly increase the chance of detection of radiation-induced by the harmonic microbunching.

### **7.3.9.3 Laser-Induced Microbunching**

The initial step in HGHG is co-propagation of a seed laser with the electron beam through a short undulator or modulator tuned to resonance as indicated schematically in Figure 1. The laser pulse length can be used to modulate a time slice of the transverse distribution or it could be lengthened to provide modulation over the whole e-beam pulse length. At 40 MeV it is impractical to satisfy the resonance condition for an 800-nm wavelength on the fundamental of an undulator based on permanent magnets. For a planar undulator, the FEL process is governed by the resonance condition:

$$\lambda = \lambda_u (1 + K^2/2)/2n\gamma^2, \quad \text{Eq. 1}$$

where  $\lambda$  is the FEL wavelength,  $\lambda_u$  is the undulator period,  $K$  is the undulator field strength parameter,  $n$  is the harmonic number, and  $\gamma$  is the relativistic Lorentz factor.

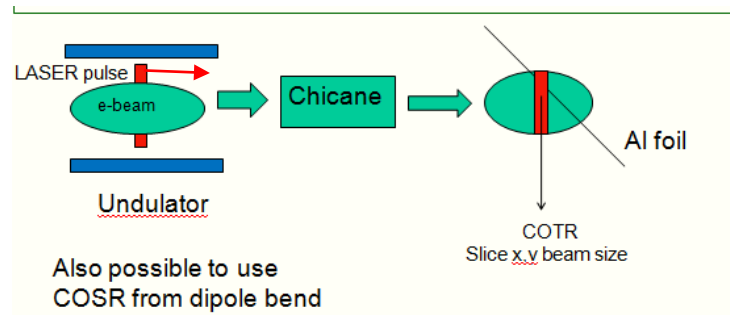


Figure 1: Schematic of laser-induced energy modulation followed by the dispersion in the chicane to produce a microbunched beam that can generate COTR or COSR in a slice. In principle the entire e-beam profile could be microbunched as well for HGHG.

However, it has been calculated that there is reasonable coupling strength at the third harmonic of the planar undulators as shown in Figure 2 from reference [18]. The coupling coefficients  $JJ_n$  for  $n=1,3,5$  versus  $K$  are reasonable, although with a rapid decrease in their values below  $K=1.5$  for  $n=3,5$  for the 780-nm case. We suggest with this concept we could modulate the energy at 800 nm in an undulator with period 1.8 cm using the third harmonic coupling of  $\sim 0.25$  and then generate harmonics of the laser wavelength in the microbunching in the dispersive section. Initially, we would use visible-UV optics to detect  $n=2,3,4$  at 400, 266, and 200 nm, respectively, in the Phase 1a experiments. Subsequently we would look for the critical higher harmonics in the VUV with appropriate diagnostics in Phase 1b as will be discussed in a later section. (Due to available 1054-nm lasers now at FNAL and LBNL, there may be some practical advantages for shifting to this wavelength. However the present S20 PC streak camera tube is insensitive at 1054 nm, it is difficult to chirp sufficiently long IR pulses to overlap uniformly the entire few-ps electron beam longitudinally, and the harmonic wavelengths will be 20% longer than the reference case. Further evaluation of this aspect is needed.)

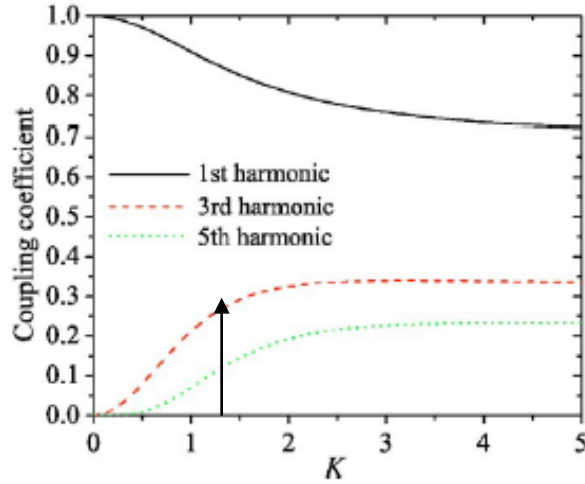


Figure 2: Coupling coefficients for odd harmonics for a planar wiggler as a function of  $K$ . The  $\gamma=80$  case with  $K=1.20$  is indicated by the arrow. [18]

#### 7.3.9.4 Coherent Optical Transition Radiation

A brief review of the source of the COTR, CUVTR, CVUVTR, etc. is in order. Transition radiation is emitted when a charged particle beam crosses the interface between two media with different dielectric constants, such as vacuum to a metal. It is a surface phenomenon, and the production time is estimated in the few-fs regime. Normally, incoherent OTR is a broadband phenomenon, but the special conditions of LIM lead to narrow band COTR. We propose that the simple modeling developed for SIM COTR [19] can be applied to LIM COTR. The coherent spectral angular distribution is given by the product of the reflection coefficients, the single electron spectral angular distribution, the interference term if applicable, and the coherence function which will be described below:

$$\frac{d^2 N}{d\omega d\Omega} = |r_{\perp, //}|^2 \frac{d^2 N_1}{d\omega d\Omega} I(\mathbf{k}) \mathfrak{S}(\mathbf{k}) \quad \text{Eq. 2}$$

where the single electron spectral angular distribution is given by,

$$\frac{d^2 N_1}{d\omega d\Omega} = \frac{e^2}{\hbar c} \frac{1}{\pi^2 \omega} \frac{(\theta_x^2 + \theta_y^2)}{(\gamma^{-2} + \theta_x^2 + \theta_y^2)^2} \quad \text{Eq. 3}$$

The coherence function is given by:

$$\mathfrak{S}(\mathbf{k}) = N + N_B (N_B - 1) |H(\mathbf{k})|^2 \quad \text{Eq. 4}$$

with the Fourier transform of the charge form factors being,

$$H(\mathbf{k}) = \frac{\rho(\mathbf{k})}{Q} = g_x(k_x) g_y(k_y) F_z(k_z) \quad \text{Eq. 5}$$

and where  $Q$  is the total charge and  $f_B = N_B/N$  is the bunching fraction. Note the coherence function reduces to just the number of particles,  $N$ , when the number of microbunched particles  $N_B$  is zero in this formalism. We expect significant fractions from the LIM process, and hence order of magnitude enhancements of COTR.

The transverse form factors are for  $i=x,y$ ,

$$g_i(k_i) = \frac{1}{\sqrt{2\pi}} e^{-\sigma_i^2 k_i^2 / 2} \quad \text{Eq.6}$$

and the longitudinal form factor for a train of  $M+1$  micropulses

$$\tilde{F}(k'_z) = f(k'_z) \sum_{m=0}^M e^{-ik'_z m \ell} = f(k'_z) \frac{\sin(Mk'_z \ell / 2)}{\sin(k'_z \ell / 2)} \quad \text{Eq.7}$$

with the longitudinal form factor for an individual microbunch

$$f(k_z) = \frac{1}{\sqrt{2\pi}} e^{-\sigma_z^2 k_z^2 / 2} \quad \text{Eq. 8}$$

Ratner, Chao, and Huang [18] have considered LSCIM COTR in their modeling, and related the effects to the bunching fractions in Eq. 9. The first term in the square bracket is the incoherent OTR, and the second term is the coherent contribution due to microbunching with bunching factor  $b_c(\mathbf{k})$  where  $\mathbf{k}$  is the wavevector of the microbunching. In their model the OTR spectral gain is the ratio of the angle-integrated second term over the angle integrated first term. The solid angle of their optics is given by  $\vartheta_m$ . One can obtain significant gain for bunching fractions of only a few per cent, needless to say, when  $N$  is large as in a 250 pC micropulse.

$$\frac{dW}{d\omega} = \int_{-\theta_m/2}^{\theta_m/2} d\theta_x \int_{-\theta_m/2}^{\theta_m/2} d\theta_y \times \left( \frac{d^2W}{d\omega d\Omega} \right)_1 [N + N^2 |b_c(\mathbf{k})|^2] . \quad \text{Eq. 9}$$

They considered the longitudinal space charge impedance of their S-band linac, the chicane's  $R_{56}$ , the energy chirp, slice energy spread, and other factors. For the broadband instability and a 3-keV slice energy spread, the model predicts a gain factor as shown by the red curve intensity compared to the incoherent OTR (blue curve) intensity as represented in Figure 3 [14].

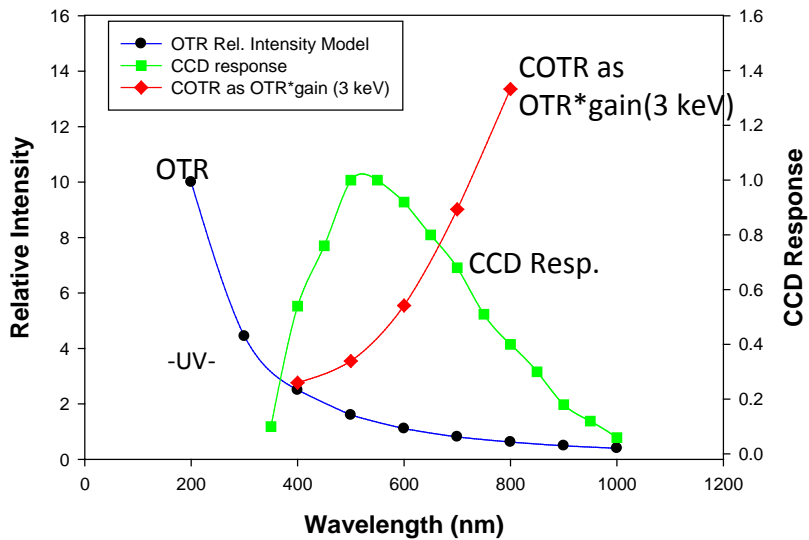


Figure 3: Plots of the nominal OTR intensity dependence on  $1/\lambda^2$ , the COTR intensity using the calculated gain factor at LCLS for a 3-keV slice energy spread [14,20], and the nominal CCD camera relative response.

These considerations describe the gain expected with LSCIM, but the narrowband nature of LIM may be best illustrated by showing the results of the narrowband microbunching in the SIM experiments at APS/ANL in 2002. Figure 4 shows a composite of the spectra obtained for a visible FEL operating near 535 nm [6]. The COTR spectra on the left are narrowband, but not quite as narrow as the SASE also observed after undulator 5 of nine undulators. The bunching fraction at saturation was calculated at about 20% of the e-beam, and enhancements of  $10^4$  for COTR and  $10^6$  for SASE were obtained. As we understand it bunching fractions of 5-10 % could be obtained in HGHG and EEHG configurations, even for harmonics of  $n=10$  or  $50$ , respectively. The potential for measuring the resultant enhanced transition radiation and elucidating LIM is high. We note that the bunching fractions would also apply to enhancing coherent optical synchrotron radiation (COSR), coherent undulator radiation (CUR), and coherent optical diffraction radiation (CODR) which mechanisms provide the potential for nonintercepting beam diagnostics for the high power beam mode of ASTA.

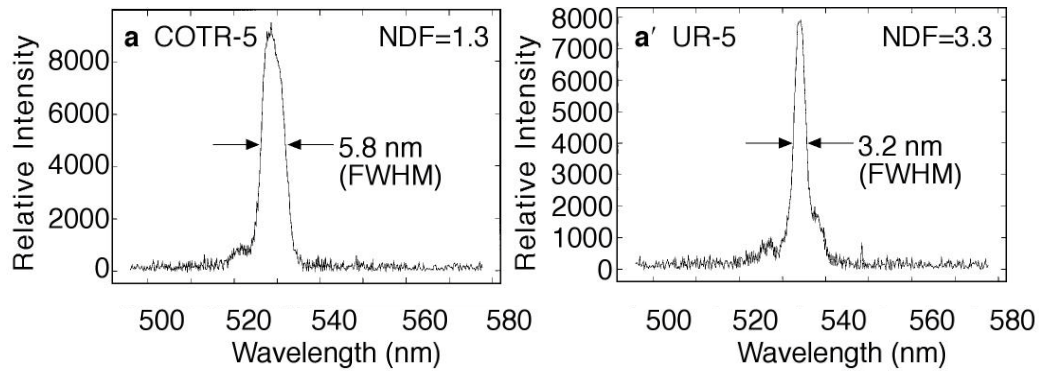


Figure 4: Example COTR (L) and SASE (R) spectra from the visible FEL experiments at ANL sampled after undulator 5 with SASE saturation occurring at about undulator 5. The SASE is  $\sim 100$  times brighter than the COTR as indicated by the use of a neutral density filter (NDF) value of 3.3 versus the 1.3 NDF value indicated for the COTR. The SASE involved 365 undulator periods versus two transition radiation converter interfaces [6].

### 7.3.9.5 Proposed studies

The ASTA linac with photocathode (PC) rf gun, two booster L-band SRF accelerators (CC1 and CC2), and beamline is schematically shown in Figure 5. The L-band accelerating sections will provide 40- to 50-MeV beams before the chicane, and an additional acceleration capability up to a total of 800 MeV will eventually be installed in the form of three cryomodules with eight 9-cell cavities with average gradient of 31 MV/m after the chicane. The phase of the CC2 section can be adjusted to energy chirp the beam entering the chicane to vary bunch-length compression. Maximizing the FIR coherent transition radiation (CTR) in a detector after the chicane will be used as the signature of generating the shortest bunch lengths. Micropulse charges of 20 to 3200 pC will be used typically. The nominal pulse format for high power ILC-like beam is 3.2 nC per micropulse at 3 MHz for 1 ms. The macropulse repetition rate will be 5 Hz. For the 1-ms period the pulse train micropulse spacing can be at a higher rate than a proposal of 100 kHz in any one of ten FEL beamlines. This aspect is unique for test facilities in the USA and highly relevant to the next generation of FELs.

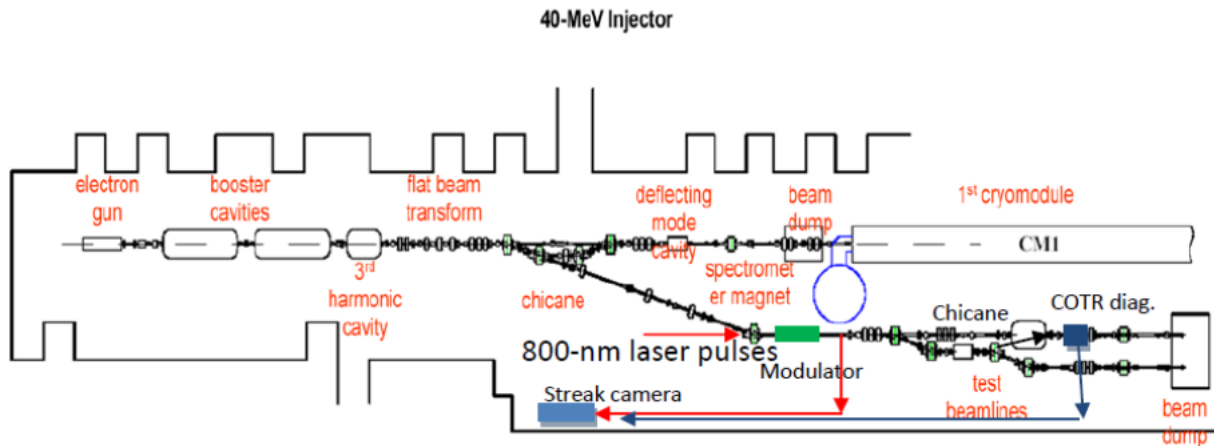


Figure 5: Schematic of the injector for the ASTA facility showing PC rf gun, booster accelerators, and beamlines. The first LIM tests are proposed in the test beamline as schematically indicated by the 800-nm laser beam injection into the beamline, modulator, chicane, and COTR diagnostics station locations. The Visible-UV streak camera could be used for both laser synchronization and COTR measurements.

### 7.3.9.6 Phase 1

We would start Phase 1 at 40-50 MeV with an 800-nm seed and a modulator with about 1.8 to 2.2 cm period,  $K \sim 1.2$ , and with length about 1 m. (The loan from LBNL of two or three 0.5-m sections with 2.18 cm period is under discussion.) The experiment location is shown in Figure 5. We would need to use resonance at the 3rd harmonic of the planar undulator as explained earlier. This is a key, and confirmation of this approach and modeling of the expected microbunching is recommended. We would need an amplifier for the 100 kHz 800-nm laser beam from the ASTA Ti:Sa laser or doubled-frequency Erbium Fiber laser to provide about 200-500  $\mu\text{J}$  per pulse, although we could start with fewer pulses in the pulse train initially. An optical parametric amplifier (OPA) could do this in principle. A laser concept developed for the EOS experiments envisioned for ASTA is shown in Figure 6. The pump laser is an existing Nd:YLF operating at 1 MHz. One might obtain higher energy pulses at the lower repetition frequency of 100 kHz and for longer pulses. The pulse train also might be shortened for initial tests. LBNL would collaborate on a solution for the OPA. The modulator should fit after the dogleg entering the low-energy test beamline at ASTA with diagnostics at both ends to align the laser and electron beam transversely. The FNAL Visible-UV streak camera would be used for timing the laser with the UR or OTR within the modulator to 1 ps or better. We have successfully done this in recent EOS tests at AOPi with the 800 nm Ti:Sa and incoherent OTR signals [21]. It also might be used to look directly at the LIM COTR within the micropulse as generated at the test station. (The system temporal resolution will be improved with narrow bandwidth COTR and also might be extended with a deflecting mode cavity [7].) The chicane configuration that is planned for an emittance

exchange (EEX) could presumably be used with its tunable  $R_{56}$  [22], but this needs to be checked. Visible-UV diagnostics would be needed after the Chicane to measure the harmonics  $n=2,3,4$  of 800 nm at 400, 266, and 200 nm, respectively.

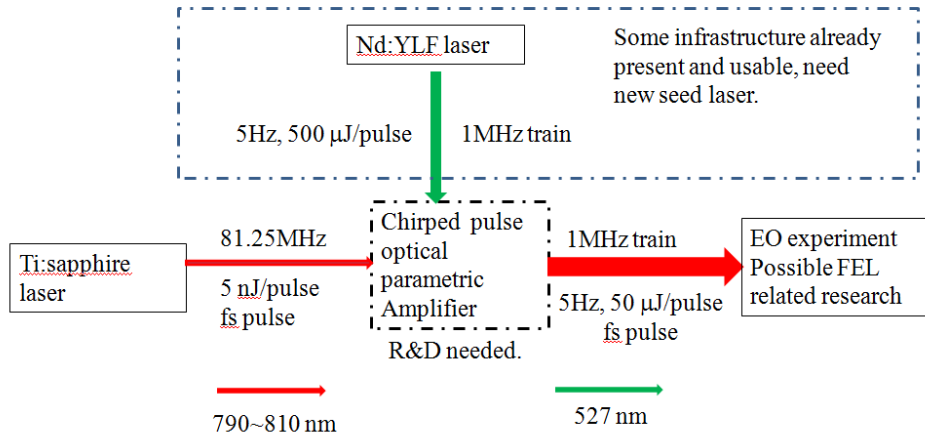


Figure 6: Schematic of the proposed ASTA diagnostics laser with OPA indicated. The pulse length and wavelengths need to be evaluated for microbunching tests. This laser system is being considered for the downstream diagnostics lab to support electro-optic tests.

In Phase 1b we would use VUV diagnostics since codes generally indicate harmonics of  $n \sim 10$  should be generated. An available in-vacuum flange-mounted 40-mm diameter microchannel plate (MCP) manufactured by BURLE Electro-Optics has been identified as a candidate 2D imager that has sensitivity from 1 eV to 50 keV. The output P43 phosphor would be viewed by a standard CCD camera, and two-dimensional images of the VUV angular distribution could be recorded. These should indicate laser/e-beam angular overlap which has been shown to impact SIM microbunching and FEL gain [23]. Evaluation of the LBNL multilayer metal mirrors at various VUV wavelengths, and testing of their robustness to electron-beam pulse trains would be of interest. As an alternative the multilayer mirrors might be located after the downstream dipole to eliminate e-beam bombardment. Development of VUV filtering schemes would also be tested. Additionally, one could use laser pulses shorter than the e-beam micropulse to probe the slice transverse beam size and centroids of the electron beam or map out the longitudinal profile as previously demonstrated at FLASH [24]. More detailed harmonic information should be obtained by use of imaging spectrometers in the UV and VUV (McPherson version has a series of gratings to use and an imaging array for display). This would provide the ultimate diagnostic of the microbunching harmonics' central wavelengths and spectral widths. LBNL would have or provide the OPA for the FNAL Ti:sapph laser oscillator, the modulator system in principle (informal discussion), the VUV mirrors, and possibly the VUV spectrometer. They also have the needed modeling capability for the HGHG and EEHG FEL processes which should include calculation of microbunching factors entering the radiator.

### 7.3.9.7 Phase 2

In Phase 2 we would move to the high-energy test lines, and the seed laser could be located in the downstream laser room. We may consider shifting to amplified 266 nm seed and look for  $n=10$ , but we should be able to start at 800 nm on the fundamental with a 20-cm-period undulator for an e-beam energy of 250 MeV. Depending on beam energy and undulator period we should be able to reach the VUV to soft x-ray regime in the microbunching. Only ASTA in the USA has the pulse train to test the technique at 100 kHz as needed, as well as the low energy jitter of a SC linac to enable generation and averaging of higher harmonics. We estimate HGHG and EEHG might be explored in a high-energy test line within a 12-15 m zone, but cascaded HGHG could be tight. At one time 30 m of z space was indicated as usable, and various configurations should be explored. A schematic is shown in Figure 7 of the layout of the simplest. With 900 MeV (4 cryomodules plus injector) and a short period undulator (maybe SCU) we could ultimately reach a few nm in the beam and the radiator. This should have strong relevance for future FELs in general.

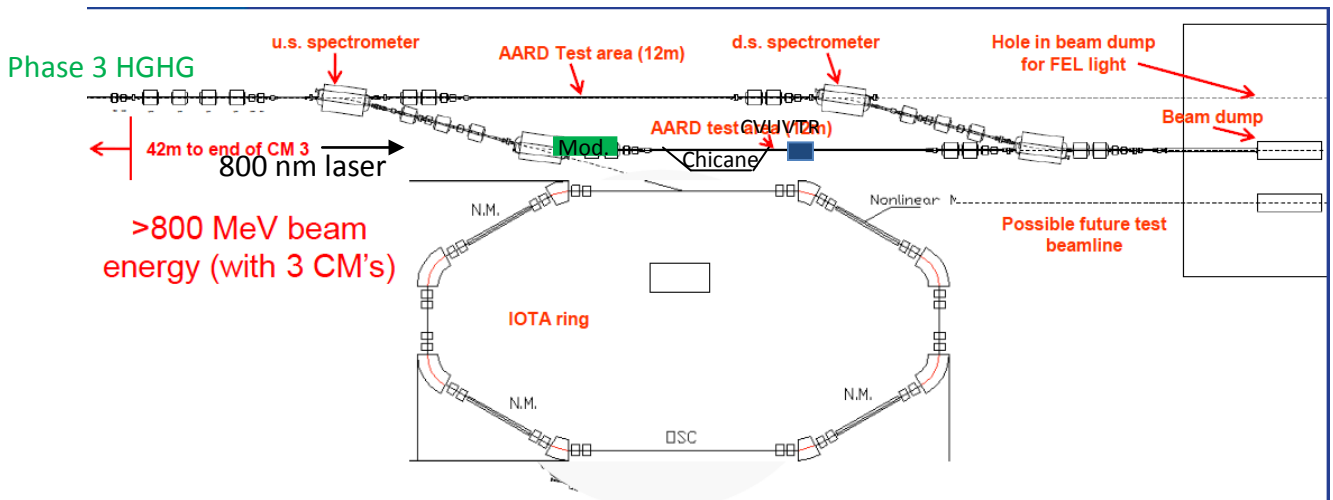


Figure 7: Schematic of the simplest microbunching experiment layout in the high-energy area. The possible configurations for HGHG and EEHG should also be considered.

Table 1 summarizes some of the configurations for the proposed studies. In some cases we are only concerned about looking at the microbunching in the electron beam post chicane so the radiator needed for HGHG is not a constraint. Phase 1 could be started in FY14 if agreements can be made soon so preparations can be made in FY13. The EEHG case is not determined yet, but we are looking for an  $n=100$  demonstration where the radiator has a short period. The last SASE case at 900 MeV invokes the use of a 4-m-long SC undulator [25] with period 1.1 cm and  $K=0.92$  to generate radiation and microbunching at 3 nm as a test since we would not have 2.5 GeV available. Separating the CXTR and SASE sources is a technology challenge to be addressed for this case.

Table 1: Summary of possible microbunching experiments at ASTA at 40-45 MeV and higher energies following the cryomodules. The potential observation wavelengths of several of the harmonics are indicated.

| Phase # | Beam Energy (MeV) | Laser Fundamental (nm) | Und. Period (cm), K, n | Microbunching Harmonics (nm) |
|---------|-------------------|------------------------|------------------------|------------------------------|
| 1a      | 44.5              | 800                    | 2.18, 1.2, 3           | 400,266, 200                 |
| 1b      | 44.5              | 800                    | 2.18, 1.2, 3           | 100,90,80                    |
| 2       | 250               | 800                    | 20.0,1.36,1            | 400,266,200,80               |
| 2       | 200               | 266                    | 5,1.2,1                | 48,29,26                     |
| 2-SASE  | 500               | ----                   | 5,1.2,1                | 42,14                        |
| 3-HGHG  | 900               | TBD                    | TBD                    | --                           |
| 4-SASE  | 900               | --                     | 1.1,0.9,1              | 3                            |
| EEHG    | 900               | --                     | TBD                    |                              |

### 7.3.9.8 Summary

In summary, we have described how a series of direct LIM experiments with diagnostics in the optical, VUV, and soft x-ray regime could be implemented at the ASTA facility. This is the only facility in the USA that has the pulse train of at least 100 kHz repetition rate to simulate proposed FEL configurations. These experiments should extend understanding of the critical phenomena of microbunching harmonic generation and preservation and allow benchmarking of codes. The potential use for HGHG and EEHG FELs at several nm with scalable results is targeted. In addition, the as-described sub-micropulse electron-beam diagnostics based on COTR could be developed into nonintercepting electron beam diagnostics if used with the COSR, CUR, or CODR mechanisms.

Notes: Assumed 50-MeV User beamline for EEX installed with chicane with tunable  $R_{56}$ ; FNAL streak camera and UV diagnostics; one meter long undulator with stand (loan from LBNL); FNAL in-vacuum MCP for VUV detection; seed laser transport line to modulator (\$25k); Miscellaneous optics (15K).

Long range: propose VUV McPherson spectrometer (\$75k) with readout camera. Need cryomodules installed and beam transport to high energy end test locations. Re-locate 1-m long undulator or other.

### 7.3.9.9 References

- [1] L.H. Yu et al., Phys. Rev. Lett. 91, 074801, (2003).
- [2] Z. Zhao et al., "Seeding Experiments at the SDUV-FEL", WEOB2, Presented at FEL11, August 24, 2011.
- [3] G. Stupakov, PRL 102, 074801, (2009).

- [4] G. Lambert et al., "High Harmonics from Gas", MOOB12, Presented at FEL11, Aug.24-27, 2011.
- [5] E. Allaria et al., "FEL Commissioning at FERMI@Elettra, Presented at FEL 11, WEOB11, Shanghai, China, Aug.24-27, 2011.
- [6] A.H. Lumpkin et al., PRL 88, 234801, (2002).
- [7] D. Xiang et al., Phys. Rev. ST-AB, 14, 112801 (2011).
- [8] Z. Zhao et al., "Seeding Experiments at the SDUV-FEL", WEOB2, Presented at FEL11, August 24, 2011.
- [9] A.H. Lumpkin, seminar presented at SINAP, Shanghai, China, Aug. 17, 2011.
- [10] See contributions to "Realizing the Potential of Seeded FELs in the Soft X-ray Regime Workshop", Berkeley, CA, Oct. 26-28, 2011.
- [11] E.L. Saldin, E.A. Schneidmiller, and M.V. Yurkov, DESY Report No. TESLA-FEL-2003-02, 2003.
- [12] Z. Huang et al., PRST-AB 7, 074401 (2004).
- [13] D.H. Dowell et al., "LCLS Injector Commissioning Results", Proc. of FEL07, Aug. 26- 30, 2007, Novosibirsk; R. Akre et al., Phys.Rev.ST-AB 11, 030703 (2008).
- [14] A.H. Lumpkin, N.S. Sereno, W. Berg, M. Borland, Y. Li, and S. Pasky, "Characterization and Mitigation of Coherent Optical Transition Radiation Signals from a Compressed Electron Beam, Phys. Rev. ST-AB 12, 080702,(2009).
- [15] M. Yan et al., "Beam profile Measurements Using a Fast Gated CCD Camera and Scintillation Screen to Suppress COTR", THPB16, presented at FEL 11, Shanghai China, Aug.24-27, 2011.
- [16] M. Veronese and E. Allaria, WEPB23, presented at FEL11, Shanghai, China, Aug.24-27, 2011.
- [17] A.H. Lumpkin, R.J. Dejus, and N.S. Sereno, Phys. Rev. ST-AB, 12, 040704 (2009).
- [18] P. Musumeci, C. Pellegrini, and J.B. Rosenzweig, Phys. Rev. E 72, 016501 (2005).
- [19] D. W. Rule and A.H. Lumpkin, "Analysis of COTRI Patterns Produced by SASE-Induced Microbunches", Proc. of PAC2001,1288 (2001).
- [20] D. Ratner, A. Chao, and Z. Huang, "Three-Dimensional Analysis of Longitudinal Space Charge Microbunching Starting from Shot Noise", Proc. of FEL08, Gyeongju, Korea, Aug. 24-29, 2008.
- [21] T. Maxwell et al., "Single-shot Electro-optic Sampling of CTR at the A0 Photoinjector", Proc. of IPAC11, Sept. 2011.
- [22] P. Piot, FNAL AAC Review, Nov. 6, 2011.
- [23] Y.-C. Chae, A.H. Lumpkin, M. Erdmann, J.W. Lewellen, and S.V. Milton, "An Experimental Study of the Beam-steering effect on the FEL Gain at LEUTL's Segmented Undulators", Proc. of FEL 2004, Trieste Italy, 100, (2004).
- [24] G. Angelova et al., PRST-AB,11, 070702 (2008).
- [25] E. Baynham et al., Proc. of PAC09, WE2RAI01, (2009).

## 7.3.10 Proposed Coherent Diffraction Radiation Measurements of Bunch Length at ASTA

### 7.3.10.1 *Abstract*

The feasibility of using the autocorrelation of coherent diffraction radiation as a non-intercepting diagnostics technique for bunch length and indirectly rf phase measurements is evaluated and proposed for the Advanced Superconducting Test Accelerator (ASTA) facility. Previous experiments on an rf thermionic cathode gun beam at 50 MeV provide a proof-of-principle reference for the ASTA injector. The technique would also be applicable at high energy in straight transport lines after the cryomodules.

### 7.3.10.2 *Introduction*

The high-power electron beams for the Advanced Superconducting Test Accelerator (ASTA) facility involve up to 3000 micropulses with up to 3.2 nC per micropulse in a 1-ms macropulse [1]. With beam energies projected from 45 to 800 MeV the need for non-intercepting diagnostics for beam size, position, energy, and bunch length is clear. In this Note, we address non-intercepting (NI) diagnostics of the bunch length and inferred rf phase by using coherent diffraction radiation (CDR) techniques [2,3]. Previous evaluations of incoherent optical synchrotron radiation indicated that the source strength for visible photons is quite weak for a single micropulse at 40 MeV from the chicane dipoles, but synchroscan streak techniques to determine the bunch length after the chicane should be viable by synchronous summing of the long pulse train's micropulses [4]. This would be complemented by optical transition radiation (OTR) and coherent transition radiation (CTR) measurements of the tune-up beam with an intercepting metal screen after the chicane. It is proposed that at this station, the metal screen would also have an insertion position where a 4-5 mm tall slit/aperture is centered on the beam position to provide a non-intercepting source of CDR from the surrounding metal surface. The autocorrelation of the far infrared radiation (FIR) CDR would then be processed for the bunch-length information, and the potential for rf phase feedback for the injector cavities would also be possible based on the signal intensity monitored by the FIR detector, whether Golay cell or pyroelectric detector. An early measurement of CDR from a screen with a circular aperture was actually an intercepting configuration because the beam subsequently struck a 45-degree metal mirror to redirect the CDR (and CTR) to the FIR detector [2]. The first non-intercepting proof-of-principle demonstration was done with an rf thermionic cathode gun beam at 50 MeV with an integrated charge of only 4 nC using a slit geometry [3]. This means that potentially one would only need a few micropulses of the ASTA injector beam at the full 3.2 nC per micropulse for 1ps rms bunch length to obtain reasonable signal levels with a Golay cell, and the full pulse train could be integrated to obtain information on even longer bunch lengths where FIR generated per pC is lower in the detector-response regime.

The implementation of the CDR converter screen at 50 MeV will take advantage of the planned THz detection system and staff expertise, and the long pulse train allows CDR to be applied to the beam-based feedback concept uniquely in HEP test facilities. In principle this could also be applied at the ASTA GeV-scale energies in a high power beam uniquely since it is a non-intercepting technique.

### 7.3.10.3 Conceptual Aspect

It is proposed that a multi-purpose station should be located after the chicane for incoherent OTR, CTR, and CDR generation and studies. As schematically indicated in Figure 1, the OTR will be transported to a Hamamatsu C5680 synchroscan streak camera (transferred from AOPI) [5], and the CTR and CDR will be transported to the Martin-Puplett interferometer (MPI) for measuring the autocorrelation of the FIR radiation [6]. A metal screen can be used for the first two mechanisms interceptively, and by centering the 5-mm slit/aperture machined in the screen on the beam axis the CDR will be generated non-interceptively as the beam transits through the aperture. In principle, this latter configuration will work for the full pulse train. Alternatively, a single plane screen with its horizontal edge positioned above or below the beam axis might be used. In this case, a beam abort would initiate the withdrawing of the screen away from the beam. The electric field scaling parameter,  $\gamma\lambda/2\pi$ , where  $\gamma$  is the Lorentz factor and  $\lambda$  is the wavelength, sets the practical scales. For example with FIR 628- $\mu\text{m}$  radiation and  $\gamma=100$ , this parameter is 10 mm so a 5-mm slit height is reasonable. One prefers a radiating surface of 100 mm, however, this is unlikely to be attained in our beam pipe so some finite screen effects may be involved.

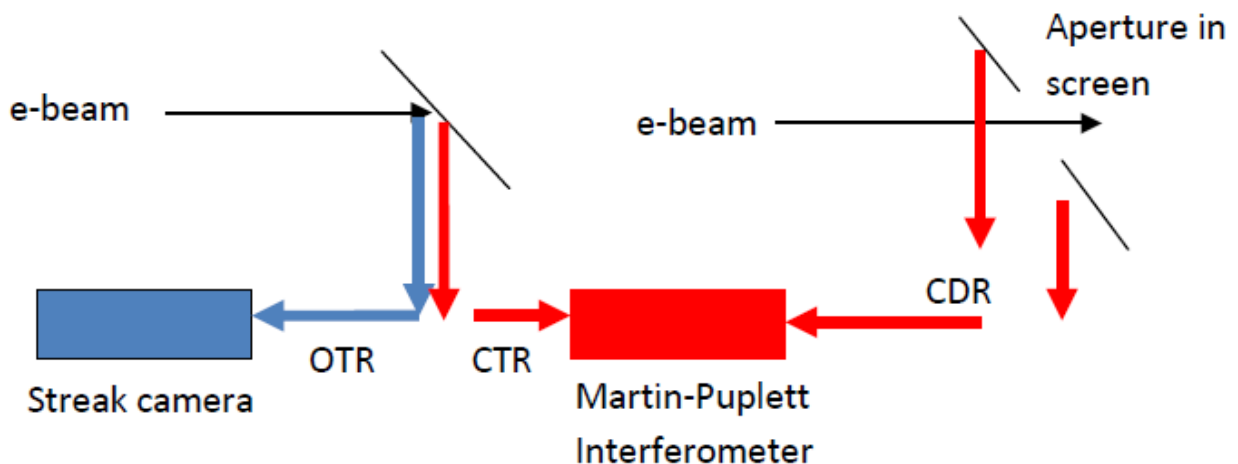


Figure 1: Schematic of a three-source option for OTR, CTR, and CDR diagnostics with the streak camera and MPI indicated. The OTR/CTR screen is at the left, and the CDR screen with aperture is at the right.

### 7.3.10.4 Coherent Radiation Analytics

A brief review [3] of the source of the CTR and CDR is in order. Coherent radiation generated by a bunch of electrons can be expressed as a product of a term representing the radiation process due to a single particle and a term which takes into account how much of the total charge in the bunch radiates together constructively, in phase. Thus the spectral, angular distribution of the radiation can be expressed as,

$$\text{Eq. 1} \quad \frac{d^2W}{d\omega d\Omega} = |r_{\perp, //}|^2 \frac{d^2W_1}{d\omega d\Omega} \mathfrak{S}(\mathbf{k})$$

where  $\frac{d^2W_1}{d\omega d\Omega}$  is the spectral angular distribution for the single particle radiation process, whether transition radiation (TR), synchrotron radiation, or diffraction radiation (DR), for example. In the present case we take it as for DR.  $\mathfrak{S}(\mathbf{k})$  is the coherence factor for a bunch of  $N$  electrons, and this term is related to the square of the Fourier transform of the spatial distribution of the bunch:

$$\text{Eq. 2} \quad \mathfrak{S}(\mathbf{k}) = N + N(N-1)H(\mathbf{k})^2$$

with the Fourier transform of the charge form factors using a simple Gaussian model being,

$$\text{Eq. 3} \quad H(\mathbf{k}) = \frac{\rho(\mathbf{k})}{Q} = g_x(k_x)g_y(k_y)F_z(k_z)$$

and where  $Q=Ne$  is the total charge. Note the first term in Eq. (2) yields the incoherent radiation produced by  $N$  electrons in the bunch, while the second term gives the coherent production, which is proportional to  $N^2$ . The transverse form factors are for  $i=x,y$ ,

$$\text{Eq. 4} \quad g_i(k_i) = \frac{1}{\sqrt{2\pi}} e^{-\sigma_i^2 k_i^2 / 2}$$

with the longitudinal form factor for an individual micropulse,

$$\text{Eq. 5} \quad F(k_z) = \frac{1}{\sqrt{2\pi}} e^{-\sigma_z^2 k_z^2 / 2}$$

Note that for the coherence factor to be sizable, the beam rms radius and the wavelength of interest  $\lambda$  must be less than  $1.4 \gamma \lambda / 2\pi$  for angles of order  $1/\gamma$ . The wavelengths of interest are determined by the longitudinal part of  $\mathfrak{S}(\mathbf{k})$  such that the rms bunch length  $\sigma_z < \lambda / 2\pi$ . The results of the calculations of CDR for several cases of  $\sigma_t$  from 0.2 to 6 ps are summarized in Figure 2 for a 50-MeV beam with 8 nC of charge transiting the center of a 5-mm tall slit in a metal plane [3]. (This was approximated as two infinite metal strips separated by 5 mm in the model.) Note the form factor results in significant enhancements

of radiation at wavelengths about three times longer than the bunch length. For the ASTA case much higher total charges are anticipated, so the signals should be even stronger if a similar geometry be used. These are basically the same wavelengths expected for the CTR measurements in the MPI, and could in principle also be used with the real-time interferometer (RTI) to generate on-line autocorrelations as demonstrated recently at AOP1 [7].

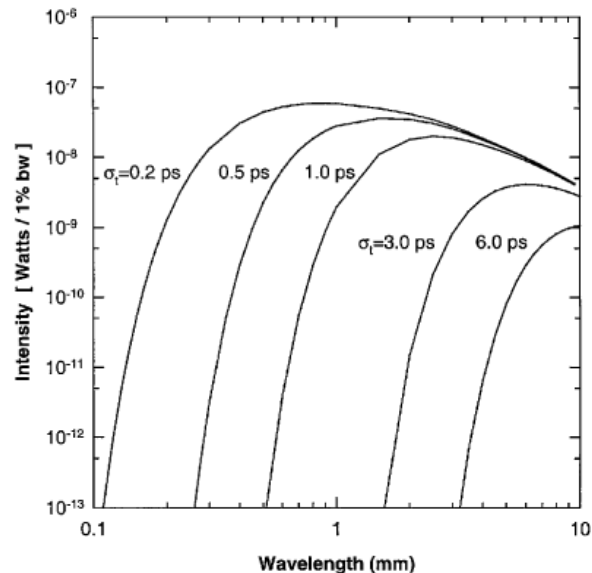


Figure 2: Calculated spectra of CDR for a 50-MeV electron beam passing through a 5-mm slit with 8 nC total charge and bunch lengths  $\sigma_t$  of 0.2, 0.5, 1.0, 3.0, and 6.0 ps [3].

### 7.3.10.5 Proposed Implementation

#### Low Energy Station (40-50 MeV)

The ASTA linac with photocathode (PC) rf gun, two booster L-band SRF accelerators (CC1 and CC2), and beamline is schematically shown in Figure 3. The L-band accelerating sections will provide 40- to 50-MeV beams before the chicane, and an additional acceleration capability up to a total of 800 MeV will eventually be installed in the form of three cryomodules with eight 9-cell cavities with average gradient of 31 MV/m after the chicane. The phase of the CC2 section can be adjusted to energy chirp the beam entering the chicane to vary bunch-length compression. Maximizing the FIR coherent transition radiation (CTR) in a detector after the chicane can be used as the signature of generating the shortest bunch lengths. An alignment laser should be planned to inject at a location after CC2 and through the straight ahead line to the bunch length monitor station and into the streak camera and FIR MPI or RTI. This will facilitate optical alignments of the transport systems to the detectors. Micropulse charges of 20 to 3200 pC will be used typically. The nominal pulse format for high power ILC-like beam is 3.2 nC per micropulse at 3 MHz for 1 ms. This aspect

is unique for test facilities in the USA and highly relevant to the next generation of free-electron lasers. The macropulse repetition rate will be 5 Hz.

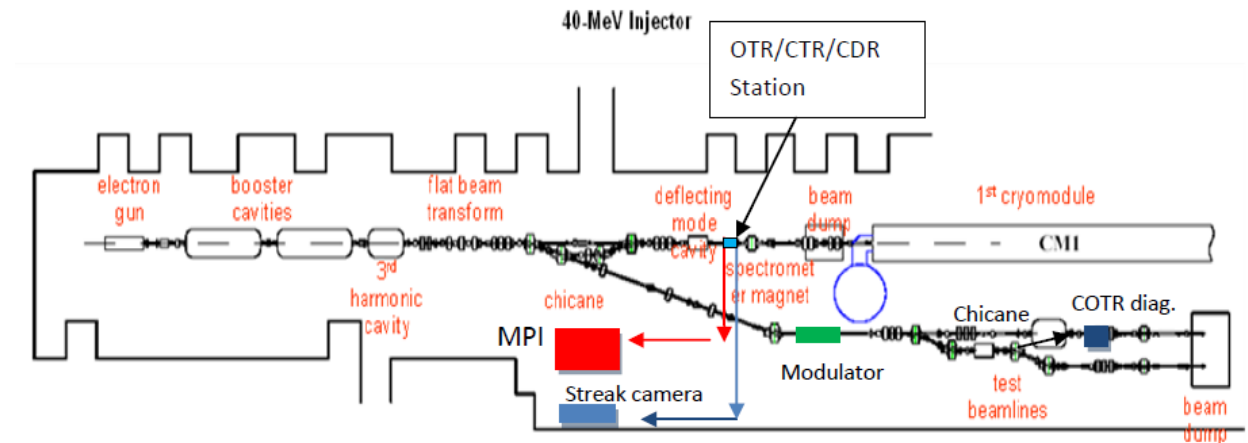


Figure 3: Schematic of the injector for the ASTA facility showing PC rf gun, booster accelerators, and beamlines. The visible-UV streak camera could be used for UV laser and OTR measurements, and the MPI for FIR CTR and CDR measurements. (modified M. Church schematic).

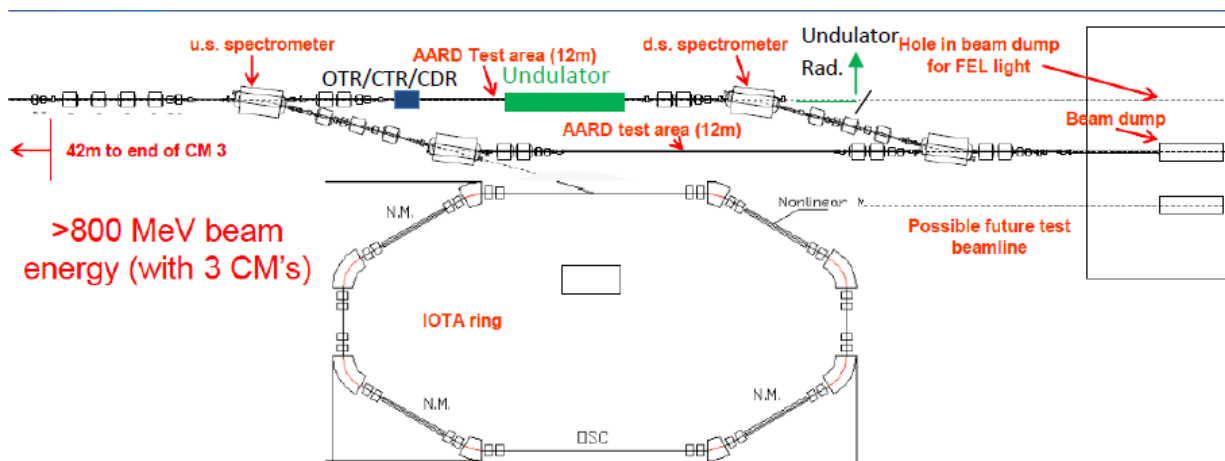


Figure 4: Schematic of the OTR/CTR/CDR monitor location in one high-energy AARD test area. This could be located just upstream of the proposed diagnostics undulator. (modified M. Church schematic).

### High-Energy Station (250-800 MeV)

These OTR/CTR/CDR techniques also scale to use at higher energies as will be found after the cryomodule string. The extension of the CDR technique to higher energies should be straight forward as the CDR signal strengths will be even closer to the CTR signal strengths for a given bunch length and similar effective apertures. This could be used after a proposed second bunch compressor located downstream of the cryomodules. A possible location would be in the AARD section after the upstream dipole as indicated in Figure 4. The streak

camera would need to be located in the high energy diagnostics laser lab upstairs, and the MPI would need to be in a locally shielded area. The EOS technique used at AOPI with CTR [8] might be employed with CDR signals to make that also a non-intercepting technique.

### **7.3.10.6      *Summary***

In summary, we have described how a combination of intercepting OTR and CTR techniques and non-intercepting CDR techniques could be implemented after the injector chicane to provide bunch length measurement capability for the 40- to 50-MeV electron beams. The bunch length and deduced phase variation could be used in combination with the beam-arrival monitors in feedback and feed forward systems for rf phase for and during the macropulse. These OTR/CTR/CDR techniques also scale to use at higher energies found after the cryomodule string. Additionally, such a spectral range with 3000, 1-ps pulses of CDR might be used as a parasitic THz source for some applications.

### **7.3.10.7      *Acknowledgements***

The author acknowledges discussions with R. Thurman-Keup on the MPI and M. Wendt, M. Church, V. Shiltsev, S. Nagaitsev, and S. Henderson of FNAL on the ASTA facility and AARD program.

### **7.3.10.8      *References***

- [1] S. Nagaitsev, talk presented at ILC-TA Workshop, Fermilab, November 28, 2006.
- [2] Y. Shibata et al., *Phys. Rev. E* **52**, 6787 (1997).
- [3] A. H. Lumpkin, N.S. Sereno, and D.W. Rule, *NIM A* **475**, 470 (2001).
- [4] Evaluations presented at NML meetings by A.H. Lumpkin and R. Thurman-Keup (2011).
- [5] A. H. Lumpkin, J. Ruan, and T.W. Koeth, "Initial Commissioning of a Dual-Sweep Streak Camera on the A0 Photoinjector", *Proceedings of Linac08, JACoW* (2008); and A.H. Lumpkin et al., *NIMA* 2012.05.068.
- [6] R. Thurman-Keup, R. Filler, and G. Kazakevich, "Bunch-length Measurement at the Fermilab A0 Photoinjector Using a Martin-Puplett Interferometer", *Proceedings of BIW08, Lake Tahoe, CA* (2008).
- [7] J. Thangaraj et al., "Demonstration of a real-time interferometer as a bunch length monitor in a high current electron beam accelerator", accepted for pub/ in *Rev. Sci. Instr.* (2012).
- [8] Timothy Maxwell, "Measurement of Sub-picosecond Electron Bunches via Electro-optic Sampling of Coherent Transition Radiation", *NIU Dissertation*, May 2012.

## 7.3.11 Non-intercepting Optical Diffraction Radiation Diagnostics at ASTA

### 7.3.10.1 Abstract

Optical diffraction radiation (ODR) imaging has been proposed as a non-intercepting beam-size monitor for the high-power electron beams in the Advanced Superconducting Test Accelerator (ASTA) facility at FNAL. Potentially the technique would be used for the high-energy end at 500-800 MeV. The application is evaluated in relation to successful experiments done at JLAB at 4.5 GeV with visible-light, near-field ODR detected by a standard CCD camera and the proof of principle at FLASH at 900 MeV with a 16-bit cooled CCD. The lower gamma beams of ASTA compared to JLAB will push the technology implementation towards the IR and the use of an ICCD and/or 16-bit camera.

### 7.3.10.2 Introduction

Characterization of the high-power electron beams of the ASTA/NML facility at FNAL will be an important aspect of demonstrating the superconducting rf (SRF) accelerator as a test bed for technology [1]. Beam size, position, divergence, emittance, and bunch length measurements are all of interest. Previously, the feasibility of using a non-intercepting (NI) technique based on near-field optical diffraction radiation (ODR) was assessed, and two experiments at other facilities were proposed and executed in the interim [2]. Due to the projected high beam power at ASTA with 3000 micropulses of up to 3 nC each in a macropulse at 5 Hz at eventually up to 800 MeV, the need for NI diagnostics is obvious. Although beam position is readily addressed with standard rf beam position monitors (BPMs), the transverse size and hence emittance are less easily monitored noninterceptively in a linear transport system. Besides an expensive laser-wire system or a wire scanner which is by definition not single pulse, one of the few viable solutions appears to be the use of ODR [1-10] which is emitted when a charged-particle beam passes near a metal-vacuum interface. Appreciable radiation is emitted when the distance of the beam to the screen edge (impact parameter)  $b \sim \gamma\lambda/2\pi$ , where  $\gamma$  is the Lorentz factor and  $\lambda$  is the observation wavelength. The first near-field imaging experiments at the Advanced Photon Source (APS) with 7-GeV beams used an impact parameter of 1.25 mm from a single edge of a plane as compared to the scaling factor of  $\sim 1.4$  mm (with an assumed operating wavelength of 0.628  $\mu\text{m}$ ) [7]. The near-field images were obtained with a single, 3-nC micropulse, while the far-field data were averaged over 10 micropulses.

We now have demonstrated extension of the technique to the 4.5 GeV beams at CEBAF/JLAB [9] and the even more challenging task at 900 MeV at FLASH [10]. The latter is close to the ASTA case with its much lower gamma. Since the fields are reduced exponentially as  $e^{-2\pi b/\gamma\lambda}$ , in principle we either have to use the longer wavelengths in the NIR or more charge integrated in the image and a more sensitive camera. Our recent modeling indicates that the FIR ODR has more photons, but it is less sensitive to the beam sizes we

anticipate. The ILC-TA design-goal beam intensity [11] gives a factor of 3000 compared to APS, and the intensified or low-noise camera should give another factor of 1000. These two factors combined should allow visible to IR near-field imaging of a beam that is up to 8-10 times lower in gamma than the JLAB case, if similar impact parameters can be used. The proof-of principle of this was demonstrated at 900 MeV at FLASH/DESY in 2008 [10] in a collaborative experiment with INFN which will be summarized in a later section.

We estimate that the ODR feasibility begins at about 500 MeV, and the reduced yield per electron will be compensated by integrating over a significant portion of the 1-ms pulse train. The integrated charge level of 500 nC is only available at ASTA. This would be a non-intercepting beam size monitor.

### 7.3.10.3 Analytical and Experimental Aspects

#### ANALYTICAL MODEL CONSIDERATIONS

The basic strategy is to convert the particle-beam information into optical radiation and to take advantage of the power of imaging technology to provide two-dimensional displays of intensity information. These images can be processed for beam size information. Possible radiation sources are optical transition radiation (OTR), ODR, and optical synchrotron radiation (OSR). For completeness, the near-field ODR model as described in Ref. 7 is provided here.

The ODR is generated as the charged-particle beam passes near the metal plane. In Figure 1a below I show a schematic of the backward ODR generated from two vertical planes with a total gap of  $a=2b$ . This far-field representation is based on Figure 1 of Fiorito and Rule [4]. As stated before, ODR is produced when an electron beam passes near a region where different dielectric materials are present. This is generally a vacuum-to-metal interface, and the theory [4-7] is usually for the *far-field* diffraction pattern produced by a beam passing through apertures or slits in conducting planes. In the present case, we effectively integrate over angle and frequency since our optical system is focused on the ODR source itself, i.e. the *near-field* image on the screen. Therefore we propose a simplified model of the near field based on the method of virtual quanta described by Jackson [12] in dealing with the photon-like fields of relativistic beams. One convolves the electron beam's Gaussian distribution of sizes  $\sigma_x$  and  $\sigma_y$  with the field expected from a single electron at point  $P$  in the metal plane. One wishes to calculate the incoherent sum of radiation from all beam particles in a pulse emitted from a given point on the ODR radiator, i.e. at  $\mathbf{u} = \mathbf{P} - \mathbf{r}_o$ , where  $\mathbf{P}$  is the field point with respect to the origin and  $\mathbf{r}_o$  is the position of the beam centroid with respect to the origin. The impact parameter is  $\mathbf{b} = \mathbf{u} - \mathbf{r}$ , where  $\mathbf{r} = \mathbf{r}(x,y)$  denotes a position in the beam measured from the beam centroid. One then can write the differential spectral intensity as:

$$\frac{dI}{d\omega}(\mathbf{u}, \omega) = \frac{1}{\pi^2} \frac{q^2}{c} \left(\frac{c}{v}\right)^2 \alpha^2 N \frac{1}{\sqrt{2\pi\sigma_x^2}} \frac{1}{\sqrt{2\pi\sigma_y^2}} \times \iint dx dy K_1^2(ab) e^{-\frac{x^2}{2\sigma_x^2}} e^{-\frac{y^2}{2\sigma_y^2}} \quad (1)$$

where  $\omega$  = radiation frequency,  $v$  = particle velocity  $\approx c$  = speed of light,  $q$  = electron charge,  $N$  is the particle number,  $\alpha = 1/\gamma\lambda$ , and  $K_1(ab) = K_1\left(\alpha\sqrt{(u_x - x)^2 + (u_y - y)^2}\right)$  is a modified Bessel function. Since one measures light intensity  $I$ , this should be proportional to  $|E_x|^2 + |E_y|^2$ , resulting in the  $K_1^2$  dependence. The incoherent photon intensity is proportional to  $N$ , the number of electrons, in contrast to the case of coherent diffraction radiation in the far infrared (FIR), which is enhanced by  $N^2$ .

The APS experiments actually started with a single plane which was inserted vertically. They evaluated the beam size parallel to the single edge. In Figure 1b I show a calculation of the signal distribution in the optical near field based on this new model for a 7-GeV beam at an impact parameter of 1.25 mm. The beam size was 1375  $\mu\text{m}$  by 200  $\mu\text{m}$  [7].

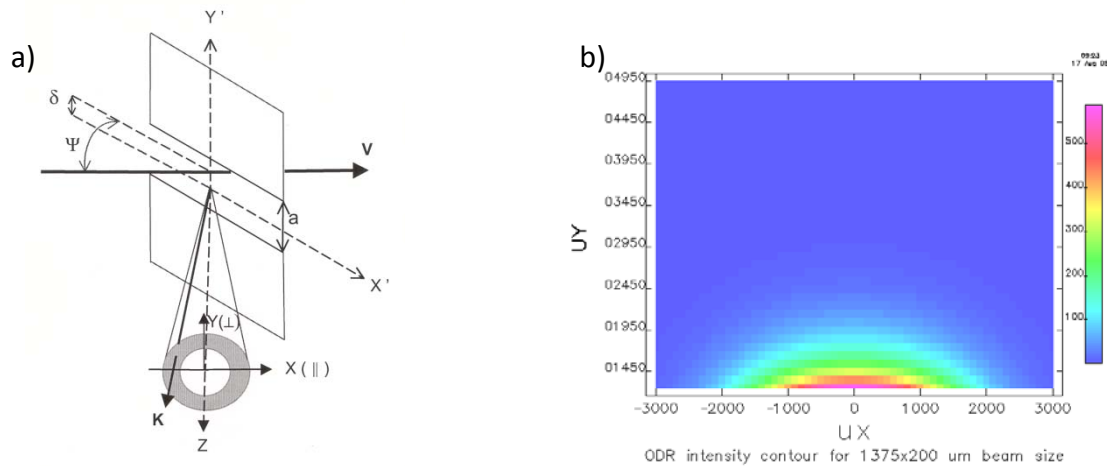


Figure 1. a) A schematic of the backward ODR angular distribution generated as the beam passes near the metal planes and b) a calculation of the ODR light generated from a single plane for the beam sizes in the experiment at an impact parameter of 1.25 mm.

### ODR Modeling Results

The model has been used to evaluate beam size sensitivity for two cases for an  $\sim 0.5$ -GeV electron beam. Previously we presented results at the 20- $\mu\text{m}$  level for the ILC regime [2]. For the ASTA case the  $x$  beam size was varied  $\pm 20\%$  around the 200- $\mu\text{m}$  sigma value to show the change in ODR profile. In Figure 2 we show the ODR perpendicular polarization component for a beam size (sigma) varied around 200  $\mu\text{m}$  (left) and around 400  $\mu\text{m}$  (right).

The calculated ODR profile is of course larger than the actual beam size, but the profiles do detectably change in size with the beam size change. A 20% change in beam size from 200  $\mu\text{m}$ , gives an  $\sim 12\%$  change in ODR profile size under these conditions.

As an additional issue we addressed the beam size sensitivity for a 400- $\mu\text{m}$  beam size, but with an impact parameter of  $12.5 \sigma_y = 5000 \mu\text{m}$  in Figure 3. Using an 800-nm wavelength, we still calculate some sensitivity to beam size changes of 12 % in the left plot, but the 10- $\mu\text{m}$  wavelength case shows very little sensitivity in its much larger horizontal profile in the right plot. It had been suggested a 14- $\mu\text{m}$  wavelength could be used to increase the photon emission number in an application for protons in the Tevatron using a far-field imaging technique, but the trade is not at all favorable in our near-field technique. So it appears that the 800-nm regime would be the better choice as has been used in far-field experiments at 680 MeV by the Frascati team using a 16-bit CCD camera [13], as well as in our more recent near-field experiment at 900 MeV using the same camera as reported at BIW08 [10].

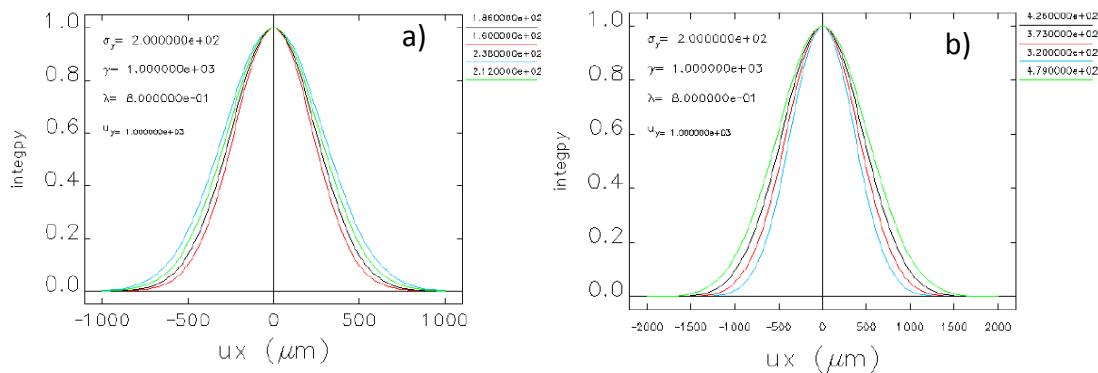


Figure 2. Numerical results for beam size sensitivity at a)  $\sigma_x=200 \mu\text{m}$  and b)  $\sigma_x=400 \mu\text{m}$ . The impact parameter was  $5 \times \sigma_y = 5 \times 200 \mu\text{m}$ , and  $\gamma=1000$  [10].

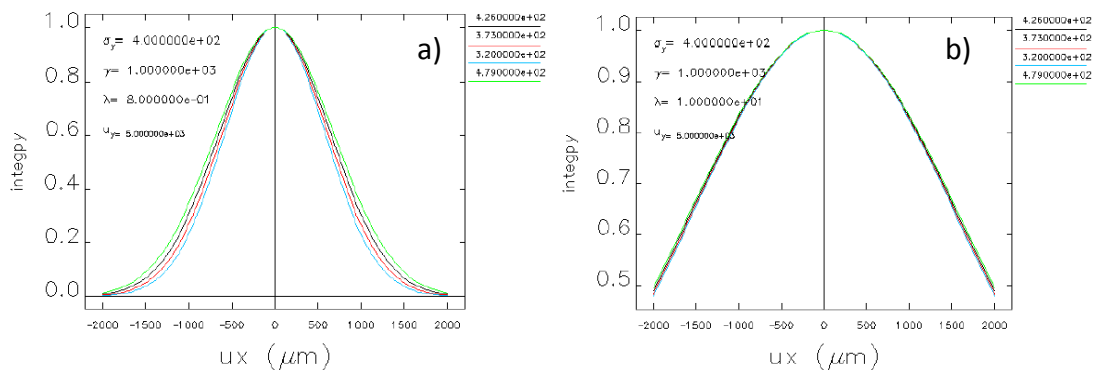


Figure 3. Numerical results for wavelength effects on beam size sensitivity at  $\sigma_x = 400 \mu\text{m}$  with a) 0.8- $\mu\text{m}$  and b) 10- $\mu\text{m}$  ODR wavelengths. The impact parameter was  $12.5 \times 400 \mu\text{m}$  ( $\sigma_y$ ) and  $\gamma=1000$  [10].

In general the linac is a linear device and has no bends. However, there can be some OSR emitted as the beam transits correctors, quadrupoles, the dipoles in a chicane, and the dipole for a spectrometer. These sources are generally out of focus or displaced from the ODR image position when near-field focusing is used. OTR from beam halo particles could be a background source, but if one uses an impact parameter of about 5-6  $\sigma_p$ , where this is the size perpendicular to the single edge, this contribution generally should be negligible.

### JLAB Experimental Results

The test station was implemented by P. Evtushenko et al. [9] to the provided general specifications on the CEBAF Hall-A transport line as shown schematically in Figure 4. The test station includes an OTR foil and an Aluminized Si converter screen with stepper motor control and the imaging system. The Al coatings were done at Fermilab by E. Hahn. The dipole that when powered directs the beam into this line is 8 m upstream of the ODR converter screen. A Pro-E version of the station is shown in Figure 5 that more clearly depicts the physical appearance of the hardware and screens. The optical transport line involves two mirrors and two relay lenses enclosed in the 2-in. diameter Thorlab tubes. The camera calibration factors in x and y are 11  $\mu\text{m}$  per pixel.

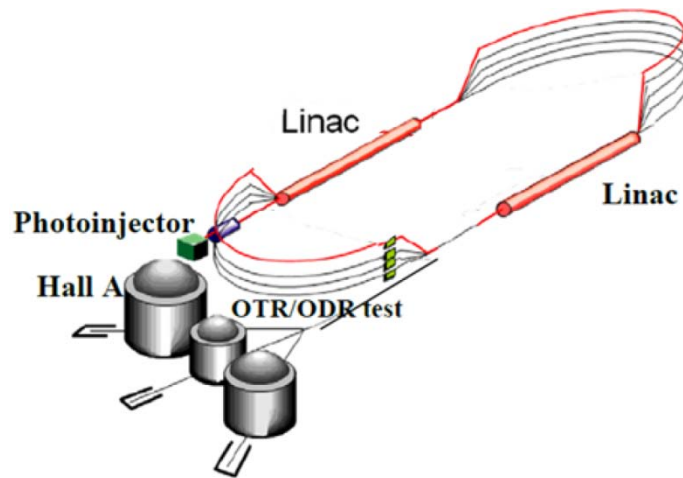


Figure 4. A schematic of the CEBAF/JLAB recirculating linac which can provide 100  $\mu\text{A}$  at 1,2,3,4, and 5 GeV and the location of the OTR/ODR test station area on the HALL A line.

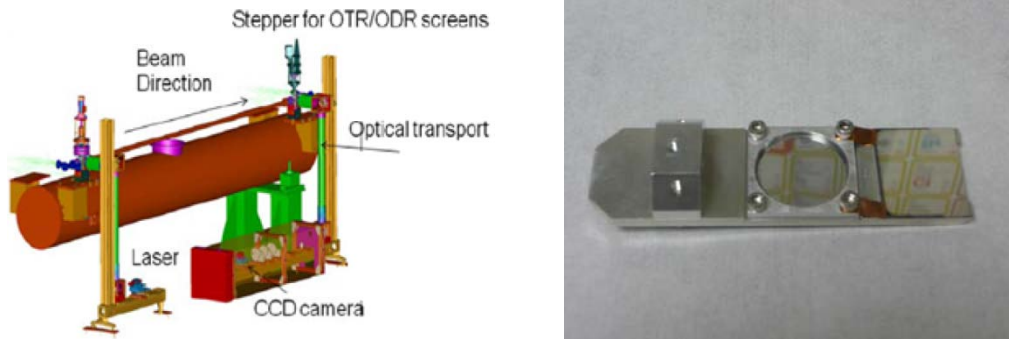


Figure 5. A Pro-E drawing (Left) of the OTR/ODR station at JLAB showing the alignment laser, ODR assembly, optical transport, and ODR CCD camera and photograph of the OTR and the ODR converter screens (Right) [9].

In this case a standard 10-bit CCD camera was used to record the near-field (focus at the object) ODR images at the Al metal screen. Reference images were taken with OTR by inserting the Al screen into the beam and using the same optics and camera. For these conditions we found the OTR about 10 times more intense than the ODR and used a neutral density filter to prevent camera saturation with OTR.

The most fundamental results are the OTR and ODR image sizes generated by the 4.5-GeV beam as it passes through and near the metal screen, respectively. These are shown in Figs. 6 and Figure 7. The OTR images in Figure 6 show the a) total intensity, b) horizontal polarization component and c) vertical polarization component. We see a 20-25  $\mu\text{m}$  smaller beam size when using the perpendicular polarization OTR components as described previously [9].

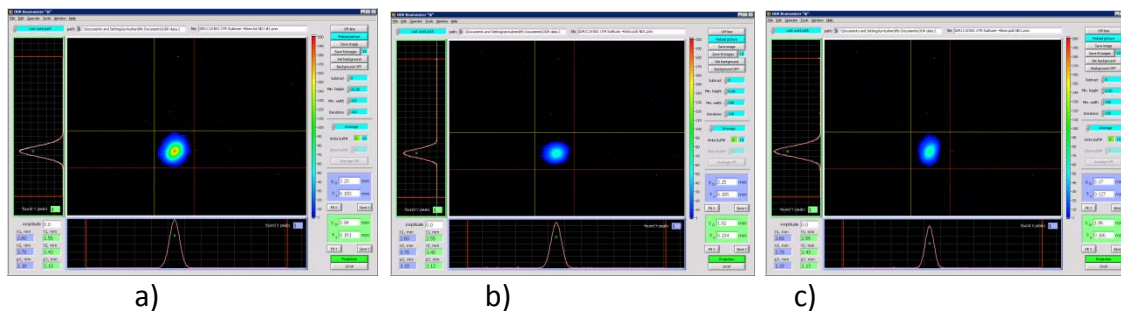


Figure 6. Results of early near-field imaging tests: the OTR images observed with a) total intensity, b) horizontal polarization, and c) vertical polarization components. The latter two show a reduced size in the perpendicular plane. Initial beam size about 150  $\mu\text{m}$  by 160  $\mu\text{m}$  for x and y, respectively, obtained with 5  $\mu\text{A}$  tune beam.

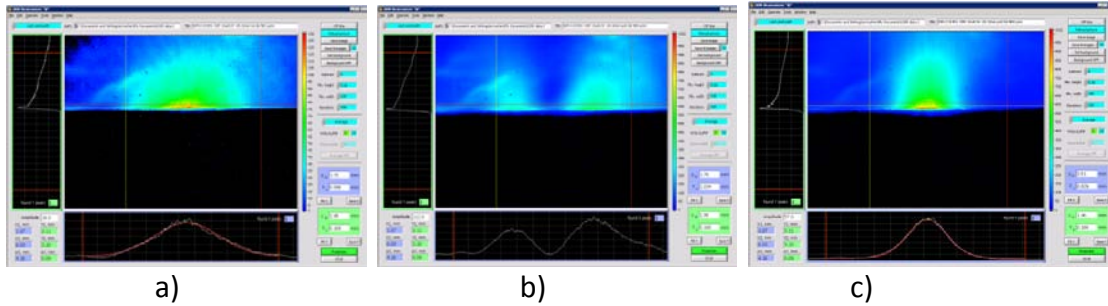


Figure 7. Results of near-field imaging tests: the ODR images observed with a) total, b) horizontal, and c) vertical polarizations for an impact parameter of 1.0 mm with the same beam size setup as Figure 6.

Another key experimental result was obtained by using the perpendicular (vertical in this case) polarization component to assess the horizontal beam size. In this case an upstream quadrupole magnet field was scanned to vary the observed beam sizes. A comparison of the OTR image profile sizes and the ODR image sizes is shown in Figure 8. There is a clear tracking of the beam-size effect with ODR. The ratio of sizes for ODR/OTR image size was tracked as the OTR determined beam size varied by a factor of two (as also seen in the wire scan data). The minimum OTR beam size was  $\sim 120 \mu\text{m}$ .

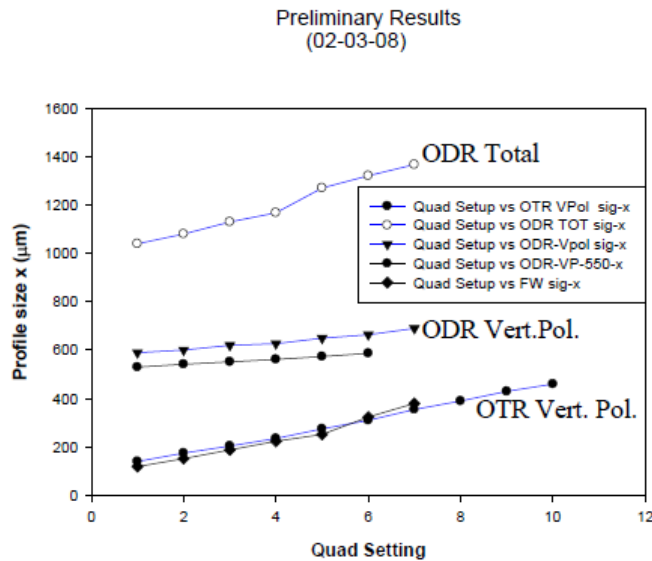


Figure 8. The observed vertically polarized ODR and OTR image size variation with the upstream quadrupole magnet current. The beam sizes determined with a wire scanner (black line with black diamond symbol) at a nearby  $z$  location are also shown as close to that of the vertically polarized OTR (blue line with black diamond symbol).

## FLASH Experimental Results

An opportunity to test the feasibility of the near-field monitor at 900 MeV was identified in discussions with staff at FLASH in Germany and Frascati in Italy. In this case a complementary test was proposed to the ongoing far-field ODR experiments of the Frascati team [12]. The FLASH facility includes a PC rf gun, two bunch compressors, and an approximately 1 GeV SRF linac as schematically shown in Figure 9. The accelerator is designed to drive a soft x-ray FEL, but in addition it has ongoing programs in diagnostics developments in electro-optic sampling, a transverse rf deflector, optical replica synthesizer, and ODR. A bypass line indicated in Figure 9 was used for the ODR tests. The converter consisted of an aluminized Si nitride wafer with a slit chemically etched of 1-mm height. A test beam with 6 bunches and 1 nC per bunch operating at 5 Hz was generated in the FLASH facility and transported to the test station. A reference OTR image as shown in Figure 10 was obtained with the screen inserted to intercept the beam. Ultimately 10 images (60 nC integrated) were summed to improve statistics for the ODR signal obtained using an 800 x 80 nm band pass filter. The beam was positioned at the top edge of the slit, and then the actuator was stepped in 100- $\mu\text{m}$  steps. An example of the image obtained with a 400- $\mu\text{m}$  beam offset from the top edge is shown in Figure 11. The dark current from the photoinjector has been subtracted from the total beam intensity. The dim ODR image is seen near both top and bottom edges. The region of interest (ROI) sampled only the top image and gave an ODR profile width of about  $\sigma_x=360 \mu\text{m}$  as shown in Figure 11 in comparison to the original OTR-measured beam size of 205  $\mu\text{m}$ .

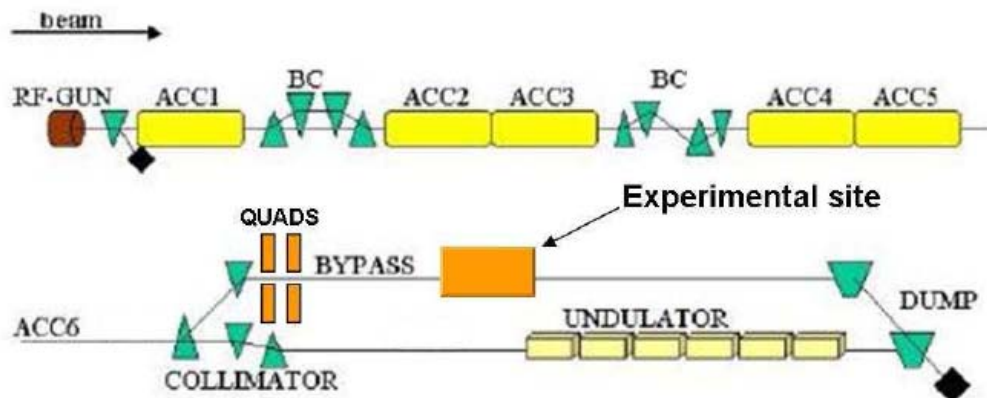


Figure 9. Schematic of the FLASH facility with the OTR/ODR experimental site in the bypass line indicated.

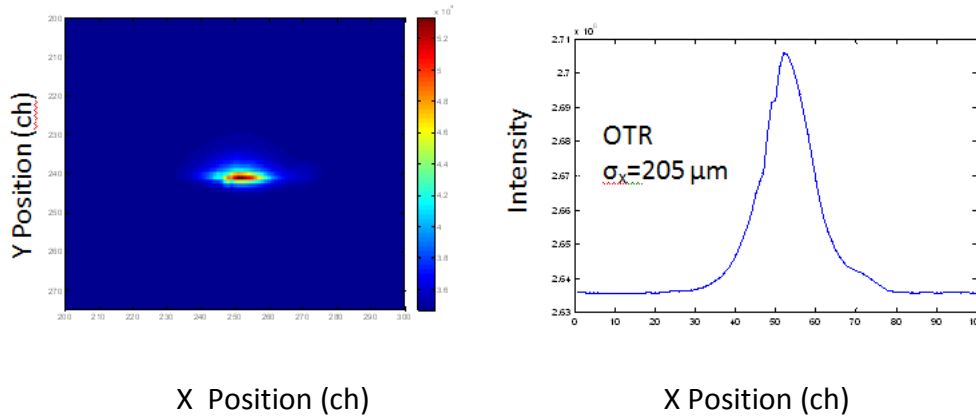


Figure 10. Near-field OTR image (L) and x profile (R) at 900 MeV on FLASH at the test site.

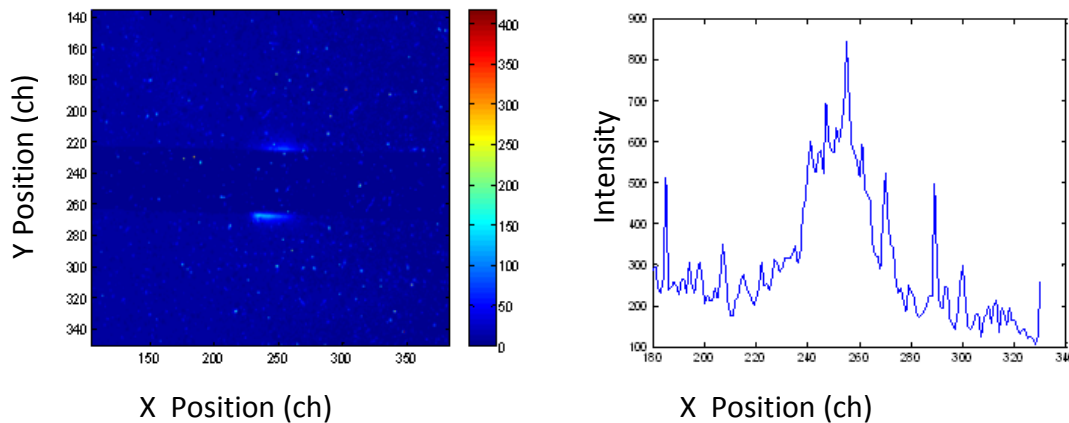


Figure 11. Near-field ODR Image (L) and x profile (R) at 900 MeV and about 30 nC image integrated obtained at FLASH with a 16-bit camera. The actual beam size is  $\sigma_x = 205 \mu\text{m}$  and the ODR image size is  $\sigma_x \sim 360 \mu\text{m}$ . The slit is 1-mm high.

With the first experimental results in the near-field at  $\gamma = 1800$ , we performed post-experiment modeling for these specific parameters. The results of the numerical evaluations by C.-Y. Yao [10] using Eq. 1 are shown in Figure 12. The left plot shows the total intensity profile for different impact parameters starting at  $500 \mu\text{m}$ . The ODR x profile was calculated to range from  $286 \mu\text{m}$  to  $400 \mu\text{m}$  for impact parameters from  $500$  to  $1200 \mu\text{m}$  for total intensity, in reasonable agreement with the experiment. The right plot shows the calculated beam-size sensitivity for the  $200 \mu\text{m} \pm 20\%$  horizontal size. The ODR x-profile clearly tracks the changes with its roughly  $30\text{-}\mu\text{m}$  change in sigma per step or 10-12% relative changes. In these cases, the dots on the curves are the ODR results and the solid lines are the Gaussian fits to those points. It is clear the Gaussian assumption is appropriate for these results.

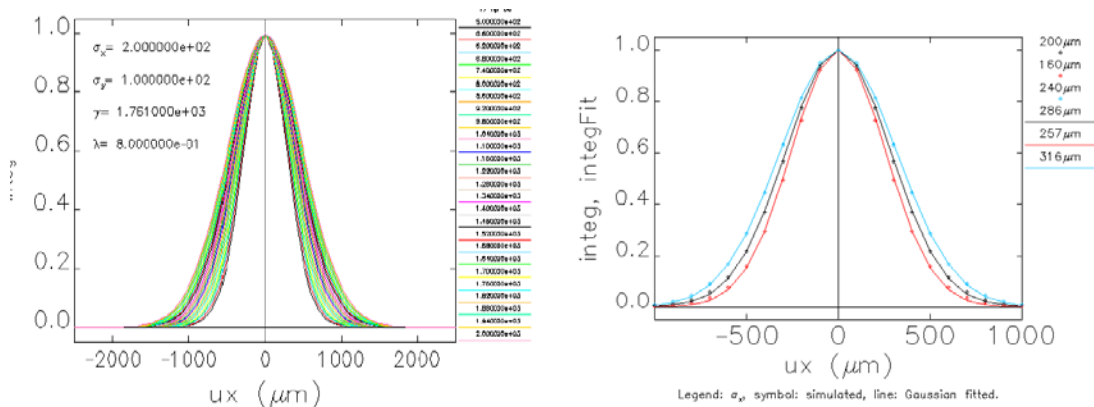


Figure 12. Calculated near-field ODR horizontal profiles for the FLASH case with the variation of impact parameter (left) and the 20% variation of initial beam size around 200 μm (right) [10].

### 7.3.10.4 ASTA Application

Beam sizes for the baseline ASTA facility appear to be between the two cases calculated in Ref. 2 and above and similar to the JLAB CEBAF case in some parameters as shown in Table 1. When the emittance is indeed degraded by the bunch compression process from 4.5 to ~25 pi mm mrad and with the beta function of 2 m, one would expect beam-size sigmas of ~160 μm at 750 MeV at ASTA. From the intensity point of view at ASTA, the factor of 3000 in charge compared to the APS case combined with an assumed camera-sensitivity factor of 1000 over a standard CCD camera should compensate for the expected reduction factor for low gamma compared to the 7-GeV case. In fact, we had added attenuation filters of about 100 before the CCD camera to avoid saturating the camera in the CEBAF full current run at 4.5 GeV, and the FLASH result at 900 MeV provided the proof of principle for the lower gamma cases such as would be at ASTA. Analytical assessments of beam size sensitivity for the specific low gamma conditions have been described in a previous section, but experiments are still warranted. In general, the basic OTR station with a stepper motor drive on the actuator that would allow selection of the OTR screen or ODR converter should be adequate as demonstrated at JLAB and APS. It would be preferable to have two vertical actuators with one screen inserted from the top and one from the bottom to establish a variable vertical slit height. A filter wheel or other device to select ND filters, bandpass filters, and two linear polarizers would be planned.

Table 1: Summary of the beam energy, beam sizes, average current, and charge per image for the APS, CEBAF, FLASH, and ASTA cases.

| <u>Parameter</u>  | <u>APS</u> | <u>CEBAF</u> | <u>FLASH</u> | <u>ASTA</u> |
|-------------------|------------|--------------|--------------|-------------|
| Energy (GeV)      | 7          | 1- 5         | 0.9-1.2      | 0.5-0.8     |
| X Beam size (μm)  | 1300       | 30-50        | 100-200      | 160-300     |
| Y Beam size (μm)  | 200        | 30-50        | 100-200      | 160-300     |
| Current (nA)      | 6          | 100,000      | 10,000       | 50,000      |
| Charge/image (nC) | 3          | 3,000        | 80 (test)    | 10,000      |

The camera for ODR needs to be evaluated, but an extended IR or NIR response with either a GaAs MCP intensifier and/or 16-bit capability would be needed. The almost flat response of a GaAs PC MCP out to 880 nm is shown in Figure 13. Such an intensified CCD camera with 10-bit dynamic range would be a candidate. The previous DESY FLASH ODR results with a 680-MeV beam and an image integrated over only ~175 nC in 2 s used a 16-bit Hamamatsu camera and supports the feasibility [13] and the simple scaling technique employed. Since the latter was a far-field test, and they used a 40-nm wide bandpass filter centered at 800 nm, they exacerbated the low photon yield issue. It's not clear from their paper what their beam-size sensitivity really is in the presence of the divergence of 30 μrad, but with near-field imaging one could use a wider bandpass filter and increase the signal. Our actual proof-of-principle, near-field experiment [10] at FLASH at 900 MeV was presented in the previous section.

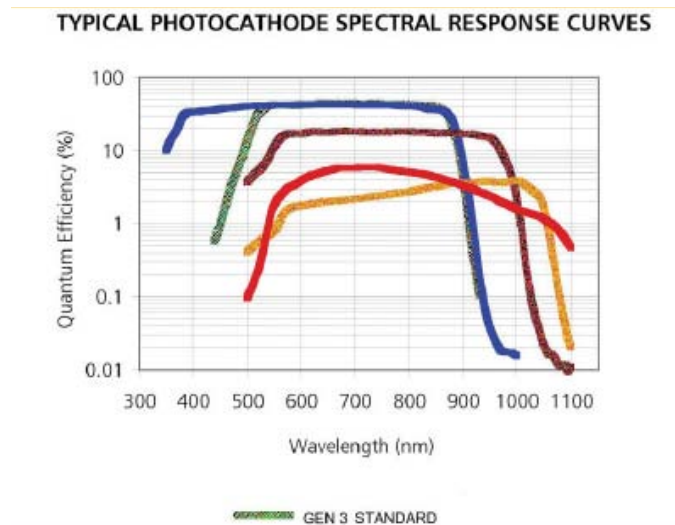


Figure 13. The reported response of the GaAs PC MCP in the NIR for the Pulnix ICCD with a Generation 3 MCP (green curve follows the blue curve at long wavelength end).

The ODR station would be initially positioned in the “test area” and/or diagnostics section where an OTR cube could be shared as indicated in Figure 14. In the test area, M. Church estimates he could provide beta functions varying from 0.2 m to 100 m for test purposes. Some optical transport to bring the radiation to the shielded camera would be needed. Operationally, one could consider a three-station configuration to provide an emittance monitor independent of the beta function determination. A beam waist generated at the center screen with adequate drift either way would simplify the emittance calculation. The expected beam sizes for the high-emittance case would be 520  $\mu\text{m}$  and 70  $\mu\text{m}$ , respectively, with about 5<sup>1/2</sup> times smaller beam sizes in the low-emittance case. Far-field imaging could be evaluated for beam-size sensitivity to the dimension perpendicular to the edge [3,4,6] or a second set of orthogonal screens could be used. The reference beam sizes at ASTA would be determined at lower macropulse charge by OTR imaging with the beam directly striking the metal screen. Depending on the actual beam sizes and the screen thickness, signals from a number of micropulses at the 3 MHz rate can be integrated to assess beam size. These screens would not be inserted at full macropulse charge, but hopefully there could be a lower charge that could be used as an overlap point with the ODR data. The ODR is then generated as the charged-particle beam passes near the metal plane in the NI mode at full current.

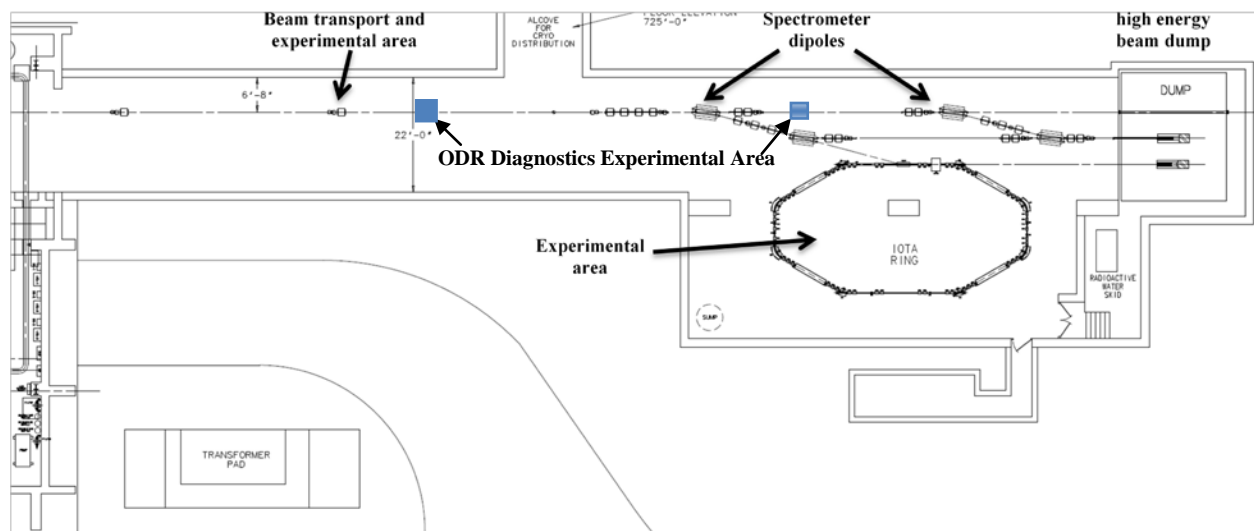


Figure14. Schematic of the ASTA Downstream beam line with ODR diagnostics experimental area indicated (courtesy of Mike Church, 8/22/12,ODR revised).

### 7.3.10.5 Summary

In summary, it is proposed that the ASTA diagnostics plans include the development of an ODR imaging station in the downstream beam line areas for a NI beam-size monitor. The baseline plan would be to use visible to IR/NIR imaging with a sensitive camera and share an

actuator on a stepper motor with the OTR screen at that station. A double vertical actuator assembly which would allow an adjustable vertical height of the horizontal slit would be preferred for the initial tests at the test position. This would also allow far-field imaging tests to be done to evaluate beam size sensitivity in the plane perpendicular to the slit direction. Complementary and proof-of-principle tests have been done at JLAB and FLASH, respectively, in FY08. We expect about 100 fs resolution from the THz-based techniques as before [6]. Subsequent beam tests at ASTA should help to establish the applicability of the diagnostic to other locations in the beam line where the OTR stations already exist, and the feasibility of an NI emittance monitor based on three ODR stations in a drift region would be evaluated.

### **7.3.10.6 Acknowledgements**

The author acknowledges discussions with S. Nagaitsev, M. Church, H. Edwards, and M. Wendt on ASTA, collaborations with P. Evtushenko, A. Freyberger, and C. Lui at JLAB, collaboration with C.-Y. Yao of ANL, and collaborations with E. Chiadroni and M. Castellano of INFN.

### **7.3.10.7 References**

- [1] Alex H. Lumpkin, "Possible ODR Imaging Diagnostics for ILCTA", talk presented at ILC-TA Workshop, Fermilab, November 28, 2006.
- [2] Alex H. Lumpkin, "Potential ODR Imaging Diagnostics for ILC-TA at NML", Fermilab Tech. Note, DocDB-2929-v1-2007.
- [3] M. Castellano, Nucl. Instrum. Methods Phys. Res. A **394**, 275 (1997).
- [4] R. B. Fiorito and D. W. Rule, Nucl. Instrum. Methods Phys. Res. B **173**, 67 (2001).
- [5] T. Muto et al., Phys. Rev. Lett. **90(10)**, 104801-1 (2003).
- [6] P. Karataev et al., Phys. Rev. Lett. **93**, 244802 (2004).
- [7] A. H. Lumpkin et al., Phys. Rev. ST AB, **10** 022802 (2007).
- [8] A.H. Lumpkin et al., "Far-Field OTR and ODR Images Produced by 7-GeV Electron Beams at APS", proceedings of PAC07, Albuquerque, June 25-29, 2007.
- [9] P. Evtushenko et al., Near-field Optical Diffraction Radiation Measurements at CEBAF", Proceedings of BIW08, JACoW, 2008.
- [10] A.H. Lumpkin et al., "Considerations on ODR Beam-size Monitoring for Gamma=1000 Beams", Proceedings of BIW08, JACoW, 2008.
- [11] M. Ross, "Challenges of the Main Linac", talk at ILC School, FNAL, July 25, 2007.
- [12] J.D. Jackson, *Classical Electrodynamics*, (John Wiley and Sons, New York, 1975) Sec. 15.4.
- [13] E. Chiadroni et al., "Non-Intercepting Electron Beam Transverse Diagnostics with ODR at the DESY FLASH Facility", Proceedings of PAC07, Albuquerque, June 25-29, 2007.

## 7.3.12 Towards Ultra-Stable Operation of ASTA with Beam Based Feedback

### 7.3.12.1 Introduction

Superconducting RF systems have been adopted in a variety of accelerator systems because of the ability to efficiently accelerate high power beams. However, because of the long RF and beam pulses used in these systems, it is also possible to use high precision feedback control of the RF systems to achieve extremely high stability of the beam parameters. In this section, we describe how such a feedback system can be implemented at ASTA, providing a unique capability for development of new accelerating techniques. For example, energy stability at the  $10^{-5}$  level and timing stability below 10 fsec would allow extremely tight synchronization with external laser systems and enable a range of advanced accelerator experiments which are either extremely difficult or impossible at existing facilities in the US.

The demonstration of a sub-femtosecond feedback system to stabilize the superconducting linac will be a very important test at ASTA.

Modern electron linacs consist of an injector and multiple accelerating sections with one or more interleaved bunch compressors. Jitter of the beam parameters such as energy, bunch length, and arrival time arises from two primary sources: 1) jitter of the beam from the injector and 2) amplitude and phase errors in the accelerating sections. In normal conducting linacs, the beam jitter is dominated by the second source because the RF pulses, typically a few microseconds long, are too short for intrapulse RF feedback to be applied. Therefore, uncorrelated errors between RF pulses cannot be corrected. In SRF systems, the RF pulses range from milliseconds to continuous and high precision feedback can be applied. Control of SC cavities has already demonstrated amplitude stability at the  $10^{-5}$  level and phase stability of  $\sim 0.01$  degrees.

However, the beam parameters depend on the vector sum of the individual cavities and it is possible for beam parameters to drift from effects such as relative drift of the phase of individual cavities. The long beam pulses also allow the possibility of using beam-based feedback to provide modulation of the set point to the RF sections preceding the bunch compressor. The energy error is measured at each dispersive section by measuring the transverse beam position at a point of dispersion. Bunch length error is measured at each bunch compressor from the coherent radiation emitted in the chicane dipole magnets. A linear combination of these measurements is then used to adjust the voltage and phase set points of the preceding RF sections. We can express this transformation as a matrix relating the measured beam errors with the changes to the RF voltages and phases. If we consider global RF and beam-based feedback for the entire linac, we can relate the measured beam parameters at several dispersion sections to the corresponding amplitude and phase correction in the different linac sections.

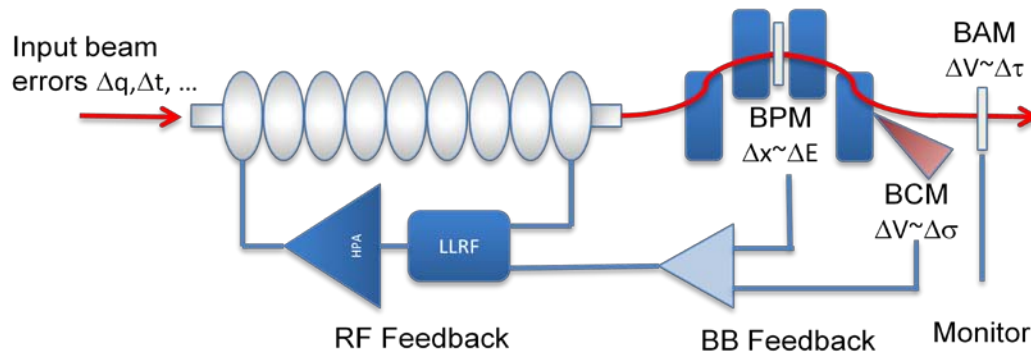


Fig. 1. Conceptual schematic view of RF and beam-based feedback control. Energy, bunch length, and arrival time measurements can provide set point modulation to the RF sections preceding the bunch compressor.

Experience with feedback control of SC linacs has been extremely positive. At FLASH, a combination of RF and BBF has been implemented. An example of the performance of this system is shown in Fig. 2. The top plot shows the arrival time error at the entrance to the bunch compressor from the injector over the first 100 bunches in a train and the lower plot shows the reduction with feedback applied. The first few bunches are not affected because of delays in the feedback. The residual noise is limited by the bandwidth and noise floor of the feedback. This performance is excellent and has already enabled high precision pump-probe experiments using x-ray free electron laser at the end of the linac. Further improvement could come from reducing the noise at the injector and improving the bandwidth and noise of floor of the feedback.

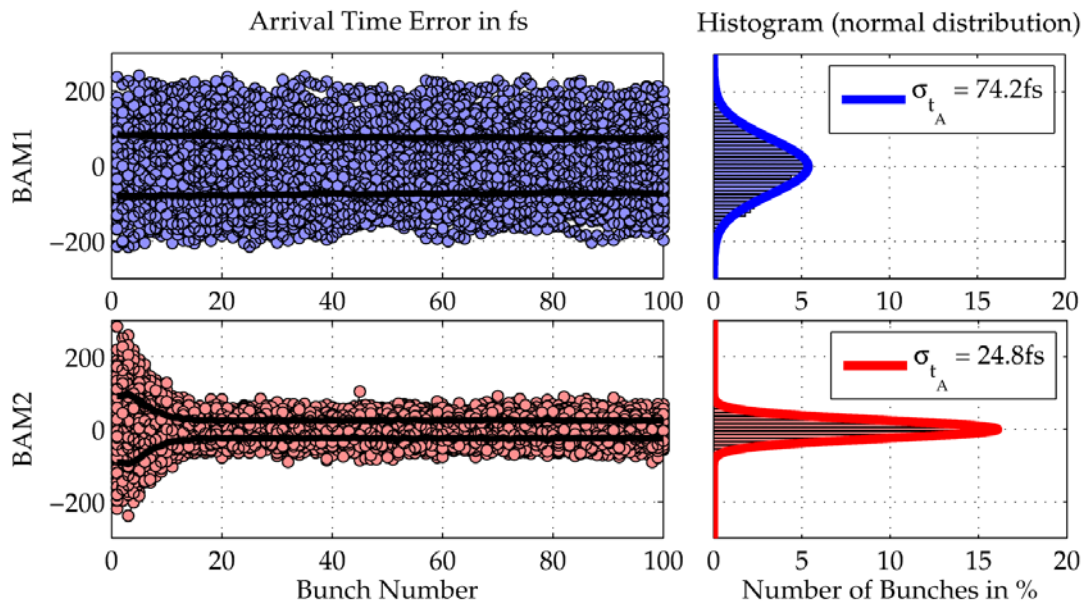


Fig. 2. Example of RF and beam-based feedback control at FLASH. The top plot shows the arrival time error at the entrance to the bunch compressor from the injector over the first 100 bunches in a train and the lower plot shows the reduction with feedback applied.

### 7.3.12.2 RF Control and Feedback

The *Low Level RF System* for ASTA shown in Fig. 3 includes all controller hardware and software required providing high precision field and resonance control of the accelerating cavities. It also delivers the Master Oscillator RF through the Phase Reference Line used to synchronize RF, instrumentation, and experimental systems. The Field Controller is capable of combining the probe signals from 24 cavities from one ASTA RF station into a single vector sum. The vector sum is used as the feedback input signal to the control loop. The FPGA-based controller uses a combination of IQ feed-forward and proportional-integral feedback driving the klystron to minimize phase errors far below the 1% amplitude and 1 degree levels with a gain of  $\sim 100$  (see Fig. 4).

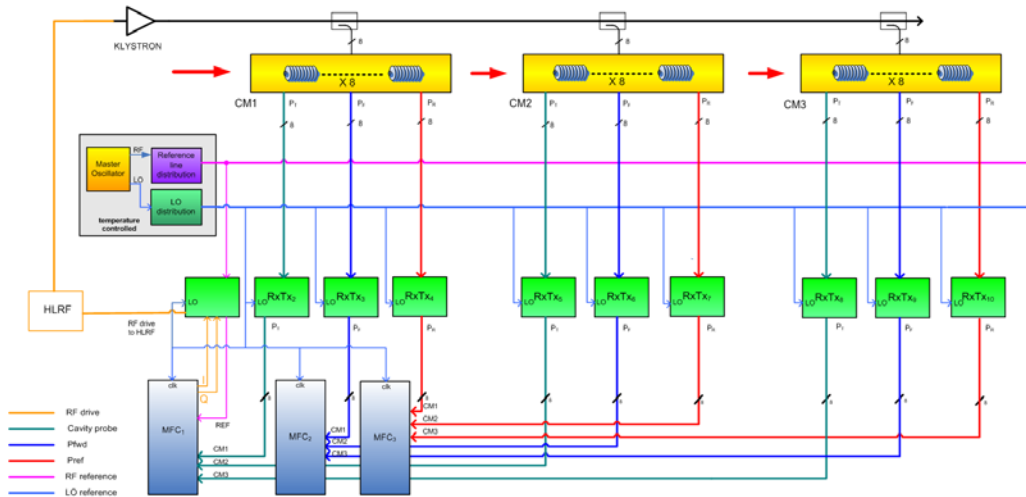


Fig. 3. ASTA LLRF system level block diagram for 3 cryomodules driven by a single klystron. A similar system is planned for booster cavities CC1 and CC2 in the

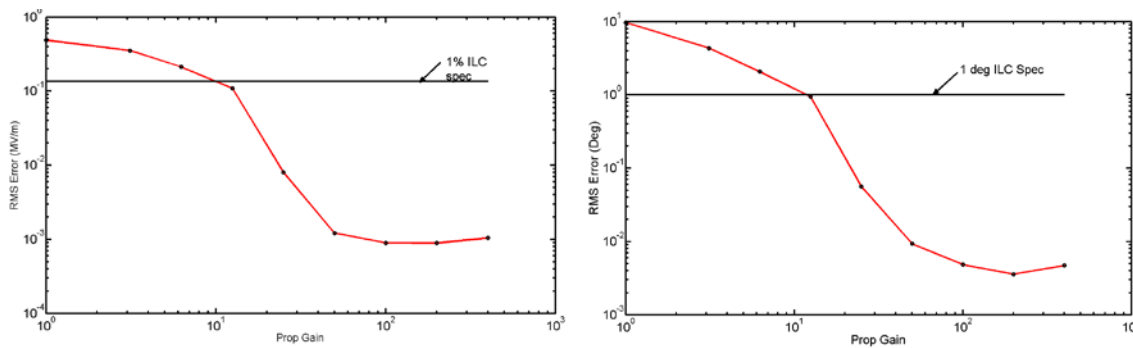


Fig.4. RMS magnitude and phase errors for Cryomodule 1 as a function of loop gain. Magnitude error is in MV/m with a 22 MV/m gradient or 3.6E-5 rms. Phase error is 3E-3 degrees rms. These measurements were made without beam through the cryomodule.

The controller can easily be adapted to use the proposed error signal matrix from the beam-based measurements with analog signals input into spare 65 MSPS digitizers or digitally with spare high speed serial links.

### 7.3.12.3 ASTA Beam-based Feedback

We propose to implement high precision feedback control at ASTA. The first stage of this work is to characterize and minimize the beam jitter from the injector. The beam energy, charge, timing and bunch length jitter can be characterized using the planned diagnostics. We expect that further control of the photocathode drive laser will be needed to reduce the charge and

timing jitter. Characterization of the phase and amplitude control of the RF gun is also critical to minimizing the beam jitter.

### 7.3.12.3.1 Beam monitors

To implement the first stage of beam-based feedback, we would implement a relative energy measurement using a beam position monitor in the BC1 bunch compressor along with a bunch length measurement following the bunch compressor. We expect the bunch length measurement to be based on detection of coherent radiation produced by either edge radiation (CER) or synchrotron radiation (CSR) from one of the chicane dipoles or from a dedicated coherent diffraction radiation (CDR) source. We also propose development of a femtosecond arrival time diagnostic to be initially used as an out-of-loop monitor of the feedback performance, but which could also be used in the loop. All of these diagnostics will be capable of operating with high precision at the bunch repetition rate of 3 MHz or close to that.

### 7.3.12.3.2 Arrival Time Diagnostics

A Bunch Arrival Monitor (BAM) is in development for ASTA and will be installed just downstream of the bunch compressor (see Figure 5). The monitor is based on the conversion of time-to-voltage via the amplitude modulation of a pulsed laser via Electro-Optical Modulation (EOM). This scheme was first proposed by the DESY group [1]. Figure 5 (left) shows the basic principle of the bunch TOA monitor. The zero-crossing voltage of a broadband beam pickup is used to amplitude modulate a single 100 femtosecond wide laser pulse. Figure 5 (right) shows how the zero-crossing voltage changes as a function of the bunch arrival time.

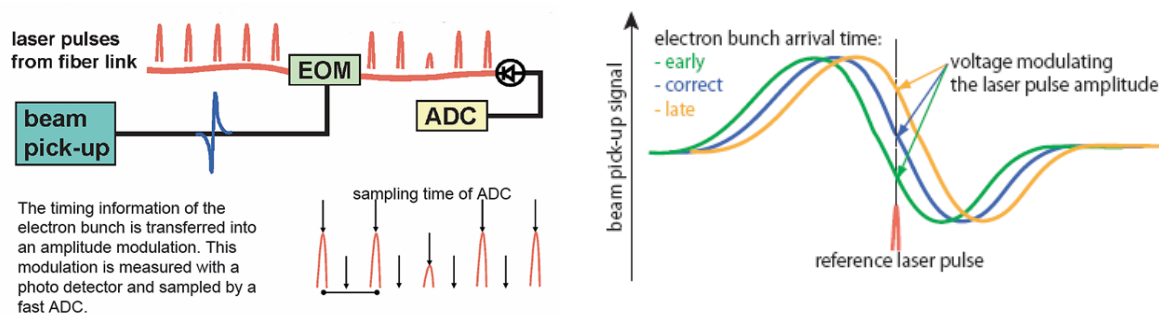


Figure 5. Left shows the basic principle of bunch time-of-arrival monitor. Right shows the relation between the modulating voltages to the bunch arrival time.

Figure 6 shows the BAM functional block diagram. The operation of the BAM starts with a wide-band beam pickup, needed to permit femtosecond time-of-arrival measurements, that acquires the bunch electric field. The pickup signal is timed to arrive at the electro-optical modulator in coincidence with the RF-locked laser pulses. The zero-crossing of the pickup signal is used to modulate the amplitude of a single 100 femtosecond wide laser pulse. A photodiode converts

the laser pulse into a voltage which is sampled by an ADC. The change in voltage then gives a measure of the time-of-arrival. The functional operation of the BAM allows for the measurement of arrival times for all bunches within the pulse train.

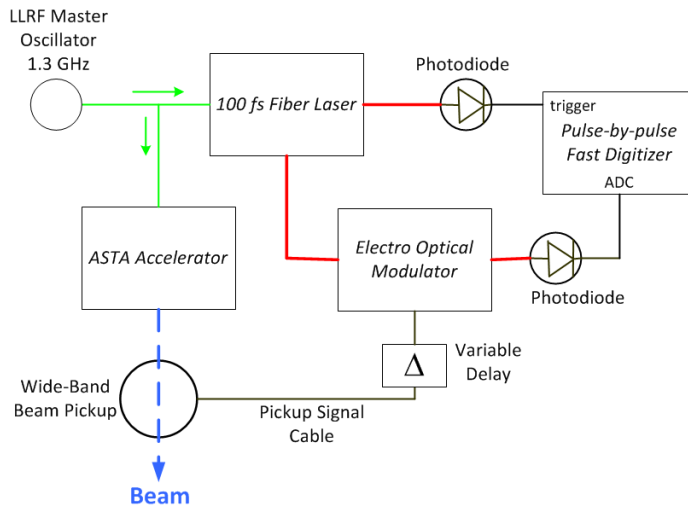


Figure 6. Functional block diagram of the proposed ASTA BAM.

For the proposed ASTA beam-based feedback system, the BAM can be used as (1) an out-of-loop monitor of the feedback performance from the bunch compressor energy and bunch length monitors or (2) as an in-loop part of the beam-based feedback system. DESY FLASH used the arrival-time information measured by a BAM to establish an intra-bunch-train arrival-time feedback acting on the amplitude of their first accelerating module. Figure 7 shows the bunch-by-bunch effect of this feedback on the arrival-time stability [2].

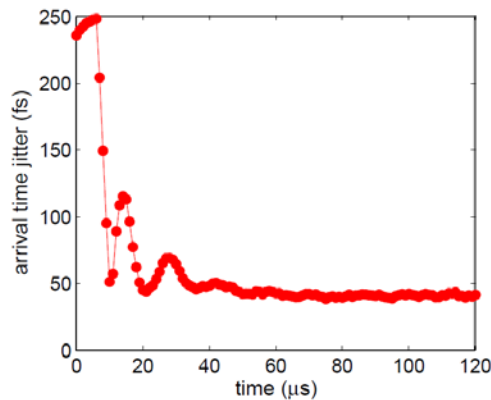


Figure 7. Effect of the intra-bunch train feedback on the arrival-time stability [2]. The first few bunches are not corrected by feedback.

One advantage of the proposed ASTA BAM system is that Fermilab already possesses a 100-fs Erbium fiber laser (MenloSystems C-Fiber femtosecond laser) and electro-optical modulators (Covega Mach-10 056). The Menlo Erbium fiber laser is designed to lock at 81.25 MHz so we will

use the 1/16<sup>th</sup> sub-harmonic of the LLRF 1.3 GHz master oscillator for the laser synchronization. The use of these pieces provides a significant cost savings toward the development of the BAM at ASTA.

One fundamental limitation of the BAM is that the slope of the beam pickup signal at the zero crossing defines the time resolution. For a high time-of-arrival resolution, the slope needs to be as steep as possible, and this requires a high bandwidth for the beam pickup [3]. As part of the ASTA BAM development, new beam pickup designs will be investigated to improve the time resolution.

#### **7.3.12.3.3 Bunch Compression Monitor**

The bunch compression measurement will utilize coherent radiation either in the form of synchrotron radiation from the center or edge of a bending magnet, or diffraction radiation from a metallic screen containing an aperture for the beam to pass through. The spectral intensity of these forms of coherent radiation is given by

$$I(\omega) = I_0(\omega) [ N + N(N - 1) | \mathcal{F} |^2 ]$$

where  $I_0$  is the single particle radiation intensity,  $N$  is the number of particles in the bunch, and  $\mathcal{F}$  is the Fourier transform of the longitudinal bunch distribution, ignoring the transverse distribution. The first term is the incoherent radiation while the second term is the coherent radiation. The Fourier transform implies that the  $N(N - 1)$  term will dominate when the wavelength of radiation is larger than the bunch length. This intensity dependence on the bunch length allows one to develop instrumentation that is sensitive to the bunch length. Figure 8 (taken from reference 4) shows the coherent synchrotron radiation intensity as a function of the phase of the accelerating cavity prior to a double bend in the A0 photoinjector. The varying phase corresponds to varying levels of energy chirp on the beam leading to varying levels of compression after the double bend.

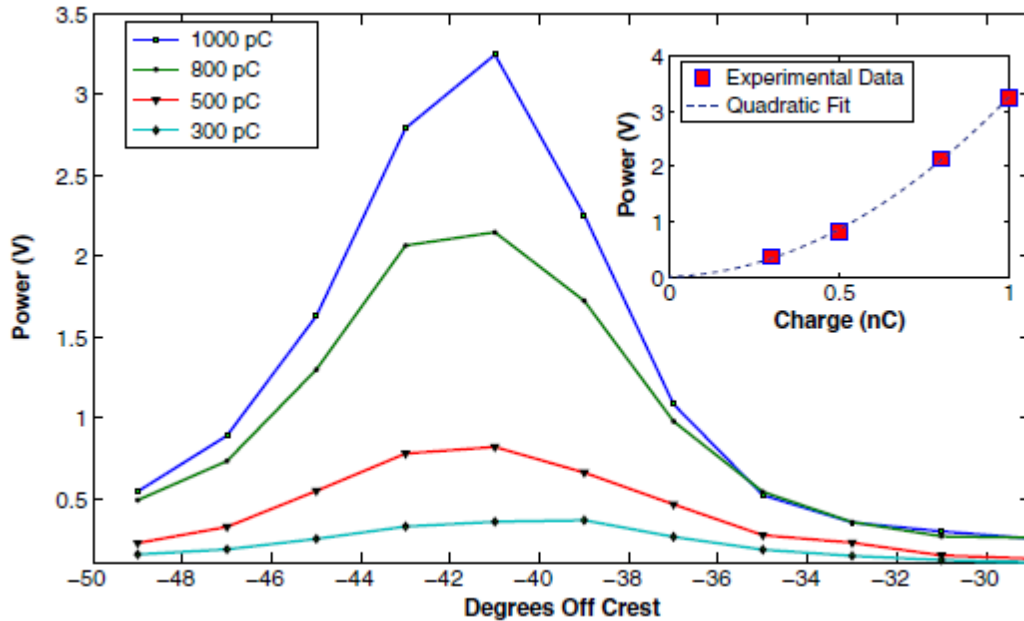


Figure 8: Coherent synchrotron radiation intensity as a function of phase of the accelerating cavity prior to a double bend.

Since typical bunch sizes are sub-picosecond to picoseconds, the frequencies of the coherent radiation is typically Terahertz. To use the coherent radiation intensity to make a bunch-by-bunch measurement of the bunch length requires a somewhat broadband and relatively fast THz detector, since the bunch spacing can be as short as  $\sim 300$  ns. Several THz devices come to mind: a pyroelectric detector, a Golay cell, a bolometer, and a schottky-diode antenna. There have been measurements made at the A0 photoinjector with a broadband pseudo-optical Schottky-diode detector [5]. This device was able to measure individual bunches, although the construction of the device could prove difficult. FLASH has developed a compression monitor using a pair of pyroelectric detectors with different gains for a larger dynamic range [6]. Pyroelectric detectors are the simplest and least expensive to build of the above list and, given the success of the FLASH system, would probably be the detector of choice, with the layout of the instrument paralleling the FLASH compression monitor. Theirs is actually based on CDR, and we already plan to install a CDR monitor after the chicane at 50 MeV for nonintercepting bunch length and relative bunch length measurements as described elsewhere in the proposal [7]. We will simply add a path to the THz detector designated for feedback.

#### 7.3.12.4 Summary

In summary, we propose the use of beam-based feedback to enhance the phase stability of the micropulse train to the 25 fs regime or better and the energy stability at the  $10^{-5}$  range in ASTA. We would take advantage of the 3-MHz micropulse repetition rate and the 1-ms macropulse length to implement the feedback with the planned LLRF system. This stable beam will enable experiments requiring these features including (but not limited to) emittance exchange,

reversible beam heating, laser-beam interactions in electro-optical sampling or microbunching studies, and free-electron laser experiments. The facility would be unique in the HEP-supported realm in the USA.

### **7.3.12.5      *References***

- [1] F. Loehl et al., "A sub 100 fs electron bunch arrival-time monitor system for FLASH", Proceedings of EPAC 2006, Edinburgh, Scotland, 2006, pp. 2781–2783.
- [2] F. Loehl et al., "Observation of 40 fs synchronization of electron bunches for FELs," Proceedings of FEL 2008, Gyeongju, Korea, 2008, pp. 490 – 493.
- [3] A. Angelovski et al., "Pickup design for high resolution bunch arrival time monitor for FLASH and XFEL," Proceedings of DIPAC 2011, Hamburg, Germany, 2011, pp. 122 – 124.
- [4] J.C.T. Thangaraj, et al., "Experimental Studies on Coherent Synchrotron Radiation in the Emittance Exchange Line at the Fermilab A0 Photoinjector", PAC11, New York, New York, 2011.
- [5] G.M. Kazakevich, et al., "Bunch Length Monitoring at the A0 Photoinjector Using a Quasi-Optical Schottky Detector", PAC09, Vancouver, British Columbia, 2009.
- [6] C. Behrens, B. Schmidt, S. Wesch, D. Nicoletti, "Upgrade and evaluation of the bunch compression monitor at the free-electron laser in Hamburg (FLASH)", IPAC10 Kyoto, Japan, 2010.
- [7] A.H. Lumpkin, "Proposed Coherent Diffraction Radiation Measurements of Bunch Length at ASTA", Section 3.5.9 as of 9-26-12 ASTA proposal draft.

### **7.3.13 Proposed Wakefield Measurements at ASTA**

#### **7.3.13.1      Introduction**

The Next Generation Light Source (NGLS) at LBNL will use a CW superconducting L-band linac to accelerate high-brightness electron beams up to 2.4 GeV at 1 MHz for injection into a farm of up to 10 free-electron laser undulators for the production of high-brightness, coherent soft x-rays. Beam stability from bunch to bunch in all coordinates is critical for such a user facility, and the impact of beam dynamics issues such as long-range wakefields must be well understood. We at LBNL therefore propose a series of beam-based and possibly RF-based measurements at the Advanced Superconducting Test Accelerator (ASTA) at Fermilab. The measurements require the installation of at least one 8-cavity cryomodule and a high-resolution electron spectrometer and beam diagnostics package to be located at the end of the Stage-I machine or similar (see Fig. 1).



Figure 1: The configuration shown above (I.2, from the ASTA proposal) might be used in this 'Stage-I' ASTA layout to measure the long-range, longitudinal wakefields induced within one cryomodule (ACC1) using the electron spectrometer and diagnostics section shown at far right.

The proposal will attempt the measurement of long-range wakefields in the superconducting linac using an ILC-type cavity. The ASTA accelerator is uniquely suited for such an experiment due to its long bunch train.

### 7.3.13.2 Beam-Based Measurements

The experimental details need further definition, but the 3-MHz micropulse repetition rate and the planned bunch-by-bunch RF beam position monitor (BPM) system provide a unique opportunity for beam-based investigations in the USA. With a single 8-cavity cryomodule installed and a high-resolution electron spectrometer available at the terminal end (100-300 MeV), it would seem quite possible to make beam-based measurements of the relative electron energy per bunch, over a bunch train of 1 ms or less, as a function of the bunch spacing (0.3-10  $\mu$ s) and the bunch charge (0.1-1 nC), and for comparison to calculated long-range wakefields over a single cryomodule. Two BPMs are already planned before and after the downstream dipole to provide both entrance and exit angle of the beam for accurate relative energy measurements at up to the 3-MHz rate. Using the first bunch in the train as a reference, the other bunches (up to 3000) will be measured using the BPM in the spectrometer bend plane. The relative electron energy per bunch is recorded by normalizing the measured beam position,  $x$ , to the spectrometer dispersion,  $\eta_x$ . A BPM resolution of 20  $\mu$ m and a dispersion function of 0.4 m (example) allows a possible resolution of 0.005%. A more detailed layout drawing of ASTA (Stage-I) is shown in Fig. 2, indicating the locations of a bunch compressor and 3.9-GHz RF linearizer cavity as well.

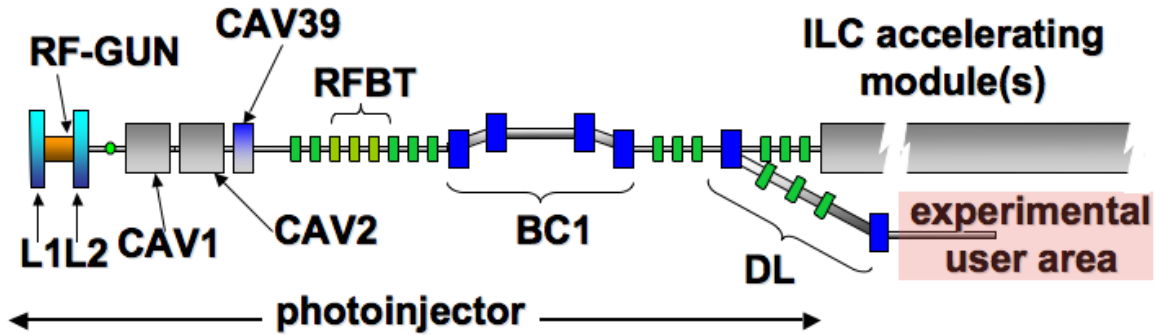


Figure 2: The layout used to measure wakefields, where the spectrometer after the “ILC accelerating module” is not shown here.

### 7.3.13.3 RF-Based Measurements

While the beam-based measurements described in the previous section can map the net effect of long-range wakefields on the beam, it is useful to directly monitor the fields excited in the corresponding higher order modes (HOMs) in the cavities themselves. This can be done using the two existing HOM coupling ports available per cavity and instrumenting them to observe the beam-induced signals in both time and frequency domain. Detailed characterization has been done on the cavities at FLASH [1].

In the study at FLASH, the authors developed a sophisticated technique for identifying the HOMs. For the dipole HOMs, they were able to use beam signals as beam position monitors and measure the alignment of individual cells within the cavity. They were also able to observe the monopole HOMs and proposed a technique to measure the relative beam phase with respect to the accelerating phase. A schematic of the electronics layout for recording the HOM signals is shown in Fig. 3 along with an example concatenated signal from the up and downstream HOM couplers. Another example measurement shown in Fig. 4 is the frequency spectrum of the monopole HOMs.

The resolution of the FLASH study was limited by the sensitivity of the charge measurement used for normalization of the signal and the phase of the local oscillator in the electronics. With use of a higher sensitivity charge measurement and better electronics, we propose to improve on this technique and use the measurement to correlate beam induced signals with the beam effects described in the previous section.

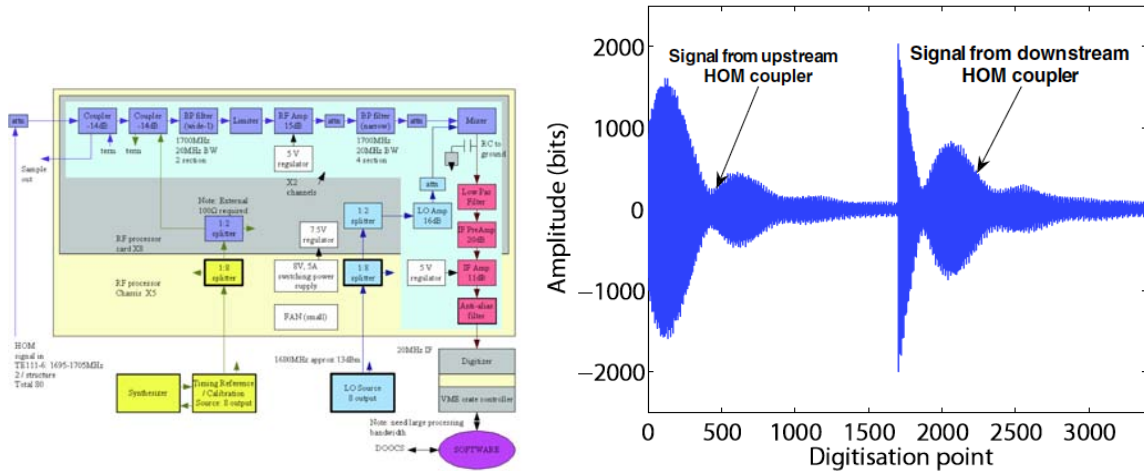


Figure 3: Left) Detailed layout of electronics for recording beam-induced signals in the FLASH HOM couplers. Right) Example signal of concatenated signal from up and downstream HOM couplers.

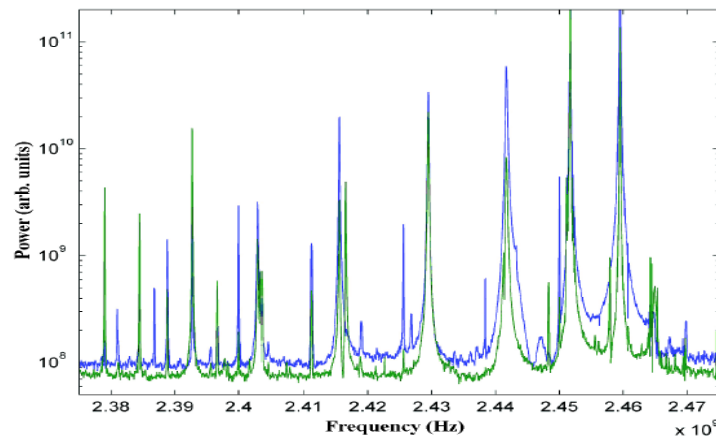


Figure 4: Frequency spectra of monopole HOMs measured on the up and downstream HOM couplers.

### 7.3.13.4 Summary

In summary, the transit of the ASTA 1-ms pulse train through a full 8-cavity cryomodule provides a unique opportunity for investigating beam dynamics effects such as long-range wakefields as a function of micropulse charge and temporal spacing that may impact beam stability in future systems. Elucidation of the effects and understanding their bounds should play a critical role in final design efforts.

### 7.3.13.5 References

[1] Molloy, et al. Phys. Rev. ST Accel. Beams **9**, 112802 (2006)].

### 7.3.14 Flat-Beam-Driven Dielectric-Wakefield Acceleration in Slab Structures

The availability of flat beams with high-repetition rate unique to ASTA would enable the testing of multi-bunch acceleration in dielectric-wakefield structures and the studying of possible dynamical effects. In the longer term, the inclusion of a transverse-to longitudinal phase space exchanger will add the capability to explore acceleration with enhanced transformer ratio.

Next generation multi-TeV high-energy-physics lepton accelerators are likely to be based on non-conventional acceleration techniques given the limitation of radio-frequency (rf) normal- and superconducting cavities. Non-conventional approaches based on the laser-plasma wakefield accelerators have recently demonstrated average energy gradients one order of magnitude higher than those possible with state-of-the-art conventional structures [1]. Another class of non-conventional accelerating techniques includes beam-driven methods which rely on using wakefields produced by high charge “drive” bunches traversing a high-impedance structure to accelerate subsequent “witness” bunches [2]; see Figure 1. Such an approach has the advantage of circumventing the use of an external power source and can therefore operate at mm and sub-mm wavelengths. Structures capable of supporting wakefield generation include plasmas [3], and dielectric-loaded waveguides (DLW's) [4].

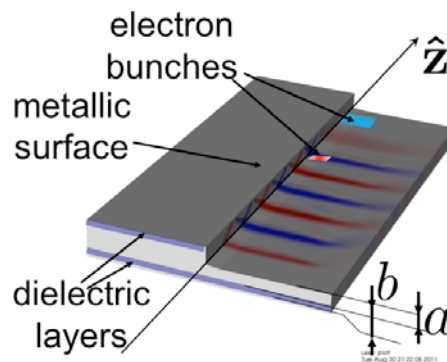


Figure 1: Configuration for beam-driven dielectric-wakefield acceleration in a slab dielectric-lined waveguide (DLW). The electron bunches include the drive (cyan) and witness (red) bunches. The darker red and blue field patterns represent the axial electric field in the structure's mid-plane.

The proposal aims at testing asymmetric dielectric-loaded waveguides driven by flat beams with high-transverse emittance ratios. ASTA's capability to generate long bunch train will be used to explore limitations associated to the acceleration of bunch trains in DLW structures. Finally, at a later stage, the bunch-current tailoring capabilities of ASTA will also be used to demonstrate high-gradient acceleration with an enhanced transformer ratio.

### 7.3.14.1 Past and current researches on dielectric-wakefield acceleration and opportunities at ASTA

Dielectrics can in principle sustain significantly higher electric surface fields. For example, in the case of fused silica tubes the onset for breakdown was observed when peak fields at the surface of the material reached approximately 13 GV/m [5]. Based on these observations it is tempting to replace the standard RF cavities with dielectric structures that can sustain much higher field gradients. Work on dielectric-lined waveguide (DLW) structures has been pioneered at Argonne in the late 80's [6].

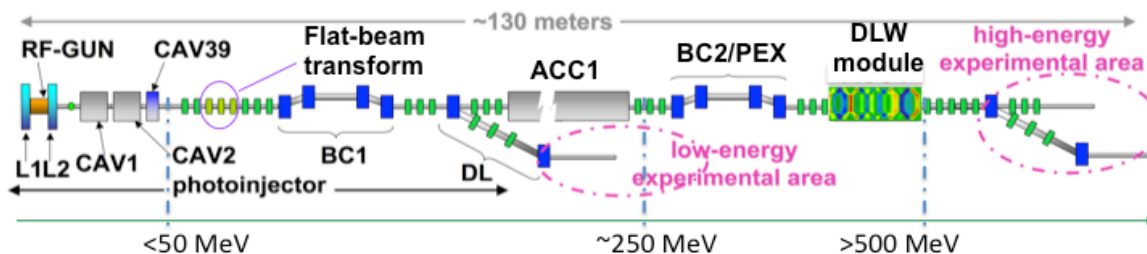


Figure 2: Overview of the ASTA facility with DLW module discussed in Ref. [10]. The beam energy could be boosted from 250 to 500 MeV and eventually from 500 MeV to 1 GeV. BC2/PEX represents an additional beamline insertion that could serve as a second-stage bunch compressor or phase space exchanger.

Until recently most of the work has been focused on cylindrical DLWs. Another class structure, the slab DLW (see Fig. 1), have been proposed as better candidates for acceleration as they offer better stability, tunability and are easier to manufacture [7,8]. Because of the high transverse asymmetry of the structures, flat drive bunches that will be readily available at ASTA are better match to fully exploit the advantages of DLWs. In addition dynamical effects related to multi-bunch effects could be investigated because of available beam format unique to superconducting linacs. To date, and very recently, only preliminary studies on slab DLWs have been carried using round beams [9]. The ability to also investigate the performance of DLW for multi-bunch acceleration would possibly provide a demonstration of a multi-user short-wavelength-FEL concept recently proposed [11]. A successful completion of a proof-of-principle experiment demonstrating acceleration in a DLW, could also form the basis of future energy upgrades of ASTA that could eventually support some of the experiments demanding beam energies around 1 GeV [10] using an implementation similar to the one detailed in Ref. [11] as outlined in Fig. 2. Finally, the experimental techniques developed for this experiment will be beneficial to other beam-driven acceleration concepts that might be tested at ASTA (e.g. plasma wakefield acceleration). This proposal builds on R&D being performed at Northern Illinois University under financial support from the Defense Threat Reduction Agency along with past or on-going collaborations between Northern Illinois University and the Argonne Wakefield Accelerator, Euclid Lab LLC, DESY, Tech X and the University of Hamburg.

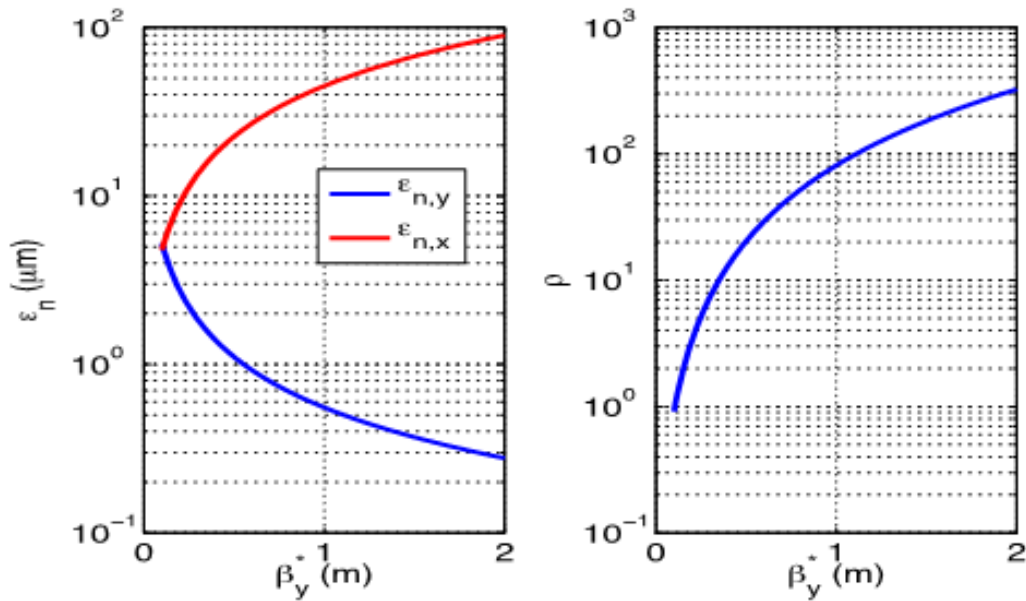


Figure 3: Required beam's transverse normalized emittances (left) and corresponding emittance ratio (right) as a function of the achieved minimum betatron function inside the DLW. The DLW's length and half-gap are respectively  $L=5$  cm and  $a=100$   $\mu\text{m}$ .

### 7.3.14.2 Technical Approach

An issue associated to the use of cylindrical-symmetric DLW structures stems from the requirement on beam parameters and especially on the beam emittances. Given the DLW structure's inner radius  $a$  and axial length  $L$ , the bunch normalized emittance has to satisfy

$$\varepsilon_{n,\perp} \leq \frac{4\gamma\beta^* a^2}{9(4\beta^{*2} + L^2)},$$

where  $\beta^*$  is the betatron function at the waist (located at the structure's center) and  $\gamma$  the beam's Lorentz factor. The latter requirement is very stringent especially for moderate values of  $\gamma$ . For instance, considering acceleration through one cryomodule  $\gamma \approx 500$ , and taking  $\beta^* = 0.1\text{m}$ ,  $a=100$   $\mu\text{m}$  and  $L=5$  cm would require a transverse emittance of 0.5 mm. Such an emittance is challenging to achieve for bunch charge larger than 1 nC. Therefore the flat beam technique developed at Fermilab combined with a slab DLW structure appear to be a viable path toward to generation of high-gradient electric field.

The previous equation sets a requirement for the normalized vertical emittance (assume to the smallest of the flat beam emittance)

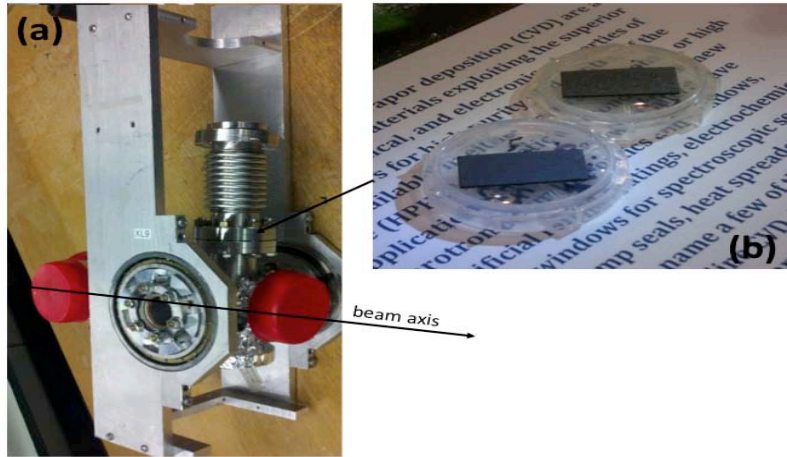


Figure 4: Assembled goniometer (a) and diamond slab structures (b) to be used in the proposed DWFA experiment. Photo (b) is courtesy of Euclid Lab LLC.

$$\varepsilon_{n,y} \leq \frac{4\gamma\beta_y^* a^2}{9(4\beta_y^{*2} + L^2)},$$

with  $a$  now being the half-gap size of the structure and the subscript  $y$  indicates the value are associated to the vertical degree of freedom. The product of the two transverse emittances is related to the four-dimensional emittance via

$$\varepsilon_{n,x} \varepsilon_{n,y} = \varepsilon_{n,4D} \equiv \sqrt{|\langle X\tilde{X} \rangle|},$$

where  $X = (x, x', y, y')$ , so that  $\langle X\tilde{X} \rangle$  refers to the four-dimensional transverse beam matrix (the absolute-value sign indicates the determinant operator). Furthermore, we can write  $\varepsilon_{n,4D} \equiv \varepsilon_{n,\perp}^2$ . In the round-to-flat beam transformation transverse emittances with ratio  $\rho \equiv \varepsilon_{n,x} / \varepsilon_{n,y} > 1$  are produced which implies that the horizontal emittance has to fulfill the inequality

$$\varepsilon_{n,x} \geq \frac{9\varepsilon_{n,\perp}^2 (4\beta_y^{*2} + L^2)}{4\gamma\beta_y^* a^2},$$

to be consistent with the requirement on  $\varepsilon_{n,y}$ . Finally, the minimum horizontal beam size inside the DLW structure is  $\sigma_x = \sqrt{\beta_x^* \varepsilon_{n,x}}$  where  $\beta_x^*$  refers to the horizontal betatron function. At ASTA we intend to take full advantage of the beam manipulations method that will be integrated in the facility.

The flat-beam method discussed in Section 5.5.2 (Advanced Phase Space Manipulations) of this proposal can be used to tailor the beam emittances such as to match the aforementioned requirements [12]. Recent simulations have shown that a 3.2-nC bunch can have its transverse emittances partitioned to  $(\epsilon_{n,x}, \epsilon_{n,y}) \approx (0.5, 50) \mu\text{m}$  consistent with typical optimized round-beam emittances of  $\epsilon_{n,\perp} \approx 5 \mu\text{m}$  [13]. The latter emittance partition with achievable minimum betatron functions of approximately 0.5 m would result in rms spot sizes of  $(\epsilon_{n,x}, \epsilon_{n,y}) = (0.5, 50) \mu\text{m}$  at 250 MeV ( $\gamma \approx 500$ ). These beam sizes are compatible with a structure's half-gap value of  $a = 100 \mu\text{m}$  which is necessary to produce THz wakefields as depicted in Fig. 2.

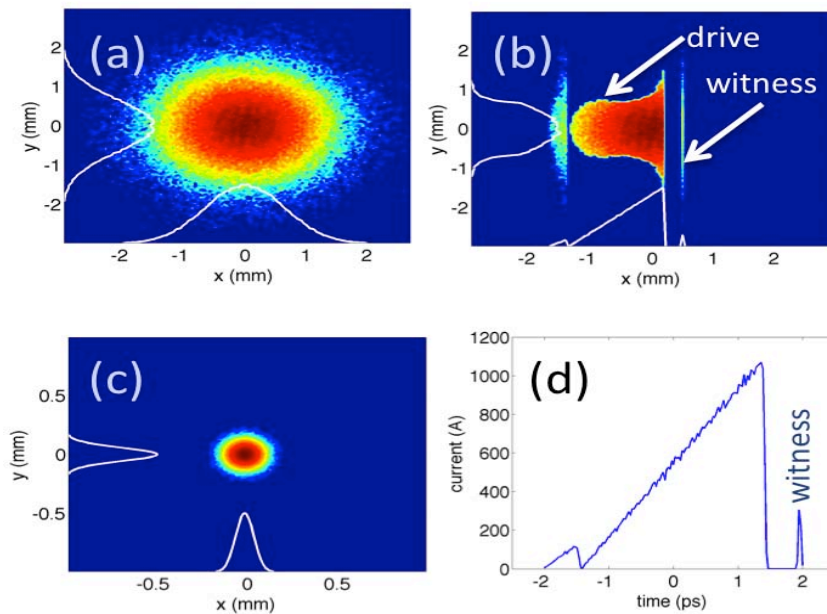


Figure 5. Double-triangular bunch generation using an EEX-based bunch shaper, where the transverse mask is tailored to generate a double-triangular bunch [“drive” in (b)] followed by a low-charge main bunch [“witness” in (b) and (d)]. (a) and (b) show the transverse beam density before and after the mask, respectively. (c)-(d) plot the beam density at the EEX exit, with (c) the transverse profile and (d) the current profile (positive time corresponds to the tail of the bunch). (from Ref. [11]). The advantages of the double-triangle distribution are detailed in Ref. [15].

Another important element to beam driven-acceleration would be the tailoring of the electron bunch's current profile. Several avenues are currently being explored to perform such bunch-shaping technique. One of them directly builds on the use of a transverse-to-longitudinal phase-space-exchange technique pioneered at Fermilab's A0 photoinjector. As discussed in Ref. [14] and depicted in Fig. 5 such a phase space exchanger could be used to tailor the profile of the

drive bunch and create a low-charge witness bunch. Other methods based the impression of nonlinear longitudinal-phase-space correlation [16] are also under investigation.

### **7.3.14.3 Experimental plans**

We expect this proposal to be carried in several stages with requirements on beam parameters consistent with the incremental upgrade of ASTA. The experimental test of dielectric structure is in itself straightforward and most of the work will be related to shaping the beam to match the desired requirements. The following four-phase approach is proposed:

#### Phase I: 50-MeV flat beams:

The goal of this phase would be to demonstrate the propagation of a 50-MeV flat beam in a slab DLW structure. The structure would be located behind the bunch compressor (BC1 in the photoinjector) or in the off-axis low-energy user line. A downstream spectrometer would enable the measurement of energy loss and self modulation (as the bunch would be longer than the wavelength of the mode supported by the DLW). The bunch charge would be varied. The structure would be located in a goniometer currently being assembled and to be tested at the HBESL facility in support to another experiment. The assembly is pictorially shown in Fig. 4.

#### Phase II: 50-MeV tailored flat beams:

The goal of this phase would be to demonstrate some acceleration using a compressed flat beam with a tailored temporal profile using a method similar to Ref. [16] (but here the nonlinearities will be introduced using another, simpler, method rather than using a 3.9-GHz cavity [17]). In this phase the photocathode would be split to provide a high-charge (1-2 nC) drive bunch followed by a low charge (<100 pC) witness bunch and acceleration of the witness bunch would be explored; see Fig. 6.

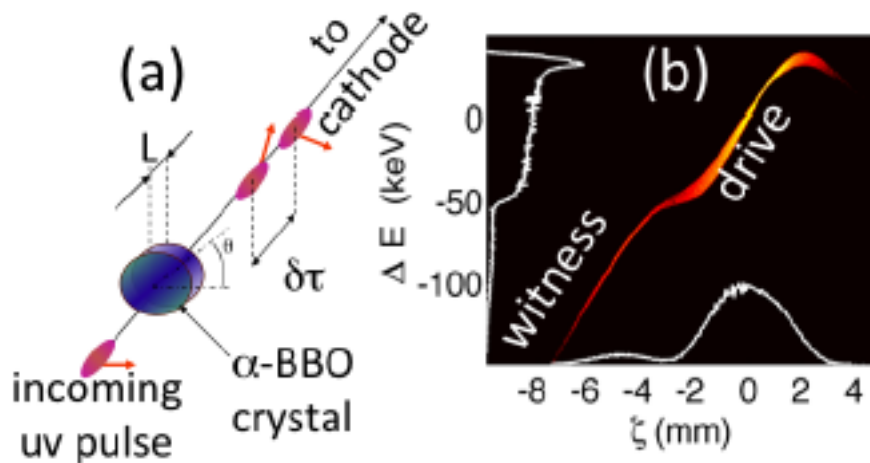


Figure 6. Photocathode drive-laser manipulation scheme to produce drive-witness bunch set (a): an alpha-BBO crystal is used to split the incoming ultra-violet photocathode laser pulse into two pulses. Corresponding simulated electron beam longitudinal phase space downstream of the RF gun (from Ref. [18]).

#### Phase III: High-energy tailored flat beam:

Upon completion of Phase II and pending the availability of a higher energy at ASTA, the tailored flat beam would be accelerated to high energy (250 or 500 MeV depending on the ASTA configuration) and a similar experiment as described in Phase II would be performed. The higher energy would enable smaller transverse beam sizes and small structure apertures (thus higher accelerating fields).

#### Phase IV: A DWFA-module as an energy doubler for ASTA:

Pending on favorable outcome of Phase III, a DLW-based accelerating module would be designed and implemented in ASTA to substantially boost the beam energy. In this configuration we could accelerate a 10-100 pC electron bunch to 1 GeV. Details of the modules would depend on the lessons learned from Phase III.

#### **7.3.14.4 References**

- [1] W. Leemans et al., *Nature Physics* **2**, 699 (2006).
- [2] G. A. Voss and T. Weiland, "Particle Acceleration by Wake Field", DESY report M-82-10, April 1982; W. Bialowons et al., "Computer Simulations of the wakefield transformer experiment at DESY", Proceedings of the 1988 European Particle Accelerator Conference (EPAC 1988), Rome, Italy, 902 (1988).
- [3] I. Blumenfeld et al., *Nature* **445**, 741 (2007).

- [4] M. Rosing, and W. Gai, Phys. Rev. D **42**, 1829 (1990).
- [5] M. C. Thompson, et al., Phys. Rev. Lett., **100**, 214801 (2008).
- [6] W. Gai, et al., Phys. Rev. Lett., **61**, 2756 (1988).
- [7] A. Tremaine, J. Rosenzweig, and P. Schoessow, Phys. Rev. E **56**, No. 6, 7204 (1997).
- [8] D. Mihalcea, P. Piot, P. Stoltz, Phys. Rev ST Accel. Beams **15**, 081304 (2012).
- [9] S. Antipov, C. Jing, A. Kanareykin, V. Yakimenko, M. Fedurin, K. Kusche, W. Gai, Appl. Phys. Lett. **100**, 132910 (2012)
- [10] P. Piot, F. Lemery, C. Prokop, D. Mihalcea, Y.-E Sun, "A DLW-based energy-doubling module for the Advanced Superconducting Test Accelerator at Fermilab", in preparation (2012).
- [11] C. Jing, P. Schoessow, A. Kanareykin, J.G. Power, R.R. Lindberg, A. Zholents, P. Piot, "A compact soft X-ray free-electron laser facility based on dielectric wakefield accelerator", ANL/APS/LS-332 (2012).
- [12] P. Piot, Y.-E Sun and K.-J Kim, Phys. Rev ST Accel. Beams **9** 031001 (2006).
- [13] P. Piot, Y.-E Sun and M. Church, Proceedings of the 2010 International Particle Accelerator Conference (IPAC10), Kyoto, Japan, (23-28 May 2010), 4316 (2010).
- [14] P. Piot, Y.-E Sun, M. Rihaoui, and J. G. Power, Phys. Rev ST Accel. Beams **14** 022801 (2011).
- [15] B. Jiang, et al, Phys. Rev ST Accel. Beams, **15**, 011301 (2012).
- [16] P. Piot, C. Behrens, C. Gerth, M. Dohlus, F. Lemery, D. Mihalcea, P. Stoltz, M. Vogt, Phys. Rev. Lett. **108**, 034801 (2012).
- [17] F. Lemery, P. Piot, in preparation (2012).
- [18] F. Lemery, P. Piot, C. Behrens, D. Mihalcea, C. Palmer, J. Osterhoff, B. Schmidt, P. Stoltz, Proceedings of the 2012 International Accelerator Conference (IPAC12), New Orleans May 20-25, 2012, p. 2166 (2012).

## 8.0 Technical Description of ASTA

### 8.1 Facility Overview

The Advanced Superconducting Test Accelerator [1] is housed in the New Muon Lab (NML) building at Fermilab. It will be capable of testing 3 or more ILC-type SRF cryomodules under full ILC beam intensity and bunch structure. In addition, test beamlines and downstream beamlines will provide a venue for advanced accelerator R&D (AARD). The original NML building had been previously used for a high energy physics experiment, but has recently been repurposed to house ASTA [2]. The original footprint has been extended to accommodate high energy beamlines, a high energy beam dump, and an experimental area for AARD. Figure 1 shows the plan view of the upstream half of the facility, and Figure 2 shows the plan view of the downstream half.

The electron beam is produced by a 1.3 GHz RF photoinjector [3] and then accelerated to 50 MeV by two 1.3 GHz SRF cryomodules, each containing a single 9-cell cavity, before being injected into the 1st 8-cavity cryomodule. Initial beam commissioning of the cryomodule string will take place with a single Tesla type III+ cryomodule [4] driven by a 5 MW klystron. The next stage of commissioning will take place with two Tesla type III+ cryomodules and one ILC type IV cryomodule. The entire string will be driven by a 10 MW multi-beam klystron, with its associated HV power supply, modulator, and waveguide distribution system. The high energy beamlines downstream of the cryomodules will provide transport to an AARD experimental area and to the high energy beam dump.

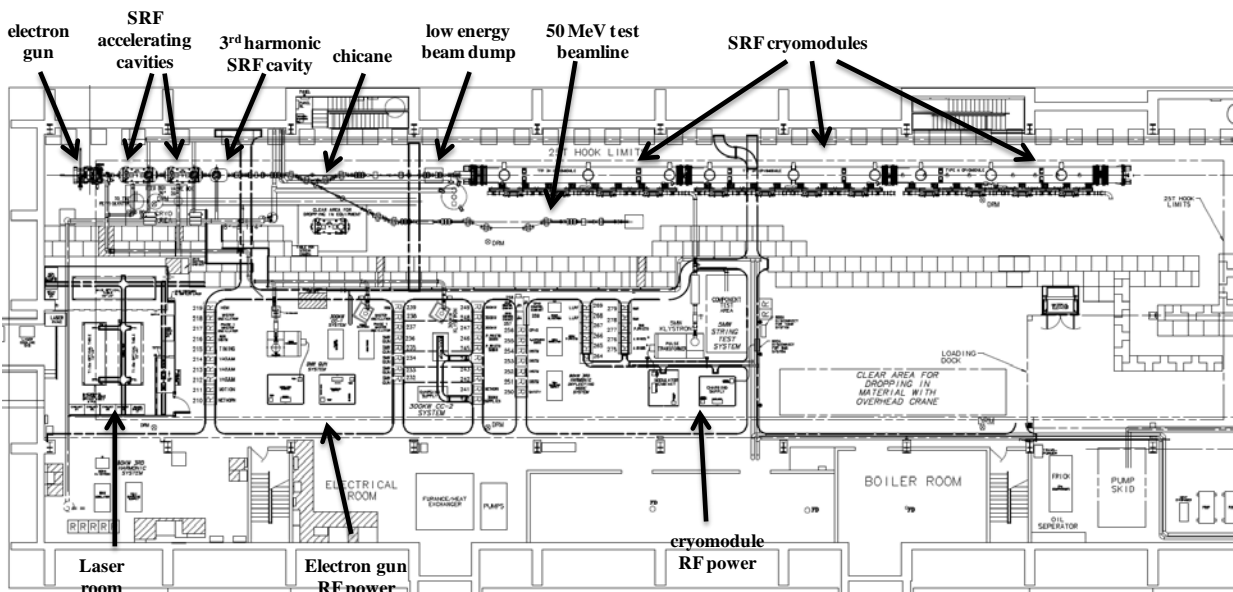


Figure 1: Upstream floor plan of the ASTA photoinjector and 3 SRF cryomodules in the original building footprint. The beamline is 1.2 m above the floor, the floor is 6.1 m below grade, and the building length is 74 m.

The cryogenic plant currently consists of 2 Tevatron-style satellite refrigerators capable of delivering a total of 110 W of 2K helium and does not have the capacity to cool all 3 cryomodules at full beam intensity and at full pulse repetition rate. The Cryomodule Test Facility (CMTF) [3] is currently being built adjacent to NML and will provide the additional capacity to deliver 600 W of 2K helium to NML and cryomodule test stands in CMTF.

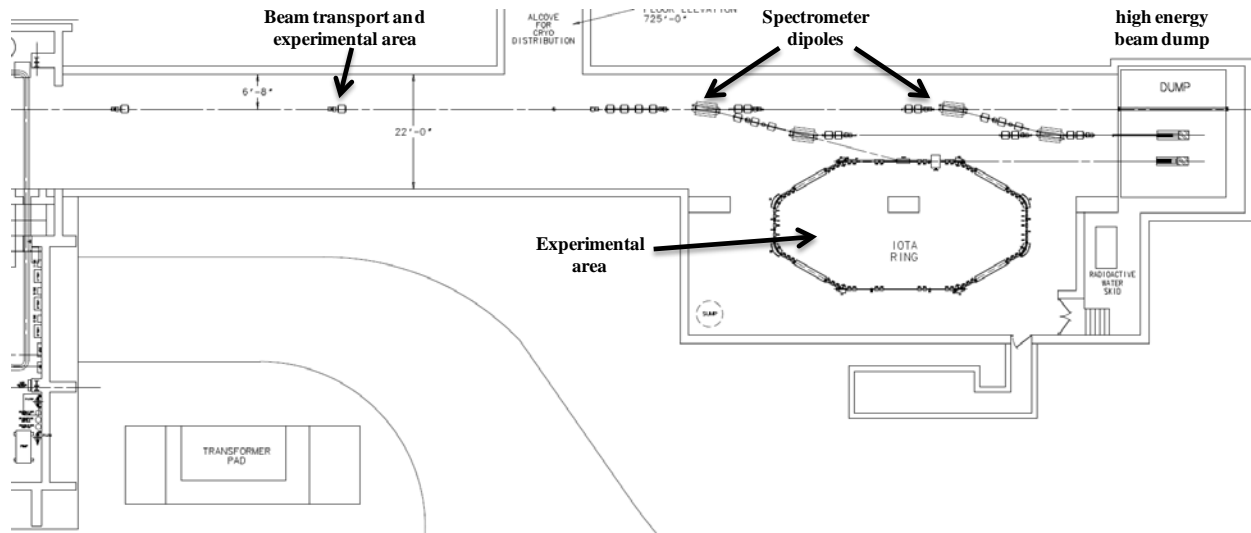


Figure 2: Downstream plan view of the ASTA high energy beamlines and experimental areas in the new underground tunnel. The tunnel extension is 70 m long. A service building is located above the experimental area.

The beam parameters for ASTA will have a wide range, depending on the particular application. Table 1 lists selected beam parameters for ILC-like conditions and the possible range for each parameter. As with all photoinjectors, many beam parameters are coupled, especially to the bunch intensity, because of space charge effects in the electron gun and low energy bunch compressor.

Table 1: Beam parameters for ASTA. The ILC-like parameter values are listed and also the range of each parameter.

| parameter                   | ILC RF unit test | range                      | comments   |
|-----------------------------|------------------|----------------------------|--|
| bunch charge                | 3.2 nC           | 10's of pC to >20 nC       | minimum determined by diagnostic thresholds; maximum determined by cathode QE and laser power            |
| bunch spacing               | 333 nsec         | <10 nsec to 10 sec         | lower laser power at minimum bunch spacing   |
| bunch train length          | 1 msec           | 1 bunch to 1 msec          | maximum limited by modulator and klystron power  |
| bunch train repetition rate | 5 Hz             | 0.1 Hz to 5 Hz             | minimum may be determined by electron gun temperature regulation and other stability considerations      |
| norm. transverse emittance  | ~25 mm-mrad      | <1 mm-mrad to >100 mm-mrad | maximum limited by aperture and beam losses; without bunch compression emittance is ~4 mm-mrad at 3.2 nC |
| RMS bunch length            | 1 ps             | ~10's of fs to ~10's of ps | minimum obtained with Ti:Sa laser; maximum obtained with laser pulse stacking                            |
| peak bunch current          | 3 kA             | > 10 kA (?)                | 3 kA based on CSRTrack simulations with low energy bunch compressor                                      |
| injection energy            | 50 MeV           | 5 MeV to 50 MeV            | may be difficult to transport 5 MeV beam to the dump; maximum determined by booster cavity gradients     |
| high energy                 | 820 MeV          | 50 MeV to 1500 MeV         | radiation shielding issues limit the maximum; 1500 MeV with 6 cryomodules                                |

## 8.2 Injector

### 8.2.1 Electron gun

The RF photocathode electron gun is identical to the guns recently developed at DESY Zeuthen (PITZ) for the FLASH facility [5]. It is a normal-conducting  $1\frac{1}{2}$  cell 1.3 GHz gun operated in  $TM_{010,\pi}$  mode, with a  $Q_L$  of 11,700, and driven by a 5 MW klystron. The power is coupled into the gun via a coaxial RF coupler at the downstream end of the gun. The gun is capable of average DC power dissipation of ~20 kW, and a temperature feedback system will regulate cooling water temperature to better than  $\pm 0.02$  °C for good phase stability. The gun will be routinely operated at peak gradients of 40-45 MV/m, and output beam kinetic energy of ~5 MeV. (For comparison, PITZ has successfully operated an identical gun at 60 MV/m for 700  $\mu$ sec pulse lengths.) The photocathode is a 10 mm diameter molybdenum disk coated with  $Cs_2Te$  with 5 mm diameter photosensitive area. It is illuminated by 263 nm wavelength laser light which is directed onto the photocathode by a 45° off-axis mirror downstream of the RF coupler.

The photocathodes are coated at a separate facility on the Fermilab site, transported under vacuum to the photocathode transfer chamber mounted on the upstream end of the gun, and inserted into the upstream end of the gun via external manipulators, all under vacuum. Several photocathodes have already been prepared and their quantum efficiency measured to be

~10%. The photocathode preparation, transport, and transfer chambers were developed and built by D. Sertore at INFN Milano [6] and commissioned at Fermilab.

For emittance compensation the gun is surrounded by 2 solenoid magnets built by Danfysik. Each magnet has a peak field of 0.28 T at 500 A. Normally the magnet currents are set so the field at the photocathode is 0 in order to minimize the beam emittance, however, the field can be set to > 1kG at the photocathode for the production of angular-momentum dominated beams and flat beam production. ASTRA [7] simulations indicate that transverse normalized emittances of 4  $\mu\text{m}$  can be attained at a bunch charge of 3.2 nC, laser pulse length of 3.2 ps RMS, and peak gun electric field gradient of 40 MV/m. Stretching the laser pulse length will produce smaller transverse beam emittance out of the gun, as will higher gun gradients.

### 8.2.2 Photocathode laser

The photocathode laser system is housed in an enclosed structure adjacent to the beam enclosure. A diagram of the laser system driving the photocathode is show in Figure 3. The seed laser is a Yb-fiber laser acquired from Calmar, Inc. The 1.3 GHz output is reduced to 3 MHz by two pulse pickers, amplified by a multipass and two 2-pass amplifiers and frequency quadrupled by two BBO crystals. The UV pulse is transported to the gun through a vacuum pipe and directed to the photocathode via a 45° off-axis mirror downstream of the gun RF coupler. The UV amplitude is sufficient to produce 10's of nC of bunch charge from the cathode, and the rms (gaussian) pulse length is 3.2 ps. In addition there will be a Ti:Sa laser for short pulse experiments (~150 fs) and laser lab space for other laser R&D efforts.

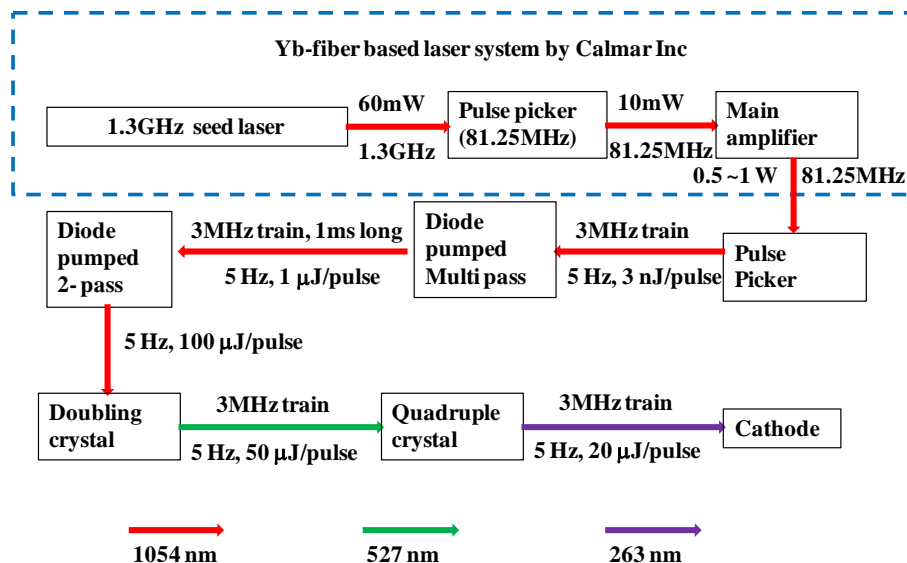


Figure 3: Schematic diagram of the photocathode laser system.

### 8.2.3 Beamline elements

The injector beamline is shown in Figure 4. After a short instrumentation section, the electron gun is followed by two SRF cryomodules to accelerate beam to 50 MeV. Each of these cryomodules contains a 9-cell L-band cavity operating at 1.3 GHz, driven by a 300 kW klystron, and capable of peak accelerating gradients of  $>22$  MV/m [8]. These cavities will also be used to “chirp” the beam, *i.e.*, generate a time-momentum correlation, in preparation for bunch compression in the chicane. Downstream of these cavities is space allotted for a future SRF 3.9 GHz cavity intended to be used for bunch linearization.

The SRF cavities are followed by a quadrupole doublet to control the beam size for the emittance measurement, 3 skew quads to generate flat beam, a matching section into the chicane, a 4-dipole chicane for bunch compression ( $R_{56} = -0.18$  m), a matching section into the vertically downward-bending dipole to the low energy beam dump, and finally a matching section into the first 8-cavity cryomodule. The  $22.5^\circ$  dipole upstream of the dump will serve as the low energy spectrometer. The 50 MeV beam dump will be capable of absorbing up to 400 W of beam power, which is 15% of the full ILC intensity [9]. In addition, there is a dogleg to deliver 50 MeV beam to a test beam area parallel to the 1<sup>st</sup> cryomodule. This test area is intended for AARD experiments which utilize low-energy beam.

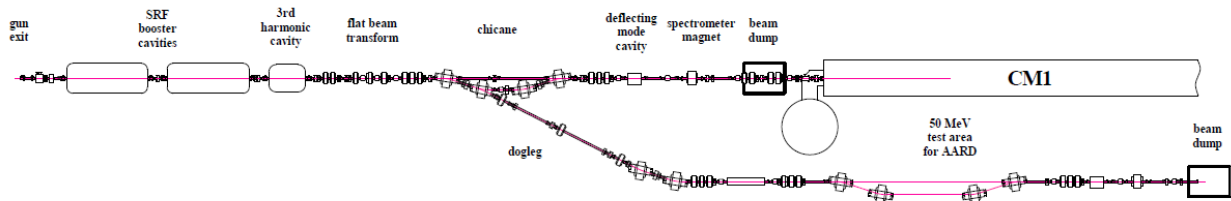


Figure 4: Injector layout.

### 8.2.4 Diagnostics

There are four primary types of diagnostics in both the injector and the high energy beamlines: BPM's to measure beam position, profile monitors to measure beam size, resistive wall monitors to measure beam current (4 in the primary injector beamline), and loss monitors ( $\sim 40$  total) to measure beam losses and serve as the primary protection element in the machine protection system.

Each BPM is a 4-button pickup measuring both X and Y position. The system will be capable of bunch-by-bunch measurements, and the anticipated accuracy is  $<25$   $\mu\text{m}$ . There will be 23 BPM's in the primary injector beamline. Signals from HOM absorbers in the cryomodules can also be used for beam position monitoring.

The profile monitors are located in 6-way vacuum crosses and were fabricated by Radiabeam Technologies. A prototype was tested at the Fermilab A0 photoinjector [10] and a resolution of

< 20  $\mu\text{m}$  has been obtained. They each contain a Ce-doped 100  $\mu\text{m}$  crystalline yttrium aluminum garnet (YAG) screen or a 100  $\mu\text{m}$  crystalline lutetium-yttrium oxyorthosilicate (LYSO) screen, a 1  $\mu\text{m}$  Al screen for OTR production, and a target screen for calibration. The screens are at right angles to the beam and are followed by a 45° mirror to deflect optical light to an optical channel and a 5 megapixel camera. There will be 12 profile monitors in the primary injector beamline. Wire scanners may be installed at a later date.

In the injector beamline, transverse emittance will be measured by the “slits method” both upstream and downstream of the chicane. Beam energy will be measured by the 22.5° spectrometer magnet. Bunch length will be measured by streak camera and interferometer both upstream and downstream of the chicane.

A 3.9 GHz 5-cell deflecting mode RF cavity will be installed upstream of the low energy spectrometer magnet for measuring the longitudinal phase space of the beam. This cavity is normal-conducting and is operated at 80 °K. It has been in operation at the A0 photoinjector for several years now.

## **8.3 Cryomodules**

### **8.3.1 Description**

Figure 5 is a photograph of a single TTF type III+ cryomodule installed at ASTA. It is driven by a single 1.3 GHz 5 MW klystron, and RF power is distributed to the eight separate cavities by variable tap-offs (VTO) in the waveguide structure alongside the cryomodule. Each cryomodule consists of a string of eight 9-cell superconducting cavities. In addition, some cryomodules will contain a superconducting quadrupole doublet package, corrector package and BPM. The goal for these cavities is to reach an operational gradient of 31.5 MV/m at 2 °K under full ILC beam conditions. This will yield a total acceleration of 250 MeV per cryomodule. The length of a single cryomodule is 11.9 m, but the cold interfaces, HOM absorbers, and warm gate valves add an additional 1.7 m in length to each end.



Figure 5: Photograph of cryomodule I installed in the ASTA beamline enclosure. View is looking downstream. Waveguide distribution structure is on the right of the cryomodule.

### 8.3.2 Initial operation

The first TESLA Type III 8-cavity cryomodule, CM-1, was installed and operated in NML for approximately 15 months ending in March 2012. CM-1 came to Fermilab as a 'kit' and was assembled at Fermilab by the technical staff here with assistance from colleagues from DESY and LASA/INFN, Milano. Commissioning and testing followed the standard protocol developed worldwide for bringing cryomodules into full operation. The steps include:

- RF Cable Calibration
- Technical Sensor/Interlock Check
- RF/Waveguide Check
- Warm Coupler Conditioning (off resonance)
- Cooldown to 2 °K
- Frequency spectra measurements
- Cavity Tuning to 1.300 GHz via motorized slow tuner
- $Q_L$  adjustment to 3.0E6
- LLRF calibrations
- Cold Coupler Conditioning (on resonance)
- Performance Evaluation including
  - Maximum gradient
  - Dynamic Heat Load ( $Q_0$  vs.  $E_{ACC}$ )
  - Dark Current and Field Emission (X-rays vs.  $E_{ACC}$ )

CM-1 was installed into its final position and aligned in January 2010 and final RF, cryogenics and vacuum connections were made thereafter. Warm off-resonance conditioning was

performed with a single cavity at a time connected to the output of the 5 MW klystron and took anywhere from 2 weeks for the first cavity to 4 days to complete. Once all eight couplers were conditioned final vacuum work was completed leading to initiation of cool down to 2 °K. CM-1 first reached operating temperature on 22 November 2010.

Continuing with the sequence of commissioning steps, each cavity was then powered on resonance to complete coupler conditioning and determine cavity performance limitations. Again each cavity was powered singly. All cavities were characterized by June 11, as shown in Table 2.

Table 2: CM-1 individual cavity performance characteristics.

| Cavity | Peak $E_{acc}$ (MV/m) | Estimated maximum $Q_0$ (E09) | Limitation/Comments   |
|--------|-----------------------|-------------------------------|---|
| 1/Z89  | 20.2                  | 11                            | 'soft' quench/heat load                                     |
| 2/AC75 | 22.5                  | 12                            | Quench  |
| 3/AC73 | 23.2                  | 0.43                          | 'soft' quench/heat load                                     |
| 4/Z106 | 24*                   | 2.3                           | *RF-limited   |
| 5/Z107 | 28.2                  | 39                            | Quench  |
| 6/Z98  | 24.5                  | 5.1                           | Quench  |
| 7/Z91  | 22.3                  | 4.7                           | 'soft' quench/heat load                                     |
| 8/S33  | 25                    | 18                            | Resonant frequency at 1300.240 MHz; tuner motor malfunction |

Full module testing was initiated on 6 July 2011. The waveguide distribution circuit was provided by SLAC and allows independent amplitude and phase control of adjacent pairs of cavities. VTO's were set based upon the gradient limits identified during cavity characterization. The bulk of the time spent powering the entire module was devoted to Low Level RF (LLRF) optimization and refining the Lorentz Force Detuning Compensation system. By the end of the run it was possible to control the RF amplitude and phase over 50 pulses to an RMS magnitude error of  $6.0 \times 10^{-3}$  % and RMS phase error of  $0.005^\circ$ . (The ILC specification for phase stability is  $0.25^\circ$ .) Much progress was made in developing a scheme to counteract the effects of Lorentz Force Detuning. An adaptive algorithm was deployed and improved which permits pulse to pulse correction.

## 8.4 High energy beamlines

### 8.4.1 Beamline elements

The beam will be initially transported from the cryomodule string to the first high energy spectrometer magnet by a 4-quad matching section, a 4-quad FODO lattice, and an additional 4 quad matching section. This region of beamline is 45 m in length and is intended to house future AARD experiments, so it will be reconfigured from time to time to accommodate new experiments. The high energy beamlines downstream of this section are shown in Figure 6. There are 2 dispersion-cancelling doglegs which allow for two 10 m sections reserved for AARD experiments. The final 2 quads in the beamline are to be used to blow up the beam size to avoid damage to the beam dump core. A slow beam sweeping system is used for both the high energy and low energy dumps in order to distribute the beam power over the dump core.

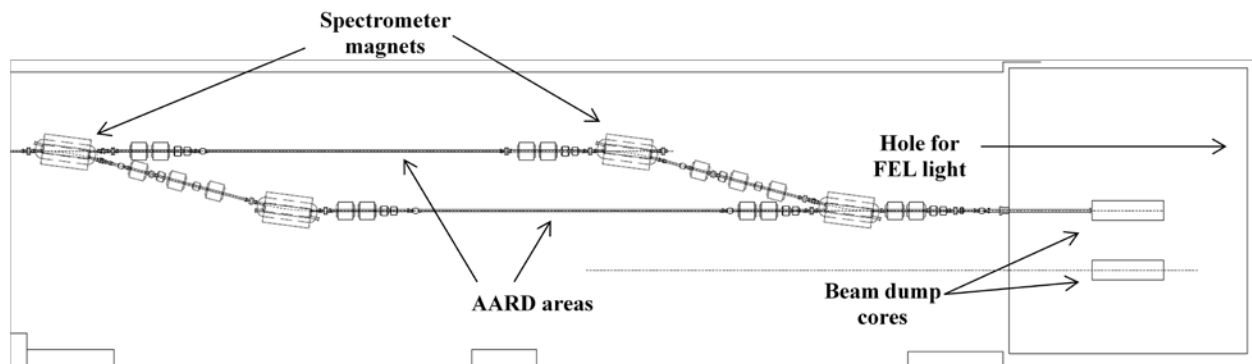


Figure 6: High energy beamline experimental area and beam dumps.

### 8.4.2 Diagnostics

Diagnostics in the high energy beamlines are identical to diagnostics in the injector beamline. There will be 27 BPM's, 9 profile monitors, 2 resistive wall monitors, and ~20 loss monitors in the initial configuration. The "quad scan" method will be used for transverse emittance measurements, and energy measurements can be made at two of the 15° dipole magnets.

### 8.4.3 Beam dump

The high energy beam dump [11] consists of stacked graphite cores, surrounded by water cooled Al in thermal contact with the graphite, surrounded by steel, backed by a copper plug, all embedded in a 6.1 m x 6.2 m x 7.5 m concrete stack. Each graphite core is surrounded by an inert gas (argon) to prevent oxidation at elevated temperatures. There are two graphite cores within the beam dump, and a third core has been left out to allow FEL light (or beam) to pass through the dump in the straight-through beamline. Each beam dump core is designed to handle 80 KW of beam power at beam energies up to 1500 MeV. The beam vacuum window consists of a 7 mm thick graphite disk enclosed by two 1 mm thick TZM disks (titanium, molybdenum, zirconium alloy).

## 8.5 Beam dynamics calculations and simulations

Extensive lattice calculations and beam simulations have been performed to validate the ASTA beamline design under a wide range of beam parameters and configurations [12][13]. ASTRA [7] is used to simulate beam to the downstream end of the 2<sup>nd</sup> acceleration cavity (8.2 m from the photocathode); Elegant [14] is used to calculate single particle (low intensity) beam dynamics from 8.2 m to the high energy dump; Impact-Z [15] or CSRTrack [16] are used to calculate multiparticle (high intensity) beam dynamics from 8.2 m to the high energy beam dump and includes the effects of space charge and coherent synchrotron radiation. As an example, Figure 7 shows results from typical beam size calculations from Elegant and Impact-Z. As another example, Figure 8 shows an Impact-Z simulation of the effects of low energy bunch compression on longitudinal phase space for varying bunch intensities.

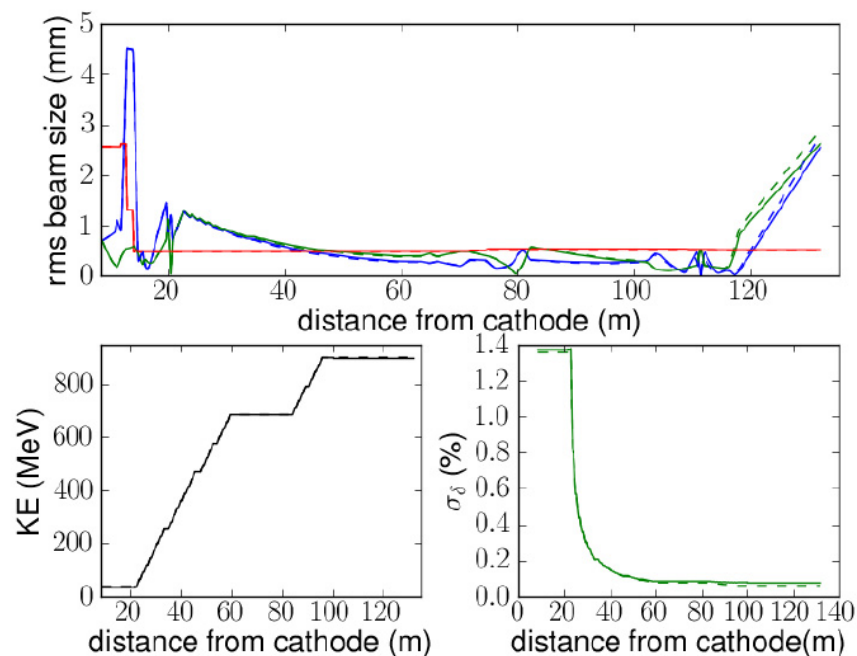


Figure 7: Top plot shows lattice functions from 8.2 m to the high energy dump in the 3-cryomodule configuration followed by a 2<sup>nd</sup> high energy bunch compressor and 4<sup>th</sup> cryomodule. The solid red, blue and green traces in the upper plot correspond, respectively, to the bunch length and horizontal and vertical spot size evolution along the beam line obtained from simulation using IMPACT-Z. The corresponding dashed lines are the same parameters simulated with ELEGANT. The solid and dashed green trace on the bottom right plot shows results from simulation carried out with IMPACT-Z and ELEGANT respectively.

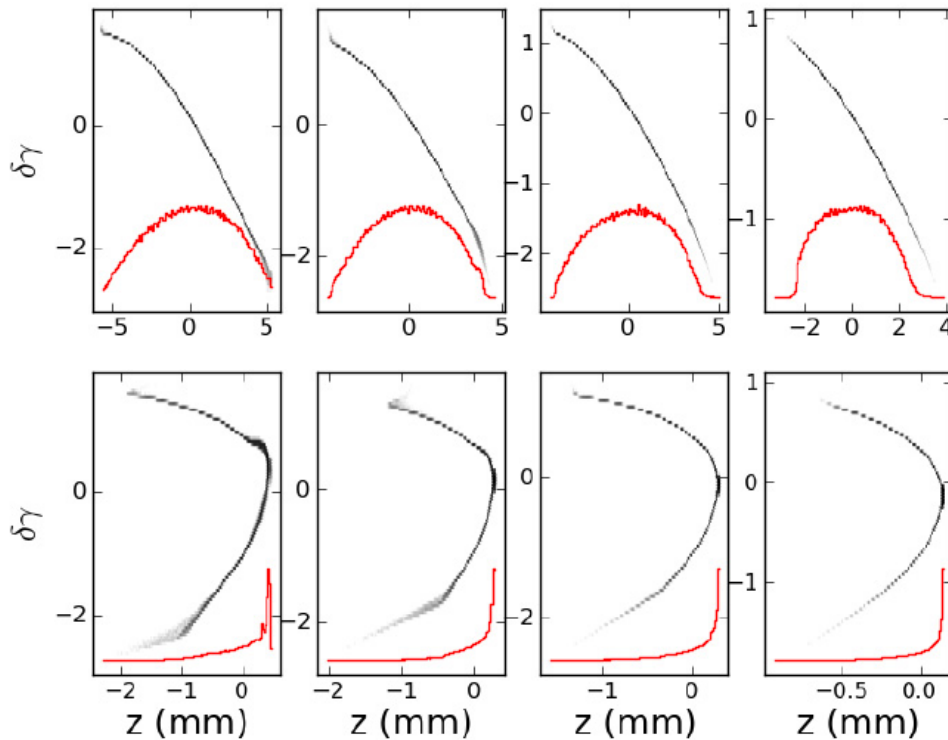


Figure 8: Longitudinal phase space plots, before (top row) and after (bottom row) low energy bunch compression. Columns are (from left to right) 3.2 nC, 1 nC, 0.25 nC, and 0.02 nC. Black trace is longitudinal phase space, and red trace is projection on  $z$  axis. For 3.2 nC, the peak beam current is 3.5 kA. These results are without a 3.9 GHz linearizing cavity.

## 8.6 References

- [1] M. Church, *et al.*, "Design of the Advanced Superconducting Test Accelerator", Fermilab Beams-doc-4212;  
[http://beamdocs.fnal.gov/AD/DocDB/0042/004212/004/ASTA\\_technical\\_description.pdf](http://beamdocs.fnal.gov/AD/DocDB/0042/004212/004/ASTA_technical_description.pdf)
- [2] J. Leibfritz, *et al.*, "Status and Plans for a Superconducting RF Accelerator Test Facility at Fermilab", MOOAC02 in IPAC2012, New Orleans, Louisiana, USA, May 2012;  
<http://www.JACoW.org>
- [3] P. Piot, Y.-E Sun and M. Church, "Beam dynamics simulations of the NML photoinjector at Fermilab", IPAC2010; <http://epaper.kek.jp/IPAC10/papers/thpd020.pdf>
- [4] E. Harms, *et al.*, "RF Test Results from Cryomodule 1 at the Fermilab SRF Beam Test Facility", MOPO013 in 15<sup>th</sup> International Conf. on RF Superconductivity (SRF2011), Chicago, IL, July 2011;  
<http://lss.fnal.gov/archive/2011/conf/fermilab-conf-11-352-ad-td.pdf>

- [5] M. Otevre, *et al.*, "Conditioning of a New Gun at PITZ Equipped with an Upgraded RF Measurement System", WEPB05 in The Proceedings of FEL2010, Malmo, Sweden, Aug. 2010; <http://www.JACoW.org>
- [6] D. Sertore, *et al.*, "Review of the Production Process of TTF and PITZ Photocathodes" MOPB009 in PAC05, Knoxville, TN, May 2005; <http://www.JACoW.org>
- [7] K. Floettman, "ASTRA – A Space Charge Tracking Algorithm", <http://www.desy.de/~mpyflo/>
- [8] J. Branlard, *et al.*, "Capture Cavity II Results at FNAL", WEPMN092 in PAC07, Albuquerque, NM, June 2007; <http://www.JACoW.org>
- [9] C. Baffes, "ASTA Low Energy Beam Dump Thermal Analysis", Fermilab Beams-Doc-4063, Feb. 2012; <https://beamdocs.fnal.gov/AD-public/DocDB/ShowDocument?docid=4063>
- [10] A. Lumpkin, *et al.*, "Initial Beam-profiling Tests with the NML Prototype Station at the Fermilab A0 Photoinjector", MOP219 in PAC11, New York, NY, Dec. 2011; <http://www.JACoW.org>
- [11] C. Baffes, "NML High Energy Beam Absorbers and Dump: Overview Talk", Fermilab beams-doc-3928, Oct. 2011; <http://beamdocs.fnal.gov/ADpublic/DocDB/ShowDocument?docid=3928>
- [12] C. Prokop, *et al.*, "Start-to-end Beam Dynamics Simulations for the SRF Accelerator Test Facility at Fermilab", WEP036 in NA-PAC'11, New York, NY, March 2011; <http://www.JACoW.org>
- [13] C. Prokop, *et al.*, "High energy Lattice for First-beam Operation of the SRF Test Accelerator at NML", Fermilab-TM-2516-APC, March 2012; <http://lss.fnal.gov/archive/test-tm/2000/fermilab-tm-2516-apc.shtml>
- [14] "Elegant – Electron Generation and Tracking", [http://www.aps.anl.gov/Accelerator\\_Systems\\_Division/Accelerator\\_Operations\\_Physics/manuals/elegant\\_latest/elegant.html](http://www.aps.anl.gov/Accelerator_Systems_Division/Accelerator_Operations_Physics/manuals/elegant_latest/elegant.html)
- [15] "Impact-Z – Integrated Map and Particle Accelerator Tracking Code", <http://amac.lbl.gov/~jiqiang/IMPACT>
- [16] "CSRTrack Version 1.1 User's Manual" [http://www.desy.de/fel-beam/csctrack/files/CSRTrack\\_User\\_Guide\\_1.100\\_01.pdf](http://www.desy.de/fel-beam/csctrack/files/CSRTrack_User_Guide_1.100_01.pdf)

## **9.0 Accelerator Science Education at ASTA**

Accelerators have taken an increasingly important role in our Society and improving their performances, downsizing their footprints, or reducing their cost will be a long and challenging endeavor that will strongly rely on future generation of accelerator scientists. In addition, the multidisciplinary nature of Accelerator Science makes accelerators ideal platforms for student education over a vast range of topics.

New beam physics issues associated with future accelerators have emerged (single-bunch and multi-bunch collective effects in high brightness electron accelerators, simulations of large emittance beams in heavy ions and/or multi state charge accelerators) and more intricate accelerator physics tools capable of accounting for all these effects are being developed and need to be carefully validated at available facilities. Such models are mandatory to efficiently design and test the performance of these accelerators prior to their construction. Similarly, future accelerators will require the development of precise diagnostics and controls capable of measuring and/or correcting unprecedented beam parameters (sub-micrometer size, femtosecond duration, with high average current). Most of these topics will be explored to some extent at ASTA and could form the basis of research projects for PhD, Masters, or internships.

Interdisciplinary research projects involving the engineering discipline will also be possible at ASTA. Examples that come to mind are fabrication of state-of-the-art accelerator components requiring precision modeling, drafting and manufacturing. RF engineering R&D examples are ubiquitous in accelerator physics. Likewise, novel synchronization techniques and feedback systems will be needed, e.g. to insure that the accelerating fields in the superconducting linear accelerators are very stable.

Over the last decade the number of Educational Institutions that have taken on developing a curriculum in Accelerator Science has increased from a couple to about 10 [1]. None of these Universities currently operates a full-fledged accelerator complex and generally rely on facilities available at National Laboratories to carry most of their experiments. National laboratories have developed programs to foster partnership with Universities. Fermilab was actually the first laboratory to initiate such a selective program, which offers to financially support students to carry-out Accelerator-Science research at Fermilab's facilities [2]. This program – the Joint University - Fermilab Doctoral Program in Accelerator Physics and Technology – has graduated close to 40 students since its initiation in 1987. More than half of the program's graduates have remained in the field of Accelerator Science, and approximately one quarter of them are prominent scientists with leadership positions in national laboratories or universities.

Fermilab also created prestigious fellowships to attract promising scientists to carry-out research in Accelerator Science: the Peoples fellowship [3] was created in 2001 and the Bardeen-Engineering Leadership fellowship [4] was created in 2005. The John Bardeen Engineering Leadership Program is designed to provide entry-level opportunities for outstanding engineering graduates who are interested in working in a cutting edge research

environment. Fermilab provides opportunities in the fields of electrical, electronics, radio frequency systems, power distribution, magnets, RF cavities, mechanical, materials science and cryogenic engineering. The Peoples Fellowship was created at Fermilab with the goal of attracting outstanding accelerator scientists early in their careers, both to enhance Fermilab's capabilities in accelerator science and related technologies, and to train and develop the accelerator scientists and technologists who will carry our field forward in the future. Together these fellowship programs have attracted and trained approximately 20 people within the last decade. Most of these fellows still carry-out research in Accelerator Science.

Finally, Fermilab has also been active in involving younger scientists (undergraduate students) through various summer programs. One of these programs, the Lee Teng Undergraduate Internship in Accelerator Science and Engineering established by Fermilab and Argonne, aims at attracting undergraduate students into the world of particle accelerator physics and technology. The selected students first attend a two-week general accelerator physics class at the summer US particle accelerator school thereby gaining a broad overview of Accelerator Science. They then work on a research project for the following weeks under the supervision of Fermilab and Argonne staff members. ASTA offers the possibility of significantly enhancing the Lee Teng program by incorporating a "hands-on" component to the students' summer research experience, making it a truly unique internship with the potential to attract future accelerator scientists at the critical undergraduate stage.

In addition to these laboratory-driven programs, Fermilab has also welcomed students from University groups carrying out research at Fermilab funded by grants to universities. Examples includes the development of photo-emission laser with University of Rochester, research on flat-beam generation with University of Chicago, or the investigation of beam-driven plasma wakefield acceleration with University of California, Los Angeles.

ASTA will be an excellent platform that could support and enhance the aforementioned education programs and support extramural research engaging students from Universities. Given the breadth of the scientific program described in this proposal, we expect ASTA to provide support for topics of research in Advanced Accelerator R&D, laser science, beam diagnostics and synchronization, accelerator-based light source, superconducting RF system, and Beam Physics. Finally, some of the proposed topics could also foster research beyond Accelerator Science such as the utilization of single-cycle Terahertz pulses for solid-state Physics research or the use of X-rays for developing phase-contrast imaging (with possible spin-off to medical imaging).

ASTA will also offer a unique opportunities for the US Particle Accelerator School [5] sessions and classes. A number of hand-on, practical training laboratory sessions can use the ASTA accelerators – the photoinjector, the SRF cryomodule and the IOTA ring. Among them, those which were very popular in the past US PAS sessions:

- Modern RF systems class
- Beam Instrumentation Lab
- Fundamentals of Accelerator Instrumentation
- Beam Measurements and Diagnostics in Linacs and Rings
- Beam Dynamics Experiments at the IOTA ring
- Beam Measurements, Manipulation and Instrumentation in SRF Linac

Proximity of the Illinois Accelerator Research Center (IARC) will make these classes attractive for the industrialists and technologists.

### **References**

- [1] W. Barletta, S. Chattopadhyay and A. Seryi, "Educating and training accelerator scientists and technologist for tomorrow", arXiv 1203:3065 (2012); available at <http://arxiv.org/pdf/1207.3065.pdf>
- [2] see [http://apc.fnal.gov/programs2/joint\\_university.shtml](http://apc.fnal.gov/programs2/joint_university.shtml)
- [3] see [http://www.fnal.gov/pub/forphysicists/fellowships/john\\_peoples/index.html](http://www.fnal.gov/pub/forphysicists/fellowships/john_peoples/index.html)
- [4] see [http://www.fnal.gov/pub/forphysicists/fellowships/john\\_bardeen/index.html](http://www.fnal.gov/pub/forphysicists/fellowships/john_bardeen/index.html)
- [5] US Particle Accelerator School <http://uspas.fnal.gov/>

## 10.0 Scope, Cost and Schedule

### 10.1 Scope

Construction of the ASTA facility at Fermilab began in 2006. Since that time, a great deal of infrastructure and equipment has been procured, installed and commissioned (Figure 1).



Figure 1: Photograph of ASTA facility in NML Building at Fermilab  
(View is looking upstream with accelerator enclosure on the right)

Many aspects of the facility are fully operational and have been in use for years. In addition, many of the technical components and systems needed to complete the ASTA facility have either already been procured or are in operation, such as:

- The recently constructed tunnel extension (\$4.9M)
- All the concrete blocks required to complete the accelerator enclosure (\$1.3M)
- All the RF power and distribution systems required for the full ASTA accelerator (\$8.0M)
- The cryogenic systems needed for the entire facility (\$16.7M)
- All magnets, power supplies, and vacuum beam tubes for the various beam lines (\$4.1M)
- The high-energy beam absorbers, dump and water cooling system (\$2.0M)

- A fully operational RF gun and injector capable of providing the 50 MeV beam in the low-energy portion of ASTA (expected to be commissioned in 2013) (\$4.4M)
- The (3) cryomodules needed to complete the accelerator portion of ASTA (\$15M)
- The controls system infrastructure, a control room and office space (\$2.6M)
- A fully operational laser room (\$1.3M)
- Electrical, water cooling, HVAC and compressed air systems capable of supporting the entire ASTA facility (\$5.4M)

The completion of ASTA has been broken up into four distinct operational stages.

#### Stage I: Beam through a single cryomodule

Stage I will provide a test area for low-energy (50 MeV) experiments (Section 6, Figures 1 and 4); a high-energy test area (Section 6, Figures 1 and 3) capable of providing (300 MeV) beam; and the IOTA storage ring. The scope of work to complete Stage I will include the following principle components, of which most of the equipment has already been procured:

- Assembly of the cave extension, connecting the existing concrete accelerator enclosure to the newly constructed downstream tunnel extension
- Installation of the low-energy test beamline (magnets, instrumentation, vacuum system, and beam absorber)
- Installation of the high-energy beam transport line (magnets, instrumentation, and vacuum system) from downstream of the first cryomodule to the high-energy beam dump.
- Installation of the IOTA storage ring (magnets, instrumentation, and vacuum system)

#### Stage II: Beam through three cryomodules

Stage II will increase the energy of the ASTA accelerator facility and provide full test capability at high energy (800 MeV). The scope of work to complete Stage II will include the following principle components:

- Installation of the 10 MW RF system (components have already been procured using ARRA funds)
- Relocating the cryogenic end cap for the cryomodule string
- Installation and commissioning of two additional cryomodules (fabrication and assembly of the cryomodules is funded elsewhere)

### Stage III: Addition of proton beam

Stage III will include the installation of a low-energy proton injector (that already exists at the HINS experimental facility) into the IOTA storage ring. The scope of work to complete Stage III will include the following principle components:

- Relocating and installing the beamline (magnets, instrumentation, vacuum system, etc.) of the HINS injector into ASTA
- Relocating and installing the RF systems from the HINS experiment to the ASTA facility
- Installation of the necessary utilities to support the proton beamline (water, power, controls, etc.)

### Stage IV: 3.9 GHz capability

Stage IV will include the addition of a 3.9 GHz superconducting cavity into the ASTA injector to expand the experimental capabilities of the facility. The scope of work to complete Stage IV will include the following principle components:

- Fabrication and testing of a superconducting linearizing 3.9 GHz cavity and cryostat
- Construction of an 80 kW, 3.9 GHz RF system
- Cryogenic modifications to the existing system to tie in the 3.9 GHz cavity

## **10.2 Cost**

### **10.2.1 Stage I Cost**

The cost to complete Stage I is broken down (Tables 1 and 2) into the various operational capabilities associated with each sub-stage, as summarized in Figure 2. These costs include the infrastructure and commissioning costs (labor and materials) required to complete each respective stage of ASTA.

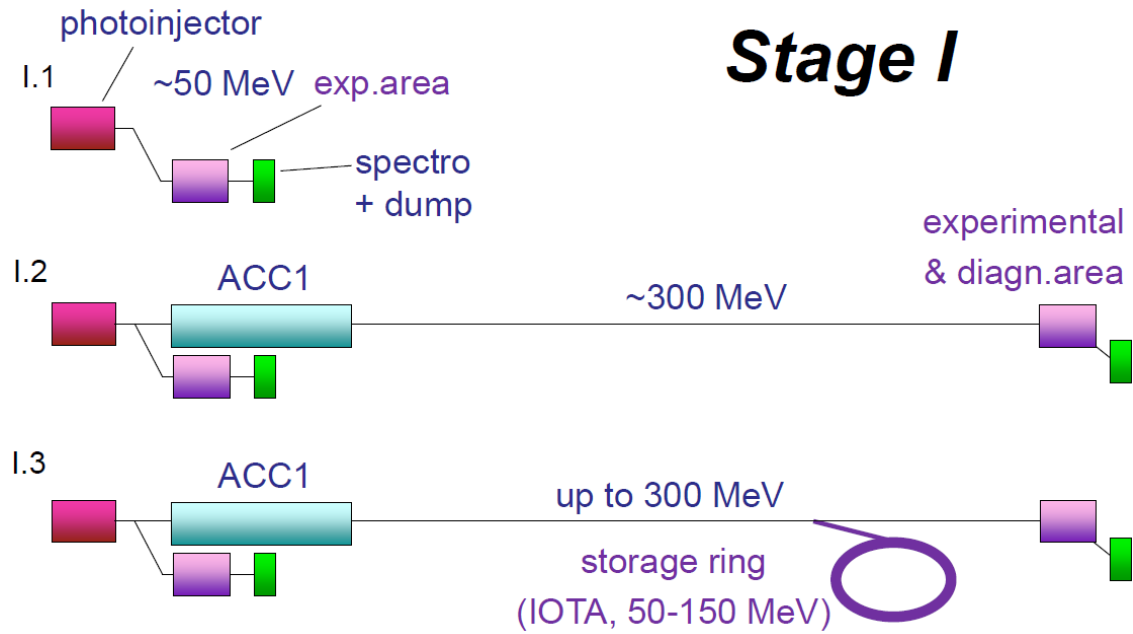


Figure 2: Stage I of the ASTA AARD User Facility construction and operational phases.

Table 1: Stage I.1 Cost (50 MeV Experimental Area)

| Description                    | FTE | Total Cost (K\$) |
|--------------------------------|-----|------------------|
| <b>Infrastructure</b>          |     |                  |
| Materials & Services/Equipment | -   | 986              |
| Labor                          | 2.0 | 472              |
|                                |     |                  |
| <b>Commissioning</b>           |     |                  |
| Materials & Services/Equipment | -   | 234              |
| Labor                          | 3.9 | 925              |
|                                |     |                  |
| <b>Total</b>                   |     | <b>2617</b>      |

Table 2: Stage I.2 Cost (300 MeV Experimental Area)

| Description                    | FTE | Total Cost (K\$) |
|--------------------------------|-----|------------------|
| <b>Infrastructure</b>          |     |                  |
| Materials & Services/Equipment | -   | 768              |
| Labor                          | 3.8 | 897              |
|                                |     |                  |
| <b>Commissioning</b>           |     |                  |
| Materials & Services/Equipment | -   | 468              |
| Labor                          | 7.3 | 1723             |
|                                |     |                  |
| <b>Total</b>                   |     | <b>3856</b>      |

### 10.2.2 IOTA Cost

The Integrable-Optics Test Accelerator (IOTA) ring is described in detail in Section 7.2. The development of IOTA is well advanced and many of the components have already been procured. The cost to complete the installation and commissioning of IOTA is summarized in Table 3. The cost to operate IOTA will be covered by the Operating Cost that is described in Section 10.2.6.

Table 3: Stage I.3 Cost (IOTA Ring)

| Description                        | FTE | Total Cost (K\$) |
|------------------------------------|-----|------------------|
| <b>Infrastructure/Installation</b> |     |                  |
| Materials & Services/Equipment     | -   | 828              |
| Labor                              | 1.7 | 401              |
|                                    |     |                  |
| <b>Commissioning</b>               |     |                  |
| Materials & Services/Equipment     | -   | 144              |
| Labor                              | 1.2 | 283              |
|                                    |     |                  |
| <b>Total</b>                       |     | <b>1656</b>      |

### 10.2.3 Stage II Cost

The cost to complete Stage II is shown in Table 4 and includes the infrastructure and commissioning costs (labor and materials) required to add two additional cryomodules, increasing the energy of ASTA to 800 MeV (Figure 3).

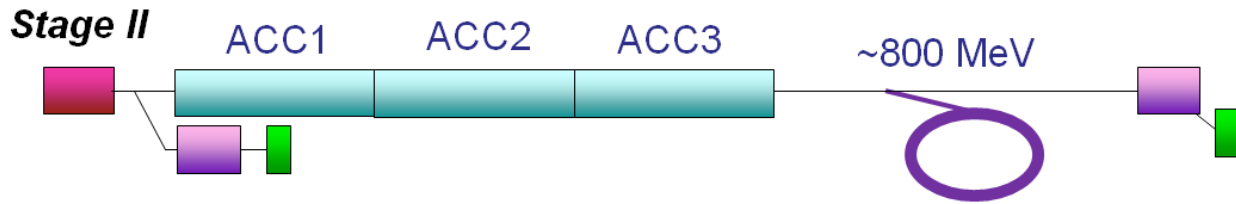


Figure 3: Stage II of the ASTA AARD User Facility

Table 4: Stage II Cost (800 MeV Experimental Area)

| Description                    | FTE  | Total Cost (K\$) |
|--------------------------------|------|------------------|
| <b>Infrastructure</b>          |      |                  |
| Materials & Services/Equipment | -    | 1068             |
| Labor                          | 8.1  | 1912             |
|                                |      |                  |
| <b>Commissioning</b>           |      |                  |
| Materials & Services/Equipment | -    | 990              |
| Labor                          | 10.0 | 2360             |
|                                |      |                  |
| <b>Total</b>                   |      | <b>6330</b>      |

#### 10.2.4 Stage III Cost

The cost to complete Stage III is shown in Table 5 and includes the infrastructure and commissioning costs (labor and materials) required to install an existing H-/proton injector into the IOTA storage ring (Figure 4).

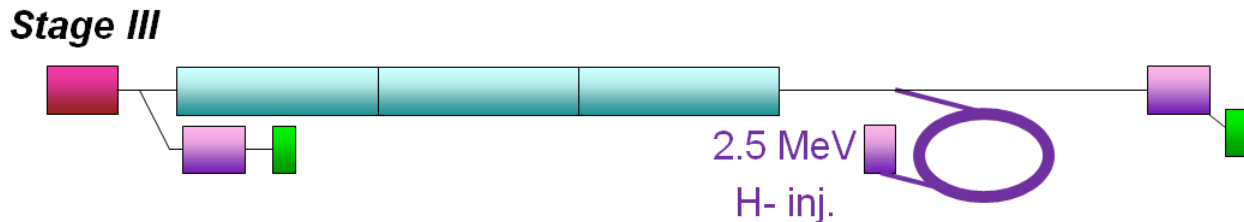


Figure 4: Stage III of the ASTA AARD User Facility

Table 5: Stage III Cost (H- Injector into IOTA Ring)

| Description                               | FTE | Total Cost (K\$) |
|---|-----|------------------|
| <b>Infrastructure &amp; Commissioning</b> |     |                  |
| Materials & Services/Equipment            | -   | 552              |
| Labor                                     | 3.5 | 826              |
|   |     |                  |
| <b>Total</b>                              |     | <b>1378</b>      |

### 10.2.5 Stage IV Cost

The cost to complete Stage IV is shown in Table 6 and includes the infrastructure and commissioning costs (labor and materials) required to fabricate and install a superconducting 3.9 GHz linearizing cavity into the ASTA injector (Figure 5).

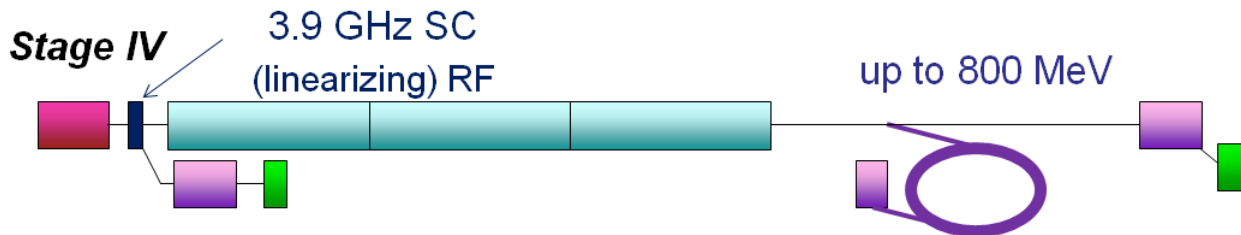


Figure 5: Stage IV of the ASTA AARD User Facility

Table 6: Stage IV Cost (3.9 GHz System)

| Description                               | FTE | Total Cost (K\$) |
|---|-----|------------------|
| <b>Infrastructure &amp; Commissioning</b> |     |                  |
| Materials & Services/Equipment            | -   | 1910             |
| Labor                                     | 6.8 | 1605             |
|   |     |                  |
| <b>Total</b>                              |     | <b>3515</b>      |

It should be emphasized that the cost of labor used in Tables 1 thru 6 is based on actual FY12 fully burdened rates for the types of specific job categories required to carry out each stage of work.

After the Stage I and Stage II infrastructure is in place, the ASTA facility will be fully operational. The long-term operational cost of the facility is described in the following Section.

### 10.2.6 Operating Cost

This estimate of the annual ASTA operating budget is the steady-state cost to operate the facility after the Stage I and Stage II infrastructure construction work has been completed. It includes the following assumptions.

- 9 months of operation and 3 months for shutdown and installation per year
- 2 shifts/day during operation
- 3 cryomodules installed
- ASTA operations department of 8 people

Furthermore, it is assumed that the experimental groups will provide funding for all experimental equipment and that Fermilab will provide only ancillary support such as standard instrumentation, beamline modifications, vacuum connections, infrastructure modifications, and other upgrades to accommodate new experiments. Labor and M&S operating cost estimates are shown in Tables 7 and 8.

Table 7: Operational Labor Estimate

| Labor Description                   | FTE          | Cost (K\$)  |
|-------------------------------------|--------------|-------------|
| ASTA Operations Department and Mgt. | 7.60         |             |
| Mechanical support                  | 1.16         |             |
| Controls & Instrumentation          | 1.66         |             |
| RF Dept.                            | 0.71         |             |
| Cryogenic Dept.                     | 1.45         |             |
| <b>Total</b>                        | <b>12.58</b> | <b>2944</b> |

The cost of labor is based on actual FY12 fully burdened rates for the types of job categories required to carry out the work. The ASTA Operations department consists of operators, engineering physicists, scientists and technical specialists whose principle responsibility is to manage the daily activities and operate the accelerator at the ASTA facility. The remaining categories are specialists (engineers, technicians, programmers, etc.) from various support departments that will be needed on a periodic basis to support and maintain the various systems of the ASTA facility. These estimates are based on the commissioning experience of ASTA over the past couple of years and the anticipated needs after the facility is completed.

Table 8: Operational M&S Estimate

| Item Description            | Cost (K\$) |
|-----------------------------|------------|
| Infrastructure/Aux. Systems | 168        |
| RF                          | 84         |
| Laser                       | 48         |
| Vacuum/Clean room           | 120        |
| Instrumentation             | 48         |
| Controls                    | 18         |
| Experimental Support        | 60         |
| Cryogenics                  | 432        |
| <b>Total</b>                | <b>978</b> |

The M&S cost estimate includes consumables, maintenance and upgrade items needed on an annual basis to support the operations and infrastructure of the ASTA facility. These estimates are based on recent historical costs over the past few years and the anticipated needs after the facility is completed and in full operation.

### 10.2.7 Cost Breakdown

A summary of the ASTA costs is shown broken down by individual operational stage in Table 9 and by fiscal year in Table 10 and in Figure 6.

Table 9: ASTA Cost Breakdown by Stage

| Stage | Description - following Figures 2,3,4 and 5                                 | Infrastructure & Commissioning Costs (\$k) | Operations Cost/yr (\$k) |
|-------|---|--|--------------------------|
| I.1   | add 50 MeV, experimental area, spectrometer, & dump                         | \$2,617                                    |                          |
| I.2   | add CM #1 (~ 300 MeV), experimental area, and diagnostics area              | \$3,856                                    |                          |
| I.3   | add IOTA Storage Ring (50-150 MeV)  | \$1,656                                    |                          |
|       | <b>Total Cost (Stage I):</b>  | <b>\$8,129</b>                             |                          |
| II    | add CM #2 and CM #3 (~ 800 MeV)   | \$6,330                                    |                          |
| Ops.  | annual operating cost of ASTA after Stage I & II infrastructure is complete |  | <b>\$3,922/yr</b>        |
| III   | add HINS 2.5 MeV H-/proton injector   | \$1,378                                    |                          |
| IV    | add superconducting 3.9 GHz linearizing cavity                              | \$3,515                                    |                          |
|       | <b>Total Project Cost (Stage I thru IV):</b>                                | <b>\$19,352</b>                            |                          |

Table 10: ASTA Cost Breakdown by Fiscal Year

| Cost by Stage (\$M) |     |     |     |      |      |      |      |                  |   |
|---------------------|-----|-----|-----|------|------|------|------|------------------|---|
| Fiscal Year         | I.1 | I.2 | I.3 | II   | III  | IV   | Ops. | Total Cost (\$M) | Details of Scope/Comments                                     |
| FY 2014             | 2.6 | 3.9 | 0.8 | -    | -    | -    | 0.2  | 7.5              | Half of IOTA cost, begin operation of 50 MeV                  |
| FY 2015             | -   | -   | 0.9 | 4.3  | 0.5  | 1    | 1    | 7.7              | Complete IOTA, begin HINS & 3.9 GHz, operation of all Stage I |
| FY 2016             | -   | -   | -   | 2    | 0.9  | 2    | 2    | 6.9              | Complete 800 MeV & HINS, complete 3.9 GHz fabrication,        |
| FY 2017             | -   | -   | -   | -    | -    | 0.5  | 3.9  | 4.4              | Install and commission 3.9 GHz, operate all stages            |
| FY 2018 & Beyond    | -   | -   | -   | -    | -    | -    | 3.9  | 3.9              | Operations of entire facility                                 |
| Cost per Stage      | 2.6 | 3.9 | 1.7 | 6.3  | 1.4  | 3.5  |      |                  |   |
| Cumulative Cost     | 2.6 | 6.5 | 8.1 | 14.5 | 15.8 | 19.3 |      |                  |   |

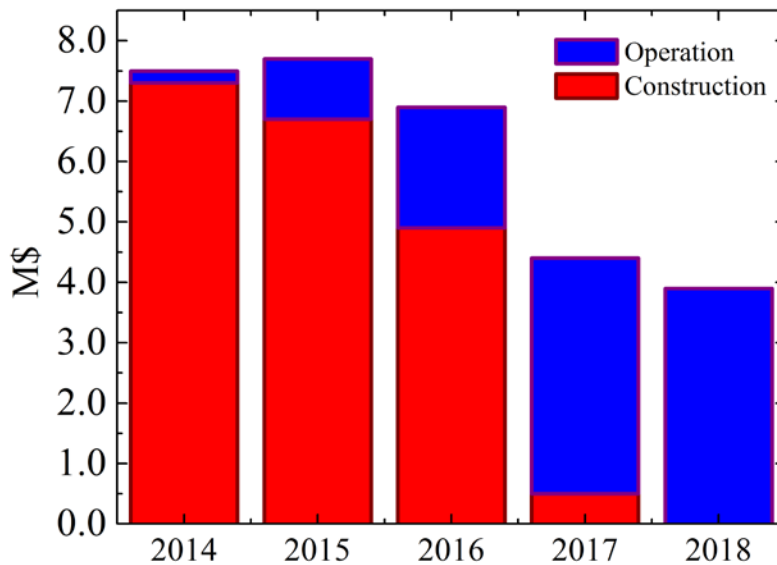


Figure 5. ASTA Costs, both Construction and Operations, by Fiscal Year

### 10.3 Schedule

Stage I of ASTA is expected to take approximately one year to install at the funding and labor levels described above. At the completion of this Stage, ASTA will be a fully operational SRF accelerator capable of supporting a 50 MeV low-energy and a 300 MeV high-energy test

program. The installation and commissioning of IOTA is also planned to occur during the Stage I schedule of ASTA.

After Stage I is complete, experimental operation of ASTA could begin on the schedule described in Section 10.2.6 (9 months of operation and 3 months of shutdown per year).

Stage II of ASTA is expected to take an additional year to complete at the funding and labor levels given in Section 10.2.3. At the completion of this Stage, the capability of the high-energy test area will increase to 800 MeV. Although low-energy (50 MeV) experimental operation of ASTA will be available during the one year installation period for Stage II, high energy (300 MeV) experimental operation of ASTA will not be possible until the installation and commissioning is complete.

The installation of Stage III and IV of ASTA will cause minor interruptions to the experimental program and can be scheduled to coincide with the annual 3-month shutdown/maintenance intervals.

A summary of the installation, commissioning and experimental schedule for the various Stages of ASTA build-out is shown in Figure 7. This schedule assumes funding for Stage I (including IOTA) is available in FY14.

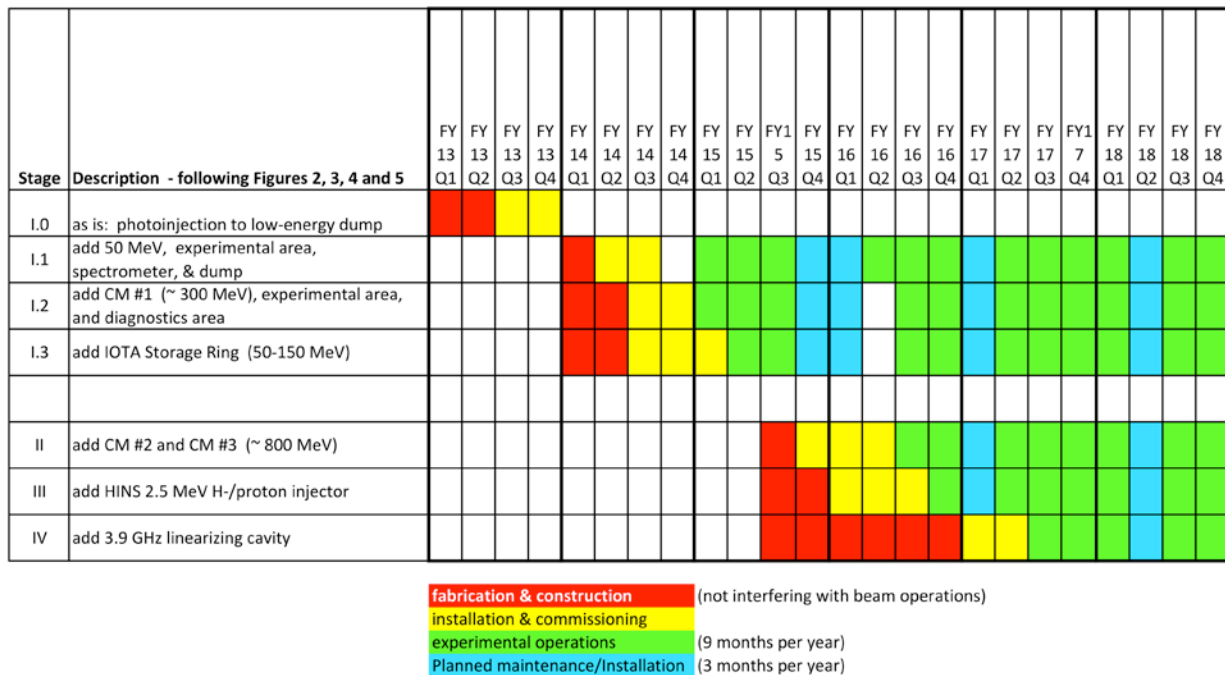


Figure 7: ASTA Schedule

## 11.0 Management of the Scientific User Program

ASTA is intended to be operated as a scientific user facility for advanced accelerator research and development. All the characteristics of a national user facility (<http://science.energy.gov/user-facilities/>) will be in evidence in the operation of ASTA and its user program. Namely,

- The facility is open to all interested potential users without regard to nationality or institutional affiliation.
- Allocation of facility resources is determined by merit review of the proposed work.
- User fees are not charged for non-proprietary work if the user intends to publish the research results in the open literature. Full cost recovery is required for proprietary work.
- The facility provides resources sufficient for users to conduct work safely and efficiently.
- The facility supports a formal user organization to represent the users and facilitate sharing of information, forming collaborations, and organizing research efforts among users.
- The facility capability does not compete with an available private sector capability.

The user program will be proposal-driven and peer-reviewed in order to ensure that the facility focuses on the highest quality research. Proposals will be evaluated by an external Program Committee (the ASTA Program Advisory Committee), consisting of internationally recognized scientists. Proposal evaluation will be carried out according to established merit review guidelines. The ASTA PAC will advise the ASTA Director on user proposal ranking. The ASTA Director is responsible for the management of the user program. In addition, ASTA will support a user's organization that will advise the facility management.

Organizationally, the ASTA Director will report to the Accelerator Physics Center Head, who has oversight responsibility for the ASTA Program. The beam operations and facility maintenance will be the responsibility of the Accelerator Division.

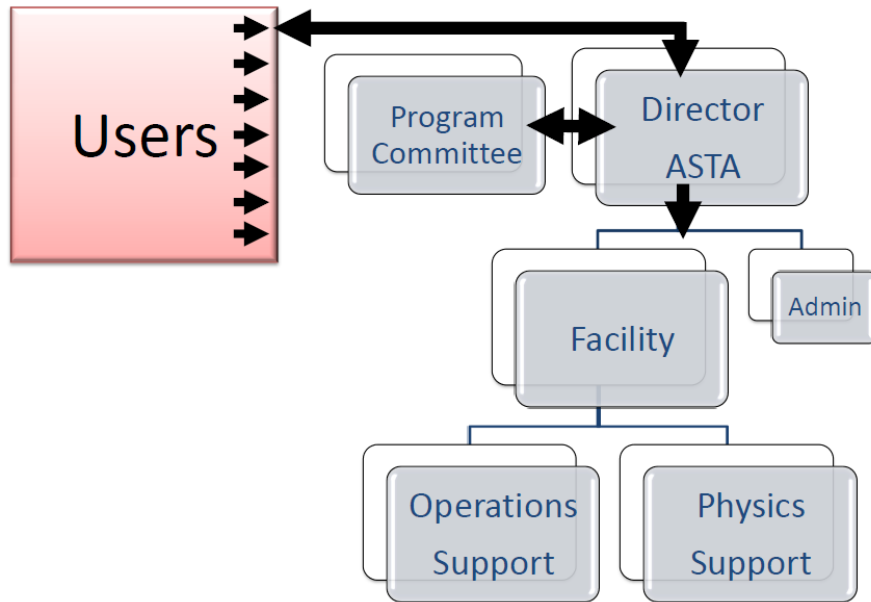


Figure 1: Proposed organizational structure of the ASTA AARD User Facility and Program.

## 12.0 List of Acronyms

ACCn: Superconducting RF Accelerating Module #n of ASTA  
ADC: Analog to Digital Converter  
ALS: Advanced Light Source at Lawrence Berkeley National Laboratory (LBNL)  
ANL: Argonne National Laboratory, Lamont, IL  
APS: Advanced Photon Source at Argonne National Laboratory, Lamont, IL  
Ar: Argon gas  
ARIEL: future Advanced Rare Isotope E Laboratory at TRIUMF  
ASTA: Advanced Superconducting Test Accelerator (this proposal for Fermilab)  
ATF: Accelerator Test Facility, at Brookhaven National Laboratory, Upton, NY  
AWA: Argonne Wakefield Accelerator at Argonne National Laboratory, Lemont, IL  
A0: AZero – location at Fermilab of the Fermilab NICADD PhotoInjector Laboratory  
now called HBESL: High-Brightness Electron Source Laboratory  
A0PI: A0 PhotoInjector Laboratory at Fermilab

BAM: Bunch Arrival Monitor  
BAT: Bormann Anomalous Transmission  
BBU: beam break-up  
BC: bunch compressor  
BELLA: Berkeley Laboratory Laser Accelerator at LBNL  
BES: Basic Energy Sciences – a division of US DOE  
BINP: Budker Institute of Nuclear Physics, Siberia, Russia  
BLIP: Brookhaven Linear Isotope Producer  
BNL: Brookhaven National Laboratory, Upton, NY  
BPM: beam position monitor  
BSM: new phenomena (outside the scope of) Beyond the Standard Model of particle physics

CAVn: superconducting RF cavity #n of the TESLA type  
CCD: charge-coupled device, as used in a camera  
CCR: Circulator Cooling Ring  
CDR: Coherent Diffraction Radiation  
CEBAF: Continuous Electron Beam Accelerator Facility – obsolete name for JLAB  
CERN: European Center for Nuclear Research, Geneva, Switzerland  
CER: Coherent Edge Radiation  
CESR-TA: CESR-Test Accelerator: Cornell Electron-Positron Storage Ring-Test Accelerator,  
Ithaca, NY  
CGH: Compressed Harmonic Generation  
CHEF: A Framework for Accelerator Optics and Simulation  
CM-n: Cryomodule #n built at Fermilab  
CNT: Carbon nanotube  
CO: molecular Carbon Monoxide  
COSR: coherent optical synchrotron radiation  
CODR: coherent optical diffraction radiation

COTR: coherent optical transition radiation  
Csl: Cesium Iodide crystal  
CSR: coherent synchrotron radiation  
CUVTR: coherent ultra-violet transition radiation  
CST: Computer Simulation Technology (a company name)  
CsTe: Cesium Telluride photocathode  
CUR: coherent undulator radiation  
CVUVTR: coherent vacuum ultra-violet transition radiation  
CW: continuous wave = constant or always active  
CXTR: coherent x-ray transition radiation

DAFNE: e+e- collider at the  $\phi$  meson and synchrotron radiation source at INFN, Frascati, Italy  
DESY: Deutsches Elektronen-Synchrotron (Laboratory), Hamburg, Germany  
DC: direct current, always on  
DEEX: Double Emittance Exchanger  
DL: dog-leg  
DPAs: displacements per atom  
DWFA: Dielectric-Wakefield Accelerator

EEHG: Echo-Enabled Harmonic Generation  
EEX: emittance exchange  
ELBE: synchrotron radiation source in Dresden, Germany  
ELIC CR: Electron-Ion Collider Cooling Ring at JLab  
EMMA: Electron Machine with Many Applications is a project at Daresbury Laboratory in the UK to build a linear non-scaling FFAG  
EOM: Electro Optical Modulation  
EOS: Electro-Optical Sampling  
e-p: electron-proton interaction  
ERL: Energy Recovery Linac  
ESH: Environmental, Safety, and Health  
EUV: extreme ultra-violet

FACET: Facility for Advanced Accelerator Experimental Tests, at SLAC  
FBT: Flat Beam Transform  
FEL: Free Electron Laser  
FELO: Free Electron Laser Oscillator  
FELEX: Free-Electron Laser EXperiment simulation code from LANL  
FERMI@Elettra: seeded Free-Electron Laser at ELLETRA, synchrotron light source, Trieste, Italy  
FFAG: Fixed Field Alternating Gradient (accelerator)  
FIR: far infra-red  
FLASH: Free-electron LASer in Hamburg - (offspring of TTF) at DESY  
FNAL: Fermi National Accelerator Laboratory, Batavia, IL  
FODO: alternating Focusing-Defocusing beam transport channel  
FPGA: field-programmable gate array

FWHM: full width at half-maximum

GHz: Giga-Hertz frequency =  $10^9$  cycles/sec

GINGER: Free-Electron Laser simulation code from LBNL

g-2: Fermilab experiment to study the anomalous magnetic moment of the muon

HBESL: High-Brightness Electron Source Laboratory at Fermilab, formerly called AOP1, also Fermilab E-1023

HEP: High Energy Physics

HEPAP: US High Energy Physics Advisory Panel reporting to both DOE and NSF

HERA: Hadron Electron Ring Anlage (facility), an electron-proton collider at DESY, Hamburg DE

HGHG: High-Gain Harmonic Generation

Higgs: a particle which likely has been recently observed at CERN which provides other particles with

mass, also the name of the theoretical physicist predicting its existence

HGHG: high gain harmonic generation

HHG: high harmonic generation

HINS: High Intensity Neutrino Source R&D program at Fermilab

HOM: higher order mode

HSR: high strain rate

H<sup>-</sup>: a negative ion formed by a proton plus two electrons

IARC: Illinois Accelerator Research Center at Fermilab, Batavia, IL

ICCD: Intensified Charge-Coupled Device, a sensitive camera

ICL: Imperial College London, UK

ICS: Inverse Compton Scattering

IIT: Illinois Institute of Technology, Chicago, IL

ILC: International Linear Collider

ILCTA: ILC Test Accelerator

INFN: Istituto Nazionale di Fisica Nucleare – Italian government agency supporting HEP

IOTA: Integrable-Optics Test Accelerator proposed for the ASTA facility at Fermilab

IR: Infra-red

JLab: Thomas Jefferson National Laboratory, Newport News, VA

LANL: Los Alamos National Laboratory, Los Alamos, NM

LASA: Laboratorio Acceleratori e Superconduttiva Applicata, INFN, Milano, Italy

LCLS: Linear Coherent Light Source at SLAC

L-band: 1-2 GHz range of RF frequencies, TESLA/TTF/FLASH and ILC are based at 1.3 GHz

LBNE: Long Baseline Neutrino Experiment – under development at Fermilab

LBNL: Lawrence Berkeley National Laboratory, Berkeley, California

LCW: low conductivity (cooling) water

LFD: Lorentz Force Detuning

LFDC: Lorentz Force Detuning Compensation

LEBT: low energy beam transport  
LHC: Large Hadron Collider at CERN  
LIM: laser-induced microbunching  
LLRF: low-level RF controls  
LN2: liquid Nitrogen  
LPS: longitudinal phase space  
LSCA: longitudinal space charge amplifier  
LSCIM: longitudinal-space-charge-induced microbunching  
LYSO: lutetium-yttrium oxyorthosilicate

MAP: Muon Accelerator Program to study feasibility of producing intense or colliding beams of muons  
MARIE: Matter-Radiation Interaction at the Extreme project at Los Alamos National Lab  
MCP: micro-channel plate photo- or electron-multiplier  
MDB: Meson Detector Building  
MEIC: Medium-energy Electron-Ion Collider at JLab  
MPI: Martin-Puplett Interferometer  
MRDL: NIU Microelectronic Research & Development Laboratory  
Mu2e: Fermilab experiment to search for direct conversion of muons into electrons  
MW: Mega-Watt ( $10^6$  watts), a unit of beam power or electrical power

NC: normal conducting (as opposed to superconducting)  
ND: Neutral Density optical filter to attenuate signal  
NI: non-intercepting diagnostic technique  
NIR: near infra-red  
NIU: Northern Illinois University, DeKalb, IL  
NGLS: Next Generation Light Source – a high-repetition-rate soft X-ray FEL proposed by LBNL  
NSF: US National Science Foundation

ODR: optical diffraction radiation  
OPA: optical parametric amplifier  
OSC: Optical Stochastic Cooling

PAC: Program Advisory Committee  
PC: photo-cathode  
PEP: Positron-Electron Project, an e<sup>+</sup>e<sup>-</sup> collider at SLAC, Menlo Park, California  
PhD: Doctor of Philosophy  
PIC: particle-in-crystal  
PITZ: Photo Injector Test Facility at DESY, Zeuthen (near Berlin), Germany  
Project X: proposed future high intensity proton accelerator program at Fermilab  
P5: Particle Physics Project Prioritization Panel – a sub-panel of HEPAP

Q: quality factor of an RF cavity =  $2\pi$  \* Energy stored in a cavity/Energy dissipated per RF cycle  
Q<sub>L</sub>: loaded Q-value = quality factor of an RF cavity while loaded with (accelerating) beam

QA: Quality Assurance

Quadrupole: shorthand for a magnet with four poles, which is used to focus the beam

RaDIATE: collaboration to study Radiation Damage in Accelerator Target Environments

RFBT: round-to-flat-beam transformer

RFQ: Radio Frequency Quadrupole magnet which accelerates and focuses low energy beams

RMS: root-mean-square

RTI: Real-Time Interferometer

RTFB: round-to-flat beam transformer

SBIR: Small Business Innovation Research – US government program (also refers to its grants)

SciDAC: Scientific Discovery through Advanced Computing, a DOE program

SRF: Superconducting RadioFrequency

SDUV FEL: Shanghai Deep Ultra-Violet (seeded) Free Electron Laser, Shanghai, China

SER: spontaneous emission radiation

Sextupole: shorthand for a magnet with six poles, usually used to improve the momentum acceptance of a beamline or accelerator by compensating for chromatic aberrations.

SIM: SASE-induced microbunching

SINAP: Shanghai INstitute of Applied Physics, Shanghai, China

SLC: SLAC Linear Collider at Stanford Linear Accelerator Center, Menlo Park, California

SNS: Spallation Neutron Source at Oak Ridge National Laboratory, Oak Ridge, TN

SRF: Superconducting RF

SSRn: Superconducting Spoke Resonator cavity #n

SWCNT: single-wall carbon nanotube

TESLA: 500 GeV e+e- collider proposed by DESY using SRF cavities

THz: Tera-Hertz ( $10^{12}$  cycles/sec) frequency

T-insert: a beam optics element described in section 3.5.1.2.1 of this proposal

TM: Transverse EM Mode

TOA: Time of Arrival

TRIUMF: Canada's particle physics laboratory in Vancouver, British Columbia

TTF: Tesla Test Facility (evolved into FLASH) at DESY

TW: Tera-Watt ( $10^{12}$  Watts) power level

UIUC: University of Illinois, Urbana-Champaign, IL

UR: undulator radiation

UV: ultra-violet

VEPP-3: accelerating-storage complex at Budker Institute of Nuclear Physics (BINP)

VLHC: Very Large Hadron Collider, a machine design considered in the early 2000's, with energy beyond that of the LHC

VORPAL: Versatile Plasma Simulation Code (by Tech-X company)

VUV: vacuum ultra-violet

VTO: variable tap-off (of power from an RF distribution system)

XUV: extreme ultra-violet

YAG: yttrium aluminum garnet

1-D: one-dimensional

2D: 2 dimensional

## **13.0 Appendix - Letters of Institutional Interest**

**13.1 Argonne National Laboratory**

**13.2 Brookhaven National Laboratory**

**13.3 CERN**

**13.4 Colorado State University**

**13.5 Community Petascale project for Accelerator Science and Simulation (ComPASS)**

**13.6 Illinois Institute of Technology**

**13.7 Indiana University**

**13.8 John Adams Institute for Accelerator Science**

**13.9 Joint Institute for Nuclear Research**

**13.10 US LHC Accelerator Physics Program (LARP)**

**13.11 Lawrence Berkeley National Laboratory**

**13.12 Northern Illinois University**

**13.13 Oak Ridge National Laboratory**

**13.14 Princeton Plasma Physics Laboratory**

**13.15 RadiaBeam Technologies, LLC**

**13.16 Thomas Jefferson National Accelerator Facility**

**13.17 US Particle Accelerator School**



Alexander Zholents  
Director

Accelerator Systems Division  
Argonne National Laboratory  
9700 South Cass Avenue, Bldg. 401  
Argonne, IL 60439

1-630-252-4810 phone  
1-630-252-7369 fax  
azholents@aps.anl.gov

December 4, 2012

Dr. Vladimir Shiltsev  
ASTA Interim Director  
Fermi National Accelerator Laboratory

Dear Vladimir,

I would like to express my strongest support for Fermilab's proposal to establish an Accelerator R&D User Facility at FNAL Advanced Superconducting Test Accelerator (ASTA). The proposed facility offers unique opportunity to enable a broad range of research in beam physics and accelerator technology at its three experimental areas (50 MeV electrons, 300-800 MeV electron, and 50-150 MeV/c electron/proton ring) and has promise to become one of the most valuable and relevant places for accelerator scientists and engineers to come and do accelerator R&D. Outstanding electron beam average and peak brightness, acceleration in superconducting RF structures and unmatched versatility of IOTA ring – all these features make ASTA a perfect testbed for many promising accelerator ideas for this country's future, such as high power beam acceleration in SC RF cryomodules, new beam optics concepts, advanced phase space manipulation, space-charge compensation and optical stochastic cooling. The range of applications of the ASTA research seems to be unmatched by any existing AARD facility in the US, and in the world, in that matter.

Argonne has long history of collaboration with Fermilab in the field of accelerators and we will be happy to see this connection further developed thanks to ASTA. Of a particular interest for ANL accelerator physicists are the opportunities which ASTA brings for the beam phase space manipulations (shaping, tailoring, microbunching) which can help to build low-cost high-efficiency FELs. Personally, I am very interested in seeing at IOTA a convincing demonstration of the optical stochastic cooling and a concept of nonlinear integrable optics. As this new facility is going to be built we will continue thinking of many other opportunities for collaborative research at ASTA which could be of importance for future beam-based facilities at Argonne.

Summarizing, I wish to express my support for the ASTA proposal at Fermilab and firm belief that such User facility will be of great value for Argonne, Fermilab, and entire US accelerator community.

Sincerely,

A handwritten signature in black ink that reads "Alexander Zholents". The signature is written in a cursive, flowing style.

Alexander Zholents



Building 911B  
P.O. Box 5000  
Upton, NY 11973-5000  
Phone 631 344-7084  
Fax 631 344-5954  
roser@bnl.gov

managed by Brookhaven Science Associates  
for the U.S. Department of Energy

December 6, 2012

Dr. Vladimir D. Shiltsev  
Director, Accelerator Physics Center  
Fermi National Accelerator Laboratory  
P.O. Box 500, MS 221  
Batavia, IL 60510-0500

**Letter of Support for an Accelerator R&D User Facility at Fermilab's Advanced Superconducting Test Accelerator (ASTA)**

Dear Dr. Shiltsev:

I write to support the proposal for an Accelerator R&D User Facility at Fermilab's Advanced Superconducting Test Accelerator (ASTA).

Accelerator R&D in the US is being performed both at existing accelerator facilities and at dedicated user facilities. Both approaches have been necessary to accomplish the goal of a vibrant R&D effort to provide the basis for future high performance accelerator facilities for the nation as well as educate the next generation of accelerator scientists. The existing dedicated facilities, pioneered by the Brookhaven Accelerator Test Facility (ATF), have focused on advanced and novel accelerating structures with very high accelerating gradients.

The proposed facility at ASTA plans to use existing equipment at Fermilab to provide very unique capabilities that can address accelerator issues ranging from limits on beam intensities and space charge dominated beams to novel beam sources. Of particular interest is the small storage ring IOTA to study beam dynamics in a ring with fully integrable optics that can accommodate very large betatron tune spread. The accelerator R&D at this facility at ASTA is of great interest to the high luminosity colliders RHIC and eRHIC at BNL and will be complementary to the work performed at the existing dedicated accelerator R&D facilities.

Please do not hesitate to contact me if you need any further information.

Sincerely,

A handwritten signature in blue ink that reads "Thomas Roser".

Thomas Roser  
Chair  
Collider-Accelerator Department  
Brookhaven National Laboratory



**ORGANISATION EUROPÉENNE POUR LA RECHERCHE NUCLÉAIRE  
EUROPEAN ORGANIZATION FOR NUCLEAR RESEARCH**

Laboratoire Européen pour la Physique des Particules / European Laboratory for Particle Physics

GENÈVE, SUISSE  
GENEVA, SWITZERLAND

Mail address: Dr Stephen Myers  
Director of Accelerators and Technology  
CERN  
CH-1211 GENEVE 23  
Switzerland

**Dr. Vladimir Shiltsev**  
**Director, Accelerator Physics Centre**  
**FNAL, PO Box 500, MS221, Batavia, IL**  
**60510 USA**

Téléphone/Telephone:  
Direct: +41 22 767 3406  
+41 22 767 8705  
Central/Exchange: +41 22 767 6111

E-mail: [Steve.Myers@cern.ch](mailto:Steve.Myers@cern.ch)  
[Oliver.Bruning@cern.ch](mailto:Oliver.Bruning@cern.ch)

Votre référence/ Your reference:  
Notre référence/ Our reference: OB\_SM\_SD/2012-004

Geneva, 11<sup>th</sup> December 2012

**Recommendation Letter for Dr. Alexander Valishev**

Dear Vladimir,

Dr. Steve Myers and I have first heard about the FNAL proposal for an Advanced Superconducting Test Accelerator (ASTA) facility from Dr. Frank Schmidt, who attended a seminar given by you in October 2012 on this proposal during his sabbatical stay at FNAL.

Several new project proposals explore the operation regime with very high intensity hadron beams (e.g. the LHC upgrade studies and its accompanying injector upgrade program LIU, neutrino facilities and spallation source proposals). Space charge effects and understanding its limits to the accelerator performance are therefore a hot topic for many accelerator projects.

A precise and reliable simulation of space charge effects is only possible with experimental validation of the simulation codes against operating accelerator installations. A dedicated accelerator test facility provides an ideal controlled environment for addressing the various space charge effects, for studying their performance limitations and for studying measures for compensating space charge effects in a running accelerator.

In addition to space charge related studies, the ASTA facility allows for tests related to Optical Stochastic Cooling, non-linear beam dynamic issues and the operational test of new installation devices such as 'electron columns' or 'electron lenses' and plasmas. Furthermore, the ASTA facility would provide a unique teaching facility for new accelerator scientists.

In light of the various potential applications and relevance for understanding space charge effects we therefore welcome the ASTA initiative and provide our full moral support for this new project proposal.



**Dr. Steve Myers**

*Director of Accelerators and Technology*



**Dr. Oliver Brüning**

*Head of the Accelerator Beam Physics (ABP)  
CERN-USLARP contact for Accelerator Systems studies.  
Deputy Project Leader of the HL-LHC upgrade project*

Electrical and Computer Engineering  
1373 Campus Delivery  
Fort Collins, Colorado 80523-1373 USA  
(970) 491-6796  
MOBILE: (708) 638-6813  
biedron@engr.colostate.edu  
www.engr.colostate.edu/ece

December 10, 2012

Dr. Piermaria Oddone  
Director  
Fermilab  
P.O. Box 500  
Batavia, IL 60510-5011

Dear Dr. Oddone,

On behalf of the Colorado State University's accelerators and beams community, we are writing to formally indicate our support for the Advanced Superconducting Test Accelerator (ASTA) proposal.

As you are aware, individuals from the Electrical and Computer Engineering Department, the Physics Department, and the Radiation and Oncology groups of the School of Veterinary medicine at Colorado State University have professional links to Fermilab in many areas, including accelerator and beam physics, high-energy physics, detector, and radiation safety, to name a few.

In the area of high-average power accelerator and beam physics, necessary to enable new science and technologies, we are enthusiastic that ASTA will facilitate much needed research including testing of:

- niobium cavities fabricated and polished with different protocols and subsequently tested with beam,
- novel cathode robustness and beam quality performance,
- high-average power beam propagation/dynamics and control,
- high-energy, space-charge dominated beams,
- non-intercepting, real-time diagnostics.

The operation of accelerators, specifically, superconducting cavities at a high repetition rates, are of interest for accelerator science and technology, for the light source user community in atomic, molecular and materials science, and for applications in nuclear and high-energy physics. For instance, a so-called "complete experiment" (reference Nature Physics, Jahnke et al, 2010) requires simultaneous detection of several particles in coincidence, thus relying upon high-average power beams.

Not only does the community require these tests for the realization of future user facilities and industrial devices for our Nation, we require ASTA for the training of our interns (high-school and undergraduate) and our graduate students as well as retention of our staff.

We applaud your proposal and are hopeful it will be funded in the near future.

Very truly yours,



Sandra G. Biedron, Ph.D.  
Associate Professor  
Electrical and Computer Engineering



Stephen V. Milton, Ph.D.  
Professor  
Electrical and Computer Engineering



**Panagiotis Spentzouris**  
**Head, Accelerator & Detector Simulation**  
**Department**

FNAL Scientific Computing Division

630.840.4342

spentz@fnal.gov

December 8, 2012

Dr. Vladimir Shiltsev,  
Director, Accelerator Physics Center  
Fermilab  
P.O. Box 500, MS221  
Batavia, IL 60510

Dear Vladimir,

I strongly support your proposal to obtain funding for the completion of the Advanced Superconducting Test Accelerator (ASTA) facility and for establishing a user accelerator R&D program there. ASTA is unique among Advanced Accelerator R&D (AARD) facilities because it focuses on the specific needs of accelerator science in support of Intensity Frontier accelerators. Researchers from the Community Petascale project for Accelerator Science and Simulation (ComPASS), which I direct, are heavily engaged in Intensity Frontier activities through our support of Project-X design. We also have a long tradition of supporting research in AARD facilities, most recently FACET and BELLA. We are excited about the prospect of collaboration on ASTA experiments, and engaging in the design and commissioning of both the superconducting rf linac and the IOTA storage ring. In particular, we are very interested in utilizing the IOTA ring to study space-charge effects and validate our numerical models. Even more importantly, we would like to model mitigation techniques for space-charge effects and verify these experimentally. In addition, we are very interested in supporting and guiding, via numerical simulation, experiments that test the ability of non-linear accelerators to reduce or eliminate beam instabilities. ASTA is the only facility that provides the infrastructure to study such instabilities and design and test techniques to mitigate them. Understanding how to control or eliminate beam instabilities and minimize beam losses is imperative for the successful operation of high-intensity accelerators.

ComPASS researchers are looking forward to working with you and your team to support and enable the planned research activities of this facility. We hope to pursue experiments and studies that will advance accelerator science and technology for the Intensity Frontier program.

Sincerely,

Panagiotis Spentzouris  
Director, ComPASS

Dr. Vladimir Shiltsev,  
Director, Accelerator Physics Center  
Fermilab  
P.O. Box 500, MS221  
Batavia, IL 60510

Prof. Linda Spentzouris  
IIT, 182 LS, Physics  
3101 South Dearborn  
Chicago, IL 60616

Dear Dr. Shiltsev,

December 6, 2012

I strongly support your proposal to obtain funding for the completion of the ASTA User's Facility at Fermilab. There is a real need for facilities that have advanced accelerator research included in their mission. It is impractical or impossible to use accelerators serving a user community to test design innovations or investigate beam dynamics under unusual conditions. Universities such as the Illinois Institute of Technology (IIT) with accelerator physics programs, but no machine on campus, rely on the availability of accelerator facilities at the national laboratories. The existence of university programs in accelerator physics and technology, in turn, contributes to the development of improved machine components. IIT is an example of this synergy; material science, engineering, and chemistry faculty who have other research options are involved with cutting edge accelerator challenges due to the proximity of resources at Fermilab.

IIT has a long history of collaboration with Fermilab in the area of accelerator development. Several of our faculty have long been involved with the research effort in muon beam production and processing. We also have faculty members collaborating with Fermilab on the development of superconducting RF structures. Condensed matter and chemistry faculty have been studying the reasons for breakdown in SRF structures, as well as investigating the production of novel SRF structures using the technique of atomic layer deposition. We also have significant research going on in the area of photocathode development. Several IIT graduate students are, or have been, in the Fermilab graduate student program in accelerator physics.

We are eager for the completion of the ASTA facility, particularly the IOTA ring. One of our faculty members is already looking at the IOTA design. The capability to run both electrons and protons in the ring is very attractive; the prospect of doing experiments using IOTA should help us recruit more accelerator physics graduate students to IIT. We look forward to the new opportunities for research and the further collaboration enabled by the availability of ASTA.

Sincerely,



Dr. Linda Spentzouris



## DEPARTMENT OF PHYSICS

INDIANA UNIVERSITY  
College of Arts and Sciences  
Bloomington

Dr. V. Shiltsev  
Fermi National Accelerator Laboratory

Dear Dr. Shiltsev,

I am happy to write a letter in support of your application of funding from the Department of Energy for the ASTA project. As you have pointed out well in your proposal that accelerator physics research is an integral part of the US High energy and nuclear physics research and development. Without accelerator physics research, it would not be possible to achieve “the particle physics today.” Accelerator physics development has also great impacts on US industries and technology.

The ASTA is an interesting project that includes Photoinjector source;  Linear accelerator based on superconducting RF cryomodules; Electron storage ring (IOTA); Low- and high-power lasers; and Experimental areas for research with low-energy and high-energy beams. The completion of such a project will provide decade of interesting physics research. The project will provide a research base for US accelerator physics for decades.

In summary, I write this letter to express my support to the importance of the ASTA proposal on the accelerator physics research in the US. I am sure that the Department of Energy realizes the importance of your project to high energy physics, to the United States high technology industries, and National Security. I support your efforts without reservation and hope to see your successful project.

Sincerely Yours,

SY Lee, Professor of Physics, Indiana University  
12/9/2012



Imperial College  
London



## The John Adams Institute for Accelerator Science

Prof. Andrei Seryi, Director  
Denys Wilkinson Building  
Keble Road, Oxford  
OX1 3RH, UK  
Mobile: [+44][0] 7722 474701  
Tel: [+44][0] 1865 273595  
Fax: [+44][0] 1865 273601

e-mail: Andrei.Seryi@adams-institute.ac.uk

10 December 2012

Dr Vladimir Shiltsev  
ASTA Interim Program Director  
Fermilab

Dear Vladimir,

With this letter I would like to express my strongest support for the plans to establish an Accelerator R&D User Facility at Fermilab's – Advanced Superconducting Test Accelerator (ASTA).

The ASTA facility will allow Fermilab to be at the forefront of the research and technology development in the areas of superconducting RF, creation of new optics concepts, investigation of promising method of space-charge compensation, developments of advanced techniques for Free Electron Lasers.

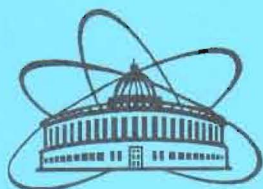
The ASTA user facility will build up very efficiently on the years of investments into advanced equipment at Fermilab, and will bring the arising opportunities close to the scientific and industrial user communities, enhancing the positive societal impact of Fermilab research.

The John Adams Institute for Accelerator Science (JAI) – a Centre of Excellence in the UK for advanced and novel accelerator technology – has a good tradition of fruitful collaborative research with Fermilab. Creating the ASTA user facility will open even more opportunities for collaborations of worldwide centres with Fermilab.

Sincerely,

Andrei Seryi

*The John Adams Institute for Accelerator Science is jointly hosted by the Departments of Physics of the University of Oxford, the Royal Holloway University of London and the Imperial College London*



ОБЪЕДИНЕННЫЙ ИНСТИТУТ ЯДЕРНЫХ ИССЛЕДОВАНИЙ  
JOINT INSTITUTE FOR NUCLEAR RESEARCH

Дубна, Московская область, Россия 141980      Dubna Moscow Region Russia 141980  
Telefax: (7-495) 632-78-80      Tel.: (7-49621) 65-059      AT: 205493 WOLNA RU      E-mail: post@jinr.ru      http://www.jinr.ru

03.12.12 № 010-27/351

на № \_\_\_\_\_ от \_\_\_\_\_

Dr. Stuart Henderson  
Associate Laboratory Director for Accelerators  
Fermi National Accelerator Laboratory

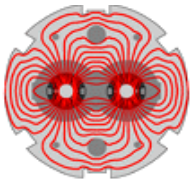
Dear Dr. Henderson,

As you may know, the Joint Institute for Nuclear Research (Dubna, Russia) is developing the project of Nuclotron based Ion Collider fAcility (NICA). The facility will consist of three cyclic accelerators including the last stage – the collider of heavy ions ( $1 \div 4.5$  GeV/u kinetic energy) and polarized protons and deuterons ( $5 \div 12.6$  GeV kinetic energy for protons). The NICA project is one of the subjects of Fermilab-JINR collaboration. We, the NICA team, are extremely interested in a progress of this collaboration and, above of all, are supporting the accelerator R&D proposal at Fermilab's Advanced Superconducting Test Accelerator (ASTA). Many of the accelerator physics research topics addressed in this proposal are of great interest to us and also overlap with issues relevant to NICA project.

Of particular interest to us are the proposed IOTA ring and its associated research program in nonlinear integrable optics, optical-stochastic cooling, and space-charge compensation. We would like to be part of this research program and to this end JINR is contributing 32 high-quality quadrupole magnets for the IOTA focusing lattice. In addition, this ASTA proposal continues our strong cooperation in the area of ILC R&D, as well as other topics, such as electron and stochastic cooling.

In the area of accelerator physics education, ASTA research program would offer many exciting opportunities which we are eager to exploit through graduate student and junior scientist exchange visits.

With best regards,  
Prof. Igor Meshkov  
JINR Directorate Adviser  
Scientific Leader of NICA project



**LARP**

**Dr. Eric Prebys**  
**Program Director, US LHC**  
**Accelerator Research Program**  
**(LARP)**

MS 221, Fermilab  
Batavia, IL 60510  
630.840.8369  
prebys@fnal.gov

December 10, 2012

**Dr. Vladimir Shiltsev,**  
**Director, Accelerator Physics Center**  
MS 221, Fermilab  
Batavia, IL 60510

Dear Vladimir,

I'm writing this letter in strong support of your proposal for the Advanced Superconducting Test Accelerator (ASTA). Although the LHC is not traditionally considered an "intensity frontier" machine, the ultimate luminosity is limited by beam brightness, which in turn is limited by intensity related effects at several points in the injector chain. The ASTA facility – and the IOTA ring in particular - will offer a powerful and unique experimental test bed to investigate these effects. The space charge compensation and optical stochastic cooling experiments, which have been proposed for ASTA, are already of great interest and it is quite likely that other experimental opportunities will present themselves. Tests done in the ASTA facility will provide invaluable data which will aid in effectively allocating resources to further tests at the LHC or the injector chain.

In addition, one of the most likely US contributions to the LHC luminosity upgrade will be the development of crab cavities, to compensate for the crossing angle of the colliding beams. It's possible that valuable R&D could be done at the ASTA facility into the affect of crab cavities on beams, which would complement that tests planned at the SPS and in the LHC.

We enthusiastically support the project, and look forward to taking part in the research opportunities it will present.

Regards,

Eric Prebys  
Program Director, LARP



ACCELERATOR & FUSION RESEARCH DIVISION  
*Director*

December 13, 2012

Dear Vladimir,

The proposed Accelerator R&D User Facility at Fermilab's Advanced Superconducting Test Accelerator (ASTA) will provide the Office of High Energy Physics with a state-of-the-art accelerator R&D platform of unique versatility. The expected beam quality and broad capabilities of the facility will be of great interest in applications outside of HEP as well, offering an opportunity for expanding the role of OHEP in accelerator R&D Stewardship. Several of our scientists in AFRD are eager to contribute to what we believe will be a diverse and exciting accelerator research program. The US, in my opinion, is severely lacking in dedicated accelerator test facilities that can focus on the improvements and generate the breakthroughs required to support a vibrant and competitive scientific community. Investment in facilities such as ASTA are vital to developing a robust R&D portfolio that will create the tools of the future. Here at LBNL we wish you great success and stand ready to assist in any way we can, now and in the future.

Sincerely,

Steve Gourlay  
Director, Accelerator and Fusion Research Division  
Lawrence Berkeley National Laboratory

December 2, 2012



NORTHERN ILLINOIS  
CENTER FOR  
ACCELERATOR AND  
DETECTOR DEVELOPMENT

Dr. Stuart Henderson, Associate Director for Accelerators  
Dr. Vladimir Shiltsev, Interim Director, Advanced Superconducting Test Acc.

DEPARTMENT OF PHYSICS  
NORTHERN ILLINOIS  
UNIVERSITY

Dear Drs. Henderson and Shiltsev,

DeKALB, ILLINOIS  
60115-2854

(815) 753-1772

We would like to express our strong support, on behalf of Northern Illinois University (NIU), of the Fermilab proposal to the Department of Energy for construction and operation of the Advanced Superconducting Test Accelerator (ASTA). NIU has been a strong partner with Fermilab in high energy and beam physics and is very pleased to further strengthen the partnership through sustained collaboration at ASTA.



The NIU-Fermilab collaboration was highlighted in 2001 with the establishment of the Northern Illinois Center for Accelerator & Detector Development (NICADD). NICADD has been successful because of extensive collaboration with and investment by Fermilab. Currently two faculty members in NICADD enjoy joint positions with the Accelerator Physics Center at Fermilab and the Department of Physics at NIU. We believe that ASTA will open new research opportunities in accelerator and beam physics and further catalyze collaborations between our institutions.



ASTA will also provide new opportunities for student training in advanced accelerator R&D. A number of students have pursued or are pursuing graduate-level degrees with research in accelerator physics or RF engineering involving Fermilab projects. NIU has also benefited locally through the collaboration as Fermilab staff have taught courses related to radiofrequency (RF) engineering in the Department of Electrical Engineering at NIU in joint effort to establish a Master degree in RF engineering.

The ASTA proposal also incorporates exciting opportunities for application of accelerator science beyond discovery science. For instance, the development of novel accelerator-based sub-picosecond x-ray, single-cycle THz sources and research on free-electron lasers could offer new research opportunities to NIU faculty. Such highly sought sources of radiation could have important applications in condensed matter, biology, and medical physics. The close proximity of ASTA to the NIU campus could lead to collaboration around the development of experimental methods utilizing these novel sources. Some of the advanced acceleration methods discussed in the ASTA proposal could also have application in medical physics, an area of increasing interest at NIU. Finally, the infrastructure needs for some of the proposed ASTA experiments, such as the

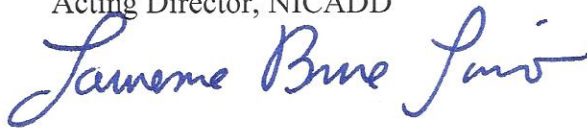
development of precision positioning for the aforementioned sources, could foster continued collaboration with the College of Engineering & Technology at NIU.

We are eagerly looking forward to the establishment of ASTA and are excited about the rich set of collaborative opportunities.

Sincerely,



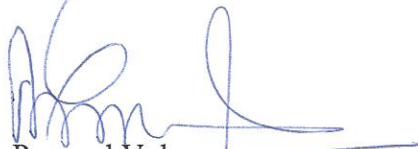
David Hedin  
Acting Director, NICADD



Lawrence Lurio  
Chair, Department of Physics



Lisa Freeman  
Vice President, Research & Graduate Studies



Promod Vohra,  
Dean College of Engineering & Engineering Technology

John Galambos  
Physics, Instrumentation and Ion Source Group Leader  
Research Accelerator Division  
Spallation Neutron Source

P.O. box 2008  
Oak Ridge, TN 37831-6462  
865-576-5482  
jdg@ornl.gov

November 20, 2012

Dr. Stuart Henderson  
Associate Laboratory Director for Accelerators  
Fermi National Accelerator Laboratory

Dear Stuart,

On behalf of the Spallation Neutron Source (SNS) accelerator effort, I wish to express support for the accelerator R&D proposal at Fermilab's Advanced Superconducting Test Accelerator (ASTA). Many of the accelerator development areas addressed in this proposal overlap with issues faced in high power proton accelerators used for spallation sources at BES neutron scattering facilities.

For instance the ASTA proposed nonlinear integrable lens tests (in the IOTA ring) is of direct interest. This technique offers potential for fundamentally improved high intensity beam storage, with avoidance of resonances, reduced possibilities of halo growth – which are major drivers in high intensity storage rings required to provide short pulse ( $\mu\text{s}$ ) neutron sources such as SNS. The nonlinear lens technique also offers promise in eliminating the problematic e-p instability, that we already see evidence of in SNS present operation. This instability could be a major obstacle for planned intensity upgrades. Additionally the proposed ASTA space charge compensation (with plasmas / electron column) tests are directly applicable to the SNS ring, as we already have a significant space charge induced beam broadening. Any possibility of reducing beam broadening can reduce beam loss, a major consideration in SNS operations.

These intensity related issues are important for both SNS upgrade plans and in the design of future high power spallation neutron sources. Additionally there will be ancillary areas of ASTA development that are applicable to SNS such as halo beam instrumentation and stable superconducting RF operation. As such we consider many of the ASTA targeted research areas as being mutually beneficial with the long-term neutron scattering scientific program within BES.

Please let me know if I can be of any further help.

Sincerely



John Galambos



**Plasma Physics Laboratory  
Princeton University  
P.O. Box 451  
Princeton, New Jersey 08543**

Dr. Vladimir D. Shiltsev  
Director  
Accelerator Physics Center  
Fermi National Accelerator Laboratory  
Batavia, IL 60510

December 10, 2012

**Re: *Proposal for an Accelerator R&D Facility at Fermilab's Advanced Superconducting Test Accelerator (ASTA)***

Dear Dr. Shiltsev:

It is a great pleasure to write this letter of strong support and participation for your proposal, "Proposal for an Accelerator R&D Facility at Fermilab's Advanced Superconducting Test Accelerator (ASTA)." The breadth and depth of the proposed research activities is quite impressive. Our PPPL Non-neutral Plasmas and Beam Dynamics Group shares many common interests with your co-authors, contributors, and you. Specifically, we are very interested in developing an improved understanding of the physics of intense beam propagation, stability, and neutralization.

In addition to our experimental expertise, our research group has significant experience in the theory and modeling of intense charged particle beams and beam neutralization by background plasma. We are also currently developing a laboratory to study the role of plasma in the formation and behavior of nanoparticles. Therefore, we look forward to collaborating with the research you are proposing in sections 7.2.2 [Integrable-optics test accelerator (IOTA) ring construction and operation], 7.2.3 [Space charge compensation in high intensity circular accelerators], and 7.2.5 [Investigation of acceleration and cooling of carbon-based crystal structures for muon accelerators].

One collaboration would include the development of supporting experiments on the Princeton Paul Trap Simulator Experiment to simulate nonlinear, integrable, transport lattices in a compact laboratory Paul trap. We will apply our expertise in pure-electron plasmas trapped in Malmberg-Penning traps to participate in the design of electron plasma diagnostics to characterize the properties of the trapped electron column used in the space charge compensation experiments. We will carry out experiments in our nanotechnology laboratory to explore the interaction of beams with carbon-based nanostructures. Further, we will apply our extensive theory and modeling tools, including fully self-consistent 3D particle-in-cell codes, to contribute to understanding topics such as emittance growth in nonlinear lattices, and two-stream instabilities in the trapped-electron/circulating proton system.

Thank you very much for the opportunity to participate.

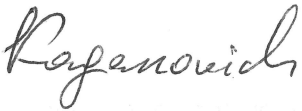
Sincerely



Ronald C. Davidson  
Professor



Erik P. Gilson  
Research Physicist



Igor D. Kaganovich  
Principal Research Physicist

December 7, 2012

Vladimir D. Shiltsev  
Director, Accelerator Physics Center  
ASTA Users' Program, Interim Director  
Fermilab  
PO Box 500, MS221  
Batavia, IL 60510 USA

Dear Dr. Shiltsev,

This letter is written in enthusiastic support of your proposal to establish an Accelerator R&D User Facility at Fermilab's Advanced Superconducting Test Accelerator (ASTA). This facility will fill an important role in providing high-energy, high average power beams for testing novel accelerator-related technologies and applications.

My company, Radiabeam Technologies, has been active in accelerator R&D and directed accelerator component and instrumentation development since its founding in 2004. We often require access to accelerator beamlines to test out new R&D concepts or new products. On the low-energy end ( $< 100$  MeV), we have used the UCLA Pegasus lab, the BNL ATF, and the Idaho Accelerator Center. However there is no facility with  $> 100$  MeV beams that will readily provide us access to the beamline. The impressive beam parameters to be available at ASTA, including the high energy, average power and brightness, will certainly enable a host of new experiments to be performed by users like us, and will no doubt spur development of new technologies with commercial applications.

For example, as you know, we have already proposed to use the ASTA beam to generate high-intensity gamma rays via the inverse Compton scattering (ICS) process. We originally became interested in an ICS gamma ray source as a probe to search for hidden Special Nuclear Materials over a long range ("active interrogation"). Our previous work resulted in the construction of a novel laser recirculator and laser-electron beam interaction system. Such a system, if configured at ASTA, would produce a beam of 5 – 20 MeV gamma rays with more than 10 W of power in a narrow bandwidth ( $\sim 1\%$ ). This would be an exciting source for homeland security applications, medical imaging and therapy, nuclear physics research, isotope production and non-destructive testing.

ASTA could also provide a test bed for the vendors to develop the accelerator instrumentation and components that will be needed for new high-intensity accelerators, such as ILC and CLIC, or a Higg's Factory. As an example, we are currently developing laser wire scanners for transverse profile measurement of high intensity beams, which would ideally be tested at a ASTA. Other companies would certainly be interested in testing their accelerator-related product at ASTA as well.

Finally, I am also excited about the development of the integrable optics accelerator as part of the ASTA program. The accelerator applications enabled by IOTA is impressive, with impact found in the areas from basic science to medicine. For example, a multi-MW proton driver is a potential workhorse in scientific applications in the intensity frontier, with applications such as: providing high fluxes of primary particles for muon production in the context of a muon collider and/or neutrino factory; spallation neutron production; transmutation of nuclear waste; and accelerator-driven sub-critical reactors (i.e. thorium cycle fission). Radiabeam has already started to look into the design of the novel nonlinear magnets required by IOTA, and we look forward to finding more opportunities to work on this exciting technology.

In conclusion, I strongly urge DOE to fund your proposal, as it would serve as a vital resource for both scientific and industrial users to develop and test novel accelerator technologies. I wish you the best of luck with this proposal, and look forward to working with you at ASTA.

Sincerely,



Salime Boucher, President  
Radiabeam Technologies, LLC

December 10, 2012

To whom it may concern,

It is with great pleasure I write this letter in support of Fermilab's Advanced Superconducting Test Accelerator (ASTA).

As Jefferson Lab's Associate Director responsible for Accelerators, I am very involved in furthering accelerator technologies and the training of future accelerator scientists and engineers.

Jefferson Lab has extensive experience in high current and high brightness electron sources used in the Nuclear Physics accelerator (CEBAF) and the Free Electron Laser (FEL). Jefferson Lab is a world leader in Superconducting Radio Frequency (SRF) accelerating structures and the interaction of electron beams with the RF fields. Due to the interest in high average currents in the present and future FELs and through our collaborations with ERL X-ray source advocates, we have worked extensively on many aspects of SRF technology suitable for high average current beams, such as cryomodules, highly HOM-damped cavities, damping couplers, high average power fundamental couplers, advanced cryogenics systems, to name a few. We will be very happy to share our expertise and the results of our continuing R&D in these areas with the ASTA effort and provide our high beam current SRF technology for use in ASTA. In order to eliminate duplication of effort, and as ASTA's future plans become more concrete, it will be advantageous to both our programs to make use of the technologies which are already here and to collaborate on mutually beneficial future research. We look forward to suitable divisions of labor with Fermilab.

As noted in the ASTA proposal itself, an area of particular interest to Jefferson Lab is developing cooling technology for our polarized Medium Energy Electron Ion Collider (MEIC). Both Brookhaven and Jefferson Lab have concluded that the luminosity of any future electron-ion collider will be high enough only through beam cooling. Brookhaven is pursuing coherent electron cooling for this purpose.

The MEIC design includes the use of Energy Recovery Linac (ERL) based Electron Cooling for the hadron beam. In order to reduce the required electron current in ERL, the cooler scheme is complemented with a Circulator Cooler Ring (CCR) operated by a fast kicker with sub-nanosecond rise times. We would like to conduct experiments with ASTA's fast kicker as part of our MEIC studies and look forward to the opportunity of collaborating with Fermilab's scientists in the cooler design at ASTA. Operating the iota ring to mimic the circulator cooler is very attractive to us.

A number of high level scientific committees have emphasized educating and training the next generation of accelerator scientists and engineers as a national priority. Fermilab's

ASTA would be an excellent facility which supplements class room teaching with hands-on training. Our experience at Jefferson Lab with accelerator physics students, (both undergraduate and graduate), is that the hands-on training enhances the understanding of critical concepts and contributes to the sustained enthusiasm for the field.

I strongly believe that ASTA will make significant contributions to accelerator science and engineering.

Sincerely,



Andrew Hutton  
Associate Director for Accelerators  
Jefferson Lab



# United States Particle Accelerator School

**Director**  
William Barletta  
MIT  
barletta@mit.edu

28 November 2012

**USPAS Board of  
Governors**

Rodney Gerig  
Chair  
ANL

Derek Lowenstein  
BNL

David Rubin  
Cornell

Stuart Henderson  
FNAL

Richard Sheffield  
LANL

Steven Gourlay  
LBNL

William Goldstein  
LLNL

Michael Syphers  
MSU

Kevin Jones  
ORNL

Alex Chao  
SLAC

Jean Delaunay  
TJNAF

Dr. Vladimir Shiltsev  
Director, Accelerator Physics Center  
Fermi National Accelerator Laboratory  
Batavia IL

Dear Vladimir,

I have read with interest your draft proposal for a test accelerator, ASTA, dedicated to beam physics studies. The opportunities for beam physics research on state of the art equipment are highly unusual. Of particular interest is the difficult task of attracting undergraduate physics and engineering students to our field. Therefore, it is natural to consider how ASTA can be used to train students in accelerator science and technology.

A highly cost-effective first use of ASTA for formal education would be an expansion of the already successful collaboration of USPAS, FNAL, and ANL in the Lee Teng Undergraduate Internship Program. In that program students take a formal course at USPAS and then spend the remainder of the summer doing research at FNAL and ANL. Were their first week of research transformed into a week of hands-on experience at ASTA, the Lee Teng Internship could be transformed into a truly unique educational experience with a strong potential to attract pre-graduate scientist

Students could spend their first week at the laboratories doing real hands-on experiments at ASTA. That would give everyone a chance to have an experimental experience even if their internship is with a theorist. As FNAL and ANL have already worked out affordable housing and transportation for the student interns, the additional costs of LeeTeng at ASTA would be minimal.

Such a program would be a great first step and also allow the ASTA staff to work out a set high quality instructional experiments for an ASTA-based curriculum that could be used on an annual basis. The USPAS would be pleased to work with you and the Lee Teng program coordinators to make this a model hands-on program.

Sincerely yours,

A handwritten signature in black ink that reads "William A. Barletta".

William A. Barletta  
Director